Transdermal iontophoresis for the controlled delivery of therapeutic agents to treat neurodegenerative diseases

Kalaria, Dhaval

UNIVERSITÉ DE GENÈVE
Section des sciences pharmaceutiques
Laboratoire de Chimie Thérapeutique

FACULTÉ DES SCIENCES
Professeur Leonardo Scapozza
Dr. Yogeshvar N. Kalia

Transdermal iontophoresis for the controlled delivery of therapeutic agents to treat neurodegenerative diseases

THÈSE

Présentée à la Faculté des Sciences de l'Université de Genève pour obtenir le grade de Docteur ès sciences, mention sciences pharmaceutiques

Par

Dhaval R. Kalaria

de L'Inde

Thèse N° 4480

GENÈVE
Atelier d'impression ReproMail
2012

UNIVERSITÉ DE GENÈVE

FACULTÉ DES SCIENCES

Doctorat ès sciences
Mention sciences pharmaceutiques

Thèse de *Monsieur Dhaval KALARIA*

intitulée :

" Transdermal Iontophoresis for the Controlled Delivery of Therapeutic Agents to Treat Neurodegenerative Diseases "

La Faculté des sciences, sur le préavis de Messieurs L. SCAPOZZA, professeur ordinaire et directeur de thèse (Section des sciences pharmaceutiques), Y. KALIA, docteur et codirecteur de thèse (Section des sciences pharmaceutiques), E. ALLEMANN, professeur ordinaire (Section des sciences pharmaceutiques), J. HIRVONEN, professeur (Faculté de pharmacie, Université d'Helsinki, Finlande), de Mesdames P. SANTI, professeure (Faculté de pharmacie, Université d'Helsinki, Finlande) et V. MERINO, professeure (Departamento de Farmacia y Tecnología Farmacéutica, Facultad de Farmacia, Universidad de Valencia, España), autorise l'impression de la présente thèse, sans exprimer d'opinion sur les propositions qui y sont énoncées.

Genève, le 26 octobre 2012

Thèse - 4480 -

Le Doyen, Jean-Marc TRISCONE

N.B. - La thèse doit porter la déclaration précédente et remplir les conditions énumérées dans les "Informations relatives aux thèses de doctorat à l'Université de Genève".

TABLE OF CONTENTS

RESUMÉ

L'utilisation de patchs transdermiques contenant la rotigotine (Neupro®) et la rivastigmine (Exelon®) pour le traitement de maladies neurodégénératives a reçu un bon accueil de la part des patients, des médecins et des soignants, ce qui a stimulé leur succès commercial. Plusieurs besoins cliniques non satisfaits ainsi que leur potentiel commercial ont relancé l'intérêt pour les systèmes de libération transdermique pour le traitement de maladies chroniques telles la maladie d'Alzheimer (MA) et la maladie de Parkinson (MP). La voie transdermique est une alternative valable pour l'administration de médicaments contre le Parkinson, dans lequel une stimulation continue des récepteurs dopaminergiques est requise si afin d'éviter des complications motrices. L'administration transdermique offre une libération cinétique de médicaments d'ordre zéro, ce qui évite une stimulation pulsatile des récepteurs dopaminergiques, ainsi que la dégradation gastro-intestinale du médicament par effet de premier passage. Les formulations transdermiques permettent aussi une réduction du fardeau que représentent les comprimés pour les patients, ce qui améliore leur compliance et l'efficacité du traitement.

L'administration transdermique de molécules hydrosolubles chargées est une tâche complexe à cause de la composition lipidique multilamellaire de la couche externe de la peau (la couche cornée). Celle-ci oppose une barrière efficace à la diffusion de médicaments polaires. Dans ce cas précis, la ionophorèse transdermique (un procédé utilisant un courant électrique) pourrait être une alternative valable. Le flux transdermique d'agents thérapeutiques est considérablement amélioré par l'application d'un courant de faible intensité à travers la peau. De plus, la ionophorèse permet l'ajustement des doses par simple modulation du courant appliqué. Ceci est d'importance capitale dans le traitement de la MP, où une augmentation graduelle de la dose est nécessaire pour réduire les effets indésirables de la thérapie dopaminergique. De plus, cette technologie transdermique est la seule à avoir été approuvée par la FDA (LidoSite™ et Ionsys™) pour l'administration topique et systémique d'agents thérapeutiques.

Le but de cette thèse est d'étudier la faisabilité de la ionophorèse pour administrer des agents thérapeutiques à travers la peau pour le traitement de la MP et de la MA. Le Chapitre 1 contient une revue complète et critique des différentes classes thérapeutiques et molécules utilisées dans des études cliniques en tant que candidats potentiels pour l'administration ionophorétique, en

insistant sur le développement des deux systèmes ionophorétiques approuvés par la FDA. Les Chapitres 2-5 montrent la faisabilité de l'administration ionophorétique de médicaments sélectionnés parmi les différentes classes thérapeutiques utilisées pour traiter la MP et la MA (p.ex. les IMAO-B, un agoniste dopaminergique pour la MP, et un inhibiteur de l'acétylcholine pour la MA). L'influence de différents paramètres comme la densité de courant, la concentration du principe actif, ainsi que le pH ont été investigués in vitro sur de la peau de porc. Les études suivantes ont comparé la libération de ces médicaments à travers la peau de porc et humaine, et ont été suivies d'une étude pharmacocinétique de la ionophorèse dans le rat. L'étude de différents paramètres ont permis d'évaluer la faisabilité de l'administration des principes actifs étudiés à des doses thérapeutiques chez l'homme.

Dans le Chapitre 2, la faisabilité et les mécanismes de l'administration transdermique ionophorétique des IMAO-B: la rasagiline et la sélégiline ont été étudiés in vitro sur de la peau humaine et porcine. La perméation passive était négligeable pour la rasagiline et la sélégiline après 7 h (respectivement, 14.2 ± 4.0 et 10.4 ± 3.4 $\mu g/cm^2$). Par contre, la ionophorèse anodale à 0.3 mA/cm^2 pendant 7 h a produit une augmentation de 64 et 48 fois de leur perméation respective. L'augmentation de l'intensité de courant a produit une croissance linéaire du flux de rasagiline et sélégiline. L'électromigration était le mécanisme dominant pour les deux médicaments, représentant ~90% du transport. Le taux de transport et l'efficacité de la libération mesurés étaient élevés pour les deux médicaments. De plus, la libération était statistiquement équivalente aussi bien à travers la peau de porc que la peau humaine. Des hydrogels à base de carbopol ont montré des taux de perméation moindres que les solutions correspondantes, mais tout de même suffisants pour atteindre un niveau thérapeutique. Sur la base de ces résultats, et en considérant la posologie et la pharmacocinétique, il serait possible d'administrer des doses thérapeutiques de rasagiline et sélégiline chez l'Homme en appliquant un courant de 0.3 mA/cm^2 à travers un patch de 2-4 cm^2.

Le Chapitre 3 décrit une investigation *in vitro* et *in vivo* de l'administration ionophorétique du pramipexole, un agoniste dopaminergique. Des études préliminaries ont montré que le pramipexole était un excellent candidat pour l'administration ionophorétique transdermique, grâce à ses propriétés physico-chimiques. Des études in vitro ont suggéré une corrélation

linéaire de l'électro-transport du pramipexole en fonction de la densité de courant et de la concentration du compartiment donneur. Ceci serait utile dans le cas d'une augmentation de la dose pour les patients présentant un état avancé de la maladie. Le transport du médicament était gouverné par l'électromigration (>80%), et le pramipexole n'a montré aucun signe d'inhibition du flux de solvent électro-osmotique. Son adéquation pour la ionophorèse a été démontrée par le taux élevé de transport et de libération (respectivement 6-7% et 14-58%). Des études pharmacocinétiques chez le rat ont montré que le taux de perfusion du pramipexole in vivo était supérieur de celui observé in vitro chez la peau de porc (respectivement 0.46 ± 0.05 et 0.19 ± 0.01 mg/h). Aussi, la ionophorèse anodale du pramipexole a permis de fournir une administration contrôlée par le courant électrique, dont les données in vivo extrapolées à l'Homme suggèrent que des doses thérapeutiques pourraient être libérées en 3 h en utilisant un patch de 2 cm^2.

La gestion de la MP est une tâche ardue, en sachant que la plupart des patients sont soumis à des traitements multiples dus aux nombreuses comorbidités (en moyenne 10 comprimés quotidiens en phase avancée). Même si la L-DOPA est souvent considérée comme "standard de référence", son utilisation prolongée mène à des complications motrices. Pour cette raison, le traitement commence par un agoniste dopaminergique, et est ensuite enrichi par la L-DOPA et d'autres agents thérapeutiques tels les IMAO-B. Un grand nombre d'études cliniques ont montré qu'une administration simultanée d'agonistes dopaminergiques et de IMAO-B ont donné comme résultat une amélioration marquée des symptômes et de la qualité de vie des patients.

Le Chapitre 4 présente l'effet de la co-ionophorèse simultanée de rasagiline et pramipexole in vitro et in vivo. L'étude met en évidence l'impact de l'administration concomitante de deux molécules et l'effet sur leur transport ionophorétique. Les différences observées entre leur perméation ionophorétique in vitro ont été attribuées à leurs différentes propriétés physico-chimiques, parmi lesquelles le LogD, la lipophilie et la surface polaire. Le pramipexole possède un caractère plus hydrophile et une plus grande surface polaire que la rasagiline, ce qui s'est traduit par un meilleur transport à travers la peau. L'effet de la composition de la formulation sur la co-ionophorèse a montré l'influence du transport sur leurs concentrations respectives. Ce principe pourra être utilisé pour concevoir un système optimisé basé sur les doses requises des

deux médicaments. Le système co-ionophorétique a montré une efficacité combinée de la libération de 64%, confirmant que la ionophorèse est bien adaptée pour leur transport à travers la peau.

La co-ionophorèse d'agents thérapeutiques était statistiquement similaire pour la peau humaine et porcine in vitro. L'ionisation des molécules étudiées a joué un rôle critique pour l'électro-transport, car il a été montré que l'électro-migration était le mécanisme dominant leur perméation. Des modèles compartimentaux obtenus à partir des données pharmacocinétiques in vivo chez le rat ont montré une libération supérieure in vivo que in vitro, attribuée aux propriétés moléculaires des médicaments, à l'irrigation sanguine, et, plus majoritairement, à la différence de concentration saline épidermique entre in vitro et in vivo. Ces résultats ont montré que des doses thérapeutiques des deux médicaments antiparkinsoniens pourraient être administrés via le même patch transdermique, ce qui offre une nouvelle approche pour le traitement de la MP.

Le Chapitre 5 décrit la ionophorère transdermique de l'hupérizine A in vitro et in vivo, et évalue aussi la faisabilité de l'administration de doses thérapeutiques pour le traitement de la MA. Il a été montré que la ionophorèse est très efficace pour l'administration d'hupérizine A à travers la peau, puisque 46-81% de la dose appliquée a été libérée en fonction de la densité de courant. L'électro-transport était proportionnel à la densité de courant appliquée ainsi qu'à la concentration d'hupérizine A dans le compartiment donneur. Les paramètres pharmacocinétiques ont été déterminés chez le rat en utilisant un modèle monocompatimental utilisant des débits d'administration soit constants, soit dépendants du temps. L'administration de médicaments à travers la peau est un processus complexe qui a montré la mauvaise adéquation du modèle d'administration à débit constant (analogue à une perfusion intraveineuse) pour simuler les profils plasmatiques à partir des données observées de l'hupérizine A. Cependant, le modèle dépendant du temps prend en considération plusieurs facteurs spécifiques à l'administration transdermique, et est de ce fait supérieur dans la simulation de la concentration observée, ce qui a permis un meilleur ajustement des données au modèle. En considérant que l'on n'a pas observé de différences dans l'absorption transdermique d'hupérizine A entre les espèces, des doses thérapeutiques pourraient être administrées via un patch de a 5 cm^2 en ~ 3 h.

SUMMARY

Transdermal delivery systems of "patches" for rotigotine (Neupro®) and rivastigmine (Exelon®) indicated for the treatment of neurodegenerative disorders have been well received by patients, physicians and care givers spurring their commercial success. Several unmet clinical needs and market potential have reinvigorated interest in the development of transdermal drug delivery systems for the treatment of chronic conditions such as Alzheimer's disease (AD) and Parkinson's disease (PD). The transdermal route is a suitable alternative for the delivery of anti-Parkinson's drugs where constant stimulation of dopaminergic receptors is required to avoid motor complications. Transdermal delivery provides zero-order drug input kinetics shunning the pulsatile stimulation of dopamine receptors as well as circumventing drug degradation in the gastro-intestinal tract and by the hepatic first pass effect. Transdermal formulations also reduce the tablet burden for patients and thereby improve patient compliance and efficacy of the treatment.

Transdermal delivery of hydrosoluble charged molecules is a formidable task due to the multilamellar lipidic composition of the skin's outermost layer (i.e., the stratum corneum) that imposes a significant barrier against the diffusion of polar drugs. For the delivery of such molecules, transdermal iontophoresis, an energy driven process can be a suitable option. Transdermal flux of therapeutics is considerably enhanced by application of a low intensity current across the skin. In addition, iontophoresis enables dose titration by simple modulation of applied current density. This is extremely important in PD therapy where gradual dose titration is required to minimize the side effect of the dopaminergic therapy. In addition, it is the only transdermal delivery technology that has managed to produce FDA approved products (LidoSite™ and Ionsys™) for topical and systemic administration of therapeutics.

The aim of this thesis was to study the possibility of using iontophoresis to deliver therapeutic agents across the skin for treatment of PD and AD. Chapter 1 contains a comprehensive and critical review of the different therapeutic classes and molecules that have been investigated as potential candidates for iontophoretic delivery in various clinical studies to-date with a special focus on the product development of the two FDA approved iontophoretic systems. Chapters 2-5 show the feasibility of transdermal iontophoretic delivery of drugs, selected from the different

therapeutic classes used to treat AD and PD (e.g., MAO-B inhibitors and a dopamine agonist for PD and an acetylcholinesterase inhibitor for AD). The influence of different parameters including the applied current density, concentration of active ingredient, effect of pH was investigated using porcine skin *in vitro*. Subsequent studies compared delivery across porcine and human skin and were followed by an investigation into drug pharmacokinetics following iontophoresis in rats. Study of different parameters enabled an evaluation of the feasibility of delivering therapeutic amounts of these drugs in humans.

The feasibility and the mechanisms of transdermal iontophoretic delivery of MAO-B inhibitors, rasagiline and selegiline across human and porcine skin *in vitro* were studied (Chapter 2). Passive permeation was minimal for rasagiline and selegiline after 7 h (14.2 ± 4.0 and 10.4 ± 3.4 $\mu g/cm^2$, respectively). In contrast, anodal iontophoresis at 0.3 mA/cm^2 for 7 h produced 64- and 48-fold increase in their permeation, respectively. Increase in current density produced a linear increase in flux for rasagiline and selegiline. Electromigration was the dominant mechanism for both rasagiline and selegiline accounting for ~90% transport. High transport and delivery efficiencies were recorded for both the drugs. Furthermore, delivery across porcine and human skin was statistically equivalent. Hydrogels formulated using carbopol showed less permeation than the corresponding solutions but it was nevertheless sufficient to deliver therapeutic amounts of each drug. Based on these results and given the posology and known pharmacokinetics, it should be possible to administer therapeutic amounts of rasagiline and selegiline in humans using 0.3 mA/cm^2 current and 2-4 cm^2 patch size.

Chapter 3 describes an investigation into the iontophoretic delivery of pramipexole, a dopamine agonist *in vitro* and *in vivo*. Preliminary studies proved that pramipexole was an excellent candidate for transdermal iontophoresis owing to its physicochemical properties. *In vitro* studies suggested linear dependence of pramipexole electrotransport on current density and donor concentration, which would be beneficial for dose ramping as patients move in to more advanced disease states. Transport was governed by electromigration (> 80%) and pramipexole did not show any signs of inhibiting electroosomotic solvent flow. Pramipexole suitability for iontophoresis was reflected by high transport and delivery efficiencies (6-7% and 14-58%, respectively). Pharmacokinetics studies in rats showed that the input rate of pramipexole *in vivo*

was more than that observed in porcine skin *in vitro* (0.46 ± 0.05 and 0.19 ± 0.01 mg/h, respectively). Thus, anodal iontophoresis provided current-controlled transdermal delivery of pramipexole and extrapolation of *in vivo* data to humans suggested that therapeutic amounts could be delivered in 3 h using a 2 cm^2 patch.

Management of PD is a daunting task, knowing the fact that most of these patients are on multiple pills due to concomitant disease conditions (mean tablet intake of 10 per day in advanced conditions). Although L-DOPA is often referred as the "gold standard" its prolonged use leads to motor complications. Hence, therapy is initiated with dopamine agonist and then supplemented with L-DOPA and other agents such as MAO-B inhibitors. A number of clinical studies have shown that simultaneous administration of dopamine agonist and MAO-B inhibitors resulted in marked improvements in symptoms and daily life of patients.

Chapter 4 presents the effect of simultaneous co-iontophoresis of rasagiline and pramipexole *in vitro* and *in vivo.* The study highlights the impact of concomitant administration of two molecules and the effect on their iontophoretic transport. The differences observed between their iontophoretic permeation *in vitro* were attributed to differences in their physicochemical properties including log D, lipophilicity and polar surface area. Pramipexole has more hydrophilic character and polar surface area than rasagiline, which resulted in its higher transport. Effect of formulation composition on co-iontophoresis demonstrated the dependence of transport on their respective concentrations, which can be utilised to design an optimum system based on the dosing requirements of two drugs. The co-iontophoretic system showed a combined delivery efficiency of 64% confirming that iontophoresis is well suited for their co-transport across the skin.

Co-iontophoretic permeation of actives was statistically similar across human and porcine skin *in vitro*. Ionization of the studied molecules played a critical role in electrotransport, as electromigration was found to be the dominant mechanism for their permeation. Compartment modelling of data from pharmacokinetic studies in rats demonstrated higher drug input rates *in vivo* than *in vitro;* attributed to molecular properties of drug, dermal blood supply, and more importantly the difference in *in vitro* and *in vivo* concentration of saline within epidermis. These

results showed that therapeutic amounts of two Anti-parkinson drugs could be administered from the same patch by transdermal iontophoresis offering a new approach towards the treatment of PD.

Chapter 5 describes transdermal iontophoresis of huperzine A *in vitro* and *in vivo* and evaluates the feasibility of delivering therapeutic amounts of the same for treatment of AD. Iontophoresis was found to be extremely efficient in delivering huperzine A across skin with 46-81% of drug load being delivered depending on current density. Electrotransport was proportional to the applied current density and concentration of huperzine A in the donor compartment. Pharmacokinetic parameters were determined in rats using one-compartment model with either constant or time-dependent input rates. Drug delivery through skin is a complex process that was reflected by inadequateness of constant input model (analogous to intravenous infusion) to simulate the predicted vs. observed plasma concentration profiles of huperzine A. However, the time-variant input model takes into consideration several factors pertaining to transdermal drug transport and was found to be superior in simulating the observed concentration, providing a better goodness of fit. With no difference observed in transdermal absorption of huperzine A between various species, therapeutic amounts of the same could be delivered in humans from a 5 cm^2 iontophoretic patch in ~ 3 h.

INTRODUCTION

Neurodegenerative Diseases

Alzheimer's Disease (AD) and Parkinson's Disease (PD) are the two most prevalent neurodegenerative disease, posing a significant burden on healthcare system [1,2]. The Alzheimer Society (US) reported that more than 5.4 million people are living with the disease in the US and estimated the direct costs at $ 200 billion [3]. PD is less prevalent affecting 1 million people in the US and 10 million people worldwide [4]. AD produces an impairment of cognitive abilities that is gradual in onset but relentless in progression, characterized by marked atrophy of the cerebral cortex and loss of cortical and subcortical neurons resulting in deficiency of acetylcholine [5]. On the other hand, the primary deficit in PD is the loss of neurons in the substantia nigra that provides dopaminergic innervation to the striatum. The clinical symptoms of PD comprise of four cardinal features: bradykinesia, muscular rigidity, resting tremor, and an impairment of postural balance [6]. Table 1 enumerates the treatment options available for the management of AD and PD.

Table 1 Commonly used therapeutic agents for the treatment of Alzheimer's Disease and Parkinson's Disease

	Class	Drugs
Parkinson's Disease	Precursor of dopamine	L-DOPA
	COMT inhibitors	Entacapone, tolcapone
	Dopamine receptor agonist	Pramipexole, rotigotine
	MAO-B inhibitors	Selegiline, rasagiline
	L-amino acid decarboxylase inhibitor	Benserazide, carbidopa
	Muscarinic receptor antagonists	Trihexyphenidyl, benztropine
Alzheimer's Disease	Acetylcholinesterase inhibitors (AChEI),	Tacrine, donepezil, rivastigmine, huperzine A
	NMDA glutamate-receptor antagonist	Memantine

Challenges in treatment of PD and AD

In healthy individuals, neurons in the substantia nigra continuously release dopamine ensuring the constant stimulation of receptors. However, in PD due to dopamine deficiency, patients are extremely sensitive to slight variations in synaptic dopamine concentration, and a non-physiologic pulsatile stimulation can cause motor complications ("on-off" effect) [7,8]. The marketed oral dosage forms show erratic absorption due to impaired gastrointestinal functions in PD patients and first pass metabolism. This leads to pulsatile stimulation of the dopamine receptors and provoke the on-off phenomena, rendering the therapy inefficacious and increasing level of discomfort for patients [9,10]. Studies have also suggested that continuous infusion of L-DOPA or dopamine agonist can reduce occurrence and severity of motor complications but such an approach is impractical for routine treatment [11].

The major concern in the treatment of AD is compliance. A clinical study in AD patients revealed that more than one third of patients stopped treatment within 6 months and of the active users, 14% had lapses of six or more weeks – obviously compromising treatment efficacy [12]. The AD patient population consists of older adults and due to higher incidence of chronic diseases in this group; these individuals are frequently on polytherapy and this can also affect compliance. Moreover, since AD patients suffer from cognitive disorders, the care giver administers and manages the medication regimen.

Currently available oral medications have severe drawbacks for the treatment of AD and PD. Oral administration of therapeutics can be cumbersome so medications that are independent of patient's state and readily controllable by the care-giver are preferred. Hence, there are several unmet clinical needs that can be addressed by the development of a patient compliant formulation. On the other hand to avoid motor complications in PD patients; a formulation that can deliver drug at a constant rate would be highly beneficial and improve the efficacy of treatment (i.e., decrease the incidence of "on-off" effects).

Transdermal formulations: Advantages and limitations

Transdermal delivery offers considerable advantages over conventional oral dosage forms for patients who are non-adherent or have difficulties swallowing solids or liquids. Transdermal

formulation can increase patient compliance and also reduce the burden of care-givers. Transdermal delivery kinetics makes it an ideal route for the continuous dopaminergic stimulation necessary in PD to avoid "on-off" episodes [13]. Transdermal therapy will offer key benefits starting from pharmaceutical aspects, as an easy, once-daily application of a patch. From pharmacokinetic perspective it can circumvent gastric drug degradation and the first pass effect with zero order drug input kinetics (no peak and trough variations) [14]. Pharmacodynamic benefits include potential for limiting motor complications as well as avoiding inhibition of enzymes present in the gastrointestinal tract or liver. For example, dietary restrictions must be imposed following oral administration of MAO-B inhibitors in order to prevent hypertensive crises [15]. In addition, when adverse effects manifest, prompt cessation of drug delivery can be ensured by simple removal of the patch. These advantages led to the development of two transdermal delivery systems: Neupro® (rotigotine) and Exelon® (rivastigmine) for the management of neurodegenerative disease [16].

However, skin's excellent barrier function (dues essentially to the stratum corneum) ensures that only selected few potent molecules with the correct physicochemical properties can be delivered transdermally in therapeutic amounts. Passive diffusion is suitable for candidates with high potency (dose <10 mg), relatively low molecular mass (< 400 Da), octanol-water distribution coefficient between 10 and 1000, and usually should be neutral in pH range from four to seven [17]. It should be mentioned that most of the drugs used in these diseases are freely water soluble base, and have an ionic character at pH 5-7. Hence, the rate of passive diffusion for such hydrosoluble charged molecule across stratum corneum is insufficient to elicit a therapeutic effect. Furthermore, commercially available patches have an application period of 24 h, causing discomfort due to skin sensitization or irritation at the site of application by various formulation components such as adhesives, penetration enhancers and even actives. Therefore, to circumvent these issues either the skin barrier function must be compromised or an active transport technology should be used to increase the transport of drugs into and across the skin. Iontophoresis is one of the more widely studied technologies to enhance the transport of charge, hydrosoluble molecules through the skin. It can provide a transdermal delivery system ideally suited to molecules with the above mentioned physicochemical properties, which are difficult to deliver through skin using conventional approaches.

Iontophoresis

Iontophoresis is a non-invasive technique that involves application of a mild electric current to enhance the penetration/permeation of molecules into and through tissues [18]. Apart from expanding the range of therapeutics that can be delivered across the skin, iontophoresis provides increased delivery efficiency and faster onset of action through enhanced permeation of actives, shortening the lag time observed with passive delivery and reducing the time of patch application. The amount of compound delivered is usually directly proportional to the applied current, the duration of current application and the area of the skin surface in contact with the active electrode. This salient feature allows control over the input rate by modulation of current density to deliver the required amount of drug in a very tightly controlled fashion and provide individualized treatment regimens as per patient needs. This would be highly beneficial for PD patients where dose escalation is required as the disease advances and such increase in therapeutic dose achievable by simple modulation of current density without any increase in the patch size. Moreover, iontophoresis is the only technology for transdermal system that has two FDA approved products: LidoSite™ topical system (lidocaine topical anaesthetic system) and Ionsys™ system (fentanyl for post-operative patient-controlled analgesia) [19,20].

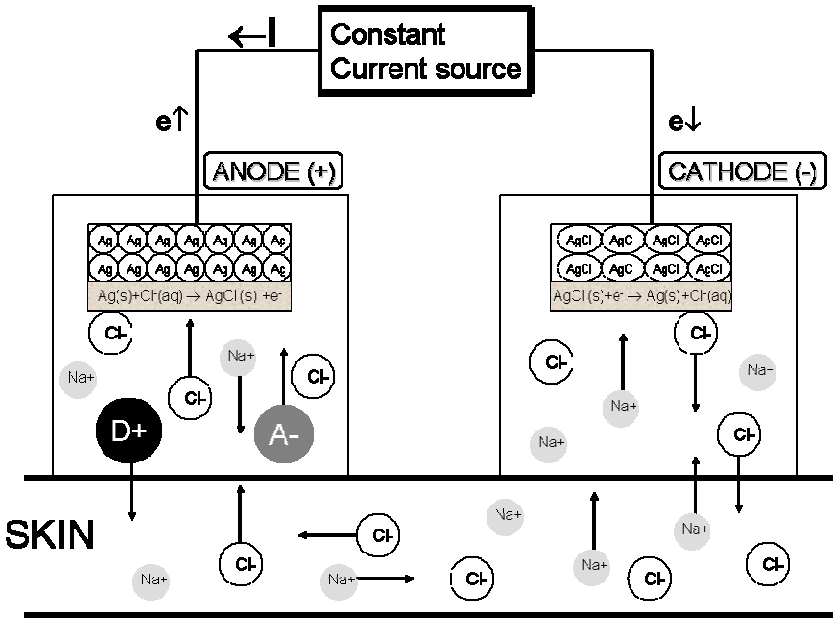

Figure1. Schematic representation of iontophoresis [16]

An iontophoretic device consists of a patch containing two electrodes (an anode and a cathode) that are connected to a power source. The active electrode is immersed in medium containing charged drug (same polarity as electrode) and the other (return electrode) is positioned in an inert conducting medium i.e., sodium chloride solution (Figure 1). During iontophoresis, the molecular transport can be attributed to three component mechanisms: passive diffusion, electromigration (EM) and electroosmosis (EO) (Nernst–Planck theory) [21]. EM is the result of charge on the molecule and EO is due to convective solvent flow generated by application of an electric field across the negatively charged skin [22]. Assuming passive diffusion is negligible, total flux for a given drug is described as follows:

$$J_{tot} = J_{EM} + J_{EO} = \left[\left(\frac{i_d}{F}\right) \times \frac{u_{DRUG}}{\sum_1^i z_i u_i c_i} + V_w\right] \times c_{DRUG} \quad (1)$$

where J_{EM} and J_{EO} represent the contribution of EM and EO to the total flux, i_d is the applied current density; z_i, u_i and c_i refer to the charge, mobility and concentration of the ions carrying charge across the membrane; u_{Drug} and c_{Drug} are the mobility and concentration of drug, respectively.

Based on the above, several drugs used in the treatment of PD and AD were selected with respect to their physiochemical and pharmacokinetic properties and were studied with the following objectives.

Objectives of the thesis

The investigations described in this thesis focus on the transdermal iontophoretic delivery of three anti-Parkinsonism drugs and one anti-Alzheimer drug. Iontophoretic transport experiments were carried out with MAO-B inhibitors (rasagiline and selegiline, chapter 2), pramipexole (chapter 3), co-iontophoresis of rasagiline and pramipexole (chapter 4) and huperzine A (chapter 5). The specific aims were: (a) to verify the feasibility of the iontophoretic transdermal delivery of above mentioned drugs; (b) to investigate the role of formulation and current density on the transdermal transport of these drugs; (c) to identify the mechanism governing iontophoretic transport; and (d) to investigate iontophoretic delivery of selected drugs *in vivo* to determine drug input rates and thus evaluate the feasibility of using iontophoresis to deliver therapeutic doses of these drugs.

References

[1] Johnston, M. V. Cognitive disorders: In Principles of Drug Therapy in Neurology, Johnston, M. V., MacDonald, R. L., Young, A.B., Eds.; Davis: Philadelphia, 1992; pp 226-267.

[2] Singh, N., Pillay V., Choonara, Y. E. Advances in the treatment of Parkinson's disease. Prog. Neurobiol. 81 (2007) 29–44.

[3] Alzheimer's Association - 24 July 2012.
http://www.alz.org/alzheimers_disease_facts_and_figures.asp

[4] Parkinson's Disease Foundation 24 July 2012. http://www.pdf.org/en/parkinson_statistics

[5] Arnold, S. E., Hyman, B. T., Flory, J., Damasio, A. R., Van Hoesen, G. W. The topographical and neuroanatomical distribution of neurofibrillary tangles and neuritic plaques in the cerebral cortex of patients with Alzheimer's disease. Cereb. Cortex 1 (1991) 103-116.

[6] Lang, A. E., Lozano, A. M. Parkinson's disease. First of two parts. New Engl. J. Med. 339 (1998) 1044-1053.

[7] Antonini, A. Continuous dopaminergic stimulation--from theory to clinical practice. Parkinsonism Relat. Disord. 13 (2007) S24-S28.

[8] Olanow, C. W., Obeso, J. A., Stocchi, F. Continuous dopamine receptor treatment of Parkinson's disease: scientific rationale and clinical implications. Lancet Neurol. 5 (2006) 677–687.

[9] Engber, T. M., Susel, Z., Juncos, J. L., Chase, T. N. Continuous and intermittent levodopa differentially affect rotation induced by D-1 and D-2 dopamine agonists. Eur. J. Pharmacol. 168 (1989) 291-298.

[10] Mouradian, M. M., Heuser, I. J., Baronti, F., Chase, T. N. Modification of central dopaminergic mechanisms by continuous levodopa therapy for advanced Parkinson's disease. Ann. Neurol. 27 (1990) 18-23.

[11] Steiger, M. Constant dopaminergic stimulation by transdermal delivery of dopaminergic drugs: a new treatment paradigm in Parkinson's disease. Eur. J. Neurol. 15 (2008) 6-15.

[12] Roe, C. M., Anderson, M. J., Spivack, B. How many patients complete an adequate trail of donepezil ? Alzheimer Dis. Assoc. Disord. 16 (2002) 49-51.

[13] Guldenpfennig, W. M., Poole, K. H., Sommerville, K. W., Boroojerdi, B. Safety, tolerability, and efficacy of continuous transdermal dopaminergic stimulation with rotigotine patch in early-stage idiopathic Parkinson disease. Clin. Neuropharmacol. 28 (2005) 106-110.

[14] Tanner, T., Marks, R. Delivering drugs by the transdermal route: review and comment. Skin Res. Technol. 14 (2008) 249-260.

[15] Culpepper, L., Kovalick, L. J. A review of the literature on the selegiline transdermal system: an effective and well-tolerated monoamine oxidase inhibitor for the treatment of depression. Prim. Care Companion J. Clin. Psychiatry 10 (2008) 25-30.

[16] Orange Book – FDA: Food and Drug administration 20 June 2012 http://www.accessdata.fda.gov/scripts/cder/ob/default.cfm/

[17] Naik, A., Kalia, Y. N., Guy, R. H. Transdermal drug delivery: overcoming the skin's barrier function. Pharm. Sci. Technol. Today 3 (2000) 318-326.

[18] Kalia, Y. N., Naik, A., Garrison, J., Guy, R. H. Iontophoretic drug delivery. Adv. Drug Deliv. Rev. 56 (2004) 619-658.

[19] Zempsky, W. T., Sullivan, J., Paulson, D. M., Heath, S. B. Evaluation of a low-dose lidocaine iontophoresis system for topical anaesthesia in adults and children: A randomized, controlled trial. Clin. Ther. 26 (2004) 1110-1119.

[20] Viscusi, E. R., Reynolds, L., Tait, S., Melson, T., Atkinson, L. E. An iontophoretic fentanyl patient-activated analgesic delivery system for postoperative pain: a double-blind, placebo-controlled trial. Anesth. Analg. 102 (2006) 188-194.

[21] Phipps J. B., Padmanabhan R. V., Lattin G.A. Iontophoretic delivery of model inorganic and drug ions. J. Pharm. Sci. 78 (1989) 365-369.

[22] Phipps, J. B., Gyory, J. R. Transdermal Ion Migration. Adv. Drug Deliv. Rev. 9 (1992) 137-176.

Chapter 1

Clinical applications of transdermal iontophoresis

Dhaval R. Kalaria, Sachin Dubey and Yogeshvar N. Kalia

School of Pharmaceutical Sciences,
University of Geneva & University of Lausanne,
30 Quai Ernest Ansermet,
1211 Geneva, Switzerland

Transdermal and Topical Drug Delivery: Principles and Practice, First Edition.
Edited by Heather A.E. Benson, Adam C. Watkinson.

The "how" and "why" of iontophoresis

Transdermal iontophoresis involves the application of a small electric potential to facilitate the transport of polar and charged hydrosoluble permeants across the skin and it has been successfully used to enhance the delivery of low molecular weight therapeutics, peptides and proteins.[1-3] The first reports describing the use of an electric current to deliver medicinal agents into the body date back to Pivati in 1747.[4] During the 18th and 19th centuries, Rossi, Palaprat, Wagner, and Morton tried to deliver various molecules using electric currents.[5] At the turn of the 20th century, Le Duc confirmed that strychnine could be driven across skin with the aid of an electric current.[6]

In addition to expanding the range of therapeutics that can be administered transdermally,[7] the key advantage of iontophoresis is that modulation of the applied current enables precise control over the rate and profile of drug delivery.[8] Thus, it is possible to achieve complex delivery kinetics, e.g., pulsatile or on-demand bolus inputs that otherwise require the use of an infusion pump. Drug input can also be titrated – e.g., in therapies that require a gradual "ramping" of the dose – and the clinician can provide individualized therapy by re-programming the device. Despite the numerous reports describing iontophoretic drug delivery *in vitro* and *in vivo* either in animals or in humans, pre-filled iontophoretic systems have only become available in the last few years. This can be attributed to advances made on three fronts: (i) progress in microelectronics and engineering processes that has enabled the development of miniaturized and cost-effective delivery systems[9]; therefore, iontophoretic systems can no longer be considered as cumbersome machines but as portable user-friendly devices readily capable of replacing more invasive systems; (ii) patient compliance and the financial success of passive transdermal patches stimulating the pharmaceutical industry to look more closely at the transdermal route; and (iii) rational drug design and recombinant DNA technology yielding increasing numbers of therapeutically important peptides and proteins where iontophoresis can provide a method for their controlled non-invasive delivery.

An iontophoretic system comprises a microprocessor, a power source and two electrode compartments – anodal and cathodal (Figure 1). The drug formulation is placed in the donor compartment based on the net charge of the therapeutic agent; for example, a cationic drug is

placed in the anodal compartment. Once the current is applied, the ions migrate out from the device and into the skin under the influence of the electric field. The electrical circuit is completed by the movement of endogenous counter-ions, primarily chloride and sodium ions, moving out from the skin and into the anodal and cathodal chambers, respectively.

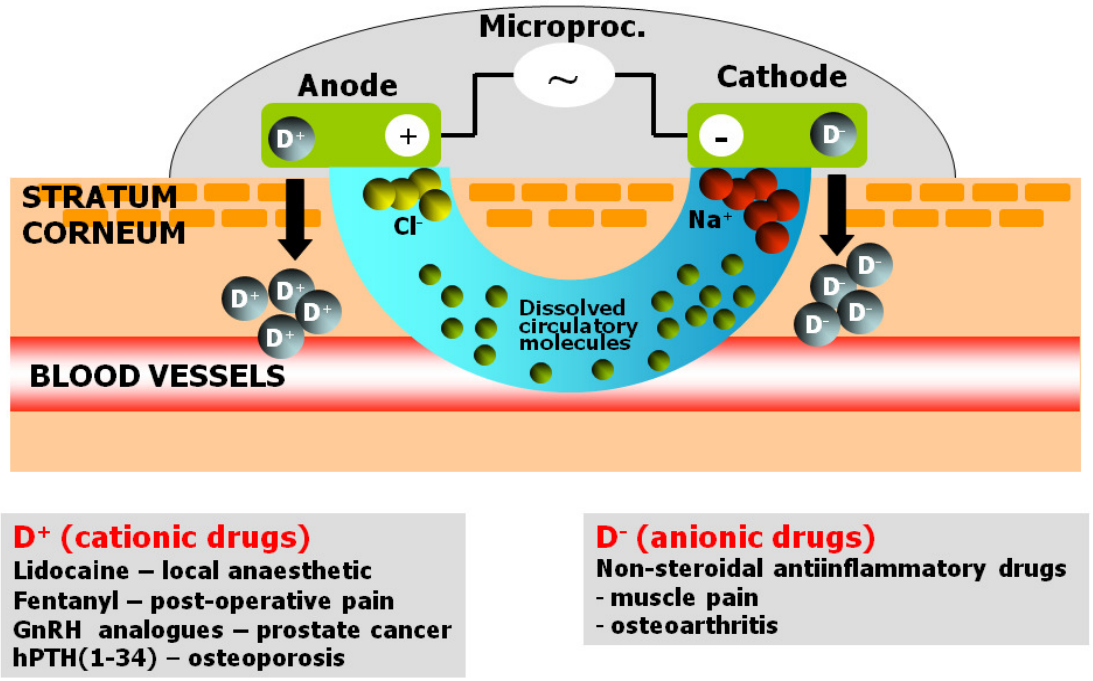

Figure 1. A schematic representation of an iontophoretic patch system. At the heart of the system is a microprocessor that controls device function and drug delivery. The patch contains active and return electrode compartments.

In addition to the duration and intensity of current application, other formulation conditions also impact upon drug delivery[2] – these include: (i) drug content which will influence drug concentration in the skin; (ii) the pH, which determines the degree of drug ionization; and (iii) the patch application area, which can be tailored as per clinical needs. Here, we provide a brief review of preliminary clinical studies that describe promising clinical applications of iontophoresis.

Topical application: using iontophoresis to increase local bioavailability

Anaesthetics – providing fast onset of action

Lidocaine, when delivered parenterally, is a fast-acting effective anaesthetic; however, the injection can be painful. For some patients, the pain and fear associated with injection reduces the likelihood that they will seek medical care, pursue diagnostic testing, receive appropriate immunization or parenteral medications.[10] In children, needlesticks can arouse more fear than major surgeries and other more invasive procedures.[11] Topical formulations such as EMLA® cream (AstraZeneca, Wilmington, DE), a eutectic mixture of lidocaine and prilocaine) have been used to provide local anaesthesia; however, they suffer from a slow onset of action (1-2 h) and the shallow depth of anaesthesia achieved (~3-5 mm).[12] These failings led to the investigation and development of fast acting iontophoretic systems for topical lidocaine delivery.

Several clinical trials have shown the efficacy of lidocaine iontophoresis in dermal anaesthesia.[13-17] Two studies suggested that lidocaine iontophoresis was superior to eutectic lidocaine and prilocaine cream for topical anaesthesia before IV cannulation.[18,19] All of the above studies used electrodes from commercial suppliers such as Iomed Inc (Salt Lake City, Utah) and Dupel® Iontophoresis System (Empi Co, St Paul, Minnesota). Treatment was initiated with a current of 1.0 mA and gradually increased to a maximum of 4.0 mA as tolerated by the subject; the total amount of charge delivered was 20, 30 or 40 mA.min.

These first generation iontophoretic devices were less convenient as they were neither pre-filled with drug nor pre-programmed and required a higher iontophoretic dose than necessary for effective topical anaesthesia, thereby increasing the risk of adverse events.[20] The LidoSite™ Topical System (Lidocaine Topical Anaesthetic System) developed by Vyteris, Inc. (Fair Lawn, NJ) and approved by the US FDA in 2005 is a small, easy-to-use, pre-programmed iontophoretic lidocaine delivery system composed of a drug-filled patch connected to a controller (Figure 2). The patch is a single use disposable drug product, which contains a 5 cm^2 circular drug reservoir (anode) that delivers lidocaine and epinephrine to the skin, and a 2.5 cm^2 oval return reservoir (cathode) containing electrolytes. The controller can be reused up to 100 times and applies a current of 1.77 mA for 10 min (i.e., 17.7 mA.min). It is designed to achieve local anaesthesia

before medical interventions such as insertion of IV catheters, needlesticks for blood withdrawal and other dermatological applications.

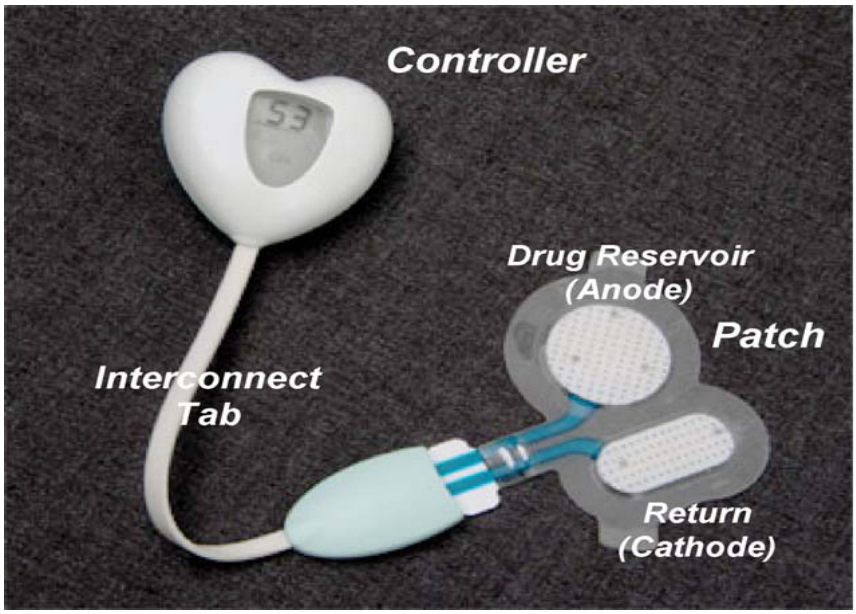

Figure 2. The LidoSite topical lidocaine delivery system comprises a reusable controller and single - use disposable patches.

Phase I clinical studies showed that 10 min of iontophoresis was sufficient to anaesthetise the skin to a depth of at least 6 mm (often 10 mm or more), which is more than adequate for needlesticks and dermatological procedures. Neither lidocaine nor epinephrine was detected in the systemic circulation. Phase II studies demonstrated the suitability of the device for paediatric patients requiring venipuncture, while Phase III clinical studies established that patients (adults and children) receiving lidocaine from the LidoSite™ system reported significantly less pain upon venipuncture or IV cannulation than the corresponding control subjects.[2,21] Furthermore, adult and paediatric patients treated with LidoSite™ experienced little or no pain during surgical procedures, such as incisional or excisional treatment of superficial skin lesions.

Pain management and delivery of nonsteroidal anti-inflammatory agents – targeted pain relief to reduce the risk of systemic side-effects

Transdermal delivery of NSAIDs is of considerable interest since it reduces the risk of GI-related side effects commonly encountered when these agents are administered orally. In addition to

minimising systemic exposure, it also enables targeted delivery and allows high local concentrations to be achieved. In a double blind study, efficacy and tolerability of pirprofen and ''lysine soluble aspirin'' (lysine acetylsalicylate) were delivered by iontophoresis to 80 patients suffering from a variety of rheumatic conditions. Treatment lasted two weeks with five administrations a week each lasting 20 minutes (direct current mean intensity, 2-3 mA). After five applications, patients showed significant improvement in pain at rest and during movement; there were no significant differences between pirprofen and aspirin. Final results were good or excellent in ~75% of the patients treated and functional improvement was satisfactory in about 80%. Furthermore, only local penetration of the drug in the inflamed area was noted without high systemic levels.[22]

Ketoprofen[23] and ketorolac[24] have also been successfully delivered by iontophoresis to human volunteers; the latter was reported to be efficient in treating pain due to rheumatic disease. Ketoprofen was delivered using Dupel® iontophoretic system with a current of 4 mA for 40 min; ketorolac was delivered using silver electrodes with a current of 2 mA for five treatment sessions with 20 min every day. Diclofenac iontophoresis has also been used clinically in patients suffering from arthritis and epicondylitis.[25] They received twenty treatments of 30 min duration with a current intensity 4-8 mA; however, several other studies have reported side-effects including a systemic adverse reaction[26] and allergic contact dermatitis.[27] Cutaneous bioavailability of piroxicam following passive and iontophoretic delivery from a commercially-available gel formulation was compared in healthy volunteers.[28] Cathodal iontophoresis was employed using silver electrodes with a current of 0.3 mA/cm^2 for 125 min. Quantification of drug levels in the stratum corneum revealed that the amount of piroxicam delivered via passive and iontophoresis was 5.4 ± 2.0 and 48.6 ± 18.8 µg/cm^2, respectively.

Iontophoresis has also been used to deliver dexamethasone in 25 patients (double blind study) suffering from Achilles tendon injury.[29] Patients received four 20 minute treatments at intervals of 3-4 days using iontophoresis in a 2 week period and were evaluated before treatment and at a series of time-points post-treatment (after 2 and 6 weeks, 3 and 6 months and 1 year). Several significant improvements in terms of physical activity were noticed in the treatment group compared to the control group. Nirschl *et al*., conducted a double blind placebo-controlled study

into the iontophoretic delivery of dexamethasone sodium phosphate in 199 patients suffering from acute epicondylitis.[30] Each patient received 40 mA.min of either the active or placebo treatment on six occasions. Patients received current up to 4.0 mA, depending on their sensitivity and once the preset dose of 40 mA.min was delivered, the current automatically ramped down to 0 mA. Iontophoretic treatment was well tolerated by most patients and was effective in reducing epicondylitis symptoms at short-term follow-up.

Dermatological applications – improving local bioavailability

Following idoxuridine iontophoresis into 14 recurrent herpes labialis lesions in six patients, the subjects reported immediate relief from discomfort and swelling, rapid appearance and coalescence of vesicles, minimal or no spread of the lesions, and accelerated healing with minimal or no scab formation.[31]

In a recent study iontophoretic application of 5% aciclovir cream was tested in a multicentre, placebo-controlled trial, for the episodic treatment of herpes labialis among 200 patients with an incipient cold sore outbreak at the erythema or papular/edema lesion stage.[32] The study was performed with a portable, hand-held, iontophoretic device with treatment for 20 min. The median classic lesion healing time was shortened by 35 h in the active treatment group with respect to the control (113 h vs. 148 h). Furthermore, in the subgroup of patients that presented lesions in the erythema stage, the median classic lesion healing time was shortened by up to 3 days for the aciclovir group, compared with the control group (49 h vs. 120 h). In addition, it was reported that the aciclovir treated group tended to have more aborted lesions than the control group (46% vs. 24%). It was concluded that single-dose topical iontophoresis of aciclovir was a convenient and effective treatment for cold sores.

In a double-blind, placebo-controlled clinical study, Gangarosa *et al*., compared iontophoresis of vidarabine monophosphate (ara-AMP) and aciclovir for efficacy against herpes orolabialis.[33] A group of 27 human volunteers with vesicular orolabial herpes were divided into three equal subgroups that received either vidarabine monophosphate (Ara-AMP) or aciclovir or NaCl. Results showed that Ara-AMP-treated lesions yielded lower viral titers after 24 h compared with lesions treated with NaCl or aciclovir. There was also a significant decrease in the duration of

virus shedding and the time to dry crust in the Ara-AMP treated group as compared to the two other groups.

Twenty-six patients with biopsy-proven Bowen's disease received eight iontophoretic treatments of 5-fluorouracil (5-FU) over a period of 4 weeks.[34] A commercially available portable iontophoretic device, Phoresor II (Iomed Inc, Salt lake City, Utah), was used with a treatment regimen of 4 mA for 10 min twice a week for 4 weeks. Three months after the last treatment, local excisions were done and in the treated group only one patient out of twenty six displayed any histologic evidence of bowenoid changes – thus, proving the efficacy of the treatment.[34] However, a case report described a cutaneous allergic reaction upon 5-FU iontophoresis, although the conclusion was derived from only one patient.[35]

Aminolevulinic acid (ALA) is a precursor of the endogenous fluorescent photosensitizer protoporphyrin IX (PpIX) which is used in the treatment of a range of cancers.[36] However, the therapeutic potential of this molecule is limited by its high polarity; simple cream formulations require several hours of application in order to penetrate into the skin.[37] Rhodes *et al*., studied ALA pharmacokinetics following iontophoretic delivery of a 2% ALA solution in the upper inner arm of healthy volunteers. Using the Phoresor II system, an iontophoretic current of 0.2 mA was applied on a circular surface of 1 cm diameter and its permeation quantified by measurement of PpIX fluorescence and phototoxicity. Studies revealed that ALA delivery was sufficient to induce tumor necrosis.[37] Gerscher *et al*., used the same conditions to compare the pharmacokinetics and phototoxicity from ALA as well as two ester derivatives in healthy human volunteers; it was reported that ALA-n-hexylester iontophoresis resulted in greater PpIX formation and lower phototoxicity relative to the other ester (ALA-n-butyl) and the parent molecule. A linear correlation between the logarithm of prodrug dose and PpIX fluorescence was observed for the three compounds[38]; a similar relationship was also observed with ALA-n-pentyl ester.[39]

Cisplatin has been iontophoresed into basal and squamous cell carcinomas (BCC/SCC).[40-42] Chang *et al*. studied 15 BCC or SCC lesions in 12 patients; 1 mg/ml of cisplatin was applied at a current of 0.5-1.0 mA for a period of 20-30 min on a lesion area of 2.9 cm x 2.0 cm. The

response was good, as 11 out of the 15 lesions showed either a complete or a 50% decrease in lesion area after iontophoresis.[40] Subsequently, this protocol was successfully applied (four cycles) to a 67-year old man with BCC.[42] Iontophoretic delivery of cisplatin also produced partial remission when applied to patients with BCC or SCC lesions on the eyelids and periorbital tissues.[41]

Recalcitrant psoriasis in a 46-year-old male with well-defined bilateral psoriatic plaques on the palms was treated by methotrexate iontophoresis (0.6 mA/cm^2 for 15 min) with aluminum foil electrodes supported by an adhesive polyethylene sheet; treatment was performed once a week for a total of 4 weeks.[43] It was suggested that the lesion on the right palm, treated with topical methotrexate iontophoresis, showed >75% improvement by the end of 4 weeks (the left palm lesion served as a control and did not receive any treatment).

Iontophoretic delivery of 1% vinblastine solution at 4 mA for 10-90 min was used to treat patients with Kaposi's sarcoma[44]; all thirty-one lesions treated showed partial to complete clearing and symptomatic improvement.

Diagnostic application

The diagnosis of cystic fibrosis by pilocarpine iontophoresis was one of the earliest clinical applications of this technology.[45] Cystic fibrosis is a hereditary systemic disorder of the mucus-producing exocrine glands that affects the pancreas, bronchi, intestine, and liver. The perspiration contains an abnormal concentration of sodium and chloride ions[46] and assay of the latter is the basis for the diagnostic test.[47] The collection of sweat for diagnostic purposes is facilitated by the iontophoretic delivery of pilocarpine, a small positively charged cholinergic agent that induces sweating. The diagnostic test was first introduced by Gibson and Cooke and received FDA approval in 1983 and several commercial iontophoretic systems for the diagnosis of cystic fibrosis have been developed[48,49] (CF Indicator®; Scandipharm, Birmingham, Alabama, Webster Sweat Inducer; Wescor Inc., Logan, Utah). It has since become a standard screening test and is commonly used by paediatricians.[50]

Systemic applications

Opioids – using iontophoresis to provide fast-acting systemic pain relief

Several opioid analgesics are good candidates for iontophoresis from both physicochemical and pharmacological standpoints. They are usually ionised at physiological pH, possess moderate molecular weight (<500 Da) and are frequently highly potent. These characteristics when combined with the ability of iontophoresis to provide fast controlled input kinetics make a compelling argument for the development of iontophoretic systems for relief from acute pain.

An early study investigated the efficacy of morphine iontophoresis in a group of post-surgery patients initially placed on IV meperidine; they were divided into two subgroups, one of which received iontophoretic morphine for a period of 6 h at the current required to deliver an equianalgesic dose of meperidine while the control group received buffer.[51] The patient controlled anaesthesia (PCA) option remained available to both sets of patients and the results demonstrated that the iontophoretic group made fewer requests for PCA than the control group. Minimally effective concentrations (~20 ng/ml) were achieved in the blood within 30 min of commencing iontophoresis and levels capable of providing consistent pain relief (~40 ng/ml) were achieved during current application. Patients in the iontophoretic group displayed a red wheal and flare under and around the anodal compartment that was attributed to local histamine release provoked by morphine.

Fentanyl is one of the most widely studied opioids when it comes to transdermal iontophoresis. In addition to its physicochemical properties, it is extremely potent – between 100- to 500-fold superior to morphine depending on the assay; moreover, it does not induce histamine release. Its physicochemical and pharmacological properties together with its pharmacokinetics – short half life, high first pass effect makes it an ideal candidate for transdermal administration.[52] Although passive transdermal fentanyl patches have been marketed for nearly 20 years for the treatment of chronic pain, they cannot provide a rapid bolus drug input for relief from acute pain.[53] The feasibility of using iontophoresis to deliver fentanyl was demonstrated *in vitro* and *in vivo*[54-56] and led to the development of the Ionsys™ system (using E-TRANS® electrotransport technology; Alza Corporation, Mountain View, CA) – a pre-programmed, self-contained, on-demand drug delivery system that is activated by the patient and can deliver 80 doses of 40 µg of

fentanyl in a 24 h period.[9] Figures 3 and 4 show a photograph and an exploded view, respectively, of the E-TRANS® fentanyl system. The system is composed of two primary components; the upper component houses the battery and electronic hardware responsible for monitoring the system. The lower component is composed of two hydrogel reservoirs – the anode containing active fentanyl hydrochloride. The other hydrogel reservoir (cathode) contains only inactive substances. The system is held in place by a polyisobutylene skin adhesive.[57]

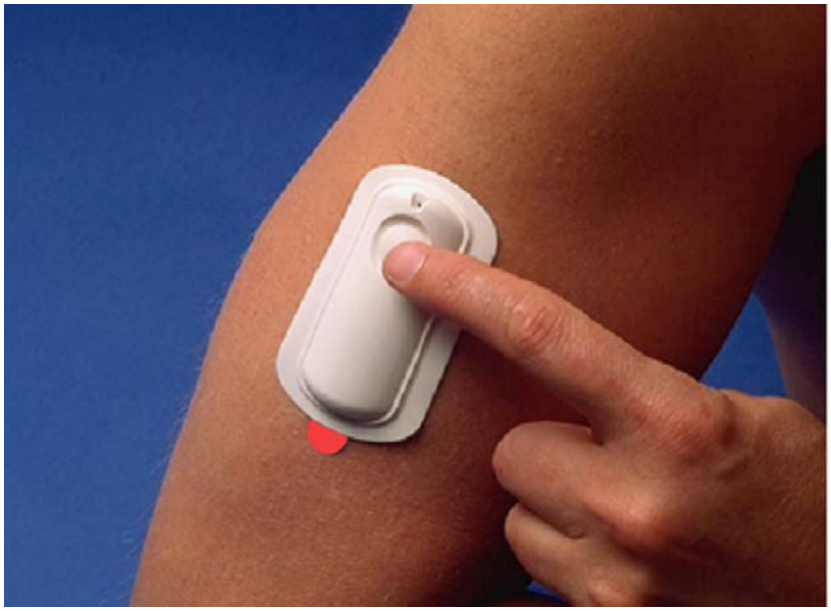

Figure 3. The fully integrated fentanyl ITS can be applied to the patient's upper arm and drug delivery initiated using the controller button.

Based on pharmacokinetic studies, a current of 170 µA was selected to deliver each 40 µg dose over 10 min.[58,59] The maximum number of 80 doses was shown to be sufficient to achieve effective analgesia and if a patient required additional analgesia, a new system could be applied to a different skin site. The size, shape, and materials of the system allowed the patient comfortable, unrestricted movement during wear (typically on the upper arm and the chest). In addition to the fundamental electronic design parameters of current intensity and duration and the number of doses allowed per system, other important safety and patient feedback features are included in the system design.[9] Clinical studies showed that the Ionsys™ system was well tolerated by patients suffering postoperative pain and was equivalent to an intravenous morphine pump demonstrating the importance of this device in medical care.[60-64] Viscusi *et al.*,compared

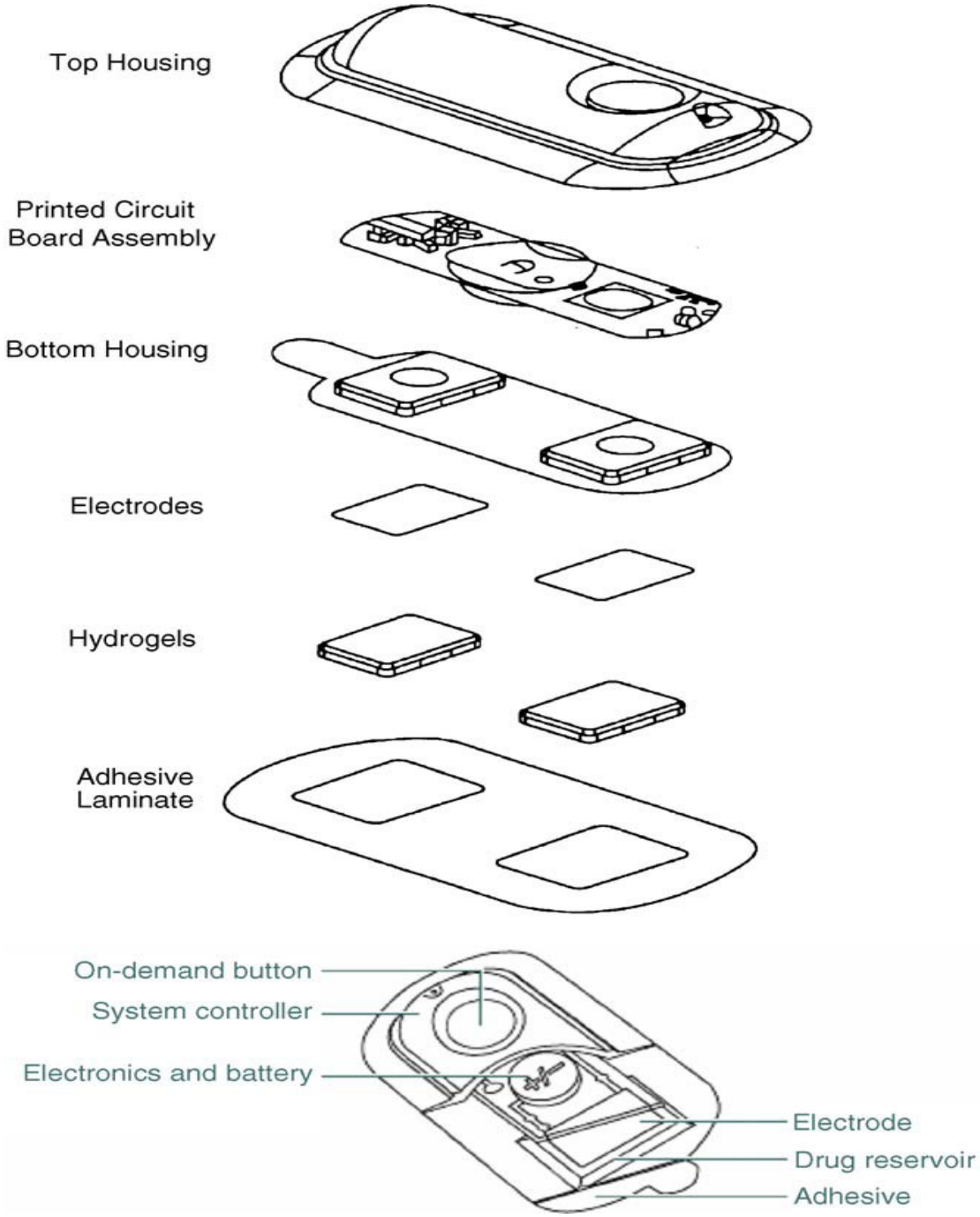

Figure 4. A detailed view inside the E - TRANS iontophoretic drug delivery system showing the major components: top housing, printed circuit board assembly that forms the controller, a bottom housing containing reservoirs for placement of electrodes and hydrogels, and an adhesive laminate. The E - TRANS technology was used to develop the Ionsys™ fentanyl.

the fentanyl iontophoretic transdermal system (ITS) with placebo in postoperative pain management among 484 patients. Supplemental IV fentanyl was available to patients upon request in both treatment groups for the first 3 hours after enrolment. The main efficacy endpoint was the patient global assessment (PGA) of the method of pain control; fewer patients receiving ITS discontinued because of inadequate analgesia compared with placebo and it was concluded that ITS was an excellent method of pain control.[60] In another multicentre study in 504 patients, the ITS (40 µg fentanyl [10-minute infusion/lockout], up to 6 doses/h) was compared with intravenous patient-controlled analgesia (IV PCA) with morphine (1 mg morphine bolus [5-minute lockout], up to 10 mg/h) for pain management following abdominal or pelvic surgery – PGA scores were used to evaluate efficacy. Results demonstrated that the fentanyl ITS and morphine IV PCA were comparable methods of pain control following abdominal or pelvic surgery; however, the fentanyl ITS was rated superior to morphine IV PCA for ease of care by patients and nurses. Overall discontinuation rates were not significantly different between groups and commonly occurring adverse events were similar between groups.[61] Ahmad *et al*., compared the efficacy and safety of the fentanyl ITS with morphine IV PCA for pain management following gynaecologic surgery – PGA success ratings were statistically equivalent between the 2 groups.[62] Pain intensity at 3 h, discontinuations due to inadequate analgesia, and the percentage of patients requesting supplemental opioids in the first 3 h were similar. Hartrick *et al*., investigated the efficacy of the fentanyl ITS and morphine IV PCA for acute pain management in patients after orthopaedic surgery.[63] PGA ratings and pain intensity scores in the first 24 h were statistically equivalent and adverse events were similar in both the groups.

Antimigraine drugs

The pharmacokinetics of alniditan, a novel $5HT_{1D}$ agonist for the treatment of migraine were studied in healthy volunteers following anodal iontophoresis using 10 cm^2 hydrophilic polyurethane foam patches containing of 0.5 mg drug.[65] A current of 0.2 mA/cm^2 was applied for two consecutive 30 min periods (separated by a 90 min interval) and patches were removed 90 min after the end of the second current application period. The mean plasma concentrations at 30 and 150 min were 4.49 and 5.37 ng/ml respectively, and were at the lower end of the

therapeutic range (5-20 ng/ml). Moreover, the plasma concentration achieved after 30 min of iontophoretic delivery was equivalent to simulated subcutaneous administration of 0.5 mg dose.

Siegel *et al*., investigated sumatriptan iontophoresis in healthy volunteers[66]; of the 6 treatment groups, two received oral sumatriptan (50 mg) and 6 mg subcutaneous injection, respectively. The remaining iontophoretic treatment groups (10 cm^2 patches) received (i) 1.0 mA current, 1.5 h dose of 1.5 mg (treatment 3) (ii) 0.5 mA current, 3 h dose of 1.5 mg (treatment 4) (iii) two patches of 1.0 mA, 3 h dose of 6 mg (treatment 5) and (iv) two patches of 1.0 mA, 6 h dose of 12 mg sumatriptan (treatment 6). The $AUC_{0–24}$ for treatments 3 and 4 were ~19% of the oral and 26% of the injection; C_{max} was 31% of oral and 14% of injection for Treatment 3 and 20% of oral and 9% of injection for Treatment 4. Treatment 5 yielded an $AUC_{0–24}$ value, which was approximately 88% of the 50 mg oral preparation and 122% of the 6 mg injection. Treatment 6 yielded an $AUC_{0–24}$ that was approximately 187% of the 50 mg oral preparation and 259% of the 6 mg injection; C_{max} was 109% of oral and 49% of injection for Treatment 5 and 131% of oral and 59% of the injection for Treatment 6. Treatments 5 and 6 maintained sumatriptan levels above 10 ng/ml for 4 and 7 h respectively, as compared to approximately 3 h for oral and 1.5 h for injectable. Thus, transdermal iontophoresis was capable of maintaining therapeutic sumatriptan levels for four times longer than the 6.0 mg injection and twice as long as the 50 mg oral preparation, offering substantially longer duration of treatment than either preparation. The T_{max} for oral and injection formulations was 1.31 and 0.28 h; while the maximum serum concentration was reached in approximately 1.5 h for all patch formulations and was sustained until patch removal. Although this was comparable to oral administration, the iontophoretic system should ideally approach the fast onset of the subcutaneous injection.

Neurodegenerative drugs

Kankkunen *et al*. investigated the iontophoretic delivery of a reversible acetylcholinesterase inhibitor, tacrine in healthy adult volunteers.[67] They performed two experiments, the first using commercially available Iogel® electrodes (Chattanooga Group, Chattanooga, TN), while in the second, a novel two compartment electrode system was employed in which the drug reservoir was separated from the electrode by a membrane to maximize the transport efficiency by avoiding competition from other ions. A 0.4 mA/cm^2 current was applied for 3 h using patches

with an active surface area of 10 cm^2. The tacrine plasma concentrations measured after iontophoresis using the "in-house" electrodes (14.9 ± 2.6 ng/ml) compared favourably with those achieved with the Iogel® electrodes (21.3 ± 5.9 ng/ml). Both values lie within the range of blood levels seen following oral administration of tacrine.

Van der Geest *et al*. iontophoresed R-apomorphine, a potent dopamine agonist, in patients with idiopathic Parkinson's disease.[68,69] Two different current intensities of 0.25 and 0.375 mA/cm^2 were applied for 1 h using patches having a surface area of 10 cm^2. Although measurable plasma apomorphine concentrations of 1.3 ± 0.6 and 2.5 ± 0.7 ng /ml, at 0.25 and 0.375 mA/cm^2, respectively, were achieved, these levels were sub-therapeutic. Furthermore, qualitative clinical improvement could only be confirmed in one patient treated with the higher current density; however, the study was not blinded so a placebo effect cannot be excluded.

Li *et al*. combined transdermal iontophoretic delivery of R-apomorphine with surfactant pre-treatment in patients with advanced Parkinson's disease.[70] Iontophoretic patches were applied in 16 patients for 3.5 h, with 0.5 h of passive delivery followed by 3 h of current application at a current density of 0.25 mA/cm^2. Eight patients were treated with a surfactant formulation consisting of laureth-3 ethyloxylene ether, laureth-7 ethyloxylene ether and sodium sulfosuccinate (in a molar ratio of 0.7:0.3:0.05 respectively) with a concentration of 5% w/w prior to iontophoresis. The surfactant formulation (20 $\mu l/cm^2$) was applied non-occlusively at the anode site on the dorsal forearm of patients for 1 h before patch placement. The patients treated with the surfactant formulations showed a higher bioavailability (BA) and steady state input rate compared to the control group (patients receiving iontophoresis without surfactant); BA – 13.2 ± 1.4 and 10.6 ± 0.8%, respectively and flux 98.3 ± 12.1 and 75.3 ± 6.6 $nmol/cm^2$ h, respectively. Clinical improvement was observed in five out of eight patients in the study group and in three out of eight patients in the control group. No clinically relevant systemic adverse effects were observed.

Antiemetics

Cormier *et al*., investigated metoclopramide iontophoresis in the presence and absence of hydrocortisone in humans in order to determine whether co-delivery of hydrocortisone was

effective in inhibiting local skin reactions.[71] Each volunteer was subjected to two identical treatments (metoclopramide alone and in combination with hydrocortisone) one after the other with a wash-out period of 1 week. A current of 500 μA was used for all the studies. There was no statistically significant difference in AUC, plasma concentration and half life of metoclopramide with or without hydrocortisone. A steady state flux of ~100 μg/cm^2 h was achieved after 1 h transport. Furthermore, hydrocortisone iontophoresis was successful in suppressing local site reactions.

Peptides and proteins

Peptides and proteins are generally inactive orally because of their susceptibility to chemical and enzymatic degradation in the GI tract. They are usually potent and can have complex secretion profiles in the body (for example, the variation in basal and post-prandial insulin levels); an ideal delivery system should be able to provide controlled drug inputs as required. In addition to being ideally suited to the delivery of polar and charged molecules with good aqueous solubility, transdermal iontophoresis permits tight control over drug transport rates and enables complex input kinetics to be used. It follows that there have been several reports into the iontophoretic delivery of peptide hormones including luteinizing hormone releasing hormone,[72,73] calcitonin,[74,75] growth hormone releasing hormone,[76] human parathyroid hormone,[77] insulin[78,79] using different iontophoretic systems.

Investigation into the effect of formulation parameters on the iontophoretic delivery of leuprolide, an LHRH superagonist, in human volunteers showed that steady state serum concentrations could be achieved within 30 min; anodal delivery from a 10 mg/ml formulation in acetate buffer using a current of 0.2 mA was able to reach mean steady state serum concentration of 0.8 ng/ml.[80] An earlier double-blind, randomized, crossover study in 13 healthy men investigating leuprolide iontophoresis (5 mg; 0.2 mA, 70 cm^2) showed that the patches, though large, were well tolerated and LH concentration was increased from a baseline of 11.3 ± 3.1 mIU/ml to 56.4 ± 49.6 mIU/ml at 4 hours.[81] Another study compared LH pharmacodynamics after iontophoretic delivery with subcutaneous injection in a group of 18 human volunteers.[82] The applied dose was kept constant at 5 mg/ml, and using a current of 0.22 μA it was observed that the time to first response was shorter for subcutaneous injection (73 ± 74 min and 147 ± 108

min, respectively) and the AUC for the first 150 min was greater for subcutaneous delivery (3655 ± 2246 and 8666 ± 4067 mIU min/ml, respectively). No major adverse effects were observed at the application site following iontophoresis; thus it might be possible to increase the current intensity in order to reduce the lag time.

A cross-over study comparing IM bolus, 6 h IV infusion and 6 h iontophoretic delivery (200 $\mu A/cm^2$) of a calcitonin analogue (MW ~3 kDa) was performed in healthy human volunteers.[83] The plasma levels observed following iontophoresis closely mimicked those seen after IM injection with similar AUC and inter-individual variability. On termination of the current at 6 h, a fairly rapid decline in the plasma levels was observed. After 6 h, the skin sites were observed for any topical effects, which suggested a slight pink coloration on skin that eventually disappeared after 24 h.

Conclusion

The results to-date demonstrate that iontophoresis is a drug delivery platform that has been used to administer a variety of therapeutic agents with many different clinical applications. Moreover, it is the only transdermal delivery technology that has managed to produce FDA approved products – although both systems (LidoSite™ and Ionsys™) contain low molecular weight therapeutics, the technique is uniquely suited to the delivery of peptides and proteins. Physicochemical properties and drug pharmacokinetics obviously put a limit on the number of drug candidates that can be delivered by transdermal iontophoresis. In the most favorable conditions (for compounds with low molecular weight and multiple charge) the maximum amount of drug that can be delivered per day from a reasonably sized patch will probably be in the range of 20-30 mg. However, technical feasibility alone cannot drive a molecule to the market – drug candidates have to address an unmet clinical need. Furthermore several issues including cost of therapy and the risk of skin irritation may also limit potential applications. Nevertheless, transdermal iontophoresis is a promising technique that requires a greater focus on research directed towards formulation development in an effort to design efficient iontophoretic patch systems, particularly with a view to the delivery of biotechnology-derived therapeutics. Stability of the drug along with other patch components for periods up to 18 months will be critical as well as challenging. The delivery of peptides and proteins, which are susceptible to

degradation in aqueous solution, may require the development of dry patches where the biomolecule is hydrated immediately prior to use.[84-88] Thus, the development of future iontophoretic systems will require a multidisciplinary effort from fields such as pharmaceutics, material sciences and electrochemistry in order to take a promising candidate from bench to bedside.

REFERENCES

1. Licht S. History of electrotherapy. In: Stilwell GK, ed. Therapeutic electricity and ultraviolet radiation. 3rd ed. Baltimore: Williams & Witkins, 1983:1-64.
2. Kalia YN, Naik A, Garrison J, Guy RH. Iontophoretic drug delivery. Adv Drug Deliv Rev 2004;56:619-58.
3. Cázares-Delgadillo J, Naik A, Ganem-Rondero A, Quintanar-Guerrero D, Kalia, YN. Transdermal delivery of cytochrome C - A 12.4 kDa protein - across intact skin by constant-current iontophoresis. Pharm Res 2007;24:1360-8.
4. Watkins AL, A manual of electrotherapy. 2nd ed. Philadelphia: Lea and Febiger, 1968.
5. Banga AK. Percutaneous absorption and its enhancement. In: Banga AK, ed. Electrically assisted transdermal and topical drug delivery. Taylor & Francis, Bristol, PA, 1998:1-12.
6. Le Duc S. Electric ions and their use in medicine. Liverpool: Rebman, 1908.
7. Abla N, Naik A, Guy RH, Kalia YN. Iontophoresis: Clinical applications and future challenges. In: Smith EW, Maibach HI, eds. Percutaneous penetration enhancers. 2nd ed. Bristol PA: Taylor & Francis, 2005:177-219.
8. Naik A, Kalia YN, Guy RH. Transdermal drug delivery: overcoming the skin's barrier function. Pharm Sci Technol Today 2000;3:318-26.
9. Subramony JA, Sharma A, Phipps JB. Microprocessor controlled transdermal drug delivery. Int J Pharm 2006;317:1-6.
10. Holmes HS. Choosing a local anesthetic. Dermatol Clin 1994;12:817-23.
11. Menke EM. School-aged children's perception of stress in the hospital. Child Health Care 1981;9:80-6.
12. Wahlgren CF, Quiding H. Depth of cutaneous analgesia after application of a eutectic mixture of the local anesthetics lidocaine and prilocaine (EMLA ceam). J Am Acad Dermatol 2000;42:584-8.

13. Zempsky WT, Parkinson TM. Lidocaine iontophoresis for topical anesthesia before dermatologic procedures in children: a randomized controlled trial. Pediatr Dermatol 2003;20:364-368.
14. Zempsky WT, Anand KJ, Sullivan KM, Fraser D, Cucina K. Lidocaine iontophoresis for topical anesthesia prior to intravenous line placement in children. J Pediatr 1998;32:1061–3.
15. Wallace MS, Ridgeway B, Jun E, Shulteis G, Rabussay D, Zhang L. Topical delivery of lidocaine in healthy volunteers by electroporation, electroincorporation, or iontophoresis: an evaluation of skin anesthesia. Reg Anesth Pain Med 2001;26:229-38.
16. Rose JB, Galinkin JL, Jantzen EC, Chiavacci RM. A study of lidocaine iontophoresis for pediatric venipuncture. Anesth Analg 2002;94:867-71.
17. Kim MK, Kini NM, Troshynski TJ, Hermes HM. A randomized clinical trial of dermal anesthesia by iontophoresis for peripheral intravenous catheter placement in children. Ann Emerg Med 1999;33:395-9.
18. Squire SJ, Kirchhoff KT, Hissong K. Comparing two methods of topical anesthesia used before intravenous cannulation in pediatric patients. J Pediatr Health Care 2000;14:68-72.
19. Miller KA, Balakrishnan G, Eichbauer G, Betley K. 1% lidocaine injection, EMLA cream, or "Numby Stuff" for topical analgesia associated with peripheral intravenous cannulation. AANA J 2001;69:185-7.
20. Zempsky WT, Ashburn MA. Iontophoresis: Noninvasive drug delivery. Am J Anesthesiology 1998;25:158-62.
21. Zempsky WT, Sullivan J, Paulson DM, Heath SB. Evaluation of a low-dose lidocaine iontophoresis system for topical anaesthesia in adults and children: A randomized, controlled trial. Clin Ther 2004;26:1110-9.
22. Garagiola U, Dacatra U, Braconaro F, Porretti E, Pisetti A, Azzolini V. Iontophoretic administration of pirprofen or lysine soluble aspirin in the treatment of rheumatic diseases. Clin Ther 1988;10:553-8.
23. Panus PC, Campbell J, Kulkarni SB, Herrick RT, Ravis WR, Banga AK. Transdermal iontophoretic delivery of ketoprofen through human cadaver skin and in humans. J Control Release 1997;44:113-21.

24. Saggini R, Zoppi M, Vecchiet F, Gatteschi L, Obletter G, Giamberardino MA. Comparison of electromotive drug administration with ketorolac or with placebo in patients with pain from rheumatic disease: a double-masked study. Clin Ther 1996;18:1169-74.
25. Vecchini L, Grossi E. Ionization with diclofenac sodium in rheumatic disorders: a double-blind placebo-controlled trial. J Int Med Res 1984;12:346-50.
26. Macchia L, Caiaffa MF, di Gioia R, Tursi A. Systemic adverse reaction to diclofenac administered by transdermal iontophoresis. Allergy 2004;59:367-8.
27. Foti C. Cassano N, Conserva A, Vena GA. Allergic contact dermatitis due to diclofenac applied with iontophoresis. Clin Exp Dermatol 2004;29:91.
28. Curdy C, Kalia YN, Naik A, Guy RH. Piroxicam delivery into human stratum corneum in vivo: iontophoresis versus passive diffusion. J Control Release 2001;76:73-9.
29. Neeter C, Thomee R, Silbernagel KG, Thomee P, Karlsson J. Iontophoresis with or without dexamethasone in the treatment of acute Achilles tendon pain. Scandinavian J Med Sci Sports 2003;13:376-82.
30. Nirschl RP, Rodin DM, Ochiai DH, Maartmann-Moe C. Iontophoretic administration of dexamethasone sodium phosphate for acute epicondylitis. Am J Sports Med 2003;31:189-95.
31. Gangarosa LP, Merchant HW, Park NH, Hill JM. Iontophoretic application of idoxuridine for recurrent herpes labialis: report of preliminary clinical trials. Methods Find Exp Clin Pharmacol 1979;1:105-9.
32. Morrel EM, Spruance S, Goldberg DI. Topical iontophoretic acyclovir cold sore study group, topical iontophoretic administration of acyclovir for the episodic treatment of herpes labialis: a randomized, double-blind, placebo-controlled clinic-initiated trial. Clin Infect Dis 2006;43:460-7.
33. Gangarosa LP, Hill JM, Thompson BL, Leggett C, Rissing JP. Iontophoresis of vidarabine monophosphate for herpes orolabialis. J Infect Dis 1986;154:930-4.
34. Welch ML, Grabski WJ, McCollough ML, et al. 5-fluorouracil iontophoretic therapy for Bowen's disease. J Am Acad Dermatol 1997;36:956-8.
35. Anderson LL, Welch ML, Grabski WJ. Allergic contact dermatitis and reactivation phenomenon from iontophoresis of 5-fluorouracil. J Am Acad Dermatol 1997;36:478-9.

36. Peng Q, Warloe T, Berg K, et al. 5-Aminolevulinic acid based photodynamic therapy. Cancer 1997;79:2282-308.
37. Rhodes LE, Tsoukas MM, Anderson RR, Kollias N. Iontophoretic delivery of ALA provides a quantitative model for ALA pharmacokinetics and PpIX phototoxicity in human skin. J Invest Dermatol 1997;108:87-91.
38. Gerscher S, Connelly JP, Griffiths J, et al. Comparison of the pharmacokinetics and phototoxicity of protoporphyrin IX metabolized from 5-aminolevulinic acid and two derivatives in human skin in vivo. Photochem Photobiol 2000;72:569-74.
39. Gerscher S, Connelly JP, Beijersbergen Van Henegouwen GM, MacRobert AJ, Watt P, Rhodes LE. A quantitative assessment of protoporphyrin IX metabolism and phototoxicity in human skin following dose-controlled delivery of the prodrugs 5-aminolaevulinic acid and 5-aminolaevulinic acid-n-pentylester. Br J Dermatol 2001;144:983-90.
40. Chang BK, Guthrie TH, Hayakawa K, Gangarosa LP. A pilot study of iontophoretic cisplatin chemotherapy of basal and squamous cell carcinomas of the skin. Arch Dermatol 1993;129:425-7.
41. Luxenberg MN, Guthrie TH. Chemotherapy of basal cell and squamous cell carcinoma of the eyelids and periorbital tissues. Ophthalmology 1986;93:504-10.
42. Bacro TR, Holladay EB, Stith MJ, Maize JC, Smith CM. Iontophoresis treatment of basal cell carcinoma with cisplatin: a case report. Cancer Detect Prev 2000;24:610-9.
43. Tiwari SB, Kumar BCR, Udupa N, Balachandran C. Topical methotrexate delivered by iontophoresis in the treatment of recalcitrant psoriasis — a case report. Int J Dermatol 2003;42:157-9.
44. Smith KJ, Konzelman JL, Lombardo FA, et al. Iontophoresis of vinblastine into normal skin and for treatment of Kaposi's sarcoma in human immunodeficiency virus-positive patients. Arch Dermatol 1992;128:1365-70.
45. Gangarosa S, Hill JM. Modern iontophoresis for local drug delivery. Int J Pharm 1995;123:159-71.
46. Huang YY, Wu SM, Wang CY, Jiang TS. Response surface method as an approach to optimization of iontophoretic transdermal delivery of pilocarpine. Int J Pharm 1996;129:41-50.

47. Gibson LE, Cooke RE. A test for the concentration of electrolytes in sweat in cystic fibrosis of the pancreas utilizing pilocarpine by iontophoresis. Pediatrics 1959;23:545-9.
48. Fogt EJ, Norenberg MS, Untereker DF, Coury AJ. Fluid absorbent quantitative test device. US patent 4,444,193, 1984.
49. Yeung WH, Palmer J, Schidlow D, Bye MR, Huang NN. Evaluation of a paper-patch test for sweat chloride determination. Clin Pediatr 1984;23:603-7.
50. Singh P, Maibach HI. Iontophoresis in drug delivery: basic principles and applications. Crit Rev Ther Drug Carrier Syst 1994;11:161-213.
51. Ashburn MA, Stephen RL, Ackerman E, et al. Iontophoretic delivery of morphine for postoperative analgesia. J Pain Symptom Manage 1992;7:27-33.
52. Chelly JE, Grass J, Houseman TW, Minkowitz H, Pue A. The safety and efficacy of a fentanyl patient-controlled transdermal system for acute postoperative analgesia: A multicenter, placebo-controlled trial. Anesth Analg 2004;98:427-33.
53. Scott ER, Phipps JB, Gyory JR, Padmanabhan RV. Electrotransport system for transdermal delivery. A practical implementation of iontophoresis. In: Wise DL, ed. Handbook of Pharmaceutical Controlled Release Technology. New York, NY: Marcel Dekker, 2000:617-59.
54. Thysman S, Tasset C, Préat V. Transdermal iontophoresis of fentanyl: delivery and mechanistic analysis. Int J Pharm 1994;101:105-13.
55. Thysman S., Préat V. In vivo iontophoresis of fentanyl and sufentanil in rats: Pharmacokinetics and acute antinociceptive effects. Anesth Analg 1993;77:61-6.
56. Ashburn MA, Streisand J, Zhang J, et al. The iontophoresis of fentanyl citrate in humans. Anesthesiology 1995;82:1146-53.
57. Hendron CM. Iontophoretic drug delivery system: focus on fentanyl. Pharmacotherapy 2007;27:745-54.
58. Gupta SK, Southam M, Sathyan G, Klausner M. Effect of current density on pharmacokinetics following continuous or intermittent input from a fentanyl electrotransport system. J Pharm Sci 1998;87:976-81.
59. Gupta SK, Sathyan G, Phipps JB, Klausner M, Southam M. Reproducible fentanyl doses delivered intermittently at different time intervals from an electrotransport system. J Pharm Sci 1999;88:835-41.

60. Viscusi ER, Reynolds L, Tait S, Melson T, Atkinson LE. An iontophoretic fentanyl patient-activated analgesic delivery system for postoperative pain: a double-blind, placebo-controlled trial. Anesth Analg 2006;102:188-94.
61. Minkowitz HS, Rathmell JP, Vallow S, Gargiulo K, Damaraju CV, Hewitt DJ. Efficacy and safety of the fentanyl iontophoretic transdermal system (ITS) and intravenous patient-controlled analgesia (IV PCA) with morphine for pain management following abdominal or pelvic surgery. Pain Med 2007;8: 657-68.
62. Ahmad S, Damaraju CV, Hewitt DJ. Fentanyl HCl iontophoretic transdermal system versus intravenous morphine pump after gynecologic surgery. Arch Gynecology Obstet 2007;276:251-8.
63. Hartrick CJ, Bourne MH, Gargiulo K, Damaraju CV, Vallow S, Hewitt DJ. Fentanyl iontophoretic transdermal system for acute-pain management after orthopedic surgery: a comparative study with morphine intravenous patient-controlled analgesia. Reg Anesth Pain Med 2006;31:546-54.
64. Viscusi ER, Reynolds L, Chung F, Atkinson LE, Khanna S. Patient-controlled transdermal fentanyl hydrochloride vs intravenous morphine pump for postoperative pain. J Am Med Assoc 2004;291:1333-41.
65. Jadoul A, Mesens J, Caers W, de Beukelaar F, Crabbe R, Preat V. Transdermal permeation of alniditan by iontophoresis: in vitro optimization and human pharmacokinetic data. Pharm Res 1996;13:1348-53.
66. Siegel SJ, Neill CO, Dubé ML, et al. Unique iontophoretic patch for optimal transdermal delivery of sumatriptan. Pharm Res 2006;24:1919-26.
67. Kankkunen T, Sulkava R, Vuorio M, Kontturi K, Hirvonen J. Transdermal iontophoresis of tacrine in vivo. Pharm Res 2002;19:704-8.
68. Van der Geest R, Danhof M, Boddé HE. Iontophoretic delivery of apomorphine: in vitro optimization and validation. Pharm Res 1997;14:1798-803.
69. Danhof M, Van der Geest R, Van Laar T, Bodde HE. An integrated pharmacokinetic–pharmacodynamic approach to optimization of R-apomorphine delivery in Parkinson's disease. Adv Drug Deliv Rev 1998;33:253-63.

70. Li GL, De Vries JJ, Van Steeg TJ, et al. Transdermal iontophoretic delivery of apomorphine in patients improved by surfactant formulation pretreatment. J Control Release 2005;101:199-208.
71. Cormier M, Chao ST, Gupta SK, Haak R. Effect of transdermal iontophoresis codelivery of hydrocortisone on metoclopramide pharmacokinetics and skin-induced reactions in human subjects. J Pharm Sci 1999;88:1030-5.
72. Heit MC, Williams PL, Jayes FL, Chang SK, Riviere JE. Transdermal iontophoretic peptide delivery: In vitro and in vivo studies with luteinizing hormone releasing hormone. J Pharm Sci 1993;82:240-3.
73. Raiman J, Koljonen M, Huikko K, Kostiainen R, Hirvonen J. Delivery and stability of LHRH and Nafarelin in human skin: the effect of constant/pulsed iontophoresis. Eur J Pharm Sci 2004;21:371-7.
74. Thysman S, Hanchard C, Preat V. Human calcitonin delivery in rats by iontophoresis. J Pharm Pharmacol 1994;46:725-30.
75. Morimoto K, Iwakura Y, Nakatani E, Miyazaki M, Tojima H. Effects of proteolytic enzyme inhibitors as absorption enhancers on the transdermal iontophoretic delivery of calcitonin in rats. J Pharm Pharmacol 1992;44:216-8.
76. Kumar S, Char H, Patel S, et al. In vivo transdermal iontophoretic delivery of growth hormone releasing factor GRF (1–44) in hairless guinea pigs. J Control Release 1992;18:213-20.
77. Suzuki Y, Nagase Y, Iga K, et al. Prevention of bone loss in ovariectomized rats by pulsatile transdermal iontophoretic administration of human PTH (1-34). J Pharm Sci 2002;91:350-61.
78. Siddiqui O, Sun Y, Liu JC, Chien YW. Facilitated transdermal transport of insulin. J Pharm Sci 1987;76:341-5.
79. Kari B. Control of blood glucose levels in alloxan-diabetic rabbits by iontophoresis of insulin. Diabetes 1986;35:217-21.
80. Lu MF, Lee D, Carlson R, et al. The effects of formulation variables on iontophoretic transdermal delivery of leuprolide to humans. Drug Dev Ind Pharm 1993;19:1557-71.

81. Meyer BR, Kreis W, Eschbach J, O'Mara V, Rosen S, Sibalis D. Successful transdermal administration of therapeutic doses of a polypeptide to normal human volunteers. Clin Pharmacol Ther 1988;44:607-12.
82. Meyer BR, Kreis W, Eschbach J, O'Mara V, Rosen S, Sibalis D. Transdermal versus subcutaneous leuprolide: a comparison of acute pharmacodynamic effect. Clin Pharmacol Ther 1990;48:340-5.
83. Green P.G. Iontophoretic delivery of peptide drugs. J Control Release 1996;41:33-48.
84. Evers HCA, Broberg FB, DeNuzzio JD, Hoke RA, User activated iontophoretic device and method for using same, World Patent Application 93/18727, 1993.
85. Konno Y, Mitoni M, Sonobe T, Yamaguchi S. Plaster structural assembly for iontophoresis. US Patent 4,842,577, 1989.
86. Haak RP, Gyory JR, Theeuwes F, Landrau FA, Roth N, Meyers RM. Iontophoretic delivery device and methods of hydrating same. US Patent 5,288,289, 1994.
87. Haak RP, Gyory JR, Theeuwes F, Landrau FA, Roth N, Meyers RM. Iontophoretic delivery device and methods of hydrating same. US Patent 5,320,598, 1994.
88. Gyory JR, Perry JR, Iontophoretic delivery device and methods of hydrating same. US Patent 5,310,404, 1994.

Chapter 2

Comparison of the cutaneous iontophoretic delivery of rasagiline and selegiline across porcine and human skin in vitro

Dhaval R. Kalaria[a], Pratik Patel[b], Vandana Patravale[b] and Yogeshvar N. Kalia[a]

[a]School of Pharmaceutical Sciences,
University of Geneva & University of Lausanne,
30 Quai Ernest Ansermet,
1211 Geneva, Switzerland

[b]Department of Pharmaceutical Sciences and Technology,
Institute of Chemical Technology,
Mumbai 400019, India

International Journal of Pharmaceutics, 438 (2012) 202-208

ABSTRACT

The objective was to investigate the anodal iontophoretic delivery of the MAO-B inhibitors rasagiline (RAS) and selegiline (SEL) across porcine and human skin *in vitro*. Passive delivery of RAS and SEL from aqueous solution was minimal; however, increasing current density from 0.1 to 0.3 and 0.5 mA/cm^2 produced a linear increase in steady-state iontophoretic flux ($J_{ss,RAS}$=49.1i_d + 27.9 (r^2=0.96) and $J_{ss,SEL}$=27.8i_d + 25.8 (r^2=0.98)). In the absence of background electrolyte, a four-fold change in donor concentration (10, 20 and 40 mM) did not produce a statistically significant increase in the cumulative permeation of either drug after iontophoresis at 0.5 mA/cm^2 for 7 h (RAS – 1200.4 ± 154.6, 1262.6 ± 125.0 and 1321.5 ± 335.2 µg/cm^2 respectively; SEL – 748.3 ± 115.2, 848.8 ± 108.3 and 859.8 ± 230.1 µg/cm^2, respectively). Co-iontophoresis of acetaminophen confirmed that electromigration was the dominant transport mechanism for both drugs (~90%). Total iontophoretic delivery of RAS and SEL across porcine and human skin *in vitro* was statistically equivalent (RAS 1512.7 ± 163.7 and 1523.6 ± 195.9 µg/cm^2, respectively; SEL 1268.7 ± 231.2 and 1298.3 ± 253.3 µg/cm^2, respectively). Transport efficiencies for RAS and SEL were good (ranged from 6.81-8.50 and 2.86-3.61 %, respectively). Furthermore, the delivery efficiency, i.e., the fraction of the drug in the formulation that was delivered was very high (>56% at 0.5 mA/cm^2). Cumulative permeation of RAS and SEL from carbopol gels, potential drug reservoirs for iontophoretic systems was 891.5 ± 148.3 and 626.6 ± 162.4 µg/cm^2, respectively; this was less than that from solution and was tentatively attributed to either different partitioning or slower drug diffusion in the gel matrix. The results demonstrated that therapeutic amounts of rasagiline and selegiline could be easily delivered by transdermal iontophoresis with simple gel patches of modest surface area.

Keywords: Parkinson's Disease, MAO-B inhibitors, Iontophoresis, Transdermal drug delivery

1. **INTRODUCTION**

Rasagiline (RAS) and selegiline (SEL) are dose-dependent selective irreversible inhibitors of monoamine oxidase B (MAO-B), an enzyme that regulates the metabolism of catecholamine neurotransmitters (e.g., dopamine and noradrenaline) (Figure 1). As such they have found therapeutic applications for the treatment of Parkinson's Disease (PD) (LeWitt, 2004) and in the treatment of Major Depressive Disorder (MDD) (Mann et al., 1989). MAO-B inhibitors are used as a monotherapy in early stage PD or as an adjunct to L-DOPA in more advanced disease states (Elmer and Bertoni, 2008). In addition to their inhibition of MAO-B, RAS and SEL also exhibit antioxidant and anti-apoptotic activity in experimental models, which may potentially translate into long-term clinical neuroprotective benefits (Elmer and Bertoni, 2008; Jenner 2004; Tabakman et al., 2004).

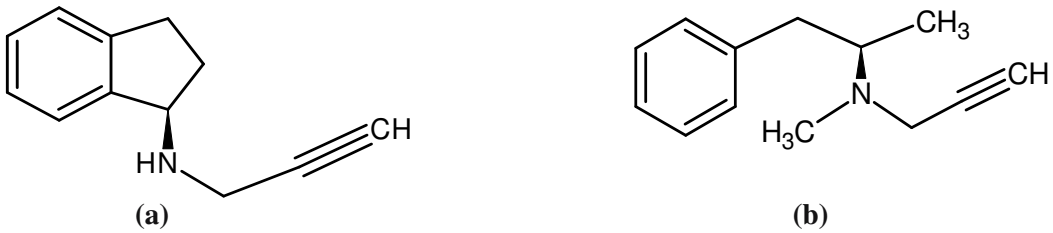

Figure 1. Chemical structure of (a) Rasagiline and (b) Selegiline.

Both molecules are subject to extensive first pass hepatic metabolism, resulting in poor and highly variable oral bioavailability (35 % for RAS and 4-10 % for SEL, respectively) (Barrett et al., 1996; Chen et al. 2007). Although RAS and SEL are preferential MAO-B inhibitors, their selectivity is dose-dependent; indeed, although SEL is approved for the treatment of depression, the dose is 3- to 6-fold higher than that for the treatment of PD causing loss of MAO-B selectivity and requiring precautions to prevent hypertensive crises (Anderson and Tipton, 1994). These are caused by inhibition of MAO-A in the intestinal barrier resulting in elevated levels of tyramine; thus, intake of food items rich in tyramine has to be restricted during therapy (Anderson and Tipton, 1994; Mawhinney, 2003). RAS is a new MAO-B inhibitor, introduced in 2006, that has 3- to 16-fold greater potency than SEL (depending on the assay). Furthermore, the principal metabolite of RAS, aminoindan, is reported to possess a neuroprotective effect. In contrast, a major drawback of SEL is that one of its principal metabolites is L-methamphetamine

and this along with desmethylselegiline is subsequently converted to L-amphetamine (Bar Am et al., 2004).

Transdermal therapy avoids the GI tract and hepatic first pass effect, increasing bioavailability and bypassing MAO-A present in the intestinal barrier. It also enables a steady zero-order drug input that eliminates peak-trough variations. This could improve efficacy since it would help to maintain relatively constant levels of dopamine in the brain and better mimic the normal state (Steiger, 2008). In addition to the pharmacologic rationale, transdermal administration is also well-suited to the treatment of patients suffering from chronic neurodegenerative conditions since the caregiver could easily apply the patch and this could help to improve patient compliance.

Table 1 Comparing physicochemical and pharmacological properties of RAS and SEL

	RAS	**SEL**
M_W (Da)	267.3[a]	302.2[b]
Aqueous solubility (g/L)	3.4[a]	3.2[b]
pKa	7.2	7.53
log P	1.67	2.68
log $D_{pH7.0}$	1.40	2.04

[a] Mesylate salt; [b] Hydrochloride salt

Although a passive transdermal patch for SEL has been approved for the treatment of MDD, there are reports of skin irritation; this may be exacerbated by the patch size (20 to 40 cm^2 depending on the dose) (Howland, 2006; Patkar et al., 2006). The physicochemical properties of RAS and SEL make them attractive candidates for transdermal iontophoresis (Table 1); they have good aqueous solubility and their pKa values mean that they have a high degree of ionization over a pH range suitable for anodal iontophoresis *in vivo* (Kalia et al., 2004). Moreover, their pharmacokinetic properties – poor systemic bioavailability, short half-life and low dosing requirements (oral daily doses are 0.5 and 1.0 mg for RAS and 1.25 and 5 mg for SEL) also justify the use of the transdermal route.

The addition of the electric potential gradient to the concentration gradient across the membrane during iontophoresis means that transport rates can be significantly increased as compared to passive diffusion. Furthermore, iontophoresis enables tight control over drug input rates since the current intensity and duration can be modulated. These can be used to provide highly individualised treatment regimens and ensure that dose ramping, an integral part of Parkinson's disease therapy, can be easily achieved. Iontophoresis can also enable faster onset of pharmacological effect, decrease lag times seen with conventional transdermal patches; more efficient delivery per unit area also corresponds to a substantial reduction in patch size.

Given the therapeutic rationale described above, the objectives of this study were (i) to investigate the transdermal iontophoretic delivery kinetics of RAS and SEL across porcine skin as a function of experimental parameters including current density, drug concentration and pH, (ii) to use co-iontophoresis of acetaminophen to identify the relative contributions of electromigration and electroosmosis to electrotransport and report on drug-skin interactions, (iii) to compare iontophoretic delivery across porcine and human skin in vitro, (iv) to investigate delivery from simple hydrogel formulations that may be considered for use as a drug reservoir in an iontophoretic patch system and hence (v) to determine the feasibility of therapeutic delivery.

2. MATERIALS AND METHODS

2.1 Materials

Rasagiline and selegiline were purchased from Jinan Jinao CDC Ltd. (Jinan City, PR China and Shaanxi Sciphar Biotechnology Co. Ltd. (Xian, PR China), respectively. Acetaminophen (ACE), sodium chloride, 4-(2-hydroxyethyl)-1-piperazineethanesulfonic acid (HEPES), triethanolamine, citric acid and sodium citrate were all purchased from Sigma-Aldrich (Buchs, Switzerland). Carbopol 980 NF was purchased from Noveon Inc. (Ohio, USA). Silver wire and silver chloride used for the fabrication of electrodes were sourced from Sigma Aldrich (Buchs, Switzerland). Methanol and PVC tubing (ID 3.17 mm; OD 4.97 mm) were purchased from VWR International (Nyon, Switzerland). All solutions were prepared using deionised water (resistivity > 18 MΩ.cm). All other chemicals were at least of analytical grade.

2.2 Skin source

Porcine ears were obtained from a local abattoir (CARRE; Rolle, Switzerland), the skin was excised (thickness 750 μm) with an air dermatome (Zimmer; Etupes, France), wrapped in Parafilm™ and stored at −20 °C for a maximum period of 1 month. Human skin samples were collected immediately after surgery from the Department of Plastic, Aesthetic and Reconstructive Surgery, Geneva University Hospital (Geneva, Switzerland), fatty tissue was removed and the skin was wrapped in Parafilm™ before storage at −20 °C for a maximum period of 7 days. The study was approved by the Central Committee for Ethics in Research (CER: 08-150 (NAC08-051); Geneva University Hospital).

2.3 Stability studies

2.3.1. Stability in the presence of skin

A 20 mM solution of either RAS or SEL in 25 mM HEPES (pH 5.2) or a 1 mM solution of either RAS or SEL in 133 mM NaCl / 25 mM HEPES (pH 7.4) were placed in contact with epidermal and dermal skin surfaces respectively for 12 h.

2.3.2 Stability in the presence of current

The electrical stability of both molecules was evaluated by placing a 20 mM drug solution (in 25 mM HEPES at pH 5.2) in the presence of 0.5 mA/cm^2 current for a period of 7 h.

2.4 Iontophoresis procedure

Electrotransport studies were performed using modified Franz diffusion cells (mean area, 2 cm^2). The anodal and cathodal (receiver) compartments were filled with 25 mM HEPES / 133 mM NaCl buffer at pH 7.4. After a 30 min equilibration period, 1 ml of drug solution (in 25 mM HEPES at pH 5.2 and containing 15 mM acetaminophen (ACE)) was placed in the donor compartment. This was connected to the anode via a salt bridge assembly (3% agarose in 0.1 M NaCl) to minimise the effect of competing ions. Acetaminophen transport reported on electroosmotic solvent flow and was used to determine the contributions of electromigration (EM) and electroosmosis (EO) to RAS and SEL delivery. The receptor compartment was sampled hourly; 0.6 ml was collected and replaced by the same volume of fresh buffer solution. Constant current was applied for 7 h via Ag/AgCl electrodes connected to a power supply

(Kepco APH 1000M; Flushing, NY). After completion of the iontophoretic permeation experiments, the drugs were extracted from the skin by cutting the samples into pieces and then soaking them in 10 ml of mobile phase for 4 h. The extraction suspensions were filtered through 0.22 μm nylon membrane filter (VWR, Nyon, Switzerland) before HPLC analysis. The extraction method was validated by spiking the stratum corneum surface of dermatomed skin samples (thickness 750 μm; area 2 cm^2) with known amounts of drug (1 ml of 100, 300 and 600 μg/ml of RAS standard solution in methanol and 1 ml of 100, 500 and 1000 μg/ml of SEL standard solution in methanol). After solvent evaporation, skin samples were subjected to extraction as mentioned above and then analyzed. The recovery was determined by calculating the ratio of the amount extracted from the skin samples to the amount applied, determined by direct injection of spiking solution in the absence of skin (Table 2). Experiments were performed with at least five replicates.

Table 2 Validation of the RAS and SEL extraction method used to quantify the amount of drug retained within the skin

	Control concentration (μg/ml)	**Sample Concentration (μg/ml)**	**Recovery (%)**	**S.D.**
RAS	100	85.2	85.2	5.2
	300	267.9	89.3	7.8
	600	554.4	92.4	5.1
SEL	250	221.0	88.4	7.3
	500	450.5	90.1	2.4
	1000	956.0	95.6	2.5

2.4.1 Effect of current density

Electrotransport experiments were performed to investigate the effect of current density (i_d; 0.15, 0.3 and 0.5 mA/cm^2) on the iontophoretic delivery of RAS and SEL (20 mM in 25 mM HEPES at pH 5.2). Control experiments were also carried out using the same experimental set-up but in the absence of current.

2.4.2. Effect of drug concentration

Iontophoretic permeation was also investigated as a function of drug concentration (10, 20 and 40 mM in 25 mM HEPES at pH 5.2) at a fixed current density of 0.5 mA/cm^2.

2.4.3. Effect of donor pH

The influence of formulation pH on the iontophoretic transport of RAS and SEL (with 20 mM donor concentration) at 0.5 mA/cm^2 was investigated by comparing delivery at pH 5.2 and pH 6.5.

2.4.4. Comparing RAS and SEL iontophoresis across porcine and human skin

Iontophoretic delivery of RAS and SEL across porcine and human skin samples was compared under the same experimental conditions – 20 mM RAS or SEL in 25 mM HEPES at pH 5.2 with 15 mM ACM iontophoresed for 7 h at 0.5 mA/cm^2 ($n \geq 4$ in both experiments).

2.4.5. Data analysis

The total iontophoretic flux (J_{tot}) of drug, assuming negligible passive diffusion, is the linear sum of fluxes due to EM (J_{EM}) and EO (J_{EO}), where J_{EO} is defined as the product of the concentration of RAS or SEL (C_{Drug}) and the linear velocity of the solvent flow (V_W), which in turn, is given by the ratio of the flux of acetaminophen (J_{ACE}) to its concentration (C_{ACE}) in the formulation (Kalia et al., 2004).

The inhibition factor (IF) is given by the ratio $Q_{ACE,Control}$ / $Q_{ACE,Drug}$ where $Q_{ACE,Control}$ and $Q_{ACE,Drug}$, represent the cumulative permeation of ACE in 7 h, in the absence and presence of drug (RAS or SEL), respectively.

2.5 Passive diffusion of RAS and SEL across mechanically microporated skin

Skin was pre-treated with a stainless steel microneedle roller (Dr. Roller; Seoul, Korea) with needle length of 0.5 mm, needle diameter of 0.1 mm and a needle density of 19.2 needles/cm^2 prior to application of 20 mM buffered solutions of RAS and SEL for 7 h.

2.6 Preparation of carbopol gel formulations

Briefly, carbopol was slowly dispersed in water, followed by addition of drug solution and then the mixture was neutralised with 10% triethanolamine until a clear, transparent gel was obtained. The loading for RAS and SEL gels was 0.6 and 0.5%, respectively. The pH of the gels was measured prior to the permeation studies by preparing 10% dispersion. For each drug, 500 mg of gel was placed in the donor compartment and iontophoretic delivery was compared with that from aqueous solution under the same conditions (0.5 mA/cm^2 for 7h).

2.7 Analytical methods

An Ultimate 3000 pump equipped with an Ultimate 3000 auto-sampler and AD25 detector (Dionex; Olten, Switzerland) was used to quantify the amounts of RAS and SEL permeated across and retained within the skin. Isocratic separation was performed using a 125 mm x 4 mm LiChrospher® column packed with 5 μm C_{18} end-capped silica reversed-phase particles. The mobile phase for quantification of SEL consisted of 75% methanol and 25% phosphate buffer (10 mM KH_2PO_4; pH 6.0) with detection at 220 nm and a column temperature of 35°C and a flow-rate of 1.0 ml/min. RAS was quantified with the same column specification and the mobile phase consisted of 70% methanol and 30% phosphate buffer (3.7mM KH_2PO_4 and 4.4mM $K_2HPO_4 \cdot 3H_2O$, pH 7.0). The flow rate was maintained at 1.1 ml/min, the column temperature was 30°C and RAS was detected by its absorbance at 264 nm. The analytical methods for RAS and SEL were validated (Table 3). ACE was analysed using the same column and the mobile phase consisted of 80% methanol and 20% citrate buffer (10mM citric acid and 7 mM sodium citrate, pH 3.0) at 1.0 ml/min flow rate, with a column temperature of 30°C and detection at 220 nm. The injection volume was 75 μl for all of the analyses.

2.8 Statistical analysis

Data were expressed as mean ± SD. Outliers determined using the Grubbs test were discarded. Results were evaluated statistically using analysis of variance (ANOVA) to compare the data sets. The level of significance was fixed at α=0.05.

Table 3 Precision and accuracy of the analytical methods used to quantify RAS and SEL

	Theoretical concentration (µg/ml)	Experimental concentration (µg/ml)	CV (%)[a]	Accuracy (%)[b]
RAS	*Intra-day (n=3)*			
	0.25	0.242 ± 0.009	3.720	96.76
	5.0	5.123 ± 0.231	4.509	102.46
	20.0	19.012 ± 0.752	3.956	95.05
	Inter-day (n=3)			
	0.25	0.259 ± 0.007	2.693	103.96
	5.0	4.564 ± 0.295	6.472	91.28
	20.0	19.134 ± 0.657	3.436	95.67
SEL	*Intra-day (n=3)*			
	0.1	0.096 ± 0.002	2.079	96.2
	5.0	4.863 ± 0.185	3.810	97.26
	20.0	20.198 ± 0.862	4.267	100.99
	Inter-day (n=3)			
	0.1	0.104 ± 0.003	2.870	104.50
	5.0	4.619 ± 0.200	4.334	92.38
	20.0	20.657 ± 0.782	3.786	103.29

[a] Precision = (SD/mean) x 100
[b] Accuracy = (obtained concentration/theoretical concentration) x 100

3. RESULTS AND DISCUSSION

3.1 Stability studies

RAS and SEL were found to be stable in the presence of epidermal and dermal skin surfaces after exposure for 12 h. After 7 h of current application, solution concentrations of RAS and SEL were 99.7 ± 2.3 and 98.3 ± 1.7%, of their initial values, respectively.

3.2 Effect of iontophoretic conditions on electrotransport of RAS and SEL

Passive delivery of RAS and SEL from 20 mM formulations after permeation for 7 h was 14.2 ± 4.0 and 10.4 ± 3.4 µg/cm^2, respectively. For comparison, treatment with the microneedle roller produced an approximately 7-fold increase in cumulative permeation for both molecules (92.7 ±

19.7 and 74.1 ± 20.2 µg/cm^2 for RAS and SEL, respectively). Significantly larger increases were observed upon current application. Cumulative permeation of RAS after 7 h iontophoresis at 0.15, 0.3 and 0.5 mA/cm^2 was 364.4 ± 67.1, 909.1 ± 80.1 and 1262.6 ± 125.0 µg/cm^2, respectively with steady state iontophoretic fluxes of 71.4 ± 12.3, 137.5 ± 18.0 and 169.6 ± 15.7 µg/cm^2 h, respectively (Figure 2). The corresponding values for SEL after iontophoresis for 7 h at 0.15, 0.3 and 0.5 mA/cm^2 were 322.8 ± 45.5, 501.9 ± 94.3 and 848.2 ± 108.3 µg/cm^2, respectively with steady state iontophoretic fluxes of 54.8 ± 6.7, 79.1 ± 15.6 and 110.5 ± 10.2 µg/cm^2 h, respectively (Figure 3). Hence, iontophoretic transport across intact skin was markedly superior to passive diffusion across microporated skin. Furthermore, increasing current density resulted in statistically significant linear flux enhancements – $J_{ss,\ RAS} = 49.1\ i_d + 27.9$ ($r^2 = 0.96$) and $J_{ss,\ SEL} = 27.8\ i_d + 25.8$ ($r^2 = 0.98$) – obviously an advantage for controlled drug delivery. The time to reach steady state for RAS and SEL at each of the current densities tested was 3 h. Drug extraction from the skin after 7 h iontophoresis showed that there was also a statistically significant increase in the amounts of RAS and SEL retained within the membrane as a function of current density (Figures 2 and 3). Higher skin deposition was seen with SEL; in contrast, RAS showed greater permeation.

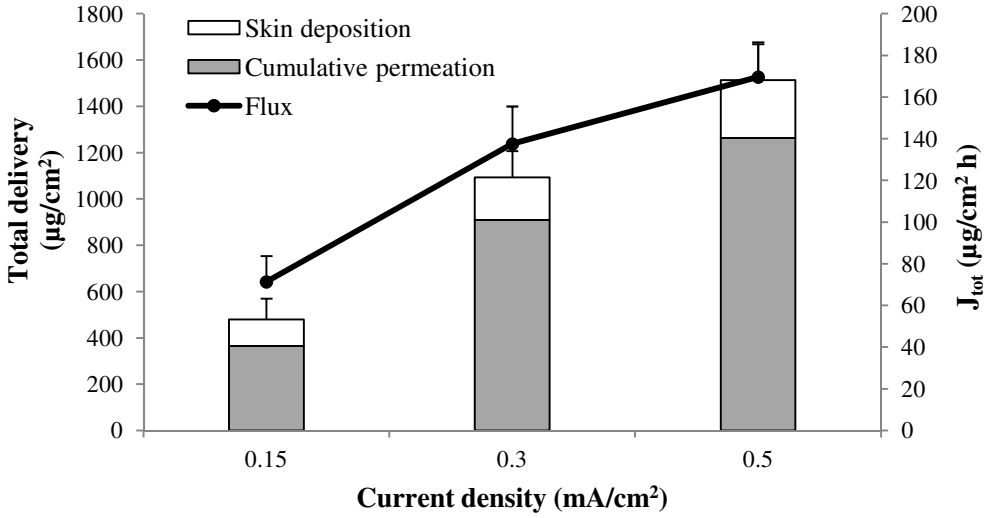

Figure 2. Total delivery (cumulative permeation + skin deposition) and steady state flux (J_{tot}) of RAS (20 mM) as a function of current density (at 0.15, 0.3 and 0.5 mA/cm^2) across porcine skin after 7 h of transdermal iontophoresis. (Mean ± SD; n≥5).

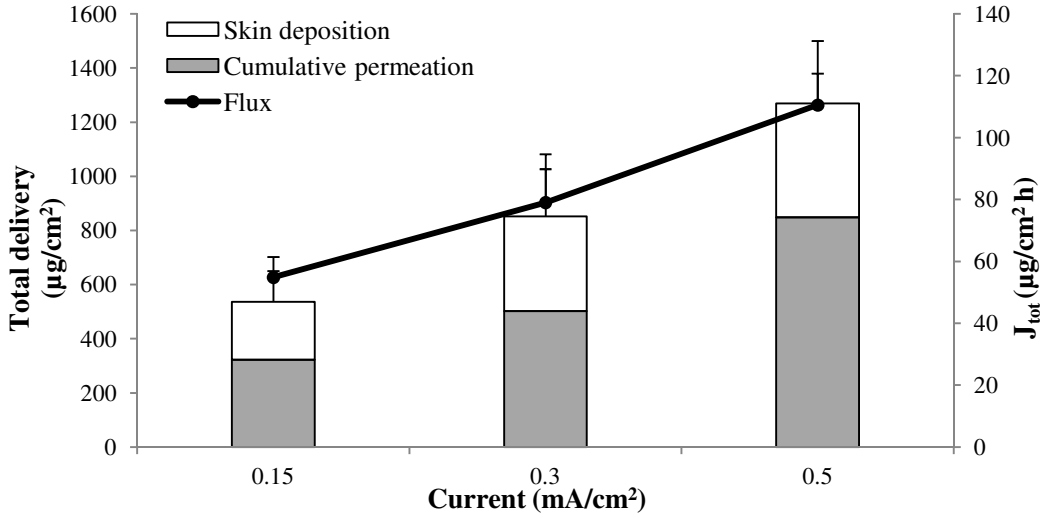

Figure 3. Total delivery (cumulative permeation + skin deposition) and steady state flux (J_{tot}) of SEL (20 mM) as a function of current density (at 0.15, 0.3 and 0.5 mA/cm^2) across porcine skin after 7 h of transdermal iontophoresis. (Mean ± SD; n≥5).

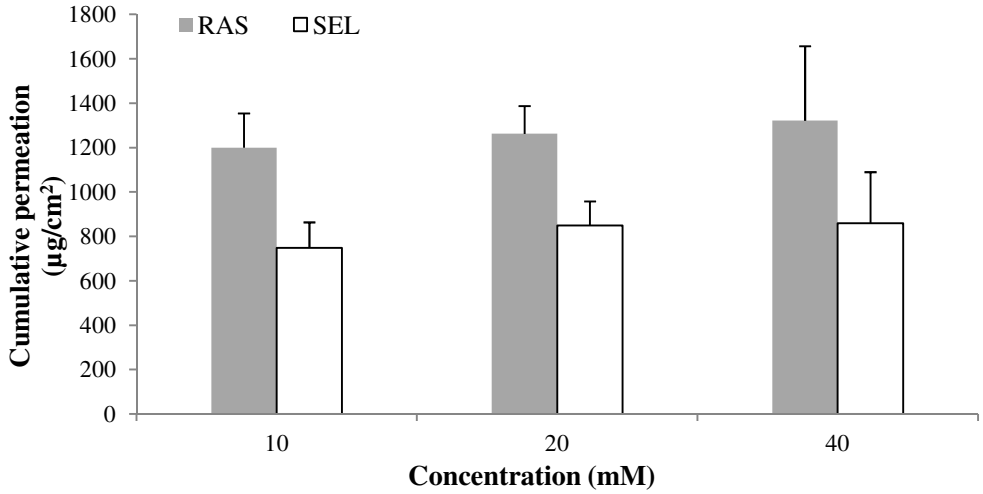

Figure 4. Cumulative permeation of RAS and SEL as a function of concentration iontophoresis at 0.5 mA/cm^2 for 7 h. (Mean ± SD; n≥5).

Cumulative permeation of RAS after iontophoresis at 0.5 mA/cm^2 for 7 h using drug concentrations of 10, 20 and 40 mM was statistically equivalent (1200.4 ± 154.6, 1262.6 ± 125.0 and 1321.5 ± 335.2 µg/cm^2 respectively); similar behaviour was observed for SEL (the corresponding values were 748.3 ± 115.2, 848.8 ± 108.3 and 859.8 ± 230.1 µg/cm^2, respectively) (Figure 4). The results were consistent with earlier studies describing the use of a salt bridge

which eliminates the presence of competing cations in the donor compartment and renders delivery independent of drug concentration (Kasting and Keister, 1989).

3.3 Comparison of RAS and SEL electrotransport across porcine and human skin

Total delivery (that is, the sum of the amounts permeated and deposited in the skin) of RAS and SEL across full thickness human skin at 0.5 mA/cm^2 was 1523.6 ± 195.9 and 1298.3 ± 253.3, respectively. This was statistically equivalent to that observed with porcine skin (Figure 5).

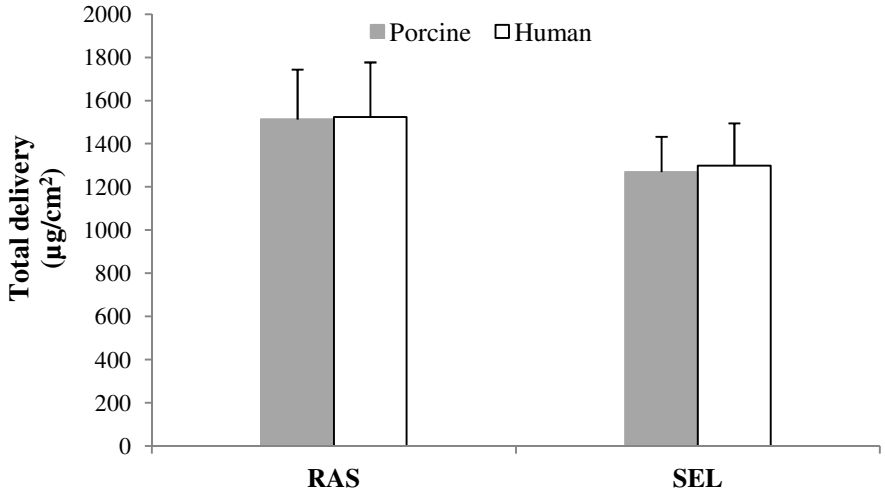

Figure 5. Comparison of total delivery (permeation + skin deposition) of RAS and SEL across human and porcine skin after iontophoresis at 0.5 mA/cm^2 for 7 h. (Mean ± SD; n≥4).

3.4 Relative contribution of EM and EO and the effect of electrotransport on RAS and SEL

Co-iontophoresis of acetaminophen (a neutral hydrophilic molecule whose iontophoretic transport is due exclusively to electrically-induced convective solvent flow) enabled deconvolution of the individual contributions of EM and EO to RAS/SEL transport. Control values for ACE flux in the absence of drug were determined independently at each current density. EM was the dominant transport mechanism for RAS and SEL accounting for 82 to 97% of electrotransport over the current densities studied (Table 4). ACE transport was also used to show that convective solvent flow was unaffected by delivery of either drug at the current densities used, suggesting that neither RAS nor SEL was binding to structures present in the transport pathway and affecting skin permselectivity.

Table 4 Iontophoretic transport kinetics of RAS and SEL and the relative contributions of electromigration and electroosmosis

	Current (mA/cm^2)	J_{tot} ($\mu g/cm^2$ h)	J_{EM} ($\mu g/cm^2$ h)	J_{EO} ($\mu g/cm^2$ h)	% EM	% EO	Inhibition factor
RAS	0.15	71.4 ± 12.3	69.6	1.8	97.5	2.5	1.82
	0.3	137.5 ± 18.0	130.9	6.6	95.2	6.6	1.63
	0.5	169.6 ± 15.7	146.9	22.7	86.6	13.4	1.32
SEL	0.15	54.8 ± 6.7	50.4	4.5	91.8	8.2	1.01
	0.3	79.1 ± 15.6	67.6	11.4	85.5	14.5	0.96
	0.5	110.5 ± 10.2	91.3	19.2	82.6	17.4	1.12

J_{tot}: total steady state flux; J_{EM}: electromigration flux; J_{EO}: electroosmotic flux; %EM and %EO are the % contributions of EM and EO to total electrotransport; IF: inhibition factor (calculated as described above).

Many studies have been conducted to understand the effect of pH on electrotransport kinetics across the skin. In theory, the pH of the formulation can influence iontophoretic transport through modification of the degree of ionisation of the permeant or by altering the skin pH and hence the degree of ionisation of pendant carboxylic acid groups. Given that the pI of the skin is 4.5, under physiological conditions the skin is permselective to cations and electroosmosis provides a secondary mechanism for cation electrotransport (Merino et al. 1999). However, increasing the pH of a formulation containing a weakly basic molecule will decrease the ionised drug fraction – reducing EM; therefore, any net benefit in transport will depend on the relative contributions of EM and EO to transport. It was found that there was no statistically significant difference between RAS or SEL delivery at pH 5.2 and 6.5 (Figure 6). As mentioned above (and in Table 4), electromigration is the main electrotransport mechanism for the delivery of both RAS and SEL. In the case of RAS (pKa 7.2), increasing pH from 5.2 to 6.5 decreased the degree of ionization from 99 to 84% and consequently, the EM contribution to RAS permeation decreased from 86.6 to 77.3%. Similarly, SEL has a pKa of 7.53 and at pH 5.2 and 6.5, it is more than 99 and 90% ionised. The convective solvent flow deduced from ACE transport indicated that the EM contribution to SEL electrotransport was reduced from 82.6 to 79.3% (smaller than that for RAS) as the pH increased from 5.2 to 6.5. Thus, for both molecules, given

that the overall delivery was statistically equivalent, the decrease in EM observed due to the lower degree of ionisation was compensated by a slightly greater EO contribution.

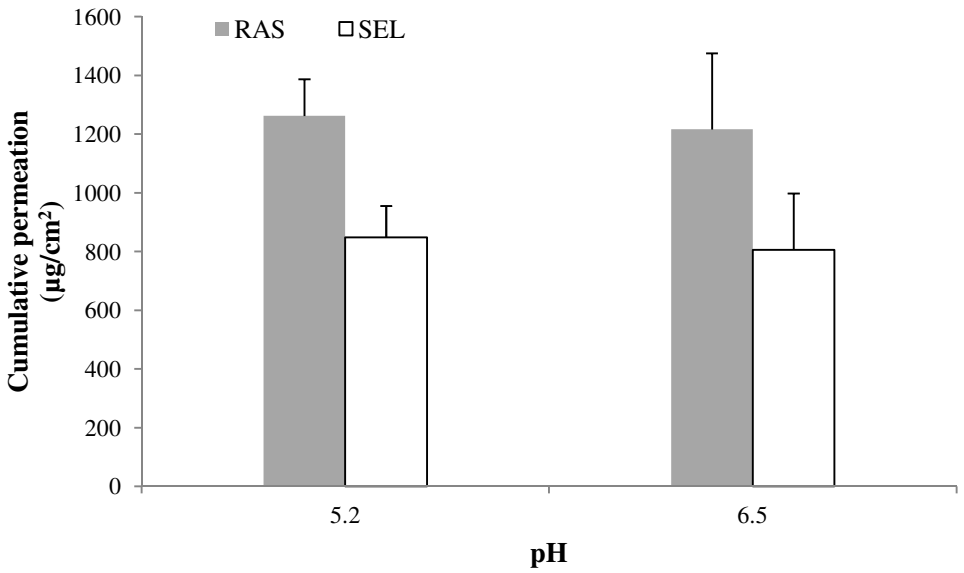

Figure 6. Comparison of RAS and SEL permeation from aqueous solutions (each drug was at a concentration of 20 mM) at pH 5.2 and 6.5 (across porcine skin after iontophoresis at 0.5 mA/cm^2 for 7 h. (Mean ± SD; n≥5).

3.5 Transport number and delivery efficiency

The transport number (t_i) is the fraction of the total current transported by a specific ion and expresses its efficiency as a charge carrier (Bellantone et al., 1986). The sum of the transport numbers of all the ionic species present during iontophoresis must add up to 1. Thus, the iontophoretic flux of the ion of interest depends on the ionic composition of the solutions contacting the outer and inner surfaces of the skin barrier. In this case, the use of salt bridges precluded the presence of competing cations in the donor compartment; however, chloride ions present in the receptor were the principal charge carriers due to their high mobility and concentration as they migrated across the skin towards the anode. Results indicate good transport efficiencies for RAS (in particular) and SEL (Table 5); for example, at 0.3 mA/cm^2, 8.50 and 2.86% of total charge was carried by RAS and SEL, respectively.

A perceived limitation of transdermal delivery systems is their low delivery efficiency since much of the drug load remains undelivered in the formulation. This unused active ingredient is a potential deterrent against developing transdermal systems prompting pharmaceutical companies to focus on the development of more cost-effective formulations. However, the results of this study show that extremely high delivery efficiencies of 56 % were achieved for RAS and SEL during 7 h iontophoresis at 0.5 mA/cm^2 (Table 5). For comparison, the marketed 20, 30 and 40 mg SEL patches deliver 6, 9 and 12 mg of selegiline in 24 h, respectively, which corresponds to delivery efficiencies of 30% (Pae et al., 2007).

Table 5 Transport and drug delivery efficiencies as a function of applied current density

	Current (mA/cm^2)	**Transport efficiency (%)**	**Drug delivered from donor (%)**
RAS	0.15	6.81	23.98
	0.3	8.50	38.09
	0.5	7.08	56.70
SEL	0.15	3.61	17.91
	0.3	2.86	40.86
	0.5	2.99	56.58

3.6 Permeation studies with carbopol gel

Iontophoretic delivery systems contain a drug reservoir and in this study carbopol gels of RAS (0.6%) and SEL (0.5%) were prepared in order to investigate delivery from a potential "drug reservoir" that could be integrated into an iontophoretic patch system. The gels were stable for 1 month at room temperature; there was no sign of drug precipitation and drug content was uniform. The pH of a 10% dispersion of gel was found to be 6.6 at ambient temperature and was thus suitable for use in vivo and conducive for electrotransport by EM. A higher drug loading was not possible for these basic drugs as solubility decreased with increasing pH (Table 1). Cumulative permeation of RAS and SEL from the gels was 891.5 ± 148.3 and 626.6 ± 162.4 μg/cm^2, respectively (Figure 7), which was statistically lower than that seen with the respective 10 mM drug solutions. This may have been due to a lower stratum corneum-vehicle partition co-efficient from the gel as compared to the buffer solution. Furthermore, in the gels the drug is

entrapped in a matrix structure that could hinder diffusion. Nevertheless, the gels still showed high delivery efficiencies and could be easily incorporated into a patch to make a patient compliant formulation.

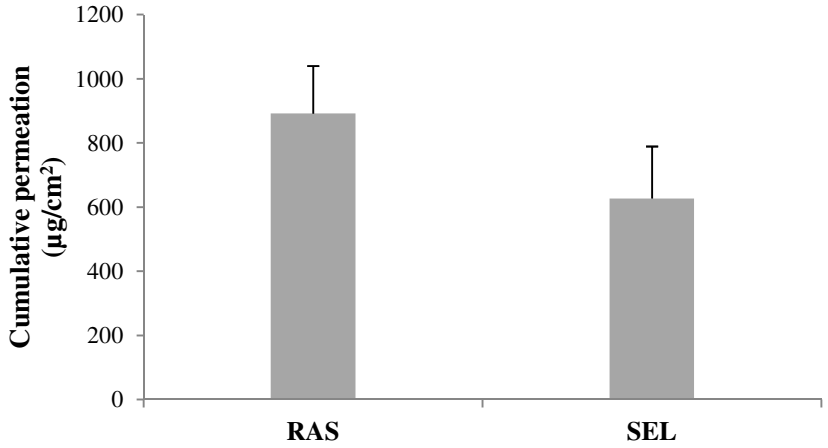

Figure 7. Cumulative permeation of RAS and SEL from carbopol gels across porcine skin after iontophoresis at 0.5 mA/cm^2 for 7 h. (Mean ± SD; n≥5).

3.7 Clinical relevance

The clinical dose of RAS is 1 mg/day – given its oral bioavailability of 35%, this means that the daily systemic dose is ~350 µg (Levy et al., 2004). The steady state iontophoretic flux of RAS at 0.3 mA/cm^2 was 137.5 ± 18.0 µg/cm^2 h; hence the therapeutic amount can be delivered in 2 h from 2 cm^2 patch. Similarly, for the treatment of PD, SEL is administered orally at a dose of 5 mg twice a day. Given that SEL has an oral bioavailability of 10%, the total systemic absorption of SEL per day would be ~1 mg. The iontophoretic flux of SEL at 0.3 mA/cm^2 was 79.1 ± 15.6 µg/cm^2 h and the required amount can be delivered in ~3 h from a 4 cm^2 patch.

4. CONCLUSION

The results presented here confirm that rasagiline and selegiline are excellent candidates for transdermal iontophoretic delivery. Electrotransport is predominantly governed by electromigration and there is no skin binding as evidenced by the lack of inhibition of electroosmosis at all of the current densities tested. Carbopol gel formulations were also shown to be efficient systems for delivering therapeutic amounts of each molecule. Based on these results and given the posology and known pharmacokinetics, it should be possible to administer

therapeutic amounts of rasagiline and selegiline using low current densities and small patch areas that are acceptable for use in humans.

5. ACKNOWLEDGEMENTS

We thank the Indo Swiss Joint Research Programme (ISJRP 123143) for financial support.

6. REFERENCES

Anderson, M.C., Tipton, K.F., 1994. Estimation of monoamine-oxidase concentrations in soluble and membrane-bound preparations by inhibitor binding. J. Neural. Transm. Supp. 41, 47-53.

Bar Am, O., Amit, T., Youdim, M.B.H., 2004. Contrasting neuroprotective and neurotoxic actions of respective metabolites of anti-Parkinson drugs rasagiline and selegiline. Neuroscience Letters. 355, 169-172.

Barrett, J.S., Rohatagi, S., Dewitt, K., Morales, R., 1996. Bioequivalence of selegiline HCl: Guidance for a "highly variable" drug. Clin. Pharmacol. Ther. 59, 206.

Bellantone, N.H., Rim, S., Francoeur, M.L., Rasadi, B., 1986. Enhanced Percutaneous-Absorption Via Iontophoresis .1. Evaluation of an Invitro System and Transport of Model Compounds, Int. J. Pharm. 30, 63-72.

Chen, J.J., Swope, D.M., Dashtipour, K., 2007. Comprehensive review of rasagiline, a second-generation monoamine oxidase inhibitor, for the treatment of Parkinson's disease. Clin. Ther. 29, 1825-1849.

Elmer, L.W., Bertoni, J.M., 2008. The increasing role of monoamine oxidase type B inhibitors in Parkinson's disease therapy. Expert Opin. Pharmacother. 9, 2759-2772.

Howland, R.H., 2006. Transdermal selegiline - A novel MAOI formulation for depression. J. Psychosoc. Nurs. 44, 9-12.

Jenner, P., 2004. Preclinical evidence for neuroprotection with monoamine oxidase-B inhibitors in Parkinson's disease. Neurology. 63, S13-S22.

Kalia, Y.N., Naik, A., Garrison, J., Guy, R.H., 2004. Iontophoretic drug delivery. Adv. Drug Delivery Rev. 56, 619-658.

Kasting, G.B., Keister, J.C., 1989. Application of electrodiffusion theory for a homogeneous membrane to iontophoretic transport through skin. J. Control. Release. 8, 195-210.

Levy, R., Thebault, J.J., Guillaume, M., 2004. The pharmacology of rasagiline: A potent, selective and irreversible MAO-B inhibitor: Results from single- and multiple-dose phase I studies. Movement Disord. 19, S158-S159.

LeWitt, P.A., 2009. Mao-B inhibitor know-how: Back to the pharm reply. Neurology. 73, 2048-2048.

Mann, J.J., Aarons, S.F., Wilner, P.J., Keilp, J.G., Sweeney, J.A., Pearlstein, T., Frances, A.J., Kocsis, J.H., Brown, R.P., 1989. A controlled study of the antidepressant efficacy and side effects of (-)-deprenyl. A selective monoamine oxidase inhibitor, Arch. Gen. Psychiatry. 46, 45-50.

Mawhinney, M., Cole, D., Azzaro, A.J., 2003. Daily transdermal administration of selegiline to guinea-pigs preferentially inhibits monoamine oxidase activity in brain when compared with intestinal and hepatic tissues. J. Pharm. Pharmacol. 55, 27-34.

Merino, V., Lopez, A., Kalia, Y.N., Guy, R.H., 1999. Electrorepulsion versus electroosmosis: Effect of pH on the iontophoretic flux of 5-fluorouracil. Pharm. Res. 16, 758-761.

Patkar, A.A., Pae, C.U., Masand, P.S., 2006. Transdermal selegiline: The new generation of monoamine oxidase inhibitors. CNS Spectrums, 11, 363-375.

Pae, C.U., Lim, H.K., Han, C., Neena, A., Lee, C., Patkar, A.A., 2007. Selegiline transdermal system: current awareness and promise. Prog. Neuropsychopharmacol. Biol. Psychiatry. 31, 1153-1163.

Steiger, M., 2008. Constant dopaminergic stimulation by transdermal delivery of dopaminergic drugs: a new treatment paradigm in Parkinson's disease. Eur. J. Neurol. 15, 6-15.

Tabakman, R., Lecht, S., Lazarovici, P., 2004. Neuroprotection by monoamine oxidase B inhibitors: a therapeutic strategy for Parkinson's disease?. Bioessays, 26, 80-90.

Chapter 3

Transdermal iontophoresis for the controlled delivery of pramipexole: Effect of iontophoretic and formulation parameters on electrotransport kinetics *in vitro* and *in vivo*

Dhaval R. Kalaria[a], Vandana Patravale[b], Virginia Merino[c] and Yogeshvar N. Kalia[a]

[a]School of Pharmaceutical Sciences,
University of Geneva & University of Lausanne,
30 Quai Ernest Ansermet,
1211 Geneva, Switzerland

[b]Department of Pharmaceutical Sciences and Technology,
Institute of Chemical Technology,
Mumbai 400019, India

[c]Departamento de Farmacia y Tecnología Farmacéutica,
Faculty of Pharmacy, University of Valencia,
Avda.Vicente Andrés Estellés s/n, 46100 Burjassot, Valencia, Spain

ABSTRACT

The objective of this study was to investigate the anodal iontophoretic delivery of pramipexole (PRAM), a dopamine agonist used for the treatment of Parkinson's disease, in order to determine whether therapeutic amounts of the drug could be delivered across the skin. Preliminary experiments were performed *in vitro* using porcine ear and human abdominal skin; these were followed by a pharmacokinetic study in male Wistar rats to determine the drug input rate *in vivo*. Stability studies revealed that after current exposure (0.5 mA/cm^2 for 6 h), the solution concentration of PRAM was only 60.2 ± 5.3% of its initial value. However, inclusion of sodium metabisulfite (0.5%), an antioxidant, increased this to 97.2 ± 3.1%. Iontophoretic transport of PRAM across porcine skin *in vitro* was studied as a function of current density (0.1, 0.3, 0.5 mA/cm^2) and concentration (10, 20, 40 mM). Increasing the current density from 0.1 to 0.3 and 0.5 mA/cm^2, resulted in 2.5- and 4-fold increases in cumulative permeation, from 309.5 ± 80.2 to 748.8 ± 148.1 and 1229.1 ± 138.6 $\mu g/cm^2$, respectively. Increasing the PRAM concentration in solution from 10 to 20 and 40 mM resulted in a 2-fold increase in cumulative permeation (816.4 ± 123.3, 1229.1 ± 138.6 and 1643.6 ± 201.3 $\mu g/cm^2$, respectively). Good linearity was observed between PRAM flux and the applied current density (r^2 = 0.98) and drug concentration in the formulation (r^2 = 0.99). Co-iontophoresis of acetaminophen showed that electromigration was the dominant electrotransport mechanism (accounting for > 80 % of delivery) and that there was no inhibition of electroosmotic flow at any current density. Cumulative iontophoretic permeation across human and porcine skin (after 6 h at 0.5 mA/cm^2) was also shown to be statistically equivalent (1229.1 ± 138.6 and 1184.8 ± 236.4 $\mu g/cm^2$, respectively). High transport and delivery efficiencies were achieved for PRAM (6-7% and 14-58%, respectively). The plasma concentration profiles obtained in the iontophoretic studies *in vivo* (20 mM PRAM; 0.5 $mA/cm^2$for 5 h) were modelled using constant and time-variant input models. The latter gave a superior quality fit and the results showed that the flux across rat skin *in vivo* was more than that obtained *in vitro* across porcine skin (0.46 ± 0.05 and 0.19 ± 0.01 mg/h, respectively). The results suggest that PRAM electrotransport rates would be sufficient for therapeutic delivery and the management of Parkinson's disease.

Keywords: Parkinson's Disease, Pramipexole, Iontophoresis, Transdermal delivery, Pharmacokinetics

1. INTRODUCTION

Pharmacotherapy of Parkinson's Disease (PD) employs two basic strategies; (i) use of the dopamine precursor, L-DOPA to compensate for the loss of dopamine synthesising neurons and (ii) administration of dopamine agonists to substitute for the depleted neurotransmitter at dopamine receptors. Adjunct treatments include the use of MAO-B inhibitors to prevent dopamine biotransformation. Although L-DOPA is often referred as the "gold standard" and considered the mainstay of therapy in PD, its prolonged use is associated with motor complications, occurrence of side effects such as dyskinesia and motor response fluctuations (i.e., "on-off" phenomena) [1]. Thus, PD treatment is frequently initiated by dopamine agonist monotherapy that is supplemented by progressively increasing doses of L-DOPA as symptomatic control becomes less effective [2]. The use of agonists can delay the motor complications that are generally considered to be inevitable after prolonged use of L-DOPA.

In contrast to the early dopamine agonists which were derived from ergot alkaloids and had several side-effects, pramipexole (PRAM) is a synthetic aminothiazole with a high relative specificity at the dopamine D_2 receptor and has been approved for the treatment of PD since 1997 [3] and is the most prescribed dopamine agonist for the treatment of PD, both as monotherapy and as an adjunctive therapy with L-DOPA [4,5]. It has also been approved for the treatment of Restless Leg Syndrome (RLS) prevalent among the geriatric population but also recognized in children and adolescents [6]. PRAM displays linear pharmacokinetics over its entire therapeutic range. It is rapidly and completely absorbed having an oral bioavailability of 90% with peak levels appearing in the bloodstream within 2 hours of dosing [7]. It is available in the form of immediate release and extended release tablets with dose typically initiated at 0.25 mg and gradually titrated to 1.5 mg thrice a day for the immediate release formulation.

The majority of the side effects associated with PD therapy have been attributed to pulsatile stimulation of the dopamine receptors [8,9]. Transdermal administration with steady zero-order drug inputs that eliminate peak-trough variations would enable continuous stimulation of dopamine receptors and so reduce these complications [10,11]. Indeed, a passive transdermal patch for rotigotine, another dopamine agonist, has already been approved for the treatment of PD and RLS and has had considerable success [12]. A transdermal delivery system for PRAM

might also offer some advantages over oral dosage forms. Apart from the pharmacokinetic aspects, adherence to therapy is an issue for elderly patients especially when they receive multiple treatments in chronic disorders such as PD (patients with advanced disease take 8-10 tablets per day [13]). Transdermal delivery could improve patient compliance due to its ease of use and once-daily administration schedule [14]. It would also benefit patients unable to take oral medications, or those with swallowing difficulties due to advanced disease state. Administration by the transdermal route could be easily performed by the care-giver, reducing their workload, and would not depend on the condition of the PD patient.

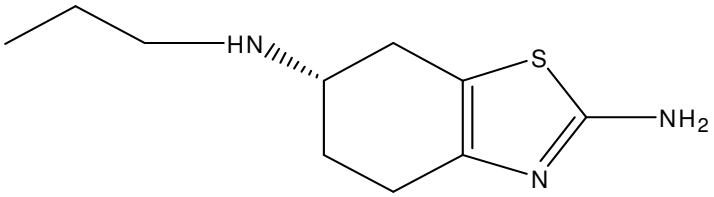

Figure 1. Chemical structure of pramipexole (MW: 211.32; pKa: 5.0, 9.6).

PRAM is a potent low molecular weight therapeutic with good aqueous solubility and two ionisable groups (pKa of 5.0 and 9.6) (Figure 1). Due to its highly polar nature, its passive delivery across the skin is difficult. In contrast, iontophoresis which involves the application of a low electric potential to enhance transdermal delivery of polar molecules and ions is a better alternative since iontophoretic transport is favoured by good aqueous solubility and the presence of multiple charged groups increases electric mobility. Thus, the physicochemical properties of PRAM lend themselves to iontophoretic administration [15]. The use of the electric potential gradient offers a second driving force resulting in a decreased lag time, faster onset time and given the improved delivery efficiency, a smaller application area compared to a conventional transdermal system. Another major advantage of iontophoresis is the control afforded over drug transport kinetics and hence, the dose administered, by simple modulation of the current density. Dose ramping is an integral part of PD where dose escalation is required as the disease progresses. Thus, iontophoresis can help in providing individualized therapeutic regimens for patients based on clinical need and the disease state, i.e., lower doses for early stage patients and higher doses for those with advanced stages of the disease. Moreover, a transdermal formulation

may also find application for the treatment of RLS, the rotigotine patch is reported to be preferred by RLS patients.

The objectives of the present study were (i) to examine the effect of experimental parameters on PRAM electrotransport in porcine skin *in vitro* and then validate with human skin, (ii) to identify the relative contributions of electromigration (EM) and electroosmosis (EO) and hence the dominant transport mechanism and, (iii) to study iontophoretic delivery in rats *in vivo* and to determine drug input rates and thus (iv) to evaluate the feasibility of using iontophoresis to deliver therapeutic amounts of PRAM for treatment of PD and RLS.

2. MATERIALS AND METHODS

2.1 Chemicals

Pramipexole dihydrochloride monohydrate was purchased from Nectar Industrial Co. Ltd (Shenzhen, China). Acetaminophen (ACE), sodium chloride, 2-(*N*-morpholino)-ethanesulfonic acid (MES), sodium metabisulfite, citric acid, sodium hydroxide and sodium citrate were all purchased from Sigma-Aldrich (Buchs, Switzerland). Silver wire and silver chloride used for the fabrication of electrodes were also sourced from Sigma-Aldrich. Potassium dihydrogenphosphate, heptanesulfonic acid sodium salt and diethyl ether were purchased from Acros Organics (Geel, Belgium). Methanol and PVC tubing (ID 3.17 mm; OD 4.97 mm) were purchased from VWR International (Nyon, Switzerland). All solutions were prepared using deionised water (resistivity > 18 MΩ.cm). All other chemicals were at least of analytical grade.

2.2 Skin preparation

Porcine ears were obtained from a local abattoir (CARRE; Rolle, Switzerland) within a few hours of sacrifice and were cleaned under cold running water. The skin was removed carefully from the outer region of the ear and separated from the underlying cartilage with a scalpel. The tissue was then dermatomed (thickness 750 μm) with an air-dermatome (Zimmer; Etupes, France), wrapped in Parafilm™ and stored at −20 ˚C for a maximum period of 1 month. Prior to the experiment, the skin was thawed at room temperature for a period of 30 min and excess hair was trimmed with clippers. Human skin samples were collected immediately after surgery from the Department of Plastic, Aesthetic and Reconstructive Surgery, Geneva University Hospital

(Geneva, Switzerland), fatty tissue was removed and the skin was wrapped in Parafilm™ before storage at −20 °C for a maximum period of 7 days. The study was approved by the Central Committee for Ethics in Research (CER: 08-150 (NAC08-051); Geneva University Hospital).

2.3 Stability studies

2.3.1 Stability in the presence of skin

PRAM solutions (20 mM in 25 mM MES; pH 5.3) and 20 mM in phosphate buffer saline (PBS; pH 7.4)) were placed in contact with the epidermal and dermal porcine skin surfaces, respectively for 12 h.

2.3.2 Stability in the presence of an electrical current

The stability of PRAM (20 mM in 25 mM MES; pH 5.3) was also evaluated in the presence of current at the highest current density used in the permeation experiments (i.e., 0.5 mA/cm^2).

2.4. Iontophoresis set-up

2.4.1 Effect of current density

Skin was clamped in vertical two-compartment diffusion cells (area ~ 2 cm^2) where the receiver compartment (lower chamber which also housed the cathode) was equipped with 2 side-arms. Prior to the start of the iontophoresis experiments, the skin was equilibrated for 30 minutes with PBS (pH 7.4). The receiver compartment was also filled with PBS. The upper chamber was used as the formulation compartment and this was connected to the anodal compartment (containing PBS) by a salt bridge to avoid competition with Na^+ ions present due to the requirement of NaCl for anodal electrochemistry. The formulation compartment contained 1 ml of PRAM solution (20 mM in 25 mM MES; pH 5.3) and 15 mM ACE (to deduce the contribution of electroosmosis). Constant current densities of 0.1, 0.3 and 0.5 mA/cm^2 were applied for 6 h via Ag/AgCl electrodes connected to a power supply (Kepco APH 1000M; Flushing, NY). Samples (0.6 ml) were withdrawn hourly from the receptor compartment and replaced with fresh buffer solution. Passive permeation experiments using the same set-up but without current application served as controls. In addition to quantifying iontophoretic permeation of PRAM, the amount of drug retained in the membrane was also determined. PRAM was extracted from the skin samples post-iontophoresis by cutting the skin into small

pieces and soaking them in 10 ml water-methanol mixture (35:65) for 4 h. The extraction mixture was then filtered through 0.22 µm nylon membrane filters (VWR; Nyon, Switzerland) and then analyzed by HPLC. Experiments were performed with at least five replicates.

2.4.2 Effect of drug concentration

The effect of concentration (10, 20 and 40 mM; in 25 mM MES, pH 5.3) on PRAM transport was investigated in a separate study. The current was fixed at 0.5 mA/cm^2 and the experimental set-up was as described above.

2.4.3 Comparing iontophoretic delivery across human and porcine skin

Iontophoretic delivery of PRAM across porcine and human skin samples was compared under the same experimental conditions – 20 mM PRAM in 25 mM MES at pH 5.3 iontophoresed for 6 h at 0.5 mA/cm^2 ($n \geq 4$).

2.4.4 Iontophoretic delivery of PRAM from a gel formulation

A carbopol gel formulation was prepared by first slowly dispersing carbopol in water (0.8% w/w) followed by the addition of PRAM (0.7% w/w). The resulting mixture was neutralized with 1% triethanolamine until a clear, transparent gel was obtained. For the permeation experiments, 500 mg of the gel was placed in the formulation compartment and iontophoretic delivery was compared with that from an aqueous buffered solution using 0.5 mA/cm^2 after 6 h. The gels were kept at room temperature for 1 month to test their stability and to detect any drug precipitation.

2.4.5 Data analysis

The total iontophoretic flux (J_{tot}) of PRAM, was considered to be the sum of the fluxes due to passive delivery ($J_{Passive}$), EM (J_{EM}) and EO (J_{EO}), where J_{EO} was defined as the product of the concentration of PRAM (C_{PRAM}) and the linear velocity of the solvent flow (V_W). The latter was calculated from the ratio of the flux of acetaminophen (J_{ACE}) to its concentration (C_{ACE}) in the formulation [15]. For convenience, it was assumed that flux due to passive delivery was negligible and thus ignored from the calculation. The inhibition factor (*IF*) is given by the ratio

$Q_{ACE,Control}$ / $Q_{ACE,Drug}$ where $Q_{ACE,Control}$ and $Q_{ACE,Drug}$, represent respectively the cumulative permeation of ACE in 6 h, in the absence and presence of PRAM.

2.5 *In vivo* studies

Male Wistar rats (260–280 g) were used and the protocol was approved by the Ethics Committee of the Animal Experimental Research Centre at the University of Valencia (Valencia, Spain). Twenty four hours before the iontophoresis experiments, the rats were anaesthetised by intraperitoneal administration of pentobarbital sodium (Dolethal solution, 40 mg/kg; Vetoquinol, Madrid, Spain). The jugular vein was cannulated using medical-grade silicon tubing (Silastic, Dow Corning Co.; ID 0.5 mm; OD 0.94 mm). Under anaesthesia, 3.4 cm of the cannula was introduced into the jugular vein toward the heart and the free end emerged from the dorsal base of the neck. The cannula was permanently filled with heparinized saline solution (20 IU/ml) and closed with a polyethylene plug.

The following day, four animals were anaesthetised and mounted on a plastic support. Two glass chambers (A = 0.78 cm^2) were then placed 2.5 cm apart on the animal's abdomen (shaved beforehand) and fixed with glue. The anode was separated from the donor compartment by means of a salt bridge. The anodal and cathodal compartments contained PBS buffer (pH 7.4). The PRAM formulation (20 mM in 25 mM MES; pH 5.3) was placed in the donor compartment. A power supply (Kepco APH 1000 M; Flushing, NY) delivered a constant, direct current of 0.5 mA/cm^2 for 5 h. Blood samples (0.8 ml) were withdrawn at hourly intervals in pre-heparinized tubes and immediately centrifuged at 10,000 rpm; the plasma collected was separated and stored at -20 ºC until analysis by HPLC. After the withdrawal of each sample, the blood volume was replaced with the same volume of saline solution. At the end of each experiment, the animals were euthanized with pentobarbital sodium.

Pharmacokinetic parameters – the volume of distribution (V_d) and the elimination rate constant (K) of PRAM in the rat were determined after intravenous (IV) administration. For these experiments, 1 mg of PRAM was injected intravenously via the cannulated jugular vein in conscious rats. Blood samples were collected at 20, 40, 60, 90 and 120 min; the plasma collected was separated and stored at -20 ºC until analysis.

2.6 HPLC analysis

A P680A LPG-4 pump equipped with an ASI-100 autosampler and a UV170U detector (Dionex; Voisins LeBretonneux, France) was used to quantify PRAM permeation and skin deposition in the *in vitro* experiments. Isocratic separation was performed using a 125 mm x 4 mm LiChrospher® C_{18} column packed with 5 µm end-capped silica reversed-phase particles. The flow rate and injection volume were 1.0 ml/min and 25 µl, respectively; the column temperature was maintained at 30˚C. The mobile phase comprised 65:35 (% v/v) MeOH / phosphate buffer (20 mM K_2HPO_4, pH 9.2) and PRAM was assayed by using its UV absorbance at 262 nm. The LOD and LOQ were 50 and 75 ng/ml, respectively. ACE was analyzed separately using the same column. The mobile phase consisted of 80% methanol and 20% citrate buffer (10 mM citric acid and 7 mM sodium citrate, pH 3.0). The flow rate was 1.0 ml/min and the column temperature was maintained at 30°C. ACE was detected by its UV absorbance at 220 nm. The LOD and LOQ were 400 and 500 ng/ml, respectively.

Table 1 Precision and accuracy for the analytical method used to quantify PRAM in plasma

Theoretical concentration (ng/ml)	**Experimental concentration (ng/ml)**	**CV (%)[a]**	**Accuracy (%)[b]**
Intra-day (n=3)			
75	73.69	6.01	98.26
500	474.28	9.89	94.96
1000	1032.47	6.40	103.25
Inter-day (n=3)			
75	69.49	2.74	92.65
500	513.14	10.72	102.63
1000	969.55	0.58	96.96

[a] Precision = (S.D./mean) x 100
[b] Accuracy = (obtained concentration/theoretical concentration) x 100

Quantification of PRAM in the plasma samples from the *in vivo* studies was performed using the same HPLC system. Isocratic separation was performed on a Phenomenex®, Jupiter, C_4 150 mm x 4.60 mm column packed with 5 µm particles. The mobile phase consisted of 10% acetonitrile and 90% buffer, which was prepared by dissolving 10.2 g potassium dihydrogenphosphate, 10.2

g sodium acetate, and 4.5 g heptanesulfonic acid sodium salt in 3 l of water and adjusting the pH to 3.5 with acetic acid. The flow rate and column temperature were 1.0 ml/min and 30ºC, respectively. A liquid-liquid extraction method was used to extract PRAM from the plasma samples [16]. Calibration standards were processed by adding 50 µl of internal standard (Selegiline) working solution to 500 µl of plasma, 75 µl of 1 M sodium hydroxide, 3 ml of diethyl ether, into polypropylene tubes. The tubes were capped and mixed on a vortex mixer for 5 minutes, and centrifuged at 5,000 rpm for 10 minutes. The aqueous layer was frozen in a dry ice-acetone bath, the organic layer was transferred to a clean tube and back-extracted with 400 µl mobile phase (ACN:Buffer; 10:90). The aqueous layer was then frozen in a dry ice-acetone bath and the organic layer was discarded. Any residual organic solvent was removed by briefly blowing under nitrogen. The injection volume used was 75 µl. The calibration range was 75-5000 ng/ml. The LOD and LOQ were 60 and 75 ng/ml, respectively and the method was validated for accuracy and precision and shown in Table 1.

2.7 Pharmacokinetic models

All pharmacokinetic parameters for the IV and iontophoretic delivery of PRAM were calculated using WinNonlin (Version 6.2.1) (Pharsight, Inc., NC). The plasma concentration versus time profile after IV injection was analysed using a one-compartment model, and the elimination rate constant (K) and volume of distribution (V_d) calculated. For the iontophoretic delivery studies with of PRAM, plasma levels were calculated using a constant input model [17] and time-variant model [18].

The constant input model is given by:

$$C_P = \left(\frac{K_{input}}{V_d\ K}\right) * (1 - e^{-K t}) \tag{1}$$

where C_P is the plasma concentration of PRAM at time (t), V_d is the volume of distribution, k_{input} is the input rate and K is the elimination rate constant.

The time-variant input model is described by:

$$C_P = \frac{\frac{I_0(K_R - K + ke^{-K_R t})}{K(K_R - K)} - \frac{I_0 K_R}{k(K_R - K)}\ e^{-Kt}}{V_d} \tag{2}$$

where C_P is the plasma concentration of PRAM at time (t), I_0 is the zero-order mass transport rate, K_R is the constant describing the first-order release rate of PRAM from skin into the plasma, K is the elimination rate constant and V_d is the volume of distribution.

Plasma profiles were fitted using a Gauss–Newton algorithm with a Levenberg–Hartley modification. $AUC_{0\text{-}300}$ was calculated in MS Excel and the cumulative amount of PRAM delivered was calculated by a deconvolution method.

2.8 Data analysis

Data were expressed as the Mean ± S.D. Outliers determined using the *Grubbs test* were discarded. Results were evaluated statistically using either analysis of variance (*ANOVA*) followed by *Student Newman Keuls test* or by *Student's t-test*. The level of significance was fixed at α=0.05.

3. RESULTS AND DISCUSSION

3.1 Stability studies in presence of skin and electric current

PRAM was stable in the presence of porcine epidermis and dermis after exposure for 12 h. However, PRAM showed significant degradation in the presence of current after 6 h. The average recovery of PRAM after exposure to current (0.5 mA/cm^2) for 6 h was 60.2 ± 5.3%. In order to increase stability and prevent this degradation, an antioxidant (sodium metabisulfite) at a concentration of 0.5% (26 mM) was added to the donor compartment. It is known that PRAM is susceptible to photodegradation and some of the products have recently been identified [19]. The addition of sodium metabisulfite was extremely effective in preventing the oxidation of PRAM and the stability in the presence of current and skin was substantially increased to 97.2 ± 3.1% after 12 h. Thus, sodium metabisulfite (0.5%) was added to all formulations used in the *in vitro* and *in vivo* studies.

3.2 Effect of iontophoretic parameters on PRAM electrotransport *in vitro*

Control experiments showed that passive permeation of PRAM from aqueous solution (20 mM in 25 mM MES, pH 5.3) after 6 h was 10.2 ± 4.6 µg/cm^2. The cumulative anodal iontophoretic permeation and steady state flux for PRAM as a function of current density (0.1, 0.3 and 0.5

mA/cm^2) using the same formulation was significantly higher (Figure 2). Increasing the current density from 0.1 to 0.3 and 0.5 mA/cm^2, resulted in 2.5- and 4-fold increases in cumulative permeation, from 309.5 ± 80.2 to 748.8 ± 148.1 and 1229.1 ± 138.6 µg/cm^2; respectively. The steady state flux showed corresponding 2.6- and 4-fold increases from 0.1 to 0.3 and 0.5 mA/cm^2. Regression analysis confirmed that the increase in steady state flux was linear (r^2 = 0.98). Current application at 0.1 to 0.3 and 0.5 mA/cm^2 afforded 30-, 73- and 120-fold enhancements over passive delivery. The ability to control drug transport kinetics through modulation of current density is very advantageous for dopamine agonists used to treat PD. As the disease advances, dose escalation is required; in the case of PRAM, the dose is gradually titrated from 0.25 to 1.25 mg. This increase in dose can be easily achieved by increasing the current intensity without any change in size of patch or drug loading as required for passive transdermal delivery systems. Skin deposition also showed appreciable increases from 138.1 ± 30.1, to 195.2 ± 44.3 and 275.8 ± 48.6 µg/cm^2 as the current density was ramped from 0.1 to 0.3 and 0.5 mA/cm^2, respectively. These values suggest that PRAM forms a depot in the different layers of skin and even after the termination of current there would be release of the therapeutic from the skin into the systemic circulation.

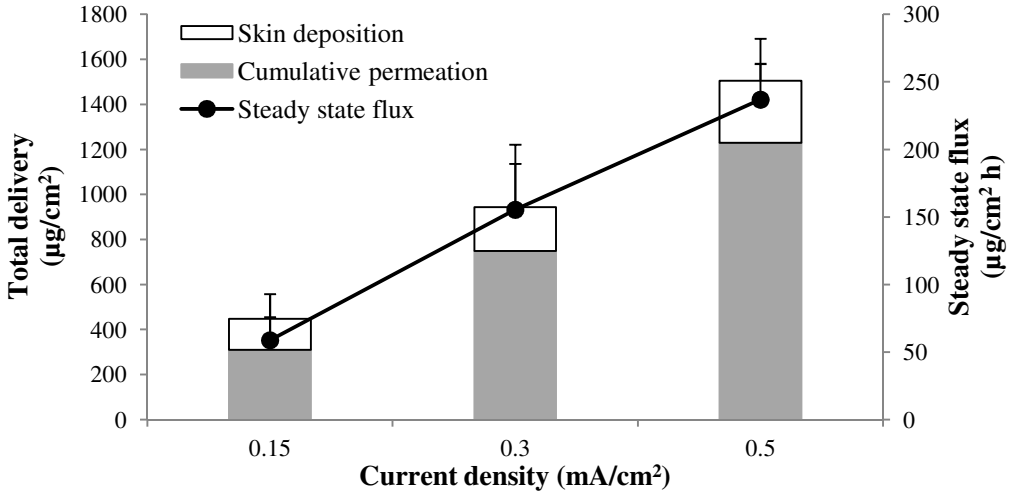

Figure 2. Total delivery (cumulative permeation + skin deposition) and steady state flux of PRAM (20 mM in 25 mM MES, pH 5.3) as a function of current density (at 0.15, 0.3 and 0.5 mA/cm^2) across porcine skin after 6 h of transdermal iontophoresis. (Mean ± S.D.; n≥5).

Table 2 Iontophoretic transport kinetics of PRAM and the relative contributions of electromigration and electroosmosis

Current (mA/cm^2)	J_{tot} ($\mu g/cm^2$ h)	J_{EM} ($\mu g/cm^2$ h)	J_{EO} ($\mu g/cm^2$ h)	% EM	% EO	Inhibition factor
0.15	58.3 ± 17.1	48.6	10.2	82.6	17.4	1.13
0.3	155.4 ± 48.2	137.6	17.8	88.5	11.5	1.01
0.5	236.9 ± 26.5	220.9	16.0	93.2	6.8	0.88

J_{tot}: Total steady-state flux, J_{EM}: Electromigration contribution, J_{EO}: Electroosmotic contribution.

Co-iontophoresis of ACE enabled deconvolution of the individual contributions of EM and EO to PRAM electrotransport [20]. Control values for ACE flux in the absence of PRAM were determined independently at each current density. It was shown that EM was the dominant transport mechanism accounting for > 83% of PRAM delivery at the current densities studied (Table 2). PRAM is a primary amine with a pKa of 9.6 indicating that it is essentially completely ionized at the experimental pH. ACE transport and the derived IF values, which ranged between 0.88-1.13, confirmed that PRAM did not affect skin permselectivity through interaction and neutralization of fixed negative charges. In addition to being conducive for electrotransport by EM, given the degree of PRAM ionization, the formulation pH which was approximately equal to the skin pH, minimized the risk of pH-induced irritation.

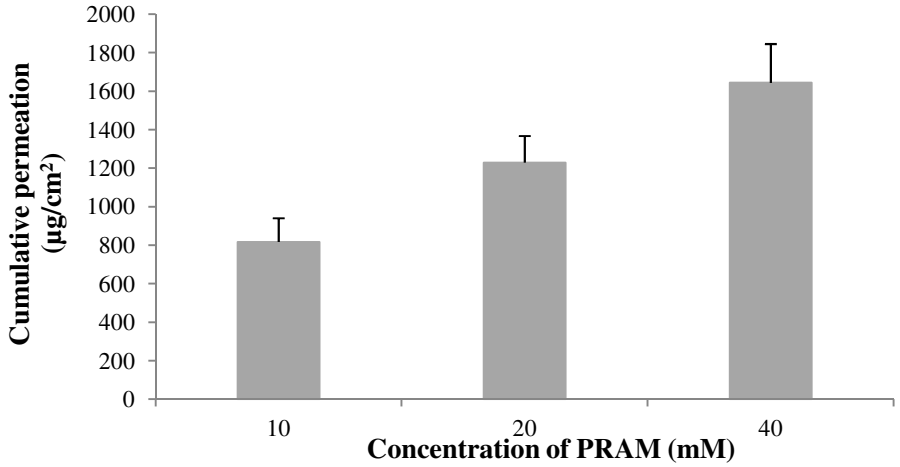

Figure 3. Cumulative permeation of PRAM as a function of concentration (10, 20 and 40 mM in 25 mM MES, pH 5.3) at 0.5 mA/cm^2 for 6 h. (Mean ± S.D.; n≥5).

Cumulative permeation of PRAM after iontophoresis at 0.5 mA/cm^2 for 6 h at drug concentrations of 10, 20 and 40 mM was 816.4 ± 123.3, 1229.1 ± 138.6 and 1643.6 ± 201.3 µg/cm^2; respectively (Figure 3). Proportionality between permeation and concentration is usually observed when competing co-ions are present in the donor solution [21,22]. The use of salt bridges usually avoids the presence of competing Na^+ ions in the donor compartment (present since NaCl is routinely used as a source of Cl^- which is required for the electrochemical reaction at the Ag anode) but the presence of sodium metabisulfite (as antioxidant, 0.5% = 26 mM) introduced Na^+ ions into the formulation that competed with PRAM to carry the current. A validation study confirmed that cumulative permeation of PRAM (20 mM) across porcine and human skin after iontophoresis was statistically equivalent (1229.1 ± 138.6 and 1184.8 ± 236.4 µg/cm^2, respectively) (Figure 4).

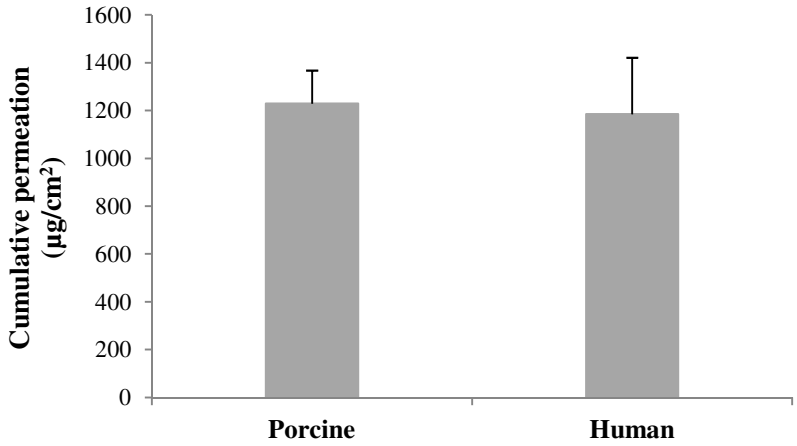

Figure 4. Comparing cumulative permeation of PRAM (20 mM; 25 mM MES, pH 5.3) after 6 h iontophoresis at 0.5 mA/cm^2 across porcine and human skin. (Mean ± S.D.; n≥5).

The preliminary feasibility studies described above were performed using aqueous buffered solutions because of the ease of preparation. However, transdermal iontophoretic devices for clinical use are microprocessor systems containing a drug reservoir in a polymeric matrix. Hence, a carbopol based semisolid hydrogel formulation of PRAM was developed that could be easily used as a drug reservoir in a patch system and provide sufficient rigidity for adhering to the skin surface. The gel formulation was stable and there were no signs of drug precipitation after 1 month and the PRAM content was found to be uniform (98.2 ± 3.5%). Furthermore, the pH of the gel was 6.5 indicating its suitability for electrotransport by EM and for use in clinical

studies. Total iontophoretic delivery after 6 h at 0.5 mA/cm^2 with the gel and aqueous buffered solution (10 mM in 25 mM MES, pH 5.3) was 910.4 ±187.9 and 1084.8 ± 178.8 µg/cm^2; respectively (Figure 5). The 10 mM solution contained 2.11 mg of PRAM content of while the 0.7% loading of PRAM in the gel meant that 500 mg of gel contained 2.44 mg of PRAM. Therefore, approximately 77% of the PRAM in solution and 58% of the drug in the gel were delivered. The statistically significant difference in delivery was assumed to be due to a retarding effect of the polymeric non-liquid nature of the carbopol matrix.

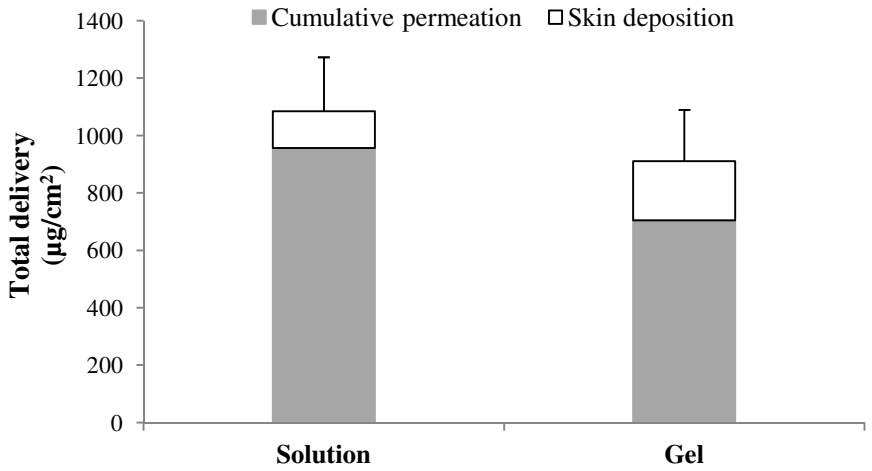

Figure 5. Comparison of total delivery (cumulative permeation + skin deposition) of PRAM from aqueous solution (10 mM in 25 mM MES, pH 5.3) and a carbopol gel (0.7% w/w, PRAM) across porcine skin at 0.5 mA/cm^2 for 6 h. (Mean ± S.D.; n≥5).

The transport number is defined as the fraction of the total charge transported by a specific ion during iontophoresis. The sum of the transport numbers of all of ions acting as charge carriers in the system (on both sides of the skin) must be equal to unity [23]. For a positively charged drug, in the absence of competing cations, the majority of current is carried by Cl^- from the receiver compartment. The presence of sodium metabisulfite in the donor compartment introduced Na^+ that entered into competition with PRAM to carry current reduced its transport efficiency. Considering all these aspects, the transport efficiency of PRAM was relatively high (Figure 6).

The delivery efficiency is defined as the ratio of the amount permeated to the amount in the formulation placed in the donor compartment. These values range from 14 to 58% for PRAM

(20 mM in in 25 mM MES, pH 5.3) after 6 h iontophoresis which are high given the presence of a highly mobile small cation such as Na^+. Based on these results, PRAM, a hydrophilic cation, which would otherwise be difficult to deliver through skin passively, is an excellent candidate for iontophoretic administration. These results illustrate that high delivery efficiencies can be achieved by energy driven processes such as iontophoresis and rebut the argument that transdermal formulations have poor efficiency *per se*.

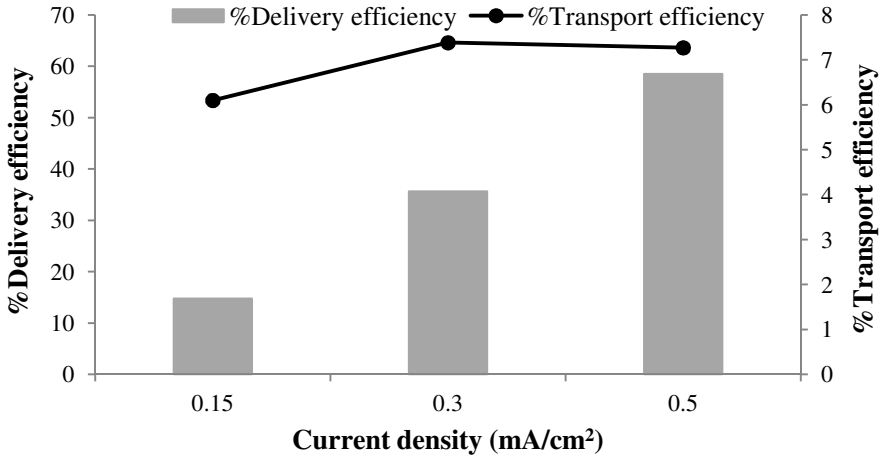

Figure 6. Delivery and transport efficiencies of PRAM after 6 h iontophoresis at current densities of 0.15, 0.3 and 0.5 mA/cm^2 at a concentration of 20 mM in 25 mM MES (pH 5.3).

3.3 Delivery kinetics in rats *in vivo*

Plasma concentrations of PRAM following IV administration were fitted using first-order elimination kinetics to derive the volume of distribution, V_d, and the elimination rate constant, K (Figure 7 and Table 3). The mean plasma concentrations of PRAM during iontophoretic current application were fitted using constant input and time-variant input model (Figure 8). The goodness of the fit was superior for the time-variant input model. It was clear that the time-variant model provided a better prediction of PRAM plasma concentrations and there was an excellent convergence to the data during the iontophoretic period. The ability of a compartmental model such as the time-variant model to simulate accurately the drug concentrations in the blood can be very useful for modelling and predicting concentrations after multiple dosing using iontophoresis, which is closer to clinical reality [18]. For PRAM, where the dose is titrated according to individual patient requirements, it may be possible to simulate

drug levels using this model to determine the necessary iontophoretic conditions required to achieve therapeutic concentrations of the drug over time. Such a model can also help to design an iontophoretic system where the drug is delivered on a need basis with complex drug input kinetics using fewer shorter application periods and thereby reducing the risk of skin irritation. It should be noted that no macroscopic changes such as erythema were observed on the skin of animals after removal of the donor compartment.

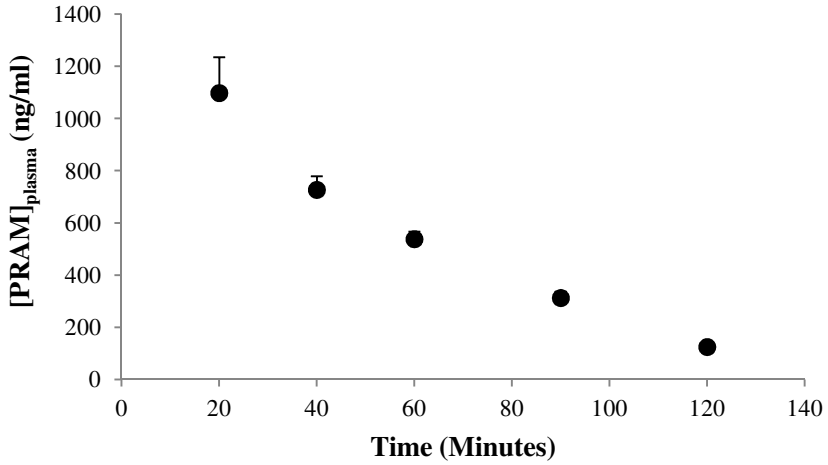

Figure 7. Plasma concentration of PRAM after IV administration at a dose of 1 mg. (Mean ± S.D.; n = 4).

The calculated transdermal absorption rate *in vivo* was 2- (constant input model) and 2.4- fold (time-variant input model) times higher than that observed *in vitro* across porcine skin (Table 3). Although porcine skin was used for the *in vitro* experiments and male Wistar rats the animal model for the *in vivo* studies performed, the prediction *a priori* of the effect of interspecies differences on electrotransport is not straightforward. For example, in previous studies, iontophoresis of granisetron and metoclopramide was lower in rats *in vivo* than across porcine skin *in vitro* [17,24]; in contrast, iontophoretic delivery of dexamethasone sodium phosphate was the same [25]. The relationship is also certainly influenced by the molecular properties of the permeant. Other studies have shown that transdermal fluxes were higher *in vivo* than a those observed *in vitro*, this was reported for hydromorphone, granisetron and naloxone [26,27,28]. It has been suggested that the lack of active microvasculature *in vitro* results in inefficient removal of the drug depot formed in the skin. Dermal blood supply has been found to play a significant role in the systemic and underlying tissue solute absorption during iontophoretic delivery, which

could explain the faster drug clearance from the skin depot by the cutaneous microcirculation *in vivo* [29,30]. It has also been hypothesized that the epidermal concentration of Na^+ and Cl^- ions *in vivo* within the transport pathway is lower than physiological saline (133 mM) which is generally used in the receptor compartment, it was reported that the best *in vitro-in vivo* correlations were observed with NaCl concentration of 90-100 mM [31]. Hence, the blood flow might affect the transport of endogenous ions from the dermis to the epidermis and *vice-versa* thereby changing the ionic composition of the different skin layers. These changes in ion concentration could impact drug electrotransport since there would be less competition *in vivo* than *in vitro*.

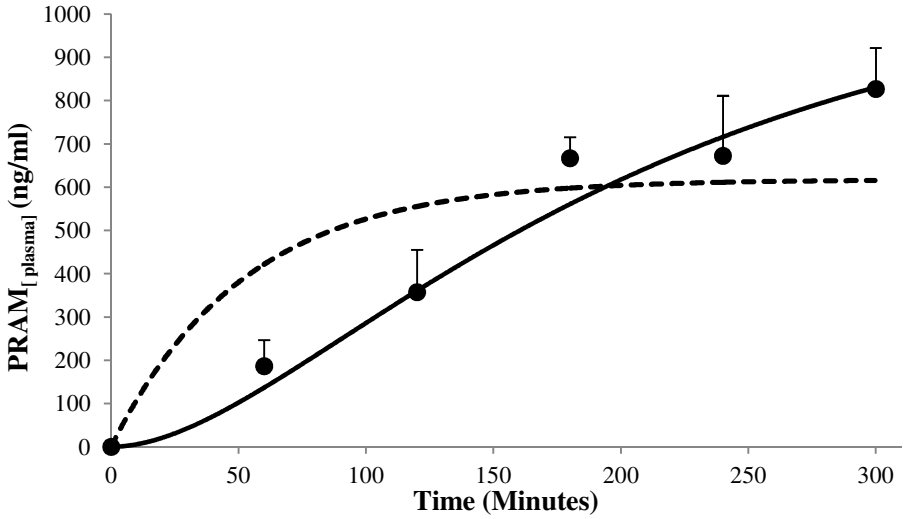

Figure 8. The observed plasma PRAM concentration vs. time profile in rats after iontophoretic administration for 5 h at 0.5 mA/cm^2 and the fits obtained using the constant input (dashed line) and time-variant input (solid line) models . (Mean ± S.D.; n = 4).

The total amount of drug delivered *in vivo* was calculated by deconvolution and was 1426 µg. PRAM pharmacokinetics obey a one-compartment model in humans [32]; extrapolation using human pharmacokinetic parameters (V_d 486 L and K = 0.693/$t_{1/2}$) and the input rate i*n vivo* observed in the present study (Table 3) was used to estimate the feasibility of achieving therapeutic delivery in humans. The calculations suggested that PRAM plasma concentrations of 2.16 to 5.22 ng/ml could be achieved after iontophoretic administration at 0.5 mA/cm^2 for 3 h using a 2 cm^2 patch. For comparison, the C_{min} and C_{max} of PRAM in humans was reported to be

in the range of 0.39–7.17 ng/ml [32]. Therefore, constant current anodal iontophoresis can attain therapeutic blood concentrations of PRAM with reasonable patch sizes and at acceptable current densities.

Table 3 Pharmacokinetic parameters estimated from plasma concentration – time profiles following iontophoretic administration of PRAM; fits obtained using constant input and time-variant input models

Parameters	Constant input model	Time-variant model
Input rate *in vivo* (ng/min)[a]	6514.6 ± 681.2[b]	7666.1 ± 821.2[c]
Input rate *in vivo* (mg/h)	0.39 ± 0.04	0.46 ± 0.05
K_R (1/h)		0.59 ± 0.33
V_d (L)[d]	0.627	
K (1/min)[e]	0.019	
In vitro input rate (ng/min)[f]	3190.7 ± 237.3	
In vitro input rate (mg/h)	0.19 ± 0.01	
C_{max} (ng/ml)	827.1 ± 94.8	
$AUC_{0\text{-}300}$ (µg.h/ml)	139.7 ± 12.6	

[a] Input rate calculated for a current application area of 0.78 cm^2
[b] K_{input} as per equation 1
[c] I_0 as per equation 2
[d] Volume of distribution calculated from IV administration
[e] Elimination rate constant calculated from IV administration
[f] porcine ear skin; input rate calculated for a current application area of 0.78 cm^2

4. CONCLUSION

The results confirm that PRAM is an excellent candidate for transdermal iontophoresis. Constant current anodal iontophoresis was used to achieve current- and concentration-proportional transdermal delivery of PRAM with no significant difference between porcine and human skin. Electrotransport was governed by EM with negligible EO inhibition. High transport and delivery efficiencies were achieved for PRAM using a carbopol gel. A subsequent *in vivo* study using rats, suggested that the transdermal absorption rate would be sufficient to maintain therapeutically relevant blood concentrations of PRAM for the management of PD. In addition to PD, this approach could also be explored for Restless Leg Syndrome.

Reference

[1] C. Lundqvist, Continuous levodopa for advanced Parkinson's disease, Neuropsychiatr. Dis. Treat. 3 (2007) 335–348.

[2] C.W. Olanow, J.A. Obeso, F. Stocchi, Continuous dopamine receptor treatment of Parkinson's disease: scientific rationale and clinical implications, Lancet Neurol. 5 (2006) 677–687.

[3] M.F. Piercey, Pharmacology of pramipexole, a dopamine D3-preferring agonist useful in treating Parkinson's disease, Clin. Neuropharmacol. 21 (1998) 141-151.

[4] C.W. Olanow, M.B. Stern, K. Sethi, The scientific and clinical basis for the treatment of Parkinson disease, Neurology 72 (2009) S1-136.

[5] M. Horstink, E. Tolosa, U. Bonuccelli, G. Deuschl, A. Friedman, P. Kanovsky, J.P. Larsen, A. Lees, W. Oertel, W. Poewe, O. Rascol, C. Sampaio, Review of the therapeutic management of Parkinson's disease. Report of a joint task force of the European Federation of Neurological Societies and the Movement Disorder Society-European Section. Part I: early (uncomplicated) Parkinson's disease, Eur. J. Neurol. 13 (2006) 1170-1185.

[6] M.A. Picchietti, D.L. Picchietti, Restless legs syndrome and periodic limb movement disorder in children and adolescents, Semin. Pediatr. Neurol. 15 (2008) 91-99.

[7] A. Antonini, P. Barone, R. Ceravolo, G. Fabbrini, M. Tinazzi, G. Abbruzzese, Role of Pramipexole in the Management of Parkinson's Disease, CNS Drugs 24 (2010) 829-841.

[8] T.M. Engber, Z. Susel, J.L. Juncos, T.N. Chase, Continuous and intermittent levodopa differentially affect rotation induced by D-1 and D-2 dopamine agonists, Eur. J. Pharmacol. 168 (1989) 291-298.

[9] M.M. Mouradian, I.J. Heuser, F. Baronti, T.N. Chase, Modification of central dopaminergic mechanisms by continuous levodopa therapy for advanced Parkinson's disease, Ann. Neurol. 27 (1990) 18-23.

[10] W.M. Guldenpfennig, K.H. Poole, K.W. Sommerville, B. Boroojerdi, Safety, tolerability, and efficacy of continuous transdermal dopaminergic stimulation with rotigotine patch in early-stage idiopathic Parkinson disease, Clin. Neuropharmacol. 28 (2005) 106-110.

[11] C.W. Olanow, Movement disorders: a step in the right direction, Lancet Neurol. 5 (2006) 3-5.

[12] B. Boroojerdi, H.M. Wolff, M. Braun, D.K.A. Scheller, Rotigotine transdermal patch for the treatment of parkinson's disease and restless legs syndrome, Drugs Today 46 (2010) 483-505.

[13] M. Fargel, B. Grobe, E. Oesterle, C. Hastedt, M. Rupp, Treatment of Parkinson's Disease: A Survey of Patients and Neurologists, Clin. Drug Investig. 27 (2007) 207-218.

[14] Y. Naidu, K.R. Chaudhuri, Transdermal rotigotine: a new non-ergot dopamine agonist for the treatment of Parkinson's disease, Expert Opin. Drug Deliv. 4 (2007) 111-118.

[15] Y.N. Kalia, A. Naik, J. Garrison, R.H. Guy, Iontophoretic drug delivery, Adv. Drug Deliv. Rev. 56 (2004) 619-658.

[16] Y.Y. Lau, G.D. Hansona, N. Ichhpurani, Determination of pramipexole (U-98,528) in human plasma and urine by high-performance liquid chromatography with electrochemical and ultraviolet detection, J. Chrom. B Biomed. Appl. 683 (1996) 217-223.

[17] J. Cázares-Delgadillo, A. Ganem-Rondero, D. Quintanar-Guerrero, A.C. López-Castellano, V. Merino, Y.N. Kalia, Using transdermal iontophoresis to increase granisetron delivery across skin in vitro and in vivo: Effect of experimental conditions and a comparison with other enhancement strategies, Eur. J. Pharm. Sci. 39 (2010) 387–393.

[18] A.K. Nugroho, O. Della-Pasqua, M. Danhof, J.A. Bouwstra, Compartmental Modeling of Transdermal Iontophoretic Transport II: In Vivo Model Derivation and Application, Pharm. Res. 22 (2005) 335-346.

[19] E. Nishimura, A. Kugimiya, H. Naoki, N. Hamanaka, Photo-degradation products of pramipexole, Bioorg. Med. Chem. Lett. 22, (2012) 2951-2953.

[20] N. Abla, A. Naik, R.H. Guy, Y.N. Kalia, Effect of charge and molecular weight on transdermal peptide delivery by iontophoresis, Pharm. Res. 22 (2005) 2069-2078.

[21] S. Thysman, C. Tasset, V. Preat, Transdermal iontophoresis of fentanyl: delivery and mechanistic analysis, Int. J. Pharm. 101 (1994) 105–113.

[22] L. Wearly, J.C. Liu, Y.W. Chien, Iontophoresis facilitated transdermal delivery of verapamil II. Factors affecting the skin permeability, J. Control. Release 9 (1989) 231–242.

[23] N.H. Bellantone, S. Rim, M.L. Francoeur, B. Rasadi, Enhanced Percutaneous-Absorption Via Iontophoresis .1. Evaluation of an In vitro System and Transport of Model Compounds, Int. J. Pharm. 30 (1986) 63-72.

[24] J. Cázares-Delgadillo, I.B. Aziza, C. Balaguer-Fernández, A. Calatayud-Pascual, A. Ganem-Rondero, D. Quintanar-Guerrero, A.C. López-Castellano, V. Merino, Y.N. Kalia, Comparing metoclopramide electrotransport kinetics in vitro and in vivo, Eur. J. Pharm. Sci. 41 (2010) 353–359.

[25] J. Cázares-Delgadillo, C. Balaguer-Fernández, A. Calatayud-Pascual, A. Ganem-Rondero, D. Quintanar-Guerrero, A.C. López-Castellano, V. Merino, Y.N. Kalia, Transdermal iontophoresis of dexamethasone sodium phosphate in vitro and in vivo: Effect of experimental parameters and skin type on drug stability and transport kinetics, Eur. J. Pharm. Biopharm. 75 (2010) 173–178.

[26] A. Chaturvedula, D.P Joshi, C. Anderson, R. Morris, W.L. Sembrowich, A.K. Banga, Dermal, subdermal, and systemic concentrations of granisetron by iontophoretic delivery, Pharm. Res. 22 (2005) 1313–1319.

[27] R. Yamamoto, S. Takasuga, Y. Yoshida, S. Mafune, K. Kominami, C. Sutoh, Y. Kato, M. Yamauchi, M. Ito, K. Kanamura, M. Kinoshita, In vitro and in vivo transdermal iontophoretic delivery of naloxone, an opioid antagonist, Int. J. Pharm. 422 (2012) 132–138.

[28] R.V. Padmanabhan, J.B. Phipps, G.A. Lattin, R.J. Sawchuk, In vitro and in vivo evaluation of transdermal iontophoretic delivery of hydromorphone, J. Control. Release 11 (1990) 123–135.

[29] S.E. Cross, M.S. Roberts, Importance of dermal blood supply and epidermis on the transdermal iontophoretic delivery of monovalent cations, J. Pharm. Sci. 84 (1995) 584–592.

[30] Y. Dancik, Y.G. Anissimov, O.G. Jepp, M.S. Roberts, Convective transport of highly plasma protein bound drugs facilitates direct penetration into deep tissues after topical application, Br. J. Clin. Pharmacol. 73 (2011) 564–578.

[31] J.B. Phipps, J.R. Gyory, Transdermal Ion Migration. Adv. Drug Deliv. Rev. 9 (1992) 137-176.

[32] C.E. Wright, T.L. Sisson, A.K. Ichhpurani, G.R. Peters, Steady-state pharmacokinetic properties of pramipexole in healthy volunteers, J. Clin. Pharmacol. 37 (1997) 520-525.

Chapter 4

Anodal co-iontophoresis for the simultaneous transdermal delivery of pramipexole (dopamine agonist) and rasagiline (MAO-B inhibitor) for more effective treatment of Parkinson's Disease

Dhaval R. Kalaria[a], Vandana Patravale[b] Virginia Merino[c] and Yogeshvar N. Kalia[a]

[a]School of Pharmaceutical Sciences,
University of Geneva & University of Lausanne,
30 Quai Ernest Ansermet,
1211 Geneva, Switzerland

[b]Department of Pharmaceutical Sciences and Technology,
Institute of Chemical Technology,
Mumbai 400019, India

[c] Departamento de Farmacia y Tecnología Farmacéutica,
Faculty of Pharmacy, University of Valencia,
Avda.Vicente Andrés Estellés s/n, 46100 Burjassot, Valencia, Spain

Abstract

Clinical therapy of Parkinson's disease (PD) involves administration of therapeutic agents with complementary mechanisms of action in order to replenish, sustain or substitute endogenous dopamine. The objective of this study was to investigate the anodal co-iontophoretic delivery of pramipexole (PRAM; dopamine agonist) and rasagiline (RAS; MAO-B inhibitor) across the skin. Preliminary *in vitro* studies to determine the effect of experimental parameters on co-iontophoretic transport of both drugs were performed using porcine and human skin. Passive permeation of PRAM and RAS (20 mM each) after 6 h was 15.7 ± 1.9 and 16.0 ± 2.9 μg/cm^2, respectively. Iontophoretic current application and increasing current density from 0.1 to 0.3 and 0.5 mA/cm^2 resulted in statistically significant increase in fluxes for PRAM and RAS. At 0.5 mA/cm^2, cumulative permeation of PRAM and RAS was 613.5 ± 114.6 and 441.1 ± 169.2 μg/cm^2, respectively – corresponding to 38- and 27-fold increases over passive diffusion. Higher electrotransport of PRAM was tentatively attributed to its greater hydrophilicity as indicated by computational analysis. Electromigration was the dominant mechanism for both molecules (> 82%) and there was no effect on convective solvent flow. Electrotransport of each molecule was dependent on its respective concentration (also mole fraction) in the formulation and this offered a simple method to design an optimized system based on the posology of the two therapeutics. The co-iontophoretic system showed high delivery efficiency (PRAM: 29% and RAS: 35%). Preliminary pharmacokinetics studies in rats showed that drugs could be detected within 30 minutes in plasma implying a rapid input kinetics. The predicted *in vivo* input rate using the time-variant model for PRAM and RAS was found to be 294.2 ± 39.8 and 160.5 ± 19.3 μg/h, respectively. These results showed that therapeutic amounts of the two anti-Parkinson drugs could be co-administered by transdermal iontophoresis.

Key words: iontophoresis, transdermal route, dopamine agonist, MAO-B inhibitors, patient compliance

1. Introduction

Parkinson's disease (PD) is the second most prevalent neurodegenerative disease; it is characterized by symptoms of tremor, rigidity and bradykinesia [1,2]. Levodopa is considered to be the most effective agent for the treatment of PD although clinical and pathologic studies have shown that it cannot slow disease progression [3]. However, the development of motor complications (e.g., on-off effect, dyskinesia) can impact its long term use. Therefore, dopamine agonists including ergot and non-ergot agents are prescribed in early stages of disease and levodopa is added as a complementary therapy when dopamine agonist monotherapy is no longer able to provide satisfactory clinical outcomes [4]. Pramipexole (PRAM) is a non ergot dopamine agonist approved for the treatment of PD since 1997 and is the most widely prescribed dopamine agonist, both as monotherapy and as an adjunctive therapy with L-DOPA [5,6]. Another class of drugs effective in PD are inhibitors of monoamine oxidase B (MAO-B), an enzyme that regulates metabolism of catecholamine neurotransmitters (e.g., dopamine) [7,8]. Rasagiline (RAS) is an irreversible dose dependent MAO-B inhibitor that also exhibits neuroprotective effects [9]. PRAM and RAS have complementary mechanisms of action and several studies have shown clinical improvements in symptoms and quality of life for patients when they are used together [10,11].

The mean intake of tablets for advanced PD patients is estimated to be 9.9 tablets per day corresponding to ~3600 tablets per year [12]. Moreover, given its short half-life, PRAM has to be administered thrice daily which is a particular inconvenience for PD patients. Drowsiness and cognitive impairment along with a rigorous dosing regimen impose a strain on the patient's life and mean an extra workload for care-givers. It is therefore not surprising that patients' principal request for improvement in treatment relates to the reduction in daily tablet intake and this opinion is shared by physicians. Furthermore, patients can have swallowing difficulties and the high tablet burden can lead to non-compliance and contribute to reduced therapeutic efficacy.

Transdermal drug delivery systems offer a promising alternative to oral administration for chronically ill patients especially in circumventing difficulties associated with swallowing, and in addition to increasing efficacy can significantly improve quality of life and bring down treatment costs by reducing care-givers' work-load. Transdermal administration of drugs also prevents problems associated with hepatic first-pass metabolism, poor absorption from the gastrointestinal tract and variable bioavailability as observed with RAS. Constant plasma

concentrations may also be achieved as a result of controlled zero order drug input even when the drug has a short elimination half-life thereby reducing peak-trough variations in blood levels. This is of particular relevance for PD therapy since motor fluctuations seen in PD patients are attributed to pulsatile stimulation of dopamine receptors when drugs are given orally [13]. Transdermal administration would provide a continuous "physiologic" stimulation of dopamine receptors and thereby help to reduce these complications [14].

Transdermal patches have been used to deliver selegiline (MAO-B inhibitor) and rotigotine (dopamine agonist) [15,16]. With these systems, plasma concentrations of the drug begin to rise after 4-6 h application and steady states are reached in 12-24 h. This would mean a longer lag phase before achieving a pharmacodynamic effect and also a greater probability of skin irritation due to longer contact time of the patch with the skin. Table 1 shows the physicochemical properties of PRAM and RAS; considering their polar and ionic nature, it would be difficult to achieve the required flux for delivering the therapeutic amounts of either drugs by passive transdermal delivery [17].

Table 1 Comparing physicochemical and pharmacological properties of PRAM and RAS

	PRAM	**RAS**
M_W (Da)	302[b]	267[a]
Aqueous solubility (g/L)	> 20[b]	3.4[a]
pKa	5.0, 9.6	7.2
log P	2.34	1.67
log $D_{pH7.0}$	0.024	1.40
Half life (h)	8-12 h	3
Oral bioavailability	90%	35%
Dosage form	Oral: 0.75-4.5 mg	Oral: 0.5-1 mg
Mechanism of action	Dopamine agonist	MAO-B inhibitor

[a] Mesylate salt; [b] Dihydrochloride salt

In contrast, transdermal iontophoresis can exploit these physicochemical properties to deliver these drugs efficiently through the skin [18]. Iontophoresis involves application of an electric potential across the membrane that will significantly increase the transport rates of ions as compared to passive diffusion. Iontophoresis enables control over drug input kinetics by modulation of current density, which can be a used to increase delivery of therapeutics in

advanced disease state without changing the drug loading or patch size. It can be used to provide highly individualised treatment regimens and hence improve efficacy and patient compliance.

The goal of this work was to investigate the co-iontophoretic delivery of PRAM and RAS, in order to optimize their transdermal administration for the treatment of PD and at the same time demonstrate that iontophoresis could be used as a means to provide controlled transdermal polytherapy. The specific aims of the study were (i) to investigate the effect of experimental parameters on anodal co-iontophoresis of PRAM and RAS in porcine skin *in vitro*, (ii) to deduce the relative contribution of electromigration (EM) and electroosmosis (EO) and so determine the dominant transport mechanism, (iii) to study simultaneous iontophoretic delivery in rats *in vivo* and hence (iv) to evaluate the feasibility of simultaneously delivering therapeutic amounts of the two anti-Parkinson's drugs *in vivo*.

2. Materials and methods

2.1 Materials

Pramipexole dihydrochloride monohydrate and rasagiline mesylate was purchased from Nectar Industrial Co. Ltd (Shenzhen, China) and Jinan Jinao CDC Ltd. (Jinan City, China), respectively. Acetaminophen (ACE), sodium chloride, 2-(*N*-morpholino)-ethanesulfonic acid (MES), sodium metabisulfite, citric acid, sodium hydroxide and sodium citrate were all purchased from Sigma-Aldrich (Buchs, Switzerland). Silver wire and silver chloride used for the fabrication of electrodes were also sourced from Sigma-Aldrich. Potassium dihydrogenphosphate, sodium salt of heptanesulfonic acid and diethyl ether were purchased from Acros Organics (Geel, Belgium). Methanol and PVC tubing (ID 3.17 mm; OD 4.97 mm) were purchased from VWR International (Nyon, Switzerland). All solutions were prepared using deionised water (resistivity > 18 MΩ.cm). All other chemicals were at least of analytical grade.

2.2 Skin source

Porcine ears were obtained from a local abattoir (CARRE; Rolle, Switzerland), the skin was excised (thickness 750 μm) with an air dermatome (Zimmer; Etupes, France), wrapped in Parafilm™ and stored at -20 °C for a maximum period of 1 month. Human skin samples were collected immediately after surgery from the Department of Plastic, Aesthetic and Reconstructive Surgery, Geneva University Hospital (Geneva, Switzerland), fatty tissue was

removed and the skin was wrapped in Parafilm™ before storage at −20 °C for a maximum period of 7 days. The study was approved by the Central Committee for Ethics in Research (CER: 08–150 (NAC08-051); Geneva University Hospital).

2.3 In vitro studies

Skin was clamped in two compartment diffusion cells (area 2 cm^2). After equilibration with phosphate buffered saline (PBS, pH 7.4), 1 ml of buffered formulation containing PRAM and RAS (20 mM each in 25 mM MES pH 5.3 with 26 mM sodium metabisulfite) was placed in the donor compartment. To avoid competition, the anodal and formulation compartments were connected by means of a salt bridge. Acetaminophen (ACE; 15 mM) was included in the formulations to report on electroosmosis (EO) and the effect of cation transport on skin permselectivity. The receptor compartment (which also contained the cathode) was filled with PBS. Samples (0.6 ml) were collected from the receiver compartment hourly and replaced with the same volume of fresh buffer. A constant current density (0.1, 0.3 and 0.5 mA/cm^2) was applied for 6 h via Ag/AgCl electrodes connected to a power supply (APH 1000M; Kepco, Flushing, NY).

In a separate study, formulations containing different concentrations of PRAM and RAS were iontophoresed at 0.5 mA/cm^2 for 6 h to investigate their transport. Five different formulations with the following concentrations were tested: Formulation A (10 mM each), B (20 mM each), C (40 mM each), D (10 mM PRAM and 30 mM RAS) and E (10 mM PRAM and 30 mM RAS).

The total iontophoretic flux (J_{tot}) is the sum of fluxes due to passive delivery ($J_{Passive}$), EM (J_{EM}) and EO (J_{EO}), where J_{EO} is defined as the product of the concentration of drug (C_{DRUG}) and the linear velocity of the solvent flow (V_W), which in turn, is given by the ratio of the flux of acetaminophen (J_{ACE}) to its concentration (C_{ACE}) in the formulation [18]. For convenience, it was assumed that flux due to passive delivery was negligible and thus ignored from the calculation.

The inhibition factor (IF) is given by the ratio $Q_{ACE,Control}$ / $Q_{ACE,Drug}$ where $Q_{ACE,Control}$ and $Q_{ACE,Drug}$, represent the cumulative permeation of ACE in 6 h, in the absence and presence of drug, respectively.

2.4 In vivo studies

Male Wistar rats (280-300 g) were used for the experiments and the study protocol was approved by the Ethics Committee for Animal Experimentation at the University of Valencia (Valencia, Spain). The rats were cannulated 24 h prior to the pharmacokinetics study. The jugular vein was cannulated using medical grade silicon tubing (Silastic, Dow Corning Co.; ID 0.5 mm; OD, 0.94 mm). The cannula was permanently filled with heparinized saline solution (20 IU/ml) and closed with a polyethylene plug.

Immediately prior to the co-iontophoresis experiments, the animals were anesthetized (Dolethal solution, 40 mg/kg) and mounted on a plastic support. Two glass chambers (area 0.78 cm^2) were then placed 2.5 cm apart on the animal's abdomen (shaved beforehand) and fixed with glue. The donor compartment contained 40 mM each of PRAM and RAS solution in 25 mM MES (pH ~5.3 with 26 mM sodium metabisulfite). The anodal compartment was separated from the formulation by the use of a salt bridge. The cathodal compartment contained PBS. A power supply (APH 1000M; Kepco, Flushing, NY) was used to deliver a constant direct current of 0.5 mA/cm^2 for 5 h using Ag/AgCl electrodes. Blood samples (1.0 ml) were withdrawn every 30 minutes and immediately centrifuged at 10,000 rpm; plasma was separated and stored at -20°C until analysis by HPLC. At each sampling time, the blood volume drawn was replaced with the same volume of saline solution. At the end of each experiment, the animals were sacrificed with a high dose of pentobarbital sodium.

Pharmacokinetic parameters of PRAM and RAS after intravenous (IV) administration in the rat were required to calculate the volume of distribution (V_d) and the elimination rate constant (K). For these experiments, 1 mg of each drug was injected intravenously via the cannulated jugular vein in conscious rats. Blood samples were collected at 20, 40, 60, 90 and 120 min; the plasma collected was separated and stored at -20 ºC until analysis.

2.4 Analytical protocol

A P680A LPG-4 pump equipped with an ASI-100 autosampler and a UV170U detector (Dionex; Voisins LeBretonneux, France) was used to quantify PRAM/RAS permeation and skin deposition in the *in vitro* experiments. Isocratic separation was performed using a 125 mm x 4 mm LiChrospher® column packed with 5 µm C_{18} end-capped silica reversed-phase particles. The flow rate and injection volume were 1.0 ml/min and 25 µl, respectively; the column temperature was maintained at 30˚C. The mobile phase comprised 65: 35 %v/v

MeOH / phosphate buffer (20 mM K_2HPO_4, pH 9.2) and PRAM/RAS were assayed by using their UV absorbance at 264 nm. The LOD and LOQ were 50 and 75 ng/ml, respectively for PRAM and 75 and 100 ng/ml, respectively for RAS. ACE was analyzed separately using the same column. The mobile phase consisted of 80% methanol and 20% citrate buffer (10 mM citric acid and 7 mM sodium citrate, pH 3.0). The flow rate was 1.0 ml/min and the column temperature was maintained at 30°C. ACE was detected by its UV absorbance at 220 nm. The LOD and LOQ for ACE were 400 and 500 ng/ml, respectively

Analysis of the samples from the *in vivo* experiments was performed on the same system as described above and the absorbance at 264 nm was used to detect both molecules. Gradient separation was performed using a Phenomenex®, Jupiter column (C_4 150 X 4.60 mm, 5 µm 300 Å). The mobile phase consisted of acetonitrile (Solvent A) and buffer (Solvent B) which was prepared by dissolving 10.2 g potassium dihydrogenphosphate, 10.2 g sodium acetate, and 4.5 g heptanesulfonic acid sodium salt in 3 litres of water and adjusting the pH to 3.5 with acetic acid. The gradient elution protocol used is shown in Table 2; the flow rate and column temperature were 1.0 ml/min and 30ºC, respectively.

Table 2 Mobile phase gradient for HPLC analysis of PRAM and RAS in plasma

Time (min)	% A	% B
0.0	10	90
5.0	10	90
5.1	25	75
12.0	25	75
12.1	10	90
15.0	10	90

Sample preparation

A liquid-liquid extraction method was used to extract PRAM and RAS from plasma samples. Calibration standards were processed by adding 50 µl of internal standard (selegiline) working solution to 500 µl of plasma, 75 µl of 1 M sodium hydroxide, 3 ml of diethyl ether, into tubes. The tubes were capped and mixed on a vortex mixer for 5 minutes, and centrifuged at 5000 rpm for 10 minutes. The aqueous layer was frozen in a dry ice-acetone bath, the organic layer was transferred to a clean tube and back-extracted with 400 µl mobile

phase (A:B 10:90). The aqueous layer was frozen in a dry ice-acetone bath, the organic layer was discarded. Residual organic solvent was removed by briefly blowing under nitrogen. The injection volume used was 75 µl. Calibration range was 75-5000 and 125-5000 ng/ml for PRAM and RAS respectively and method was validated for accuracy and precision (Table 3). The LOD and LOQ were 60 and 75 ng/ml, respectively, for PRAM and 100 and 125 ng/ml, respectively, for RAS.

Table 3 Precision and accuracy values for the analytical method used to quantify PRAM and RAS in plasma

	Theoretical concentration (ng/ml)	**Experimental concentration (ng/ml)**	**CV (%)[a]**	**Accuracy (%)[b]**
PRAM	*Intra-day (n=3)*			
	75	66.42	9.006	88.57
	500	443.05	1.75	88.61
	1000	984.62	7.17	98.46
	Inter-day (n=3)			
	75	75	66.76	4.05
	500	500	458.95	7.07
	1000	1000	952.03	2.60
RAS	*Intra-day (n=3)*			
	125	119.36	1.25	95.49
	500	483.06	5.50	96.61
	1000	981.51	4.15	98.15
	Inter-day (n=3)			
	125	120.70	2.78	96.56
	500	495.78	4.34	99.16
	1000	975.97	3.31	97.60

[a] Precision = (SD/mean) x 100
[b] Accuracy = (obtained concentration/theoretical concentration) x 100

2.5 Pharmacokinetic models

All pharmacokinetic parameters for the IV and iontophoretic delivery experiments were calculated using WinNonlin software Pharsight, Inc., Apex, NC (Version 6.2.1). The plasma concentration versus time profile after IV injection was analysed using a one-compartment

model and the elimination rate constant (K_{el}) and volume of distribution (V_d) calculated. For the co-iontophoretic delivery of PRAM and RAS, plasma levels were calculated using constant input [17] and time-variant models [18]. Plasma profiles were fitted using a Gauss–Newton algorithm with a Levenberg–Hartley modification.

The constant input model is given by:

$$C_P = \left(\frac{K_{input}}{V_d\ K_{el}}\right) * \ (1 - e^{-K_{el}\,t}) \tag{1}$$

where C_P is the plasma concentration of drug at time (t), k_{input} is the input rate and K_{el} and V_d as defined above.

The time-variant input model is described by:

$$C_P\ = \frac{\frac{I_0(K_R\ -\ K_{el}\ +\ ke^{-K_R t})}{K_{el}(K_R - K_{el})} - \frac{I_0 K_R}{K_{el}(K_R - K_{el})}\ e^{-K_{el}t}}{V_d} \tag{2}$$

where C_P is the plasma concentration of drug at time (t), I_0 is zero-order mass transport, K_R is the constant describing the first-order release rate of drug from skin into the plasma, K_{el} and V_d as above.

2.6 Statistics

Data were expressed as the Mean ± SD. Outliers determined using the *Grubbs test* were discarded. Results were evaluated statistically using either analysis of variance (*ANOVA*) followed by *Student Newman Keuls test* or by *Student's t-test*. The level of significance was fixed at α=0.05.

3. Results and Discussion

3.1 Effect of current density on PRAM and RAS co-iontophoretic transport rate

The aim of this study was to determine the factors affecting the co-iontophoretic transport of PRAM and RAS *in vitro.* The passive permeation of PRAM and RAS (20 mM each) after 6 h was 15.7 ± 1.9 and 16.0 ± 2.9 µg/cm^2, respectively (Figures 1, 2). Co-iontophoresis of PRAM and RAS from the same donor compartment at different current densities produced substantial increases in the permeation of both molecules (Figures 1, 2). Regression analysis

suggested that electrotransport of RAS increased linearly with current density (Q_{RAS} (μg/cm^2) = 938.02 i_d, R^2 = 0.9191). Similar observations were made with PRAM where increase in current density also produced statistical significant increase in permeation and flux (Figures 1, 2) (Q_{PRAM} (μg/cm^2) = 1280.3 i_d, R^2 = 0.9713). The results are in perfect agreement with Phipps and Gyory [19], as the flux of the drug ion increases in a linear fashion with the applied current density according to the equation: $J = t_d I/FZ_d$ where J_d, t_d and Z_d are the flux, the transport number and the valence of cation, I is the current density and F is the Faraday constant. The linear dependence of flux on current density is an important feature for the iontophoretic delivery of PRAM, as the dose requirement differs depending on the individual patient, on the phase of therapy and on disease progression. More generally, dose titration is easily achieved with transdermal iontophoretic system, by simply changing the current density and this is an important advantage for the delivery of dopamine receptor agonists. Similarly, increased doses of RAS are also required as the disease progresses.

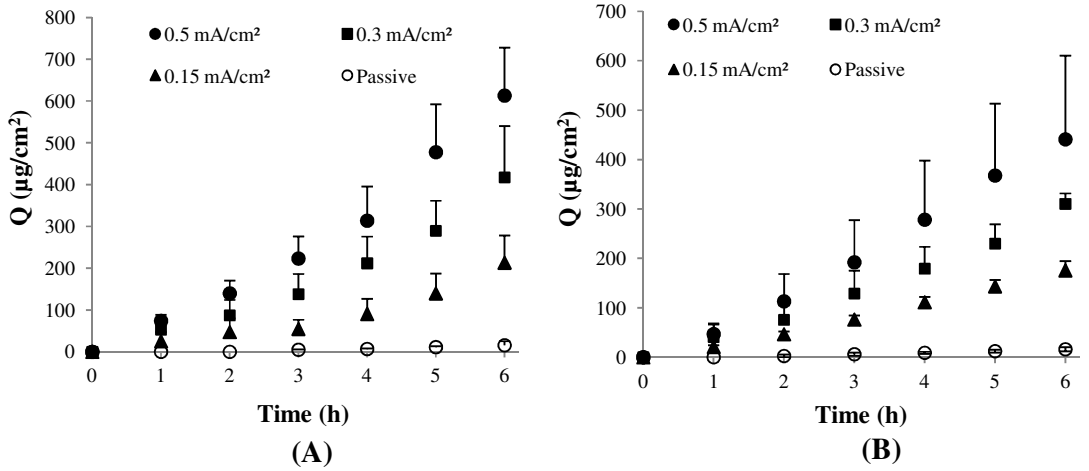

Figure 1. Cumulative permeation (Q) of PRAM (A) and RAS (B) across porcine skin *in vitro* as a function of current density and time. (Data represented as Mean ± S.D.; n ≥ 5).

The individual iontophoretic transport of PRAM and RAS across porcine skin after 6 h at 0.5 mA/cm^2 with the same donor concentration was and 1229.1 ± 138.6 μg/cm^2 and 1104.6 ± 131.2, respectively. Hence, PRAM and RAS showed a 2 and 2.5-fold reduction respectively in cumulative permeation when they were co-iontophoresed. There is competition between the two ions to carry current. The difference in their electrotransport when co-iontophoresed together can be correlated to their physicochemical properties. The log D values of PRAM and RAS at pH 5.3 are -0.84 and 1.69, respectively (determined by Advanced Chemistry

Development Labs Software Version 12.01) indicating higher polarity of PRAM. Computational analysis of both structures revealed that lipophilic potential of unionized RAS (Min 0.063 and Max 0.123) was higher than PRAM (Min 0.035 and Max 0.092). The polar surface area for PRAM and RAS are 50.94 and 12.03, respectively with polarizability of 24.47 and 20.25, respectively. PRAM has two nitrogen atoms that can be ionized depending on the pH. At the experimental pH (i.e., 5.3), one of the nitrogen in PRAM would be completely ionized while the other would be 33% ionized. There is no change in pH during the experiment due to the presence of buffer and to maintain the equilibrium; there will be always 33% of PRAM which will be double charged while 67% would be single charged. On the other hand, RAS has one ionisable group and will only carry a single charge. Computational studies of both molecules in their respective ionization state showed that PRAM (Min -0.171 and Max 0.052) had lower lipophilic potential than RAS (Min -0.047 and Max 0.078) which is also confirmed by their 3D structure (Figure 3 A, B). Thus, PRAM has a more hydrophilic character than RAS due to presence of two ionisable groups, more polar surface area that gives the former an edge over the latter with respect to its delivery by iontophoresis.

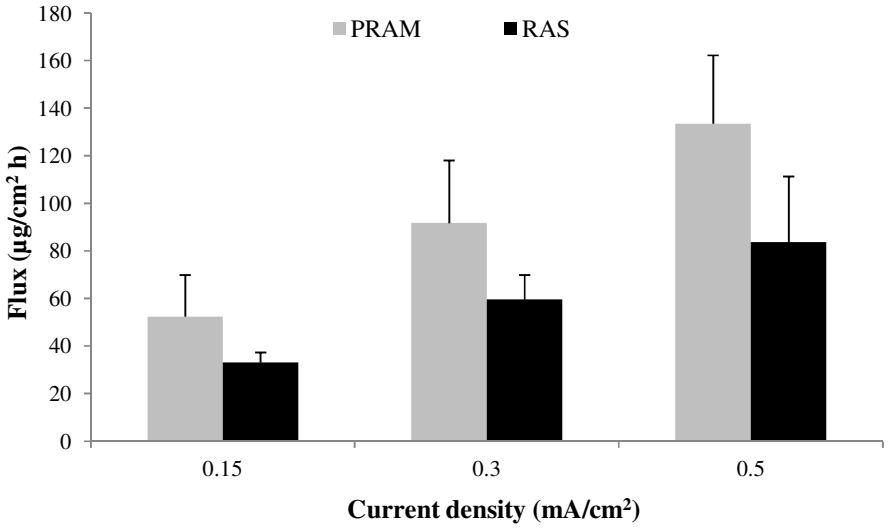

Figure 2. Steady-state fluxes of PRAM and RAS at different current densities after 6 h of iontophoresis with a donor concentration of 20 mM of each drug. (Mean ± S.D.; n ≥ 5).

3.2 Mechanism of PRAM and RAS transport

Iontophoresis of ACE, a neutral molecule, whose transport is governed by EO was used to ascertain the effect of iontophoresis on convective solvent flow at different current densities;

it was also used to determine the contribution of EM and EO towards the electrotransport of PRAM and RAS. As the current density increased the contribution of EO increased for both the molecules (Figure 4). Nevertheless, EM accounted for and 86-97% and 82-93% of total flux for PRAM and RAS; respectively. There was no inhibition of ACE transport (IF values 1.08-1.13) indicating no binding of either cation to structures in the transport pathway and their electrotransport left skin permselectivity unperturbed.

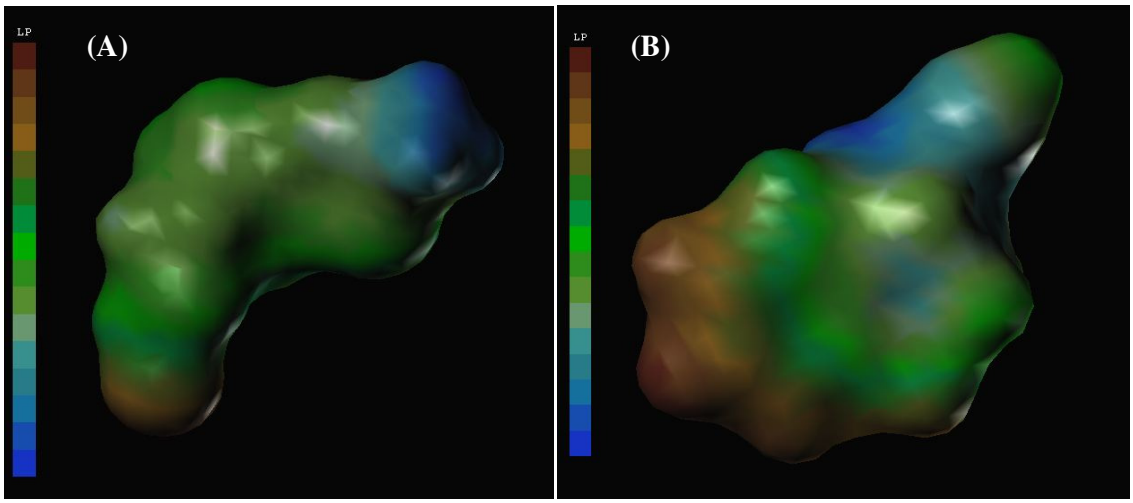

Figure 3. Three-dimensional structure of ionized PRAM (divalent cation) (A) and ionized RAS (monovalent cation) (B) showing their lipophilic potential using SYBYL-X1.1.

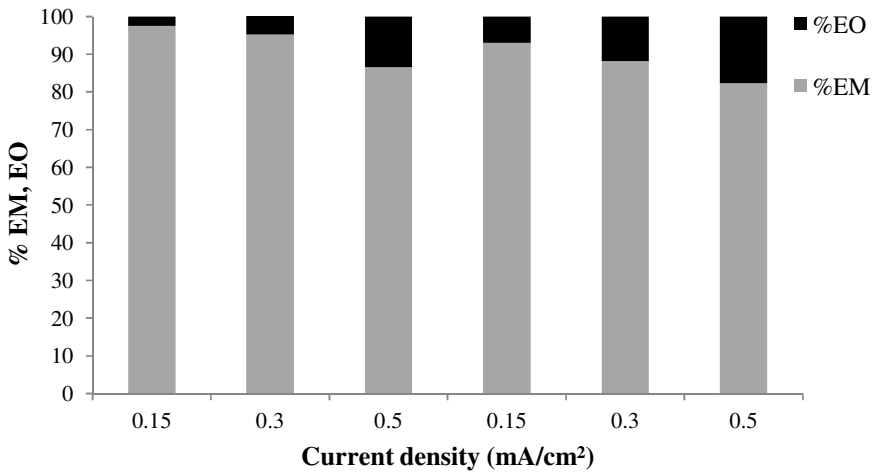

Figure 4. Relative contributions of electromigration (EM) and electroosmosis (EO) to the total flux of PRAM and RAS as a function of current density (The first three columns represent PRAM and the last three represent RAS).

3.3 Transport and delivery efficiency

The transport number is the fraction of the total charge transported by a specific ion during iontophoresis [20]. This number depends on the charge and mobility of the ion suggesting that cations and anions such as Na^+ and Cl^- are the major charge carriers. However, PRAM and RAS showed good transport numbers given that the formulation in the donor compartment contained 26 mM sodium metabisulfite and Cl^- ions from the receiver were present at much higher concentration (and were the primary charge carriers) (Table 4).

Table 4 Transport and drug delivery efficiencies of PRAM and RAS as a function of applied current density

Current (mA/cm^2)	**% Transport efficiency**		**% Delivery efficiency**	
	PRAM	RAS	PRAM	RAS
0.15	3.05	3.01	10.16	12.19
0.3	2.99	2.69	19.91	23.97
0.5	2.58	2.3	29.22	35.05

The excellent barrier function of the skin means that transdermal administration is best suited for potent drugs but even these molecules must possess the appropriate balance of physicochemical properties. These constraints coupled with low delivery efficiency can make transdermal delivery systems less appealing to the pharmaceutical industry. However, this co-iontophoretic system showed a combined delivery efficiency of 64% which is quite remarkable for a transdermal formulation. Such results should help to resuscitate interest in the transdermal route and underline the need for the careful selection of a delivery technology based on the properties of the drug candidate.

3.4 Effect of formulation composition on PRAM and RAS permeation

The cumulative permeation for PRAM and RAS from formulations A–E after iontophoresis at 0.5 mA/cm^2 for 6 h is presented in Fig. 5. The results demonstrate that cumulative permeation for each molecule increased with concentration. It has been predicted theoretically and verified experimentally that the highest flux for anodal iontophoresis is achieved when the drug is the only cation in the donor solution [21]. In such cases, the cation will compete to carry current with the counter-ion in the subdermal compartment and its flux is independent of concentration. In these electrotransport experiments there was competition

between PRAM, RAS, Na^+ and, of course, Cl^-. Reports have also shown that iontophoretic delivery of drugs is proportional to drug mole fraction in the donor [21,22]. All the formulations had a different mole fraction for PRAM and RAS which also led to a change in their permeation profile. In an ideal iontophoretic system, a formulator would like to have no competition in donor to maximize the transport efficiency of a cation. However, for co-iontophoresis from the same electrode one cannot avoid competition among the two ions of interest which can be a drawback for the system. In this case, competition between ions can be helpful in delivering different amounts of a particular ion. PRAM has almost four times the dose requirements of RAS. Hence, by having a system where the concentration of PRAM is much higher than RAS in the donor compartment the required therapeutic amounts of both drugs can be delivered from the same system. In formulation D the concentration of PRAM is thrice that of RAS and there is 3.6-fold increase in permeation of PRAM than RAS (701.2 ± 145.8 and 190.4 ± 65.3 µg/cm^2, respectively). Therefore, iontophoresis can be a very efficient technique in delivering two ions with different input kinetics by changing the donor concentration of the drugs or with a linear increase in their input by modulation of current density along with high delivery efficiency.

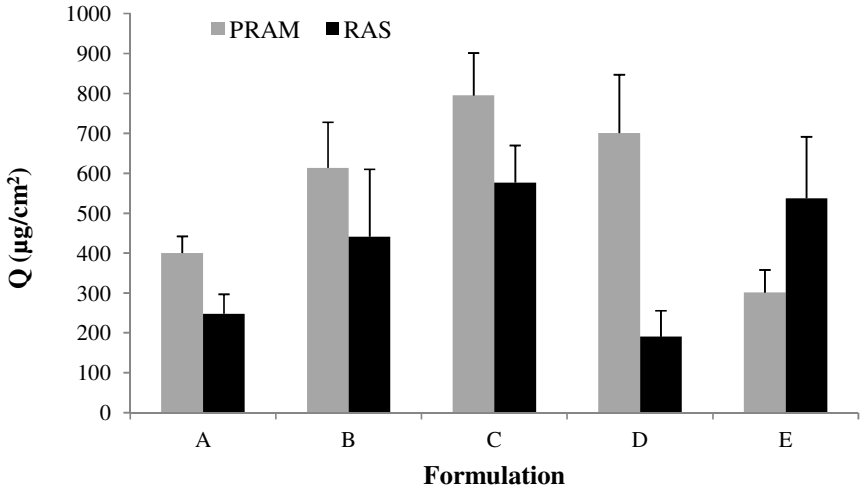

Figure 5. Influence of formulation composition on PRAM and RAS delivery after 6 h of iontophoresis at 0.5 mA/cm^2. (Mean ± S.D.; n>5).

3.5 Comparison of PRAM and RAS electrotransport across porcine and human skin

Cumulative permeation observed with human skin after 6 h iontophoresis at 0.5 mA/cm^2 for PRAM and RAS was 589.34 ± 86.7 and 420.3 ±98.6 µg/cm^2, respectively, which was statistically equivalent to that observed with porcine skin (Figure 6).

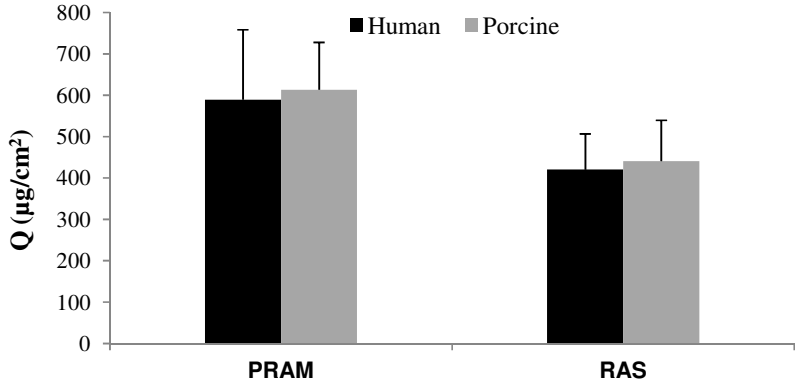

Figure 6. Comparison of cumulative permeation of PRAM and RAS across human and porcine skin after their co-iontophoresis at 0.5 mA/cm^2 for 6 h using a formulation containing 20 mM of each drug. (Mean ± S.D.; n≥4).

3.6 Pharmacokinetics studies

The first objective of this experiment was to estimate the pharmacokinetic parameters of PRAM and RAS in Wistar rats following IV administration (Figure 7). Plasma levels of both drugs were fitted by using a one compartment model. The volume of distribution (V_d) and elimination rate constant (K_{el}) were calculated for each molecule and used in equations (1) and (2) to model the plasma concentrations achieved with iontophoresis.

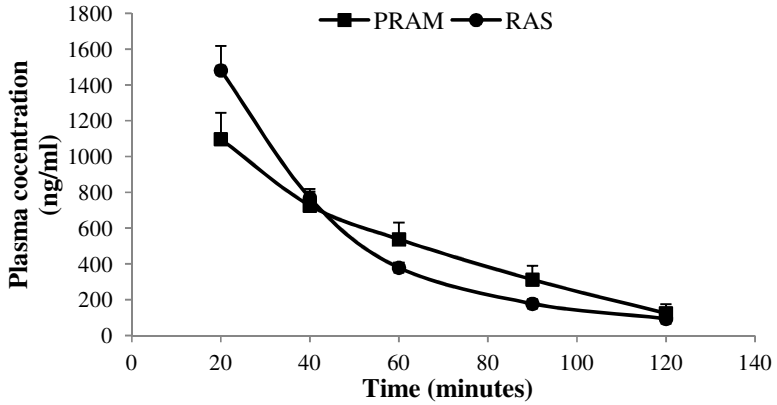

Figure 7. PRAM and RAS plasma concentrations measured after an IV administration in rats. (Mean ± S.D.; n = 4).

The plasma concentration–time profiles of PRAM and RAS upon co-iontophoretic administration at 0.5 mA/cm^2 are shown in Figures 8 and 9. Significant drug levels were achieved rapidly for both drugs in 30 minutes. Iontophoretic delivery of PRAM was superior to that of RAS again pointing to the better charge carrying ability and hydrophilic character

of PRAM. Moreover, there was little variability in the plasma concentrations for either drug, which is also an advantage of using iontophoresis over passive delivery where large variations are sometimes observed. It should also be mentioned that no macroscopic changes were noted on the skin of animals after the termination of the electric current.

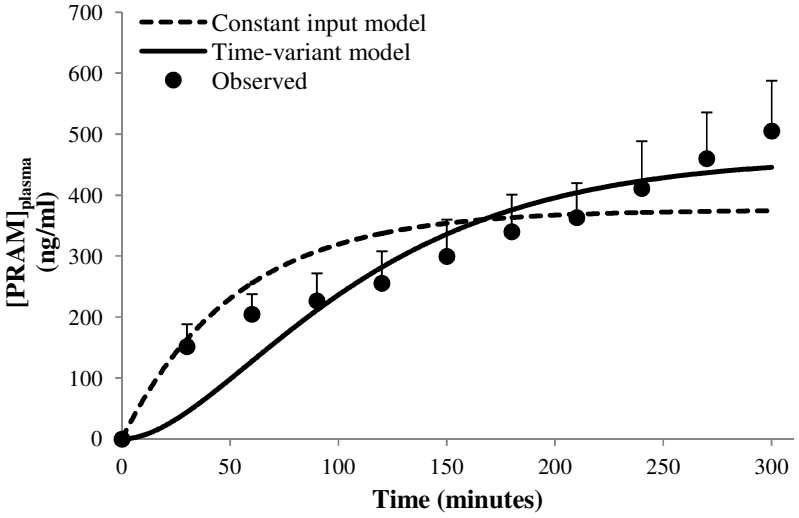

Figure 8. The observed plasma PRAM concentration vs. time profiles in rats after iontophoretic administration for 5 h at 0.5 mA/cm^2 and the fits obtained using the constant input (dashed line) and time-variant input (solid line) models. (Mean ± S.D.; n = 6).

The mean plasma concentrations of PRAM and RAS during iontophoretic current application were fitted using constant input and time-variant input models (Figures 8 and 9). It was observed that the time-variant input model was better in simulating the plasma concentration for both drugs. The constant input model tended to overestimate drug levels at the initial time-points and underestimated those in the later stages. The underlying reason for this is the fact that constant input model assumes that steady states are achieved rapidly. In reality for transdermal iontophoresis, the permeation of therapeutics is a multi-step process where the drug will initially partition from formulation to stratum corneum, followed by diffusion through stratum corneum and epidermis (i.e., release from the skin matrix) and finally uptake by blood vessels. The time-variant input model gave a better picture in prediction of plasma drug levels but slightly underestimated initial time points. The ability of compartmental modelling to simulate the plasma drug concentration can be very helpful in designing an iontophoretic system for PRAM and RAS. These drugs have different pharmacokinetics and dosage requirements depending on the state of the disease. Such models can predict plasma

profiles for PRAM where dose titrations are required and also help to ascertain the input rates required for achieving a therapeutically relevant concentration. More detailed pharmacokinetic study with different current density and donor concentration of actives will provide more detailed information for the better utility of such compartment modelling approaches in designing a drug delivery system with complex input kinetics for simultaneous administration of two or more drugs.

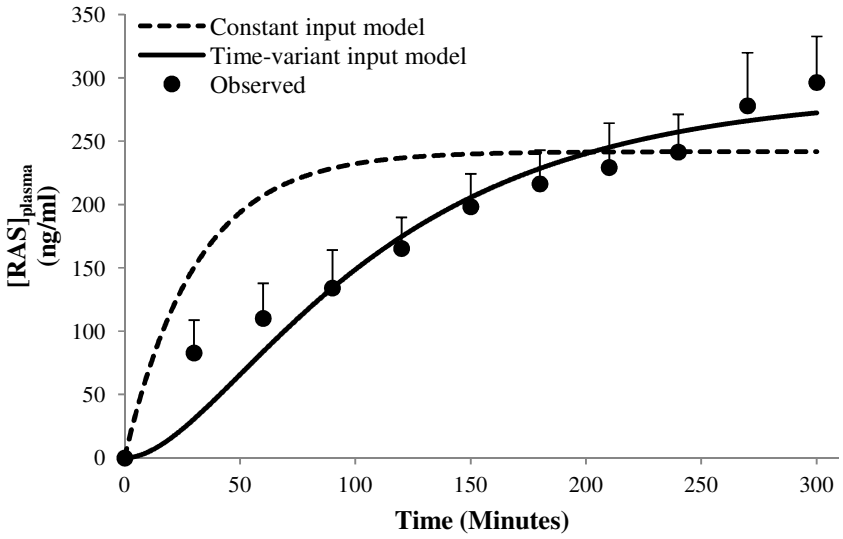

Figure 9. The observed plasma RAS concentration vs. time profiles in Wistar rats after iontophoretic administration for 5 h at 0.5 mA/cm^2 and the fits obtained using the constant input (dashed line) and time-variant input (solid line) models. (Mean ± S.D.; n = 6).

The calculated transdermal absorption rate *in vivo* for RAS was 1.7- (constant input model) and 1.6- fold (time-variant input model) times higher than that observed *in vitro* across porcine skin (Table 5) and was statistically different. Similarly, PRAM exhibited 1.8- (constant input model) and 2.0- fold (time-variant input model) higher *in vivo* absorption rate than that obtained in porcine skin *in vitro*. The results obtained with PRAM are in agreement when PRAM was iontophoresed alone in rats where the *in vivo* predicted rates were higher than those *in vitro*. It has been previously reported that *in vitro* flux measurements can underestimate the transport of certain ions *in vivo* mainly due to the use of higher NaCl concentrations in the receiver compartment *in vitro* than would be present in the epidermis *in vivo* [19]. The "clearance" *in vitro* of the permeant might also be different from the clearance *in vivo* by the microcirculation in the skin contributing to the variation in fluxes [23,24]. There are several other reports where there is a discrepancy in transdermal fluxes obtained *in*

vitro and *in vivo* [25-27]. In many cases the experimental conditions *in vitro* differed from those *in vivo* and therefore a correlation is not always possible [28].

Table 5 Pharmacokinetic parameters estimated from plasma concentration – time profiles following iontophoretic administration of PRAM and RAS; fits obtained using constant input and time-variant input models

Parameters	**PRAM**		**RAS**	
	Constant	*Time-variant*	*Constant*	*Time-variant*
Input rate *in vivo*[a] (µg/h)	268.3 ± 47.6[b]	294.2 ± 39.8[c]	167.2 ± 21.7[b]	160.5 ± 19.3[c]
K_R (1/h)		0.81 ± 0.16		0.93 ± 0.27
V_d (L)[d]	0.627		0.357	
K_{el} (1/min)[e]	0.019		0.032	
Input rate *in vitro*[f] (µg/h)	146.3 ± 34.2		100.5 ± 20.4	
C_{max} (ng/ml)	505.4 ± 82.6		296.5 ± 36.5	
AUC_{0-300} (µg.min/ml)	97.2 ± 17.6		68.2 ± 9.11	

[a] Current application area (0.78 cm^2)
[b] K_{input} as per equation 1
[c] I_0 as per equation 2
[d] Volume of distribution calculated from IV administration
[d] Elimination rate constant calculated from IV administration
[f] Porcine ear skin *in vitro*; input rate calculated assuming a current application area of 0.78 cm^2

The drug levels obtained *in vivo* were then compared with human pharmacokinetics of both drugs in order to evaluate the feasibility of using their co-iontophoresis for therapeutic delivery. PRAM and RAS follow one-compartment pharmacokinetics in humans [29,30]. The values of V_d and K from human pharmacokinetics studies for RAS were 87 l and 0.332 1/h and for PRAM were 486 l and 0.057 1/h, respectively. The *in vivo* input rate (Table 5) were then used to estimate the plasma concentration of respective drugs after 2 h, which were 1.67 and 0.91 ng/ml for PRAM and RAS respectively after 3 h from 1 cm^2 patch. The reported C_{max} and C_{min} in humans for PRAM are 4.66 and 7.17 with a dose of 1.5 mg administered every 8h. Similarly, the C_{max} for RAS is 8.5 ng/ml after a once a daily administration in Parkinson's patients at a dose of 1 mg. Therefore, constant current anodal iontophoresis can attain therapeutic blood concentrations of PRAM and RAS with reasonable patch sizes with at acceptable current densities.

4. Conclusion

The results confirmed the feasibility of delivering therapeutic amounts of PRAM and RAS across the skin by transdermal co-iontophoresis. Transdermal fluxes increased for both drugs with current density and donor concentration. Permeation across human and porcine skin was statistically equivalent. The pharmacokinetics studies in rats suggested that the transdermal iontophoretic flux would be sufficient to maintain therapeutically relevant blood concentrations of PRAM and RAS for the management of PD.

References

[1] J.G. Nutt, G.F. Wooten, Diagnosis and initial management of Parkinson's disease, N. Engl. J. Med. 353 (2005) 1021-1027.

[2] I. Litvan, G. Halliday, M. Hallett, C.G. Goetz, W. Rocca, C. Duyckaerts, Y. Ben-Shlomo, D.W. Dickson, A.E. Lang, M.F. Chesselet, W.J. Langston, D.A. Di Monte, T. Gasser, T. Hagg, J. Hardy, P. Jenner, E. Melamed, R.H. Myers, D. Parker Jr, D.L. Price, The etiopathogenesis of Parkinson disease and suggestions for future research Part 1, J. Neuropathol. Exp. Neurol. 66 (2007) 251-257.

[3] C.G. Goetz, W. Poewe, O. Rascol, C. Sampaio, Evidence-based medical review update: pharmacological and surgical treatments of Parkinson's disease: 2001 to 2004, Mov. Disord.20 (2005) 523–539.

[4] C.W. Olanow, M.B. Stern, K. Sethi, The scientific and clinical basis for the treatment of Parkinson disease, Neurology 72 (2009) S1-136.

[5] M.F. Piercey, Pharmacology of pramipexole, a dopamine D3-preferring agonist useful in treating Parkinson's disease, Clin. Neuropharmacol. 21 (1998) 141-151.

[6] M. Horstink, E. Tolosa, U. Bonuccelli, G. Deuschl, A. Friedman, P. Kanovsky, J.P. Larsen, A. Lees, W. Oertel, W. Poewe, O. Rascol, C. Sampaio, Review of the therapeutic management of Parkinson's disease. Report of a joint task force of the European Federation of Neurological Societies and the Movement Disorder Society-European Section. Part I: early (uncomplicated) Parkinson's disease, Eur. J. Neurol. 13 (2006) 1170-1185.

[7] P.A. LeWitt, Mao-B inhibitor know-how: Back to the pharm reply, Neurology. 72 (2009) 1352-1357.

[8] L.W. Elmer, J.M. Bertoni, The increasing role of monoamine oxidase type B inhibitors in Parkinson's disease therapy, Expert Opin. Pharmacother. 9 (2008) 2759-2772.

[9] P. Jenner, Preclinical evidence for neuroprotection with monoamine oxidase-B inhibitors in Parkinson's disease, Neurology 63 (2004) S13-S22.

[10] J.P. Hubble, W.C. Koller, N.R. Cutler, J.J. Sramek, J. Friedman, C. Goetz, A. Ranhosky, D. Korts, A. Elvin, Pramipexole in patients with early Parkinson's disease, Clin. Neuropharmacol. 18 (1995) 338–347.

[11] P. Navan, L.J. Findley, J.A.R. Jeffs, R.K.B. Pearce, P.G. Bain, Randomized, double-blind, 3-month parallel study of the effects of pramipexole, pergolide, and placebo on parkinsonian tremor, Mov. Disord. 18 (2003) 1324–1331.

[12] M. Fargel, B. Grobe, E. Oesterle, C. Hastedt, M. Rupp, Treatment of Parkinson's Disease: A Survey of Patients and Neurologists, Clin. Drug Investig. 27 (2007) 207-218.

[13] M.M. Mouradian, I.J. Heuser, F. Baronti, T.N. Chase, Modification of central dopaminergic mechanisms by continuous levodopa therapy for advanced Parkinson's disease, Ann. Neurol. 27 (1990) 18-23.

[14] W.M. Guldenpfennig, K.H. Poole, K.W. Sommerville, B. Boroojerdi, Safety, tolerability, and efficacy of continuous transdermal dopaminergic stimulation with rotigotine patch in early-stage idiopathic Parkinson disease, Clin. Neuropharmacol. 28 (2005) 106-110.

[15] B. Boroojerdi, H.M. Wolff, M. Braun, D.K.A. Scheller, Rotigotine transdermal patch for the treatment of parkinson's disease and restless legs syndrome, Drugs Today 46 (2010) 483-505.

[16] R.H. Howland, 2006. Transdermal selegiline - A novel MAOI formulation for depression. J. Psychosoc. Nurs. 44, 9-12.

[17] A. Naik, Y.N. Kalia, R.H. Guy, Transdermal drug delivery: overcoming the skin's barrier function, Pharm. Sci. Technolo. Today 3 (2000) 318-326.

[18] Y.N. Kalia, A. Naik, J. Garrison, R.H. Guy, Iontophoretic drug delivery, Adv Drug Deliv. Rev. 56 (2004) 619-658.

[19] J.B. Phipps, J.R. Gyory, Transdermal Ion Migration, Adv. Drug Deliv. Rev. 9 (1992) 137-176.

[20] N.H. Bellantone, S. Rim, M.L. Francoeur, B. Rasadi, Enhanced Percutaneous-Absorption Via Iontophoresis .1. Evaluation of an In vitro System and Transport of Model Compounds, Int. J. Pharm. 30 (1986) 63-72.

[21] R.V. Padmanabhan, J.B. Phipps, G.A. Lattin, R.J. Sawchuk, In vitro and in vivo evaluation of transdermal iontophoretic delivery of hydromorphone, J. Control. Release 11 (1990) 123–135.

[22] D. Marro, Y.N. Kalia, M.B. Delgado-Charro, R.H. Guy, Contributions of electromigration and electroosmosis to iontophoretic drug delivery, Pharm. Res. 18 (2001) 1701-1708.

[23] S.E. Cross, M.S. Roberts, Importance of dermal blood supply and epidermis on the transdermal iontophoretic delivery of monovalent cations, J. Pharm. Sci. 84 (1995) 584–592.

[24] Y. Dancik, Y.G. Anissimov, O.G. Jepp, M.S. Roberts, Convective transport of highly plasma protein bound drugs facilitates direct penetration into deep tissues after topical application, Br. J. Clin. Pharmacol. 73 (2011) 564–578.

[25] A. Chaturvedula, D.P Joshi, C. Anderson, R. Morris, W.L. Sembrowich, A.K. Banga, Dermal, subdermal, and systemic concentrations of granisetron by iontophoretic delivery, Pharm. Res. 22 (2005) 1313–1319.

[26] R. Yamamoto, S. Takasuga, Y. Yoshida, S. Mafune, K. Kominami, C. Sutoh, Y. Kato, M. Yamauchi, M. Ito, K. Kanamura, M. Kinoshita, In vitro and in vivo transdermal iontophoretic delivery of naloxone, an opioid antagonist, Int. J. Pharm. 422 (2012) 132–138.

[27] R.V. Padmanabhan, J.B. Phipps, G.A. Lattin, R.J. Sawchuk, In vitro and in vivo evaluation of transdermal iontophoretic delivery of hydromorphone, J. Control. Release 11 (1990) 123–135.

[28] R. Van der Geest, T. Van Laar, J.M. Gubbens-Stibbe, H.E Bodde, M. Danhof**,** Compartment Modeling of Transdermal Iontophoresis *in Vivo*, and. Iontophoretic delivery of apomorphine. II: An in vivo study in patients with Parkinson's disease, Pharm. Res. 14 (1997) 1804–1810.

[29] C.E. Wright, T.L. Sisson, A.K. Ichhpurani, G.R. Peters, Steady-state pharmacokinetic properties of pramipexole in healthy volunteers, J. Clin. Pharmacol. 37 (1997) 520-525.

[30] V. Oldfield, G.M. Keating, and C.M. Perry, Rasagiline: a review of its use in the management of Parkinson's Disease, Drugs 67 (2007) 1725-1747.

Chapter 5

Controlled iontophoretic transport of huperzine A across skin *in vitro* and *in vivo*: Effect of delivery conditions and comparison of pharmacokinetic models

Dhaval R. Kalaria,[†] Vandana Patravale,[§]
Virginia Merino,[‡] and Yogeshvar N. Kalia*[,†]

[†]School of Pharmaceutical Sciences,
University of Geneva & University of Lausanne,
30 Quai Ernest Ansermet,
1211 Geneva, Switzerland

[§]Department of Pharmaceutical Sciences and Technology,
Institute of Chemical Technology,
Mumbai 400019, India

[‡]Departamento de Farmacia y Tecnología Farmacéutica,
Faculty of Pharmacy, University of Valencia,
Avda.Vicente Andrés Estellés s/n, 46100 Burjassot, Valencia, Spain

ABSTRACT

The aim of this study was to investigate constant current anodal iontophoresis of Huperzine A (HupA) *in vitro* and *in vivo* and hence to evaluate the feasibility of using electrically-assisted delivery to administer therapeutic amounts of the drug across the skin for the treatment of Alzheimer's disease. Preliminary experiments were performed using porcine and human skin *in vitro*. Stability studies demonstrated that HupA was not degraded upon exposure to epidermis or dermis for 12 h and that it was also stable in the presence of an electric current (0.5 $mA.cm^{-2}$). Passive permeation of HupA (2 mM) was minimal (1.1 ± 0.1 $\mu g.cm^{-2}$); iontophoresis at 0.1, 0.3 and 0.5 $mA.cm^{-2}$ produced 106-, 134- and 184-fold increases in its transport across the skin. Surprisingly, despite the use of a salt bridge to isolate the formulation compartment from the anodal chamber, which contained 133 mM NaCl, iontophoresis of HupA was shown to increase linearly with its concentration (1, 2 and 4 mM in 25 mM MES, pH 5.0) ($r^2 = 0.99$). This was attributed to the low ratio of drug to Cl^-, in the receiver compartment, its depletion and to possible competition from the zwitterionic MES. Co-iontophoresis of acetaminophen confirmed that electromigration was the dominant electrotransport mechanism. Total delivery across human and porcine skin was found to be statistically equivalent (243.2 ± 33.1 and 235.6 ± 13.7 $\mu g.cm^{-2}$, respectively). Although the transport efficiency was ~1%, the iontophoretic delivery efficiency (i.e., the fraction of the drug load delivered) was extremely high, in the range of 46-81% depending on the current density. Cumulative permeation of HupA from a carbopol gel formulation after iontophoresis for 6 h at 0.5 $mA.cm^{-2}$ was less than that from solution (135.3 ± 25.2 and 202.9 ± 5.2 $\mu g.cm^{-2}$ respectively) but sufficient for therapeutic delivery. Pharmacokinetic parameters were determined in male Wistar rats *in vivo* (4 mM HupA; 0.5 $mA.cm^{-2}$ for 5 h with Ag/AgCl electrodes) using a one-compartment model with either constant or time-dependent input rates. A superior fit was obtained using the time-variant model and the input rate i*n vivo* was significantly greater than that *in vitro* (67.94 ± 10.99 vs. 51.88 ± 5.00 $\mu g.h^{-1}$, respectively). Based on these results and the known pharmacokinetics, it was estimated that therapeutic amounts of HupA could be delivered for the treatment of Alzheimer's disease using a reasonably sized patch.

KEYWORDS: Transdermal iontophoresis, Alzheimer's disease, Huperzine A, Pharmacokinetics, Drug delivery

INTRODUCTION

Alzheimer's disease (AD) is a progressive neurodegenerative illness whose incidence and health burden are increasing as a consequence of demographic changes. Cholinergic enhancement strategies have been at the forefront of efforts for the pharmacological treatment of cognitive impairment.[1,2] Among the various therapeutic approaches, acetylcholinesterase inhibitors (AChEIs) are the first family of compounds to have produced modest improvements in cognitive function of AD patients.[3]

Huperzine A (HupA), an alkaloid isolated from the Chinese herb *Huperzia serrata*, is a highly selective, reversible AChEI.[4,5] It is more potent than galantamine, tacrine or rivastigmine and has the least anti-butyrylcholinesterase activity, suggesting a better selectivity and tolerability profile.[6] HupA also displays better penetration of the blood–brain barrier and a longer duration of acetylcholinesterase inhibition compared to other AChEIs.[7] It was approved in China in 1994 and has been widely used to improve memory deficits in elderly people and patients with AD and vascular dementia.[8,9] As a result, HupA has generated considerable interest in recent years in western countries leading to the development of various derivatives as potential new anti-AD drugs.[10] Clinical trials have shown that twice daily oral administration of 500 µg HupA elicited beneficial effects in patients. However, this dosing regimen is sub-optimal given the patient population and the symptoms of AD (i.e., memory loss), and there is a high probability of missing a scheduled dose.[11] In addition, several side-effects including nausea and anorexia have been reported following oral administration.

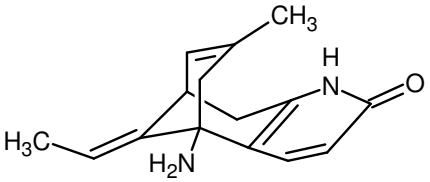

Figure 1. Chemical structure of huperzine A (HupA; MW: 242.32, pKa 6.97).

Transdermal iontophoresis can help to circumvent these problems and provide a smoother, controlled and continuous delivery resulting in steadier plasma levels over time. HupA has an aqueous solubility of 1.43 mg/ml (pH 7) and a pKa of 6.97, suggesting that at pH 5, the approximate pH at the skin surface, it exists predominantly as a monocation (Figure 1).[12,13] Hence, its physicochemical properties and low dosing requirements make it a good candidate

for iontophoresis.[14] In addition, iontophoresis enables easy modulation of HupA delivery kinetics by simply changing the current density, thus enabling dose titration according to individual patient need. Furthermore, transdermal administration is also beneficial for patients unable to take oral medications or those with swallowing difficulties in advanced disease states. As a result, it may increase patient compliance, reduce the caregiver's workload and contribute to bringing down the cost of therapy.

The objectives of this study were: (a) to investigate the effect of experimental parameters on the iontophoretic transport of HupA *in vitro*; (b) to deduce the relative contribution of electromigration (EM) and electroosmosis (EO) and so determine the dominant transport mechanism; (c) to investigate iontophoretic delivery *in vivo* and to compare iontophoretic transport rates determined using constant-input and time-variant one compartment models and hence to examine the *in vitro-in vivo* correlation and finally (d) to estimate the feasibility of delivering therapeutic amounts of HupA across the skin.

MATERIALS AND METHODS

Materials

Huperzine A was purchased from Ningbo Liwah Plant Extraction Technology Company Limited (Ningbo, China). Acetaminophen (ACE), sodium chloride, 4-(2-hydroxyethyl)-1-piperazineethanesulfonic acid (HEPES), 2-(*N*-morpholino)ethanesulfonic acid (MES), triethanolamine, citric acid, chloroform and sodium citrate were all purchased from Sigma-Aldrich (Buchs, Switzerland). Silver wire and silver chloride used for the fabrication of electrodes were also sourced from Sigma-Aldrich. Methanol and PVC tubing (ID 3.17 mm; OD 4.97 mm) were purchased from VWR International (Nyon, Switzerland). All solutions were prepared using deionised water (resistivity > 18 MΩ.cm). All other chemicals were at least of analytical grade.

Skin supply

Porcine ears were obtained from a local abattoir (CARRE; Rolle, Switzerland). The skin was excised (thickness 750 µm) with an air-dermatome (Zimmer; Etupes, France), wrapped in Parafilm™ and stored at −20 ˚C for a maximum period of 1 month. Human skin samples were collected immediately after surgery from the Department of Plastic, Aesthetic and Reconstructive Surgery, Geneva University Hospital (Geneva, Switzerland), fatty tissue was removed and the skin was wrapped in Parafilm™ before storage at −20 °C for a maximum

period of 7 days. The study was approved by the Central Committee for Ethics in Research (CER: 08-150 (NAC08-051); Geneva University Hospital).

In vitro protocol

Stability in the presence of skin and electrical current

The stability of HupA in the presence of skin (both human and porcine) was evaluated using two compartment vertical diffusion cells (area ~ 2 cm^2). A 2 mM solution of HupA in 10 mM MES (pH 5.0) was placed in contact with the epidermal and dermal surfaces of both skin types for 12 h. In addition, the stability of HupA in the presence of current was also investigated prior to the iontophoretic permeation studies. A 2 mM solution of HupA in 10 mM MES (pH 5.0) was subjected to a current density of 0.5 $mA.cm^{-2}$, the highest to be used in the experiments, for 6 h. The initial concentration of HupA in solution was compared to that following exposure to skin or electric current, quantification was by HPLC (see below). Experiments were performed in triplicate.

Iontophoretic permeation studies in vitro

(1) Effect of drug concentration

Skin was clamped in two compartment vertical diffusion cells (area ~ 2 cm^2) where the receiver compartment (which also housed the cathode) was equipped with 2 side arms. The upper chamber was used as the formulation compartment and this was connected to the anodal compartment by a salt bridge. All compartments were initially filled with 133 mM NaCl/25 mM HEPES (pH 7.4) solution. After equilibration for 30 min, the NaCl-HEPES solution, in the upper chamber (or formulation compartment), was replaced by a 1 ml HupA solution (1, 2 and 4 mM in 10 mM MES, pH 5.0) that also contained acetaminophen (ACE; 15 mM), which was used to report on electroosmotic solvent flow.[15] A constant current was applied for 6 h via Ag/AgCl electrodes connected to a power supply (Kepco APH 1000M; Flushing, NY). The receptor compartment was sampled hourly; 0.6 ml of solution was withdrawn and replaced by the same volume of fresh buffer solution. After current application for 6 h, the cells were dismantled and bound HupA was extracted from the skin post-iontophoresis by cutting the skin samples into small pieces and soaking them in 10 ml water-methanol mixture (45:55) for 4 h. The extraction mixture was then filtered through 0.22 µm nylon membrane filters (VWR; Nyon, Switzerland). The method was validated by spiking the stratum corneum surface of dermatomed skin (750 µm thickness) with known concentrations of drug (1, 5 and 50 µg/ml in mobile phase). After solvent evaporation, skin

samples were subjected to extraction using the above-mentioned procedure. The recovery of HupA was determined by adding a known amount of substance on the skin surface and calculating the ratio of the amount extracted from skin samples to the amount added by spiking; the results are shown in Table 1. Experiments were performed with at least five replicates.

Table 1 Validation of the HupA extraction method used to quantify drug retained within the skin during experiments *in vitro* (n = 3)

Control concentration (µg.ml^{-1})	**Sample concentration (µg.ml^{-1})**	**Recovery (%)**	**S.D.**
1	0.83	83.0	6.7
5	4.32	86.4	7.8
50	47.45	94.9	3.2

(2) Effect of current density

This was investigated in separate studies using a 2 mM HupA solution (buffered in 10 mM MES, pH 5.0) that was iontophoresed at 0.15, 0.3 and 0.5 mA cm^{-2}. The current was applied for 6 h and all other conditions were as described above.

The total flux (J_{tot}) of HupA during iontophoresis, assuming negligible passive permeation, is given by the equation:

$$J_{tot} = J_{EM} + J_{EO} = \left[\left(\frac{i_d}{F}\right) \times \frac{u_{HupA}}{\sum_1^i z_i u_i c_i} + V_w\right] \times c_{HupA} \quad (1)$$

where J_{EM} and J_{EO} represent the contribution of EM and EO to the total flux, and i_d is the applied current density, and z_i, u_i and c_i refer to the charge, mobility and concentration of the ions carrying charge across the membrane and u_{HupA} and c_{HupA} are the mobility and concentration of HupA, respectively. J_{EO} is given by the product of the linear velocity of solvent flow (V_W) and drug concentration (c_{HupA}). For each experiment, co-iontophoresis of ACE enabled the calculation of V_W and the inhibition factor (IF) to report on the effect of HupA transport on skin permselectivity:

$$IF = \frac{Q_{ACE\ Control}}{Q_{ACE}} \quad (2)$$

where $Q_{ACE\ Control}$ and Q_{ACE} represent the cumulative permeation of ACE in 6 h in the absence and presence of drug; respectively.

(3) HupA delivery from gel formulation

A carbopol gel formulation was prepared by slowly dispersing carbopol in water at 0.8% w/w followed by addition of HupA at 0.7% w/w. The resulting mixture was neutralized with 10% triethanolamine until a clear, transparent gel was obtained. For the permeation experiments, 500 mg gel was placed in the formulation compartment and iontophoretic delivery was compared to that from an aqueous buffered solution. The gels were kept at room temperature for 1 month to test their stability and to detect any drug precipitation.

***In vivo* experimental protocol**

Male Wistar rats (260–280 g) were supplied by the Animal Experimental Research Centre at the University of Valencia (Valencia, Spain). Experimental protocols were approved by the Ethics Committee for Animal Experimentation at the University of Valencia. Twenty four hours before the iontophoresis experiments, the rats were anaesthetised by intraperitoneal administration of pentobarbital sodium (Dolethal solution, 40 mg kg^{-1}; Vetoquinol, Madrid, Spain). The jugular vein was then cannulated using medical-grade silicon tubing (Silastic, Dow Corning Co.; ID 0.5 mm; OD 0.94 mm). Under anaesthesia, 3.4 cm of the cannula was introduced into the jugular vein towards the heart and the free end emerged from the dorsal base of the neck. The cannula was filled with heparinized saline solution (20 IU ml^{-1}) and closed with a polyethylene plug.

The following day the animals were again anaesthetised and mounted on a plastic support. Two glass chambers (area 0.78 cm^2) were then placed 2.5 cm apart on the animal's abdomen (shaved beforehand) and fixed with glue. The anodal chamber was separated from the donor compartment by means of a salt bridge. The anodal and cathodal compartments contained buffer solution (25 mM HEPES/133 mM NaCl, pH 7.4). The HupA formulation (4 mM in 10 mM MES; pH 5.0) was placed in the donor compartment. A power supply (Kepco APH 1000 M; Flushing, NY) delivered a constant, direct current of 0.5 mA cm^{-2} for 5 h. Blood samples (0.5 ml) were withdrawn at hourly intervals in pre-heparinzied tubes and immediately centrifuged at 10,000 rpm; the plasma collected was separated and stored at -20 ºC until analysis by HPLC. After the withdrawal of each sample, the blood volume was

replaced with the same volume of saline solution. At the end of each experiment, the animals were euthanized with pentobarbital sodium.

Analytical procedure for quantification of HupA

A P680A LPG-4 pump equipped with an ASI-100 autosampler and a UV170U detector (Dionex; Voisins LeBretonneux, France) were used to assay HupA. Isocratic separation was performed using a 125 mm x 4 mm LiChrospher® column packed with 5 µm C18 end-capped silica reversed-phase particles. The flow rate and injection volumes were 0.8 ml min^{-1} and 25 µl, respectively; the column temperature was maintained at 30 ˚C. The mobile phase consisted of 60:40 (% v/v) methanol: water (with 0.05% triethylamine) and HupA was assayed using its UV absorbance at 306 nm. The LOD and LOQ were 250 and 300 ng/ml, respectively. ACE was analyzed separately using the same column at a flow rate of 1.0 ml/min, with a column temperature of 30°C and using 220 nm as the detection wavelength. The mobile phase consisted of 80% methanol and 20% citrate buffer (10 mM citric acid and 7 mM sodium citrate, pH 3.0). The LOD and LOQ were 400 and 500 ng/ml, respectively.

Table 2 Precision and accuracy values for the analytical method used to quantify HupA in rat plasma

Theoretical concentration ($ng.ml^{-1}$)	**Experimental concentration ($ng.ml^{-1}$)**	**CV (%)[a]**	**Accuracy (%)[b]**
Intra-day (n=3)			
25	23.17	3.54	92.70
100	95.33	7.45	95.33
500	481.40	4.29	96.28
Inter-day (n=3)			
25	24.02	5.14	96.10
100	97.68	10.73	97.68
500	489.49	6.08	97.90

[a] Precision = (SD/mean) x 100
[b] Accuracy = (obtained concentration/theoretical concentration) x 100

Analysis of plasma extracts was performed using the same HPLC system and column coupled to a RF2000 fluorescence detector (Dionex; Voisins LeBretonneux, France). The mobile phase comprised water-methanol-triethanolamine (45:55:0.05, v/v/v), the flow rate

was 1.0 ml/min and the temperature of the column oven was 40 ˚C. Fluorescence detection was performed at excitation and emission wavelengths of 310 and 370 nm, respectively. The extraction procedure was adapted from a previous report.[16] In brief, 75 µl of 1 M NaOH was added to 0.2 ml of plasma. After vortexing, the mixture was extracted with 1.5 ml chloroform by vortex-mixing for 5 min. The mixture was subjected to centrifugation at 10,000 rpm for 10 min; the organic phase was then transferred to another tube and evaporated to dryness under a gentle stream of nitrogen. The residue was reconstituted in 400 µl of mobile phase and then 50 µl was injected into the HPLC. A calibration curve was prepared over a concentration range of 20-1000 ng/ml in triplicate and the method was validated for accuracy and precision (Table 2). The LOD and LOQ were 15 and 20 ng/ml, respectively.

Pharmacokinetic models

Pharmacokinetic parameters for the iontophoretic delivery of HupA were calculated using constant- and time-variant input models. [17,18] Both models are based on a one-compartment model with zero order absorption and were plotted using WinNonlin® software (version 6.2.1; Pharsight, Inc., Apex, NC).

The constant input model is described by:

$$C_P = \left(\frac{K_{input}}{V_d\ k_{el}}\right) * \left(1 - e^{-k_{el}\,t}\right) \tag{3}$$

where C_P is the plasma concentration of HupA at time (t), V_d is the volume of distribution, K_{input} is the constant input rate and k_{el} is the elimination rate constant.

The time-variant input model is given by:

$$C_P = \frac{\frac{I_0(K_R - k_{el} + k_{el}e^{-K_R t})}{k_{el}(K_R - k_{el})} - \frac{I_0 K_R}{k_{el}(K_R - k_{el})}\, e^{-k_{el}t}}{V_d} \tag{4}$$

where C_P is the plasma concentration of HupA at time (t), I_0 is zero-order mass transport rate, K_R is the constant describing the first-order release rate of HupA from skin into the plasma, k_{el} is the elimination rate constant and V_d is the volume of distribution.

Plasma profiles were fitted using a Gauss–Newton algorithm with Levenberg–Hartley modification. $AUC_{0\text{-}300}$ was calculated in MS Excel and the cumulative amount of HupA delivered was calculated by using a deconvolution method. The volume of distribution and elimination rate constant of the drug were obtained from literature.[19]

Data analysis

Data were expressed as the Mean ± S.D. Outliers determined using the *Grubbs test* were discarded. Results were evaluated statistically using either analysis of variance (*ANOVA*) followed by *Student Newman Keuls test* or by *Student's t-test*. The level of significance was fixed at α=0.05.

RESULTS AND DISCUSSIONS

Stability studies

HupA was found to be stable in the presence of both human and porcine epidermis and dermis after 12 h (97.3 ± 3.5%). After 6 h of current application at 0.5 mA.cm^{-2}, the HupA concentration in solution was 98.7 ± 2.1% of that measured initially, confirming the stability of the drug in the presence of an electric current.

Effect of increasing HupA concentration on transport

Passive permeation of HupA after 6 h from a 2 mM solution was 1.1 ± 0.1 µg.cm^{-2}. In contrast, anodal iontophoresis of HupA at 0.5 mA.cm^{-2} using a 1, 2 and 4 mM buffered solution resulted in cumulative permeation of 82.5 ± 12.5, 202.9 ± 5.2 and 318.4 ± 90.1 µg.cm^{-2}, respectively after 6 h. Cumulative HupA permeation and steady-state iontophoretic flux as a function of donor concentration are illustrated in Figure 2. Increasing HupA concentration in the solution from 1 to 4 mM gave a proportional ~4 fold increase in cumulative permeation and steady state flux. Regression analysis confirmed that the flux (J_{tot}) increased linearly with the concentration (r^2 = 0.99). Thus, in this case, increasing HupA concentration in the formulation resulted in a statistically significant (ANOVA, α=0.05) increase in steady state flux even in the "apparent" absence of competing ions since the formulation was separated from the anodal chamber by a salt bridge. It has previously been hypothesized and confirmed experimentally, that iontophoretic flux is independent of drug concentration in the absence of other co-ions and is largely determined by the ratio of drug diffusivity in the skin to that of the predominant counter-ion on the opposite side of the membrane (i.e., Cl^-).[20] These observations were made when the ratio of drug to Cl^- ions was

in the range of 0.1-10. It is reasonable to assume that there has to be some threshold concentration below which this ratio cannot be maintained due to the presence of insufficient amounts of permeant in the formulation. The 4-fold flux enhancement seen here occurs when the HupA/Cl^- concentration ratio is much lower (0.007-0.03) and at this ratio the flux appears to show a dependence on the concentration of the permeant. Thus, increasing the Hup A concentration in the formulation may have decreased the effect of drug depletion from the formulation in the donor compartment (the fraction of the drug load permeated across the skin was between 66 and 84%) and hence resulted in the observed increase in flux. However, zwitterionic MES (used to buffer the solution) may also compete – to some degree – to carry current and the effect of this competition would also be reduced by increasing HupA concentration. Increase in HupA concentration also produced a significant increase in the skin deposition.

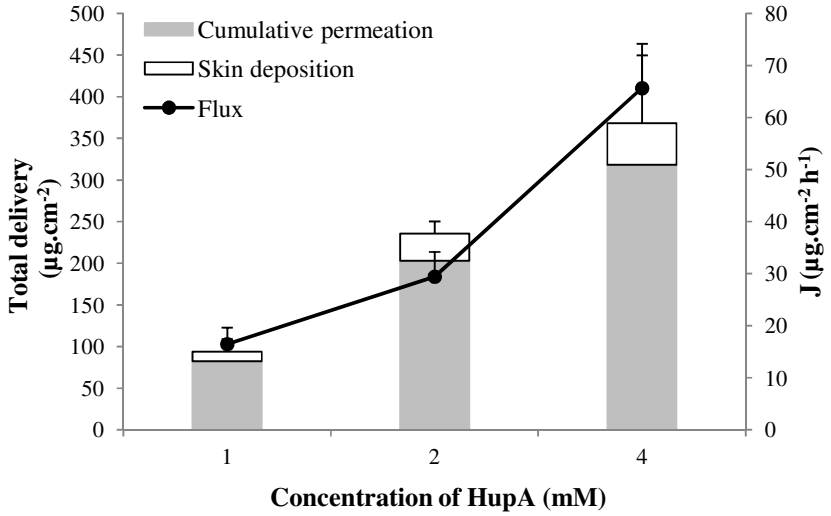

Figure 2. Total delivery (cumulative permeation + skin deposition) and steady state flux (J) of HupA as a function of concentration (at 1, 2 and 4 mM in 10 mM MES; pH 5) across porcine skin after transdermal iontophoresis for 6 h at 0.5 $mA.cm^{-2}$ (Mean ± S.D.; n≥5).

Effect of increasing current density on HupA permeation

Upon increasing current density from 0.15 to 0.3 and 0.5 $mA.cm^{-2}$, cumulative iontophoretic permeation of HupA (2 mM in 10 mM MES; pH 5.0) increased from 116.7 ± 14.1 to 147.8 ± 22.1 and 202.9 ± 5.2 $\mu g.cm^{-2}$, respectively (Figure 3). Data analysis confirmed that there was a statistically significant increase in HupA flux upon increasing current density from 0.15 to 0.3 and 0.5 $mA.cm^{-2}$ (ANOVA (α=0.05) followed by *Student Newman Keuls test*). According to Phipps and Gyory, the flux of an ion is linearly proportional to the applied

current density and holds for almost all ions.[21] This relationship can be used to control input kinetics and the delivery of drug can be increased to get better efficacy. Drug extraction from the skin carried out at the end of the iontophoretic experiments also showed a statistically significant (ANOVA (α=0.05) increase in skin deposition with increase in applied current density (Figure 3). The tendency of HupA to form a depot in the skin may be exploited to provide a sustained post-iontophoretic release of drug into the bloodstream. Thus, it might be possible to use to avoid shorter duration current application and so reduce the risk of skin irritation caused by patch components or current.

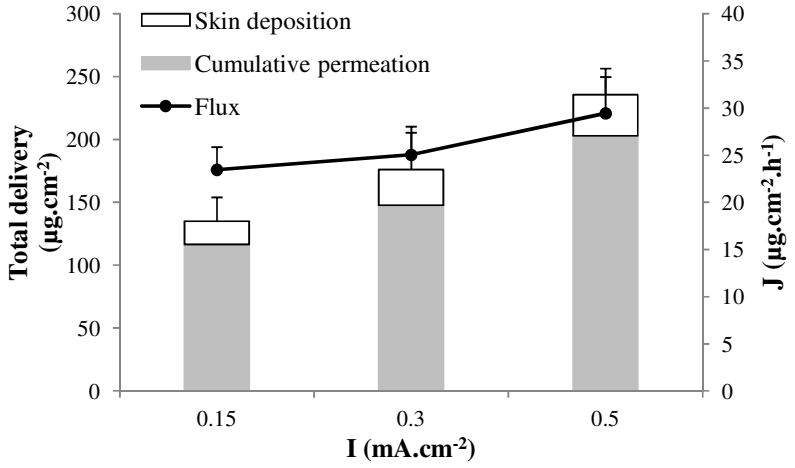

Figure 3. Total delivery (cumulative permeation + skin deposition) and steady state flux (J) of HupA (2mM in 10 mM MES; pH 5) as a function of current density (at 0.15, 0.3 and 0.5 mA.cm^{-2}) across porcine skin after transdermal iontophoresis for 6 h (Mean ± S.D.; n≥5).

Table 3 Iontophoretic transport kinetics of HupA and the relative contributions of electromigration and electroosmosis

Current (mA.cm^{-2})	J_{tot} (µg.cm^{-2} h^{-1})	J_{EM} (µg.cm^{-2} h^{-1})	J_{EO} (µg.cm^{-2} h^{-1})	% EM	% EO	Inhibition factor
0.15	23.4 ± 2.4	22.7	0.77	96.7	3.3	1.32
0.3	25.0 ± 3.0	23.5	1.54	94.0	6.0	0.99
0.5	29.5 ± 4.7	28.1	1.37	95.5	4.5	1.03

J_{tot}: total steady state flux; J_{EM}: electromigration flux; J_{EO}: electroosmotic flux; %EM and %EO are the % contributions of EM and EO to total electrotransport; IF: inhibition factor.

Mechanism of HupA transport

Co-iontophoresis of ACE enabled the contributions of EM and EO to HupA electrotransport to be estimated at each current density (0.15, 0.3 and 0.5 mA.cm^{-2}). Iontophoretic transport of ACE is exclusively dependent on the electrically-induced convective solvent flow and, as such, it can be used to report on EO.[15,22] Calculation of the iontophoretic flux of ACE enabled the linear solvent velocity (V_W) to be determined, which in turn was used to estimate the contributions of EM and EO to HupA electrotransport. The results showed that > 92 % of HupA delivery could be attributed to EM (Figure 4); hence, EO played only a minor role. HupA is a primary amine with a pKa of 6.97 implying that it is almost completely ionized at pH 5 and hence well suited to delivery by EM. The inhibition factor (IF) – i.e., the ratio of ACE flux in the absence or presence of HupA – was between 0.99-1.32 showing that convective solvent flow was not inhibited by HupA electrotransport at any of the current densities (Table 3). Thus, HupA did not appear to interact with the fixed negative charges in the skin and hence did not affect skin permselectivity.

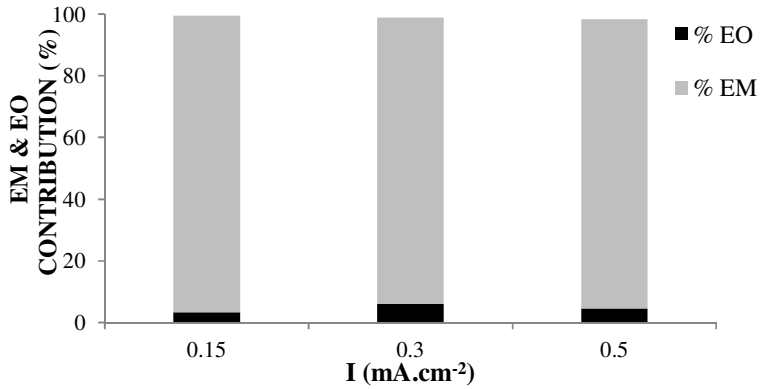

Figure 4. Relative contributions of EM and EO to the total HupA flux as a function of current density (0.15, 0.3 and 0.5 mA.cm^{-2}) with 2 mM HupA solution (in 10 mM MES; pH 5) (Mean ± S.D.; n≥5).

Transport and delivery efficiency

The transport number is defined as the fraction of the total charge transported by a specific ion during iontophoresis. The sum of the transport numbers of all of the ions acting as charge carriers in the system (on both sides of the skin) must equal 1. The transport efficiency of HupA at the different current densities is low which is due to its low concentration and low mobility as compared to endogenous ions, Na^+ and in particular Cl^- present in the receiver compartment which is the principal charge carrier (Figure 5). In contrast, the delivery efficiency of HupA, defined as the ratio of the amount permeated to the amount present in the

formulation in the donor compartment, was extremely high confirming that HupA is ideally suited for iontophoretic delivery (Figure 5). High delivery efficiency is rare in transdermal systems where the maximum efficiency usually achieved is ~20%. Hence, an optimized transdermal iontophoretic system for HupA would contain minimal amounts of undelivered drug and hence offer an industrially feasible alternative to solid oral dosage forms.

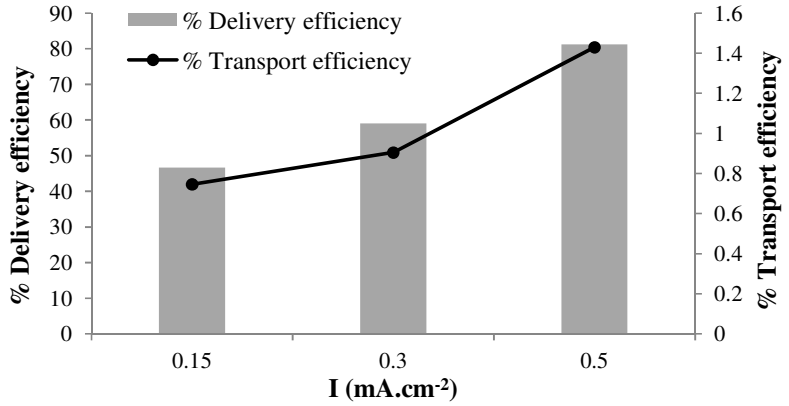

Figure 5. Delivery and transport efficiency (%) of HupA after 6 h iontophoresis at different current densities (at 0.15, 0.3 and 0.5 mA.cm^{-2}) with 2 mM HupA (in 10 mM MES; pH 5).

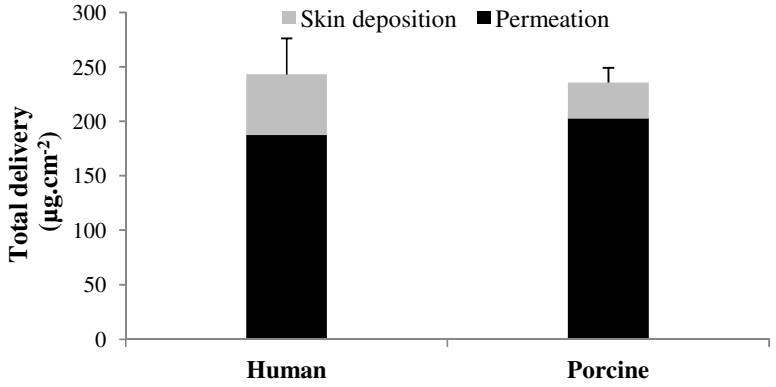

Figure 6. Total HupA delivery (sum of amounts permeated and deposited within the skin) across porcine and human skin after 6 h iontophoresis at 0.5 mA.cm^{-2} with 2 mM HupA in 10 mM MES; pH 5) (Mean ± S.D.; n≥5).

Validation with human skin

Electrotransport of HupA across porcine skin was compared to that using human skin to identify any species-related differences in HupA transport kinetics.[23] Total delivery of HupA, that is, the sum of the amounts permeated and deposited, across human and porcine

skin after iontophoresis at 0.5 mA.cm^{-2} for 6 h was shown to be statistically equivalent (243.2 ± 33.1 and 235.6 ± 13.7 µg.cm^{-2}, respectively; (Student's t-test; (α=0.05)) (Figure 6).

Permeation studies with carbopol gel

The preliminary iontophoretic studies investigating HupA delivery were performed using aqueous solutions; therefore, in a second step, carbopol gel formulations were developed in order to better simulate conditions in an iontophoretic patch system where the drug would be formulated in a reservoir. The gel formulation was stable, there were no signs of drug precipitation after 1 month and drug content was found to be uniform. A statistically significant difference was observed between cumulative permeation of HupA from the gel and buffered solution (2 mM in 10 mM MES) after iontophoresis for 6 h at 0.5 mA.cm^{-2} (135.3 ± 25.2 and 202.9 ± 5.2 µg.cm^{-2} respectively) (Figure 7). The lower transport seen with the gel was attributed to the retarding effect of polymeric matrix that acted as an additional barrier to diffusion. Another possible factor was decreased partitioning of the drug from the gel formulation to the stratum corneum. The 2 mM solution contained 0.5 mg of HupA while the 0.7% loading of gel equated to 0.35 mg in 500 mg of gel. Therefore, an almost equivalent percentage of the drug loading was delivered from the two formulations (77.3% for the gel and 81.2% for the solution); delivery from the gel would be sufficient for therapeutic effect.

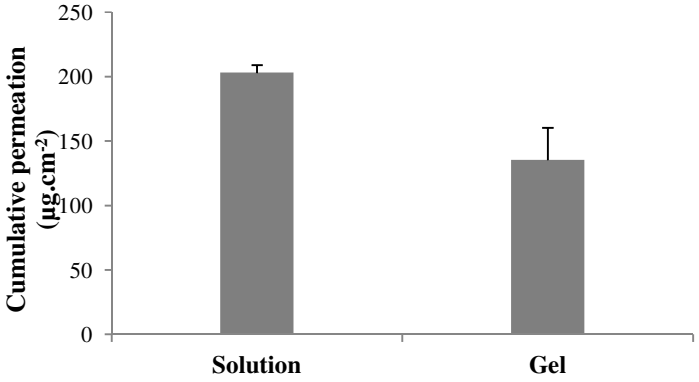

Figure 7. Cumulative permeation of HupA from carbopol gel across porcine skin at 0.5 mA.cm^{-2} for 6 h (Mean ± S.D.; n≥5).

Iontophoretic delivery kinetics of HupA *in vivo*

Drug concentrations in the blood during iontophoretic administration are usually fitted using a constant input pharmacokinetic model similar to that for treating intravenous infusion data in order to derive pharmacokinetic parameters. However, as the name suggests, it is assumed

that the drug input rate is constant throughout the entire period of iontophoretic current application. Moreover, whereas intravenous infusion introduces drug directly into the bloodstream, transdermal iontophoretic delivery *in vivo* is a multi-step process involving release from the formulation into the stratum corneum, transport through the stratum corneum and viable epidermis, entry into the dermis and the capillary network. Therefore, for many, if not most drugs, achieving steady-state flux is not instantaneous and this model can over-estimate plasma drug levels at early time-points and this has led to the development of time-variant pharmacokinetic models.[18] The ability of the constant input and time-variant input models to accurately describe HupA delivery kinetics was compared by fitting the plasma profiles observed upon HupA iontophoresis in rats (Figure 8). The mean plasma concentration–time curve during iontophoretic current application fitted using the constant-input model and its goodness, as indicated by the correlation between the measured and estimated values (predicted from the fit) are shown in Figure 8A and 8B; the corresponding plots for the time-variant input model are shown in Figure 8C and 8D. The much closer approximation of the fitted values to the experimental data demonstrates the superiority of the time-variant model as confirmed by the respective correlation coefficients (Figure 8B and 8D). Furthermore, the akaike information criterion (AIC; measure of the relative goodness of fit) for the time-variant model was also less than that for the constant input model (Table 4).

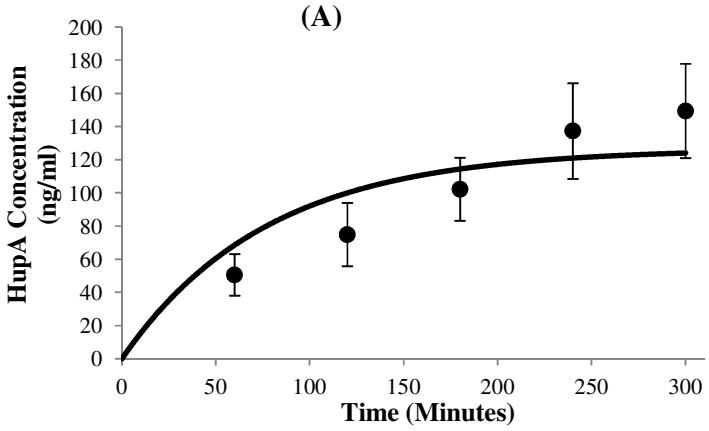

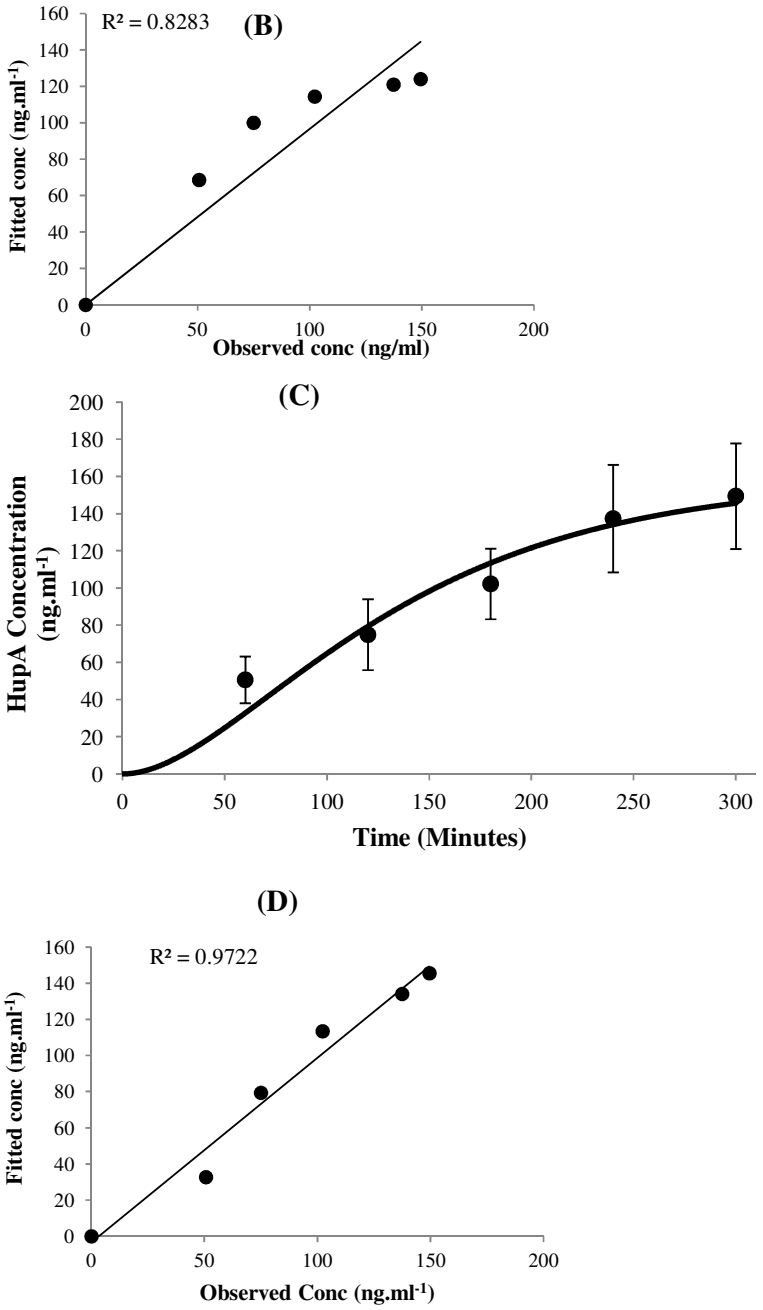

Figure 8. The observed (solid filled circles) and predicted (solid line) mean plasma HupA concentration–time profiles in rats after iontophoretic administration. Data were fitted using constant input (A, B) and time-variant input (C, D) models (Mean ± S.D.; n = 4).

The calculated transdermal absorption rate *in vivo* with both models and the *in vitro* flux (Table 4) across porcine skin were statistically equivalent (ANOVA; α=0.05). As iontophoresis is an energy driven process, this may help to reduce the interspecies variations seen with passive delivery. The control afforded over drug input kinetics as evidenced by the

small standard deviations from the mean values seen in the HupA plasma concentrations may also result in decreased inter-individual variability. Deconvolution revealed that the total amount of drug delivered from the formulation was 532 µg, which corresponded to an exceptional delivery efficiency of 69%. It should also be noted that no erythema was observed at the site of iontophoresis after current application for 5 h.

Table 4 Pharmacokinetic parameters for HupA following iontophoretic administration

Parameters	Constant input model	Time Variant input model
Input rate *in vivo* ($ng.min^{-1}$)	1022.22 ± 85.28[a]	1132.35 ± 183.20[b]
Input rate *in vivo* ($\mu g.h^{-1}$)	61.33 ± 5.12[a]	67.94 ± 10.99[b]
K_R (h^{-1})		1.05 ± 0.39
AIC	47.43	40.95
V_d (L)[c]	0.621	
K_{el} (min^{-1})[d]	0.013	
Input rate *in vitro*[e] ($ng.min^{-1}$)	864.71 ± 83.34	
Input rate *in vitro*[e] ($\mu g.h^{-1}$)	51.88 ± 5.00	
C_{max}	149.48 ± 28.39	
AUC_{0-300} ($ng.h.ml^{-1}$)	26068.05 ± 5545.35	

[a] Input rate calculated for a current application area of 0.78 cm^2
[b] K_{input} as described in equation 3
[c] I_0 as described in equation 4
[d,e] adapted from (16)
[f] porcine ear skin; input rate calculated for a current application area of 0.78 cm^2

There are no reports available on the PK-PD correlation for HupA so the following calculation was made from the known posology. The bioavailability of HupA is 90% and the dose is 1000 µg, indicating a daily input of 900 µg. Based on the calculated transdermal absorption rate *in vivo* and no difference in the absorption between various species the required amount could be delivered from a 5 cm^2 iontophoretic patch in ~ 3 h.

CONCLUSION

Constant-current anodal iontophoresis was successfully used to deliver HupA with high delivery efficiencies (~80%) suggesting that it was an almost perfect candidate for transdermal iontophoresis. The linear dependence of the electrotransport rate on the applied

current density provides a simple means to control the amount of drug delivered *in vivo* and to individualize dosing. Electrotransport was governed by EM and there was negligible EO inhibition, indicating that HupA did not interact with fixed negative charges in the skin. Pharmacokinetic analyses using constant and time-variant-input one compartment models with zero order absorption demonstrated the superiority of the latter. Comparison of the data showed that there was an excellent *in vitro-in vivo* correlation; drug inputs in porcine skin *in vitro* and in rats *in vivo* were statistically equivalent. Based on the delivery *in vivo*, known posology and pharmacokinetics, transdermal iontophoresis could be used to deliver therapeutic amounts of HupA from a reasonably sized patch in only a few hours.

ACKNOWLEDGEMENTS

We thank the Indo Swiss Joint Research Programme (ISJRP 123143) for financial support.

REFERENCES

(1) Johnston, M. V. Cognitive disorders: In *Principles of Drug Therapy in Neurology*, Johnston, M. V., MacDonald, R. L., Young, A.B., Eds.; Davis: Philadelphia, 1992; pp 226-267.

(2) Perry, E. K. The Cholinergic Hypothesis - 10 Years On. *Br. Med. Bull.* **1986,** 42, 63-69.

(3) Wolfe, M.S. Therapeutic strategies for Alzheimer's disease. *Nat. Rev. Drug Discov.* **2002,** 1, 859-866.

(4) Tang, X. C.; Desarno, P.; Sugaya, K.; Giacobini, E. Effect of Huperzine-A, a New Cholinesterase Inhibitor, on the Central Cholinergic System of the Rat. *J. Neurosci. Res.* **1989,** 24, 276-285.

(5) Wang, R.; Yan, H.; Tang, X. C. Progress in studies of huperzine A, a natural cholinesterase inhibitor from Chinese herbal medicine. *Acta Pharmacol. Sin.* **2006,** 27, 1-26.

(6) Wang, B.; Wang, H.; Wei, Z.; Song, Y.; Zhang, L.; Chen, H. Efficacy and safety of natural acetylcholinesterase inhibitor huperzine A in the treatment of Alzheimer's disease: an updated meta-analysis. *J. Neural Transm.* **2009,** 116, 457–465.

(7) Bai, D. L.; Tang, X. C.; He, X. C. Huperzine A, a potential therapeutic agent for treatment of Alzheimer's disease. *Curr. Med. Chem.* **2000,** 7, 355-374.

(8) Little, J. T.; Walsh, S.; Aisen, P. S. An update on huperzine A as a treatment for Alzheimer's disease. Expert Opin. Invest. Drugs **2008,** 17, 209-215.

(9) Kelley, B. J.; Knopman, D. S. Alternative medicine and Alzheimer disease. Neurologist **2008,** 14, 299-306.

(10) Wong, D. M.; Greenblatt, H. M.; Dvir, H.; Carlier, P. R.; Han, Y. F.; Pang, Y. P.; Silman, I.; Sussman, J. L. Acetylcholinesterase complexed with bivalent ligands related to huperzine A: Experimental evidence for species-dependent protein-ligand complementarity. *J. Am. Chem. Soc.* **2003,** 125, 363-373.

(11) Rafii, M. S.; Walsh, S.; Little, J. L.; Behan, K.; Reynolds, B.; Ward, C.; Jin, S.; Thomas, R.; Aisen, P. S. A phase II trial of huperzine A in mild to moderate Alzheimer disease. *Neurology* **2011,** 76, 1389-1394.

(12) Hwang, K. W.; Liu, S. Transdermal rate-controlled delivery of Huperzine A for treatment of alzheimer's disease. **2002**, U.S. Patent 6,352,715.

(13) Tao, T.; Zhao, Y.; Chen, H. Q. Determination of Dissociation Constant, Apparent Solubility and Apparent Partition Coefficient of Huperzine A. *Chin. J. Pharm.* **2005,** 36, 487-489.

(14) Kalia, Y. N.; Naik, A.; Garrison, J.; Guy, R. H. Iontophoretic drug delivery. *Adv. Drug Delivery Rev.* **2004,** 56, 619-658.

(15) Padula, C.; Sartori, F.; Marra, F.; Santi, P. The influence of iontophoresis on acyclovir transport and accumulation in rabbit ear skin. *Pharm. Res.* **2005,** 22, 1519-1524.

(16) Yue, P.; Tao, T.; Zhao, Y.; Ren, J. F.; Chai, X.Y. Determination of Huperzine A in rat plasma by high-performance liquid chromatography with a fluorescence detector. *J. Pharm. Biomed. Anal.* **2007,** 44, 309-312.

(17) Cázares-Delgadillo, J.; Ganem-Rondero, A.; Quintanar-Guerrero, D.; López-Castellano, A. C.; Merino, V.; Kalia, Y. N. Using transdermal iontophoresis to increase granisetron delivery across skin in vitro and in vivo: Effect of experimental conditions and a comparison with other enhancement strategies. *Eur. J. Pharm. Sci.* **2010,** 39, 387–393.

(18) Nugroho, A. K.; Della-Pasqua, O.; Danhof, M.; Bouwstra, J. A. Compartmental Modeling of Transdermal Iontophoretic Transport II: *In Vivo* Model Derivation and Application. *Pharm. Res.* **2005,** 22, 335-346.

(19) Wang, Q.; Chen, G. Pharmacokinetic Behavior of Huperzine A in Plasma and Cerebrospinal Fluid after Intranasal Administration in Rats. *Biopharm. Drug Dispos*. **2009,** 30, 551–555.

(20) Kasting, G. B.; Keister, J. C. Application of Electrodiffusion Theory for a Homogeneous Membrane to Iontophoretic Transport through Skin. *J. Control. Release* **1989,** 8, 195-210.

(21) Phipps, J. B.; Gyory, J. R. Transdermal Ion Migration. *Adv. Drug Delivery Rev.* **1992,** 9, 137-176.

(22) Abla, N.; Naik, A.; Guy, R. H.; Kalia, Y. N. Effect of charge and molecular weight on transdermal peptide delivery by iontophoresis. *Pharm. Res.* **2005,** 22, 2069-2078.
(23) Dick, I. P.; Scott, R. C. Pig Ear Skin as an Invitro Model for Human Skin Permeability. *J. Pharm. Pharmacol.* **1992,** 44, 640-645.

Annexure 1

Expert Opinion

informa
healthcare

Non-invasive iontophoretic delivery of peptides and proteins across the skin

Taís Gratieri, Dhaval Kalaria & Yogeshvar N Kalia†
University of Geneva & University of Lausanne, School of Pharmaceutical Sciences, Geneva, Switzerland

Introduction: Peptides and proteins are playing an increasingly important role in modern therapy. Their potency and specificity make them excellent therapeutic agents; however, their physicochemical properties and stability requirements almost invariably necessitate their administration by subcutaneous, intramuscular or intravenous injection. Controlled non-invasive administration using more patient-friendly advanced delivery technologies may combine the precision afforded by parenteral administration with improved compliance and the potential for individualized therapy.

Areas covered: Transdermal iontophoresis enables hydrophilic charged molecules to be administered through the skin in an effective, non-invasive, patient-friendly manner. This review presents the basic concepts and an analysis of the effect of iontophoretic parameters and molecular properties on electrotransport rates across the skin along with a summary of experimental studies with peptides and proteins. The last section covers other techniques used in conjunction with iontophoresis.

Expert opinion: It has long been known that iontophoresis can administer therapeutic amounts of biologically active peptides into the body. More recent studies have shown that it is also capable of delivering structurally intact, functional proteins non-invasively into and across intact human skin. The next step is to develop cost-effective and easy-to-use iontophoretic patch systems that ensure biomolecule stability, optimize delivery efficiency and address unmet therapeutic needs.

Keywords: iontophoresis, non-invasive, peptide and protein therapeutics, skin, topical, transdermal

Expert Opin. Drug Deliv. (2011) 8(5):645-663

1. Introduction

In recent years an increasing number of peptides and proteins have been proposed as active pharmaceutical ingredients. The average number of new candidates studied has steadily increased from 1.2 a year in the 1970s, to 4.6 a year in the 1980s, to 9.7 a year in the 1990s, to 16.8 a year so far in the 2000s [1]. Given the improved efficacy of peptide synthesis and protein production, it is likely that these potent, selective therapeutics will be the subject of further investment from the pharmaceutical industry [2]. New rational synthetic strategies could also shorten the time spent on research and development and reduce production costs [3] and together with the traditional benefits of peptides (high biological activity, high specificity and low toxicity) make them even more attractive as therapeutic candidates [4,5]. Indeed, advances in biotechnology and bioinformatics have enabled significant progress in the identification of

10.1517/17425247.2011.566265 ISSN 1742-5247

Article highlights.

- The control afforded by constant current iontophoresis over transport rates means that peptide/protein delivery kinetics can mimic endogenous secretion profiles.
- Moreover, complex input kinetics can be used to optimize and individualize therapy.
- Several therapeutic peptides, including luteinizing hormone-releasing hormone and its analogues, vasopressin, somatostatin, somatorelin calcitonin, human parathyroid hormone and insulin, have been investigated in preclinical and Phase I clinical trials; importantly, these confirmed that biological activity was retained post-iontophoresis.
- More recently, it has been demonstrated that it is possible to deliver intact functional proteins across the skin non-invasively. Two-pronged approaches combining iontophoresis with the use of drug carriers or the reversible impairment of skin barrier function have been proposed in order to find potential synergies and to expand further the range of molecules that can be delivered by the transdermal route.

This box summarizes key points contained in the article.

proteins and rational drug design [6,7]. Medicinal chemistry approaches have been used to produce proteolytically stable molecules and to increase receptor selectivity [8]. In many cases chemical modifications have also been applied successfully to overcome the short half-lives of peptide and protein drug candidates [9]. However, the challenge of reaching and maintaining therapeutic levels in the target tissue remains. Poor oral bioavailability means that biopharmaceuticals are primarily administered by subcutaneous, intramuscular or intravenous injection; these invasive procedures entail varying degrees of discomfort and pain for patients and may have an impact on compliance. Furthermore, the pharmacokinetics may result in appreciable variability in blood concentrations with associated side effects [10].

In common with injection-based therapy, the more patient-friendly transdermal route avoids degradation in the gastrointestinal tract and potential first-pass metabolism; although the skin does contain metabolizing enzymes, drug molecules encounter a significantly less challenging enzymatic barrier [11]. Approved peptide and protein therapeutics vary significantly with respect to their physicochemical properties; for example, the molecular mass of romiplostim is almost 170-fold higher than that of thyrotropin-releasing hormone (60 kDa and 360 Da, respectively). Given the properties of their constituent amino acids it is to be expected that they have significant hydrophilic character and are often charged at physiological pH. These physicochemical properties do not favor their partitioning into the lipid-rich intercellular space in the stratum corneum. Nevertheless, these so-called 'undesirable' properties make peptides and proteins excellent candidates for iontophoretic delivery [12,13].

Iontophoresis is a non-invasive technique that involves application of a mild electric current to enhance the penetration of hydrosoluble, ionized molecules into and through tissues [14]. The amount of substance delivered is directly proportional to the quantity of charge passed and depends on the intensity of the applied current, the duration of current application and the area of the skin surface in contact with the active electrode compartment. In addition to precise control over delivery, other advantages include faster onset and offset times. Moreover, the current profile can be customized to enable complex drug input kinetics, for example, pulsatile delivery. This makes iontophoresis very attractive for the treatment of metabolic diseases, as natural physiological secretion profiles can be mimicked. Iontophoresis has been investigated for the delivery of peptides since the 1980s [15,16], with insulin being the most studied molecule at that time [17,18]. Progress in the last decade in microelectronics and engineering processes enabled the development of miniaturized and cost-effective delivery systems [19]; thus, compact fully integrated iontophoretic systems are now available that are far-removed from the first-generation fill-on-site devices. Transdermal iontophoresis is one of the few transdermal technologies that has resulted in the development of products approved by the regulatory authorities – LidoSite® (Vyteris Inc., Fairlawn, NJ, USA) (topical lidocaine delivery for local anesthesia) and Ionsys™ (Alza Corporation, Mountain View, CA, USA) (systemic fentanyl for acute postoperative pain). Although both lidocaine and fentanyl are low-molecular-mass therapeutics, given the excellent patient compliance for passive transdermal systems and their financial success, the appeal of delivering peptides and proteins less invasively should encourage the pharmaceutical industry to explore transdermal technologies such as iontophoresis. The first part of the review presents the basic concepts and an analysis of the effect of iontophoretic parameters and molecular properties on electrotransport rates across the skin; the second part provides an overview of studies with therapeutic peptides and proteins, and the paper concludes with a summary of combination approaches using iontophoresis with a second delivery technology.

2. Iontophoretic transport mechanisms

Molecular transport during iontophoresis can be attributed to three component mechanisms: (enhanced) passive diffusion, electromigration (EM) and convective solvent flow, also called electroosmosis (EO) (**Figure 1**). Assuming that each phenomenon is independent, the total flux of a molecule during iontophoresis can be described as the sum of the fluxes resulting from these three processes (Nernst–Planck theory) [20]:

$$J_{TOT} = J_P + J_{EM} + J_{EO} \quad (1)$$

where J_{TOT} is the total flux, J_P is the passive flux, and J_{EM} and J_{EO} are the fluxes resulting from EM and EO,

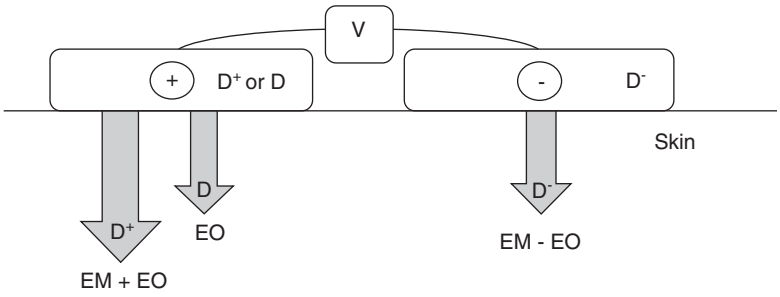

Figure 1. Electromigration (EM) and electroosmosis (EO) and their roles in the transport of charged and neutral molecules during iontophoresis under physiological conditions.

respectively. The role of passive diffusion in iontophoretic delivery is usually minor compared with the two other mechanisms [21].

2.1 Electromigration

Electromigration refers to the ordered movement of the ions in the presence of the applied electric field. This process may be described by Faraday's law [14,20,22-24]:

$$J_{EM} = \frac{It_D}{AFz_D} \quad (2)$$

where I is the applied current (amperes), t_D is the transport number of the drug, A is the cross-sectional area through which transport occurs, F is the Faraday constant (coulombs/mole) and z_D is the drug charge.

The rate of drug delivery is proportional to the applied current (I) and the ability of the drug to function as a charge carrier, which is expressed by the transport number ($0 < t_D < 1$). This parameter describes the fraction of the total charge carried by each species. The transport number of a drug depends on its mobility and concentration and how they compare with the corresponding properties of the other charge carriers present in the system, and is a measure of their relative efficiency as charge carriers [25-27]. Specifically,

$$J_{EM} = \left(\frac{1}{Z_D F}\right)\frac{z_D u_D c_D}{\sum_{n=0}^{i} z_i u_i c_i} I_d \quad (3)$$

where I_d is the applied current density (equal to I/A), and z_D, u_D and c_D refer to the charge, mobility and concentration of the drug in the membrane, respectively; the denominator is the sum of the products of these parameters for each ion in the system contributing to charge transfer across the membrane [14,28]. As peptides and proteins have a high molecular mass, they tend to have lower mobilities than other ions often present in the system, such as Na^+ or Cl^-. Therefore, to increase delivery efficiency, the system needs to be designed to avoid competition with these highly mobile ions. In theory, other approaches would be to increase drug ionization by modulating the pH to increase z_D, or increasing drug concentration in the donor, c_D; however, in practice these changes in the formulation are not always possible and other factors must be taken into account, such as drug stability or skin tolerance to a specific pH.

2.2 Electroosmosis

The skin has an isoelectric point (pI) of ~ 4 – 4.5 [29] and at physiological pH it is negatively charged and acts as a cation-selective ion-exchange membrane. As a consequence, under the influence of an electric field, a convective solvent flow is generated in the anode-to-cathode direction [30-33].

The practical consequence of EO is that it contributes to the permeation of cations but opposes the movement of anions. Furthermore, under physiological conditions, neutral molecules can also be transported from the anode into the body [34]. The relative importance of EM and EO to the total flux of proteins and peptides has been the subject of much investigation [12,21,35,36].

In these studies, a neutral polar molecule with negligible passive transdermal transport (e.g., acetaminophen or mannitol) was used as an EO 'marker' and its flux used to report on EO solvent flow from anode to cathode and hence estimate the EO contribution to the total transport of the molecule of interest. During iontophoresis, the linear velocity (V_w) of the current-induced water flow (centimeters per hour) across the skin can be estimated using [33]:

$$V_W = \frac{J_M}{C_M} \quad (4)$$

where J_M and c_M are the flux and donor concentration of the marker, respectively. It follows that a measurement of J_M at known c_M allows V_w to be determined. It is then possible to calculate the EO contribution to the flux of the peptide drug by multiplying V_w by its concentration in the donor solution (c_D) [29]:

$$J_{EO} = V_W \cdot c_D \quad (5)$$

Three assumptions are implicit in this analysis: i) that drug and marker are transported in a similar fashion by convective solvent flow; ii) that transport of drug and marker is independent and there is no interaction between the two species; and iii) that electroosmotic transport of the marker molecule is proportional to its concentration in the solvent [37].

Using EO markers, it was observed that certain cationic peptides and proteins are able to decrease or even abolish EO flow; surface hydrophobic regions participate in van der Waals-type interactions with structures in the transport pathway, allowing exposed cationic amino acid side chains to form electrostatic interactions with fixed negative charges in the skin [38]. The neutralization of the fixed negative charges results in reduced convective flow. The magnitude and significance of electroosmotic flow inhibition can be expressed by calculating the inhibition factor (*IF*) [36]:

$$IF = \frac{[Q_M, \text{control}]}{[Q_M, \text{peptide}]} \quad (6)$$

where Q_M, control is the amount of marker transported after an iontophoretic experiment when no peptide is present in the donor solution and Q_M, peptide is the corresponding quantity in the presence of the peptide (or protein).

The EO inhibition caused by peptides and proteins can be influenced by their physicochemical properties and the applied current density. As this is increased, more charge has to be transported across the skin; this is partly carried by the peptide, which is driven into the membrane in greater amounts, leading to a more extensive neutralization of the skin's negative charge and a more pronounced EO inhibition.

As, in principle, electric mobility tends to decrease with molecular mass, it was putatively suggested that electroosmosis would become increasingly important for larger molecules and might even be the sole electrotransport mechanism for molecules approaching ~ 1000 Da [39]. However, studies using EO markers have shown that EM can be the dominant transport mechanism for peptides and proteins; for example, for triptorelin (a decapeptide, molecular mass 1311 Da) EM accounted for ~ 80% of overall transport [12]. In such cases the impact of molecule–skin interactions and the reduction of EO flow on total flux can be negligible – as observed during the iontophoretic delivery of cytochrome *c*, a 12.4 kDa protein [35]. When a current density of 0.5 mA/cm^2 was applied, although skin permselectivity decreased, there was no significant impact on the total flux, as EM accounted for ~ 90% of total protein delivery [35]. Similarly, in the case of Ribonuclease A, an RNA cleaving enzyme with a molecular mass of 13.6 kDa, EM was the major driving force, accounting for > 80% of the total flux. Increasing current density from 0.1 to 0.3 mA/cm^2 led to a near fourfold increase in J_{EM} and a twofold increase in J_{EO}. However, a further increase in current density to 0.5 mA/cm^2 produced a decrease in J_{EO} ($IF \sim 5$), indicating either interactions between the permeant and the transport pathway or a more efficient concentration-dependent screening of membrane charge that decreased convective solvent flow. **Figure 2** shows similar marker transport at either 0.1 or 0.3 mA/cm^2 in the presence and absence of the protein; however, there was a significant decrease of marker transport at 0.5 mA/cm^2 in the presence of protein, indicating EO inhibition [40].

3. System parameters affecting delivery

3.1 System design

Iontophoretic systems comprise three main components: the active and return electrode compartments and a microprocessor-controlled power supply (**Figure 1**). Charged drugs are normally placed in the electrode compartment with the same polarity; under physiological pH, neutral molecules are placed in the anode compartment. According to Equation 3 the optimal situation for iontophoresis would be the so-called 'single-ion' case where competing co-ions are absent from the formulation [28]. However, in practice it is difficult to create a 'single-ion system'; competing ions may be present in the pharmaceutical formulation (buffering agents, viscosity modifiers and preservatives), or highly mobile inorganic ions necessary for (or generated by) electrode reactions [25].

Although there are many different types of electrode, the one most suited to iontophoresis is the Ag/AgCl couple, which is reversible at low potential, chemically stable and does not elicit pH changes [14,20,24]. Ag/AgCl electrodes need chloride ions for anodal electrochemistry; thus, the anodal compartment must contain a supply of such ions derived either from the active agent (e.g., present as a hydrochloride salt) or from an external source (e.g., NaCl), in which case the concentration of competing cations in the anodal formulation is greatly increased and the delivery efficiency of the positively charged drug decreased. Strategies to reduce this competition can involve physical (but not electrical) separation of the drug and electrode compartment, such as that based on the well-known 'salt-bridge' concept in electrochemistry (**Figure 3**).

Several recent studies on the iontophoretic delivery of peptides and proteins have been done using salt-bridge assemblies normally composed of agarose and NaCl [35-37,40]. In addition to increasing the proportion of charge carried by the peptide/protein, salt bridges allow its isolation from the electrode compartment. However, it is important to verify whether the protein adsorbs onto the salt bridge [41]. It was demonstrated that reducing the number of competing ions in the formulation significantly increased the transport of a series of tripeptides across porcine skin *in vitro* (**Figure 4**) [37]. The use of a salt bridge increased the EM contribution (which accounted for 77 – 93% of the overall transport); however, as more peptide was carrying the charge, it also increased the inhibition factor of molecules with a propensity to interact with the membrane [37].

Patch-based iontophoretic systems using the same principles have been developed in which the electrode compartment contains an ion-exchange resin to trap Ag^+ ions released from the anode and is separated from the drug reservoir by a size exclusion membrane [42,43].

3.2 Current

Many studies have demonstrated that the iontophoretic flux of a peptide can be enhanced by increasing the

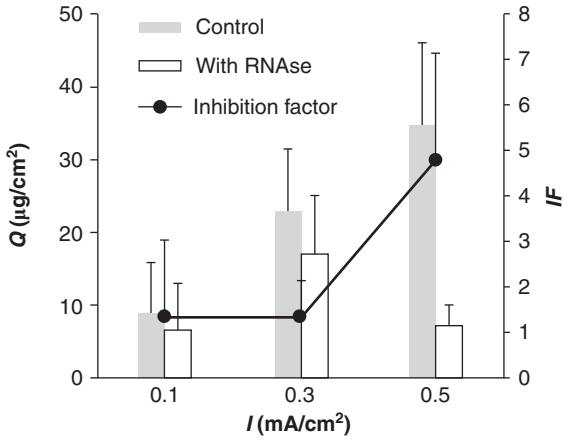

Figure 2. Cumulative acetaminophen permeation (*Q*) across the skin after 8 h of transdermal iontophoresis at 0.1, 0.3 and 0.5 mA/cm^2 in the presence and in the absence of Ribonuclease A [40].

applied current [21,44,45]; linear correlations between flux and current density have been reported for thyrotropin (362 Da) [15] and triptorelin (1311.5 Da) [12].

Although an increased current density usually results in increased permeation, straightforward linear correlations are not always observed. For example, a poor correlation was found between DGAVP (9-desglycinamide, 8-arginine-vasopressin) flux and applied current; a more than sixfold increment in current density did not even double the flux [46]. When working with cationic peptides and proteins one point to be considered with respect to the effect of increasing the current is the potential inhibition of the electroosmotic flow caused by neutralization of the skin's negative charge [36]. This may reduce the response to increases in current. However, lack of response to increases in current can also be a result of concentration polarization of the molecule in the transport pathways; this results in a plateauing of the current–response profile. This behavior was observed with cytochrome *c* [35] and in the iontophoretic delivery of Ribonuclease A [40]. In this study, a threefold increase in current density from 0.1 to 0.3 mA/cm^2 resulted in a corresponding increase in protein permeation; however, a further increase in applied current density to 0.5 mA/cm^2 did not produce a statistically significant increase in transport (**Figure 5**).

Linear relationships between steady-state flux and current intensity provide flexibility in controlling drug input kinetics. In terms of patient compliance and current tolerability, the upper limit for the current density applied *in vivo* is considered to be ~ 0.5 mA/cm^2 [47]. Although tingling and itching sensations as well as erythema (which resolves without sequelae) are frequent and well-tolerated side effects, higher current densities can provoke pain and discomfort [47]. Another approach to reduce patient discomfort and skin irritation is the use of a pulsed current profile (direct current with a varying on/off ratio) instead of a continuous direct current [48-51]. The hypothesis is that pulsed waveforms allow time for the skin to depolarize and return to its initial state before the onset of the next pulse, provided that the depolarization period is sufficiently long to discharge the membrane capacitance. In this way, charge does not accumulate in the stratum corneum and skin irritation resulting from polarization is presumably avoided [52,53]. It has been shown that a pulsed direct current profile using 0.5 mA/cm^2 is more efficient at transporting luteinizing hormone-releasing hormone (LHRH) and nafarelin than direct current profiles across the human epidermis *in vitro* [54]. Although the use of a pulsed current profile seems to be promising for the delivery of peptides and proteins, few groups have worked with these current profiles. More mechanistic studies on the efficiency of such systems are needed.

3.3 Drug concentration

A priori, Equations 2 and 3 suggest that increasing the drug concentration in the formulation will result in an increased transdermal flux via an increase in t_D, and indeed this has been observed in some cases. The steady-state flux of H-Tyr-D-Arg-OH (molecular mass 337 Da, charge = +1) increased linearly with donor peptide levels over the concentration range examined (**Figure 6**). EM was the dominant transport mechanism, accounting for > 70% of iontophoretic delivery. Both EM and EO contributions displayed a linear dependence on peptide concentration, suggesting that peptide–peptide and peptide–skin interactions were of an insufficient level to have an impact on electrotransport. Moreover, the relative contribution of EO to peptide electrotransport was not significantly different at each concentration, confirming the absence of an inhibition effect [21].

For certain molecules, however, the flux–concentration profiles reach a plateau above which further increases in concentration have only a limited or negligible effect on flux. One fact to be considered is the concentration and mobilities of competing ions. When the donor formulation contains a source of competing ions, the initial linear dependence that is observed between flux and drug concentration may fade as concentration increases: once the product of the drug concentration and mobility is in sufficient excess of the corresponding values for the competing ions, the flux may become independent of drug concentration. A second factor to be considered is the ability of the molecule to bind with skin structures along the iontophoretic transport pathway. The transport of some positively charged peptides that interact with skin and affect the EO, such as nafarelin and leuprolide, shows a nonlinear dependence on concentration [38,55-62]. In these cases, the impact on drug delivery can depend on the relative contribution of EO to the iontophoretic transport of the molecule in question [59,63].

A third factor is that simply increasing the amount of drug in the formulation may not increase the number of molecules

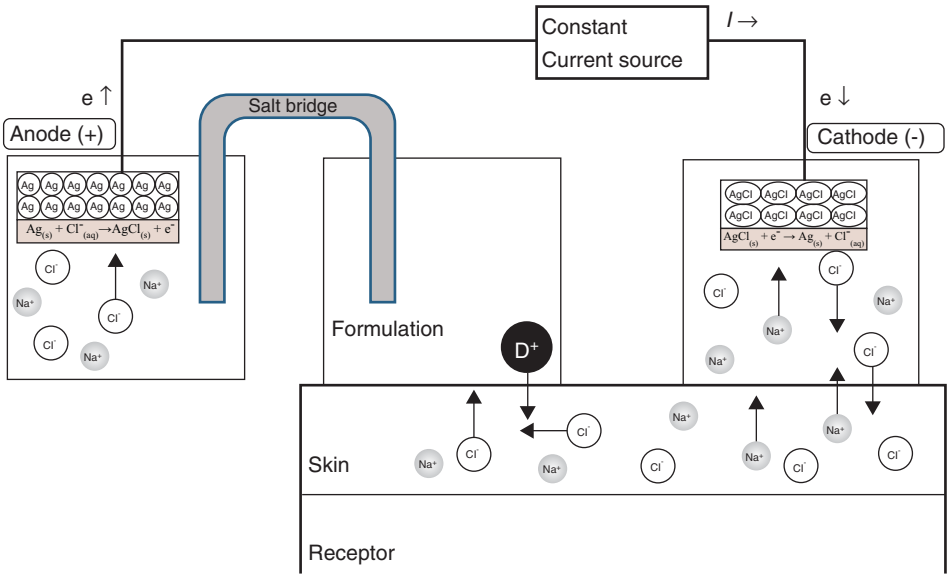

Figure 3. Iontophoresis using a Ag/AgCl electrode system. The anodal compartment is connected to the drug-containing compartment by a salt bridge. Application of an electric potential causes a current to flow through the circuit. At the anode–solution interface, the Ag^+ and Cl^- react to form insoluble AgCl, which is deposited on the electrode surface. Electromigration transports the cations, including the drug molecule, from the anodal compartment into the skin. At the same time, endogenous anions, primarily Cl^-, move into the anodal compartment. In the cathodal chamber, Cl^- ions are released from the electrode and electroneutrality requires that either an anion is lost from the cathodal chamber or that a cation enters the chamber from the skin.
Adapted from [13].

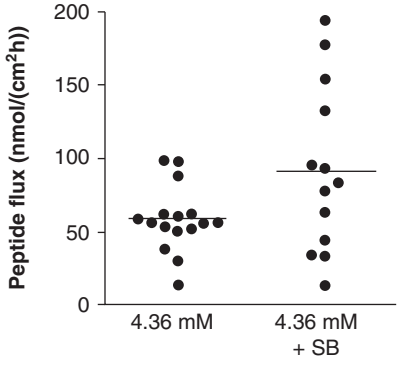

Figure 4. The influence of the salt bridge (SB) on the transport of a series of tripeptides across porcine skin *in vitro*.
Adapted from [37].

in the membrane. The formation of aggregates may hinder peptide delivery, reducing drug mobility and affecting EM. This was reported as being responsible for the anomalous iontophoretic behavior observed with triptorelin, where a twofold increase of peptide in the formulation produced a twofold decrease in delivery [12].

3.4 pH

In principle, drug permeation can be optimized by controlling the ionization state of the drug and/or that of the skin through manipulation of formulation pH. The degree of drug ionization will affect the mobility and hence EM, whereas the ionization state of the skin determines EO solvent flow. As peptides generally possess a mixture of weakly acidic and basic groups, then, depending on the specific pH value, they can be predominantly anionic, cationic or neutral. With respect to the skin, its charge should be such that it favors EO flow in the direction of drug movement. For example, for basic peptides with pI > 8, it will usually be more appropriate to keep the pH at least one unit below the pI (~ 7) so that the molecule will be positively charged and the skin negatively charged, facilitating both EM in the anode and EO, whereas in the case of acidic peptides with pI < 4, it may be useful to use pH 5 or 6, providing EM in the cathode and reducing the effect of EO [14]. The effect of pH on the iontophoretic delivery of two amino acids, histidine and lysine, was compared at pH 4 and 7.4 [64]. In the case of lysine (pK_a 9.59), increased delivery was observed at pH 7.4 because then EO also contributed to the transport of the charged amino acid. By contrast, for histidine (pK_a 6.5), higher transport was observed at pH 4 than at pH 7.4 because histidine is > 90% uncharged at pH 7.4 and is no longer subject to EM and, as a result, its iontophoretic transport depends exclusively on EO [64]. Conversely, the transport of thyrotropin-releasing hormone (TRH) at pH 8 with 98% uncharged peptide was twice that at pH 4 where TRH is ~ 99% protonated [15].

Although modulation of formulation pH can certainly be used to improve transport, in practice the formulator has

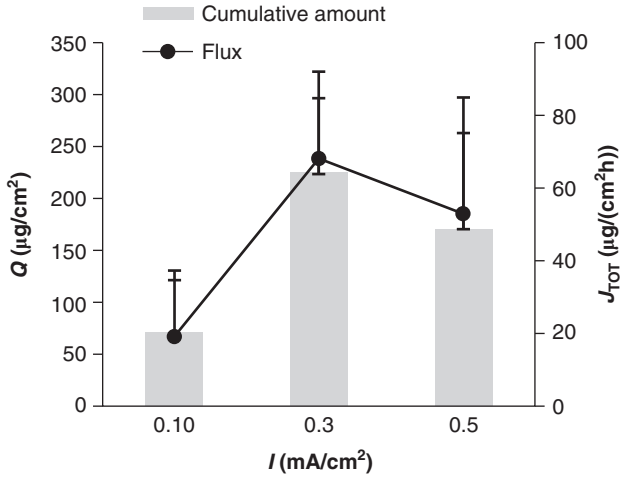

Figure 5. Effect of current density on cumulative permeation (Q) and steady-state flux (J_{TOT}) of Ribonuclease A across porcine skin [40].

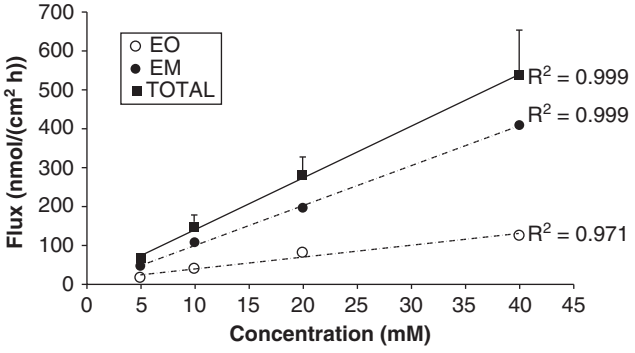

Figure 6. Electroosmosis (EO) and electromigration (EM) contributions to the iontophoretic delivery of tyrosine-D-arginine dipeptides (YdR). Data show the mean steady-state flux (± s.d.) as a function of YdR concentration in the formulation [21].

only limited options. Realistically, for a formulation to be acceptable for skin application it will probably have a mildly acidic to neutral pH (5 – 7.4) – extreme pH values can irritate the skin or even cause chemical burns. In addition, a key issue will be the stability of the biopharmaceutical as a function of pH, and a compromise is required that ensures both applicability and stability. Thus, although low pH (3.6) has been used during anodal iontophoresis of cationic insulin to decrease peptide degradation, this is not an option for application *in vivo* [65]; similarly, cathodal iontophoresis of anionic insulin has been studied at pH 10 in order to decrease aggregate formation – at pH > 9 aggregation is reduced and monomers and dimers are present in higher percentages. Indeed, the results showed much higher plasma levels in rats following iontophoresis at pH 10 as compared with a formulation at pH 7 [66]. However, such a basic formulation cannot be envisaged for use in patients.

In addition, at extremes of low and high pH, there will, by definition, be substantial concentrations of hydroxonium and hydroxide ions, respectively. These ions have high electrical mobilities and at elevated concentrations can cause significant reduction in the iontophoretic delivery of larger drug molecules, which have lower mobilities and may be present at low concentrations in the formulation. With respect to skin pH, although this can be changed for *in vitro* experiments by modifying the pH of the bathing solution in contact with the membrane, this is rather more difficult to achieve *in vivo* owing to the skin's intrinsic buffering capacity [67].

3.5 Formulation

The most obvious formulation factors affecting iontophoretic delivery are the formulation pH (discussed previously) and the presence of competing ions. As discussed in Section 3.1, in cases where the electrodes can be separated from the drug reservoir the so-called 'single-ion' situation can be applied, where the drug is the only ionic species that can contribute to charge transport, that is, all other competing cations have been eliminated from the formulation. Under these conditions, the drug competes only with endogenous counter-ions, for example a cationic drug will compete with subdermal chloride. However, in some cases addition of excipients such as stabilizers and preservatives may be necessary and the efficiency of drug delivery can be lowered [68]. In such cases, the drug concentration relative to that of competing co-ions, not the nominal drug concentration *per se*, should be considered; in fact, the use of molar fraction has also been suggested [23,26,63,69,70].

Another important point to consider is the ease of application of the formulation in a clinical situation. Although *in vitro* experiments are usually performed using aqueous solutions, pre-filled iontophoretic patch drug reservoirs will most probably use hydrogels, and these have attracted increasing attention in recent years in view of their adhesiveness and biocompatibility [71,72]. Hydrogels are three-dimensional networks of hydrophilic polymers capable of retaining large amounts of water or biological fluids within their structure; because of the high water content they possess good electrical conductivity and can be used for transdermal iontophoretic delivery [73-78]. Furthermore, network structure and composition can be manipulated to influence the permeation and diffusion characteristics of a drug within the hydrogel [79]; these changes must take into account the charge of both the polymer and the drug. Normally, drug release is reduced when the molecule has the opposite charge to the polymer and is favored when they have the same charge [80].

The combined use of drug carriers and iontophoresis has also been reported. Liposomes [81-85], microemulsions [86,87] and solid lipid nanoparticles [88] have been used as vehicles for iontophoretic drug delivery. Some reports claim that charges could be imparted to neutral drugs by encapsulating

them in charged drug carriers, which could be delivered by iontophoresis [88]. Higher accumulation of drug carriers in the hair follicle has also been shown [83]. Furthermore, enhanced transport and drug accumulation in the skin have been observed on incorporation into nanoparticles [89-91]. However, information on whether these carriers can penetrate the skin is still controversial. Some reports show that the drug but not the carrier is delivered [92,93]. Therefore, with respect to the iontophoretic delivery of peptides, the concomitant use of a drug carrier system would probably be justifiable only if it represented a significant increase in molecular solubility and/or stability. Indeed, it has been suggested that encapsulation could protect a peptide from degradation [84]. Iontophoretic delivery of ciclosporin A across human cadaver epidermis has been investigated using colloidal systems (lecithin vesicles and microemulsion) [94]; the liposomes enhanced aqueous solubility ~ 100-fold. Of the formulations tested, highest drug permeation was observed from lecithin vesicles under anodal iontophoresis, followed by anodal iontophoresis of a microemulsion. Although both the microemulsion and lecithin vesicles were negatively charged, cathodal iontophoresis resulted in the lowest permeation of ciclosporin A, suggesting that the carriers were not penetrating the skin themselves. However, by improving drug solubility, they increased the concentration gradient and hence the flux. So far very few studies have focused on the use of formulation conditions to improve the iontophoretic delivery of peptides. However, that should change because peptides and proteins are comparatively high-cost molecules and an increase in drug solubility and/or stability could make possible therapy using lower more cost-effective drug loads in patch systems.

4. Molecular factors affecting delivery

For a long time the molecular mass was considered to be the main factor affecting transdermal iontophoretic transport. However, it has recently been shown that molecular mass or size is not a sufficiently discriminating parameter to explain subtle differences in transport. An investigation into the effect of charge and molecular mass on the electrotransport of a series of dipeptides showed that an increase in charge could compensate for an increase in molecular mass [95]. For example, a comparison of lysine and H-Lys-Lys-OH transport revealed that the twofold increase in molecular mass was compensated by doubling the charge; by contrast, H-His-Lys-OH, with approximately the same molecular mass as H-Lys-Lys-OH but unit charge (at pH 7.4), had a significantly lower flux. The ratio of charge to molecular mass (and hence molecular volume) will influence the electric mobility of a molecule.

Even though the charge/molecular mass ratio explains the different delivery profiles of small peptides, the effective mobility of a peptide or a protein will also depend on volume, shape and charge distribution within the molecule. It is therefore likely that secondary, tertiary and quaternary structure of a protein will be important in determining iontophoretic transport. Indeed, different sequences of the same three amino acids within a tripeptide have been shown to affect transport behavior significantly [96]. Capillary zone electrophoresis (CZE) may be a promising tool to determine the effective mobility, providing an estimation of the EM contribution to transdermal iontophoretic flux [97,98]. However, if the molecule of interest interacts with the skin transport pathway, then CZE will not provide an accurate prediction of transport [35].

5. Iontophoretic delivery of therapeutic peptides and proteins through the skin

Several studies have been performed on the iontophoretic delivery of therapeutic peptides, and these are briefly described below (see also **Table 1**).

5.1 Diabetes and insulin delivery

One of the greatest challenges for non-invasive peptide and protein delivery concerns insulin. Iontophoretic delivery of insulin has been studied extensively both *in vitro* [99-106] and *in vivo* in small animals [105,107-109]. However, the physicochemical properties of insulin hinder its iontophoretic delivery: the insulin monomer is a ~ 6000 Da negatively charged peptide (51 amino acids) with pI ~ 5.4. This means that when insulin is delivered as a cation from the anode it will tend to become 'neutral' on contact with the skin's outermost layers (pH ~ 5) before becoming predominantly negatively charged within the skin (pH > 5.4 in the inner layers) – hindering its anodal transport [24]. Conversely, when it is delivered as an anion from the cathode, not only will cathodal delivery be opposed by EO, but also insulin may decrease its anionic character in the upper layers of the skin. Hence, its pI plays an important role in its iontophoretic transport, explaining its poor permeation by both anodal and cathodal deliveries [110]. Moreover, the formation of dimers and hexamers at relatively low concentration complicates delivery further. Thus, the iontophoretic delivery of insulin analogues may be more favorable; the highest iontophoretic flux was observed for a sulfate analogue of monomeric porcine insulin, which had a pI ~ 2.5 and a net -8 charge at pH 7.4 [100]. The iontophoresis of a monomeric insulin analogue in diabetic rats (with intact skin) was also reported to reduce plasma glucose levels [107].

Although early studies showed that iontophoretic delivery of insulin resulted in a reduction in blood glucose levels in small animals, the challenge is to extrapolate these results to humans, where significantly greater quantities of the hormone are required for pharmacologic effect. A normal healthy individual produces 18 – 40 IU (where 1 IU ~ 0.04 mg) of insulin a day, which corresponds to 0.2 – 0.5 IU/(kg day). Approximately half of this is secreted in the basal state and the rest is secreted in response to meals. Therefore, the basal secretion rate is ~ 0.5 – 1.0 IU/h; an iontophoretic system would have to provide a drug input rate of 0.02 – 0.04 mg/h to match the

Table 1. List of relevant studies applying iontophoresis for delivery of therapeutic peptides and proteins *in vitro* and *in vivo*.

Therapeutic agent	Approximate molecular mass (Da)	Model	Observations
Insulin	6000	Diabetic rats	Monomeric human analogue (intact skin) and bovine insulin (impaired barrier) induced decrease in blood glucose level [107]
		Porcine epidermis *in vitro* and diabetic rats	Combination approach with permeation enhancers increased transport [105]
Human calcitonin	3500	Rats	Hypocalcemia comparable to intravenous [120]
Salmon calcitonin	3430	Rabbits	Therapeutic effect [121]
		Shaved rats	Therapeutic effect [118]
		Rats	Comparable to subcutaneous injection [10]
hPTH	4117	Rats, hairless rats, beagle dogs	Absorption via hair follicles [122]
		Ovariectomized rats	Similar results to subcutaneous injection [123]
LHRH	1182	Yorkshire pigs	Pharmacologically active LHRH delivered [131]
Nafarelin	1322	Human skin *in vitro*	75% pulsed DC current was most efficient in delivery [54]
Leuprolide	1210	Healthy males	Pharmacologically effect [61]
		Healthy males	Comparable to subcutaneous injection [134]
Triptorelin	1311	Porcine skin *in vitro*	Therapeutic amounts delivered [36]
Vasopressin	1084	Human and rat skin *in vitro*	Therapeutic dose delivered [137]
9-desglycinamide vasopressin	1028	Human skin *in vitro*	Transport achieved mainly by electroosmosis [46]
Desmopressin	1183	Diabetic rats	More effective than oral and nasal route [138,139]
Octreotide	1019	Rabbits	Increased flux as function of current and concentration [44]
Vapreotide	1131	Porcine skin *in vitro*	Peptide irreversibly binds to skin but therapeutic concentrations achieved [36]
Somatorelin	3929	Hairless porcine skin *in vitro*	Linear increase in flux with current density but independent of type of current and frequency [50]
		Hairless guinea-pig	Steady-state levels similar to subcutaneous [141]
GHRP	817	Rats	Therapeutic levels achieved [142]
Botulinum toxin	150,000	Humans with hyperhidrosis	Amelioration of symptoms [147,148]
		Rats	Toxin found in hair roots, sebaceous glands and arrector pili muscle fibers [150]

GHRP: Growth hormone-releasing peptide; hPTH: Human parathyroid hormone; LHRH: Luteinizing hormone-releasing hormone.

physiological rate of insulin secretion, and for a conveniently sized 4 cm^2 patch, this equates to drug fluxes of 5 – 10 μg/(cm^2 h) [14]. Furthermore, it is always important to bear in mind the clinical feasibility of the treatment; given the requirements for basal insulin, amounts of ~ 1 mg may need to be given and the duration of current application may become an issue for patients receiving chronic therapy. In addition, in most of the animal studies, significant barrier impairment was necessary to deliver sufficient insulin to decrease blood glucose levels [107,108]. These problems may explain why despite the considerable amount of work so far, there are no reports of successful clinical investigations into the transdermal iontophoretic delivery of insulin in humans.

More recently, effort has been directed at combining other methods with iontophoresis to increase its efficiency. For example, chemical penetration enhancers have been used in combination with iontophoresis in an attempt to increase the permeability of the skin without severe irritation or damage to its structure [105,106,111]. In these studies, a pretreatment with penetration enhancers was usually done before iontophoresis. However, it is important to evaluate the practicality of the different protocols because the duration of pretreatment may be too long; for example, a 2 h pretreatment with saturated and unsaturated fatty acids before iontophoresis was used to produce synergistic enhancement of insulin flux through rat skin *in vitro* [103]. Although an insulin flux of nearly 7 IU/(cm^2 h) was observed from a hydrogel patch using 2 min pretreatment with different classes of permeation enhancers (5% 1,8 cineole, oleic acid and sodium deoxycholate in propylene glycol:ethanol (7:3)) used synergistically followed by 1 h of anodal iontophoresis with a sinusoidal waveform (0.5 mA/cm^2 with 1 kHz frequency), the experiment was performed *in vitro* at pH 3.6 across porcine epidermis prepared by trypsin digestion [105]. Electroporation [66], encapsulation into liposomes [112] and nanovesicles as well as microneedles [113] have been used in combination with iontophoresis to enhance penetration ability of insulin through skin. These techniques are treated in more detail in Section 6.

5.2 Osteoporosis and Paget's disease

5.2.1 Calcitonin

Calcitonin is a 32-amino acid peptide secreted by the thyroid gland. Its major physiological role is to control calcium concentration and metabolism in the body in conjunction with parathyroid hormone. Clinically, it is indicated in the treatment of Paget's disease, in the therapy of postmenopausal osteoporosis, and in malignant hypercalcemia. It is generally given as a subcutaneous or intramuscular injection [114]. However, owing to a short half-life multiple injections are required for optimal pharmacological effect, thus patient compliance is low. The other marketed alternative is a nasal spray, which suffers from low bioavailability [115]. Other disadvantages include irritation of nasal mucosa and variable absorption in the case of nasal disease conditions.

Several studies, both *in vitro* and *in vivo*, have investigated the iontophoretic delivery of this peptide, which carries a positive charge at physiological pH [10,79,109,115-120]. A pulsed current iontophoretic protocol (30 kHz, 30% duty cycle applied for 45 min) was used to deliver salmon calcitonin to shaved rats [118]; in this study, no significant difference in the hypocalcemic effect was observed on increasing the dose, suggesting that a dose–response plateau had been reached [118]. This was also observed by Santi *et al.*, who demonstrated that increasing the intravenous dose of salmon calcitonin from 10 to 25 IU/kg did not produce a significant increase in the hypocalcemic effect [121]. A cutaneous first-pass effect during salmon calcitonin delivery has been proposed [117,118], and the enzymatic inhibitors aprotinin and camostat mesilate were shown to enhance the hypocalcemic effect of salmon calcitonin in rats [117], although aprotinin was not found to modify human calcitonin delivery kinetics across hairless rat skin *in vitro* [120]. More recently, salmon calcitonin was iontophoresed to hairless rats using a wearable and disposable device (WEDD, Travanti Pharma, Inc., (Mendota Heights, MN, USA)); the decrease in calcium levels was similar to that after subcutaneous injection [10]. This device uses Zn and AgCl as the anode and cathode, respectively; when the circuit is closed oxidation of Zn and reduction of AgCl occur spontaneously because of the difference in potential between the two metals. However, such a device imposes a constant voltage (1 V) across the skin, and not a constant current, therefore drug fluxes may vary with skin resistance. Further, this voltage is insufficient for certain applications, including the above study, which required an external power source providing an extra 9 V.

5.2.2 Human parathyroid hormone

Human parathyroid hormone (hPTH) is an 84-amino acid residue peptide that is used in the treatment of osteoporosis because it promotes osteoblast growth. It can have either an anabolic or a catabolic effect on bones, depending on its input kinetics – pulsatile delivery favors its anabolic and antiosteoporotic effects. Suzuki *et al.* conducted a detailed *in vivo* investigation into the pulsatile anodal iontophoretic delivery of hPTH (1 – 34), a pharmacologically active fragment, in Sprague-Dawley rats, hairless rats and in beagles [122]. It was found that an increase in peptide concentration or current density resulted in increased plasma levels of the peptide. The study also demonstrated a linear relationship between the absorption rates and the ratio of hair follicles to epidermal thickness. Based on these results, the main transport route for hPTH (1 – 34) during iontophoresis was suggested to be via the hair follicles, implying that absorption in man might be intermediate between that in hairless rats and beagle dogs. In a subsequent study the anabolic effect of hPTH as measured by changes in bone mineral density in an ovariectomized rat model following pulsatile iontophoresis was compared with that after subcutaneous injection [123]. Their results suggested that a thrice-weekly three pulse protocol (3 × 30 min application of 0.1 mA/cm^2 using a 120 µg patch loading) was equivalent to daily subcutaneous injections of 5 µg/kg.

5.3 Luteinizing hormone-releasing hormone and its analogues

Luteinizing hormone-releasing hormone (LHRH, gonadorelin, molecular mass ~ 1182 Da) is a decapeptide that is secreted by the hypothalamus in a pulsatile mode to activate pituitary release of luteinizing hormone (LH) and follicle-stimulating hormone (FSH). Pulsatile administration of LHRH is used in the therapy of hypogonadotropic hypogonadism. Its positive charge at physiological pH along with its short half-life of ~ 5 min makes it an ideal candidate for transdermal iontophoresis. The iontophoretic delivery of LHRH has been investigated both *in vitro* [54,124-130] and *in vivo* [131]. Iontophoresis of LHRH using the IPPSF model was performed at pH 6 for 2 h; LHRH delivery was monitored for a further 3 h after terminating current application [131]. The flux gradually increased during iontophoresis and decreased rapidly on terminating current flow. It was also shown that the iontophoretically delivered hormone retained its biologic activity.

Nafarelin is a LHRH superagonist with increased efficacy that can be attributed to its high binding affinity to the LHRH receptor and its relatively long biological half-life. Several studies have reported the transdermal iontophoresis of nafarelin *in vitro* [54,57,58,132]. A recent study compared constant/pulsed iontophoresis of nafarelin across human skin [54]; five different current profiles – 100% DC, 75% on/25% off or 50% on/50% off pulsed DC, 75%+/25%- or 50%+/50%-AC – were used in the iontophoretic experiments (current density 0.5 mA/cm^2, pulsed current frequency 500 Hz). The results showed that the 75% on/25% off pulsed DC was the most efficient current profile followed by the 75%+/25%- AC current profile (**Figure 7**). Transdermal administration of lipophilic peptides such as nafarelin with adjacently located positively charged and lipophilic moieties has been difficult owing to adsorption in the negatively charged transport pathways in the skin [38,58].

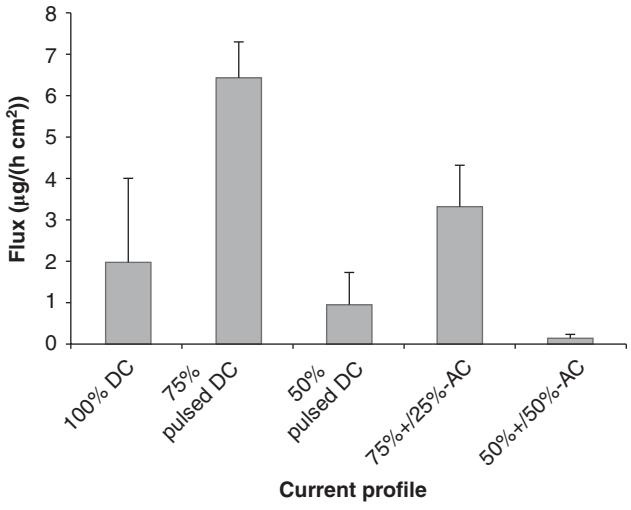

Figure 7. Iontophoretic flux of nafarelin as a function of various current profiles.

Leuprolide, another LHRH superagonist, has also been investigated [61,133,134]. A double-blind, randomized, crossover study in 13 healthy men (5 mg; 0.2 mA, 70 cm^2) showed that the patches, though large, were well tolerated and LH concentration was increased from a baseline of 11.3 ± 3.1 to 56.4 ± 49.6 mIU/ml at 4 h [133]. The iontophoresis of triptorelin (molecular mass ~ 1311 Da), another LHRH analogue, used for the treatment of sex hormone-dependent tumors and other benign gynecologic disorders, has also been studied across porcine skin *in vitro* [12]. Based on the results, application of a total iontophoretic current of 0.6 – 0.8 mA, over a 4 cm^2 contact area, would be sufficient to provide therapeutic delivery rates (27 – 36 µg/h).

Miller *et al.* conducted iontophoretic transport of LHRH, a poorly water-soluble antagonist and a superagonist (D-Trp6,Pro9-NHEt)LHRH across hairless mouse skin; the latter was delivered successfully at 0.1, 0.3 and 0.5 mA/cm [135].

5.4 Vasopressin and analogues

Vasopressin, a nonapeptide with a molecular mass of 1084 Da, is an anti-diuretic used to control polyuria and used in the management of variceal bleeding. Transdermal iontophoretic delivery of vasopressin was first investigated across rat skin [136]. Subsequent iontophoresis across human cadaver skin at a current density of 0.5 mA/cm^2 showed that the cumulative amount of intact vasopressin permeated during 8 h of iontophoretic transport was 15.37 ± 5.31 µg/cm^2, corresponding to only 1% permeation of the applied dose [137]. Nevertheless, given that the therapeutic dose of vasopressin is 25 µg, this could easily be delivered using an optimized formulation and a reasonably sized iontophoretic patch (2 – 4 cm^2). No intact vasopressin was found to permeate under passive conditions.

A vasopressin analogue, 9-desglycinamide vasopressin (molecular mass 1028 Da), which is more potent and more resistant to metabolism than vasopressin, has also been iontophoresed across dermatomed human skin [46].

Iontophoretic delivery of desmopressin acetate has been investigated *in vivo* with a diabetes insipidus model in rats [138,139]. Repeated short duration iontophoretic treatments with low current density were found to be best at maintaining a constant response. In another study, prolongation of the anti-diuretic response to desmopressin acetate in diabetic rats was compared with other routes of administration. Delivery by iontophoresis was comparable to that via the nasal route and was two to three times more effective than oral administration [140].

5.5 Somatostatin analogues

Octreotide (molecular mass 1019 Da), a synthetic octapeptide, is a somatostatin analogue available for the treatment of acromegaly and carcinoid tumors that carries a net positive charge under physiological conditions. Iontophoretic delivery of octreotide acetate has been investigated in rabbits [44]. Plasma levels of octreotide were negligible in the absence of current application, but increased in proportion to current density within the range 0.05 – 0.15 mA/cm^2 and declined rapidly after removal of the device. Similar proportional increases in plasma levels were observed when peptide concentration was increased from 2.5 to 5 mg/ml but not beyond this concentration.

Vapreotide (molecular mass ~ 1131 Da), another long-acting synthetic analogue of somatostatin used in the treatment of acromegaly and gastroenteropancreatic tumors, was iontophoresed across porcine skin *in vitro* [36]. Despite the susceptibility of vapreotide to enzymatic degradation, a flux of 1.7 µg/(cm^2 h) was achieved after 7 h of constant current iontophoresis (0.15 mA/cm^2). Post-iontophoretic extraction revealed that, depending on the experimental conditions, 80 – 300 µg of peptide were bound to the skin. Based on the clinical pharmacokinetics and observed transport rates of vapreotide across porcine skin, therapeutic concentrations might be achieved with a patch area of 15 cm^2

5.6 Somatorelin and analogues

Somatorelin, or growth hormone-releasing hormone (GRF), is a 44-residue endogenous peptide (molecular mass 5039 Da) secreted by the hypothalamus and is used to treat children with growth hormone deficiency. The iontophoretic delivery of a shortened GRF analogue, Ro 23–7861 (molecular mass 3929 Da), was studied across hairless guinea-pig skin *in vitro* [50]. A subsequent *in vivo* study in hairless guinea-pigs compared the serum GRF concentration profiles following iontophoresis with those obtained after subcutaneous and intravenous administration (10 µg/kg). Iontophoresis yielded a steady-state plasma concentration of 0.2 ng/ml that was similar to the peak plasma level achieved after a subcutaneous dose [141].

Ellens *et al.* investigated iontophoretic delivery of a growth hormone-releasing peptide (GHRP) (elimination half-life of 30 min and 71 min after intravenous and subcutaneous injection) at a current density of 0.15 – 0.2 mA/cm^2 for 2 h from a patch system specially designed for iontophoresis [142]. Blood levels of peptides persisted for at least 2 h after the current was turned off, indicative of depot formation in the skin, and flux of 0.8 – 1.2 μg/(cm^2 h) was achieved with peak plasma concentration of 20 ng/ml. The results suggested that a skin reservoir was formed during current application that released the peptide slowly into the systemic circulation after iontophoresis. Given the flux obtained with iontophoresis and the dose required to elicit a pharmacological response (21 μg/h in 70 kg adults), delivery of therapeutically relevant amounts of peptide would require use of a 15 – 20 cm^2 patch.

5.7 Botulinum toxin

Botulinum toxin A was first described for use in axillary hyperhidrosis in 1996 [143]. The safety and efficacy of this treatment have been documented [144-146]; the first case report on the successful iontophoresis of this protein to treat two patients appeared in 2004 [147], and this was followed by a pilot study performed on eight patients who were refractory to conventional therapy [148]. It is believed that the toxin works by inhibiting the release of acetylcholine at the neuromuscular junction and affecting the postganglionic sympathetic innervation of sweat glands [149]. Botulinum toxin A is a two-chain protein with a 100 kDa heavy chain joined by a disulfide bond to a 50 kDa light chain and has a pI of 6.06. An *in vivo* study found the toxin in hair roots, sebaceous glands and arrector pili muscle fibers of Wistar rats after only 10 min of iontophoresis [150]. More studies would be helpful to understand the degree of permeation and the duration of the pharmacological effect of this toxin after iontophoretic application.

6. Combination strategies to improve transdermal iontophoretic delivery

These strategies can involve either a modification of the formulation or the use of a complementary strategy to increase membrane permeability. The concomitant use of a drug carrier system and iontophoresis may result in a significant increase in molecular solubility and/or stability, for example, protect a peptide from degradation and thereby increase delivery [84]. Alternatively, other strategies involving skin barrier impairment have been proposed. As iontophoresis acts principally on the permeant, barrier impairment may offer some degree of synergy.

6.1 Iontophoresis in conjunction with electroporation

Transdermal electroporation involves the application of short (< 1 s), high voltage (50 – 500 V) pulses to the skin that disorganize the stratum corneum lipids and thereby increase drug transport. Electroporation (6 pulses of 120 V, 10 ms each) increased the transdermal iontophoretic delivery of salmon calcitonin across human epidermis fourfold; however, pulsing at lower voltages (60 and 100 V) before iontophoresis was not superior to iontophoresis alone [151]. Similarly, electroporation increased iontophoretic flux of parathyroid hormone 17-fold over 24 h [151]. Another study showed 10- and fivefold enhancements in human parathyroid hormone delivery when using electroporation pulses of 100 and 300 V followed by iontophoresis at 0.2 mA/cm^2 in comparison with the flux with electroporation alone [152]. The application of a single pulse (500 V, 5 ms) to initiate the experiment resulted in a nearly twofold increase in LHRH concentration at the end of 30 min of iontophoresis (0.4 mA/cm^2) [153]. In contrast to iontophoresis alone (0.4 mA/cm^2), electroporation of insulin (150 or 300 V, 10 ms and 10 pulses) resulted in high plasma levels of the hormone, and the combined use of electroporation and iontophoresis led to a further increase in insulin delivery in rats [66]. A single electroporation pulse before iontophoresis was found to double the iontophoretic transport of dextran sulfate as compared with iontophoresis alone (144.5 ± 10.35 and 276 ± 45.2 μg/cm^2, respectively), supporting the hypothesis that the structural rearrangement of the lipid bilayers can lead to enhanced permeability and improved transport [154].

6.2 Iontophoresis in conjunction with chemical enhancers

The use of chemical penetration enhancers is one of the more widely studied techniques for increasing transdermal drug permeation [103,105,106,111,124-128,155]. Various mechanisms have been postulated to explain how they increase permeation – including acting as solvents to dissolve skin lipids/denature skin proteins, affecting drug partitioning from the applied formulation or modifying drug solubility in the skin.

Pillai *et al.* investigated the effect of pretreatment with commonly used vehicles such as EtOH, Propylene Glycol (PG), water and their binary combinations, dimethyl acetamide (DMA), 10% dimethyl acetamide in water, ethyl acetate (EtAc) and isopropyl myristate (IPM) on insulin iontophoresis [103]. The skin barrier was severely compromised with DMA, less so by EtOH and EtAc, whereas IPM and PG had relatively minimal skin barrier-altering potential. All the solvents produced synergistic enhancement with iontophoresis. Fourier transform infrared studies showed that EtOH and EtAC caused lipid extraction, whereas IPM caused an increase in lipid fluidity. Thermogravimetric studies showed that EtOH and PG caused dehydration of skin.

6.3 Iontophoresis in conjunction with microporation

Microneedles, as the name suggests, are micrometer-scale needles (typically ~ 500 μm in length) that are used for transdermal delivery of drugs. In principle, they are sufficiently long to penetrate the stratum corneum, but

short enough not to stimulate nerves and hence pain receptors in the deeper tissues.

A study performed to evaluate the potential of combining microneedles and iontophoresis on skin permeation of D_2O and FITC-dextrans of variable molecular mass ranging from 3.8 to 400 kDa showed that convective solvent flow (electroosmosis) was unaffected by microneedle pretreatment [156]. The combination strategy significantly enhanced FITC-dextran flux compared with microneedle pretreatment alone or iontophoresis alone, whereas no synergistic effect was found on the flux of D_2O. A similar study was conducted to assess the skin transport behavior of daniplestin (molecular mass 12.7 kDa, pI 6.2) across hairless rat skin [157]. The combination approach gave higher flux values compared with iontophoresis alone. The authors followed up with an *in vivo* study in rats using a current of 0.2 mA/cm^2 for 6 h along with microneedles. Individual approaches were unable to produce detectable levels of the protein in the plasma [158]. By contrast, the combination of microneedles and iontophoresis resulted in controlled delivery over a period of 10 h.

Chen *et al.* investigated transdermal delivery of insulin from nanovesicles iontophoresed through microchannels in diabetic rats [113], which resulted in a 713-fold increase in insulin flux as compared with passive diffusion *in vitro*. *In vivo* studies in diabetic rats showed that iontophoresis of the cationic vesicles through microporated skin produced 33.3 and 28.3% reductions in blood glucose levels at 4 and 6 h; these were comparable to decreases induced by subcutaneous injection of insulin.

It has also been shown that iontophoresis across microporated skin in hairless rats results in a twofold increase in the dose of IFN-α_{2b} delivered [159].

7. Conclusion

Transdermal iontophoresis enables the controlled non-invasive delivery of therapeutics into and across the skin; numerous studies have demonstrated its ability to deliver peptides and now we are beginning to see evidence that it can also be used for proteins. Crucially, the use of activity assays and the quantification of downstream biological markers have confirmed that biological activity is retained post-iontophoresis. Despite earlier hypotheses that electrotransport of high-molecular-mass cations would be governed exclusively by electroosmosis (thus limiting potential applications), it is now clear that electromigration may play a major, if not pivotal, role in peptide and protein iontophoresis – the dominant transport mechanism being dependent on the properties of the permeant. Hence, much larger molecules can be considered as legitimate candidates for iontophoretic delivery. Transport rates are governed by: i) intrinsic physicochemical properties, although the exact relationship between delivery rates and the complex three-dimensional structures and concomitant spatial distribution of different molecular properties remains to be elucidated; and ii) iontophoretic conditions – most importantly, formulation composition and current density. So far, pre-filled iontophoretic systems for low-molecular-mass therapeutics have been approved by regulators; the challenge now is to develop commercial iontophoretic systems for the non-invasive administration of peptides and proteins that could dramatically change the delivery options of these potent and increasingly used therapeutics.

8. Expert opinion

Iontophoresis is one of the few transdermal delivery technologies that has succeeded in producing FDA-approved products – although both systems (LidoSite and Ionsys) contain low-molecular-mass therapeutics for local anesthesia and postoperative pain relief, respectively. Physicochemical properties – including good aqueous solubility and the presence of charged groups – that can render peptides and proteins 'difficult to deliver' by other approaches are ideal for iontophoresis. It offers the key advantage of enabling the controlled delivery of these therapeutics using complex input kinetics that can mimic endogenous secretion profiles – a so-called 'non-invasive infusion pump'. Until recently, it was thought that protein delivery was beyond the scope of iontophoresis; however, it has now been shown that functional proteins can indeed be iontophoresed across intact human skin. Thus, there are now published reports describing the successful non-invasive iontophoretic delivery of biomolecules ranging from thyrotropin-releasing hormone (359.5 Da) to Ribonuclease A (13.6 kDa) across intact skin; these include Phase I/II trials evaluating peptide pharmacokinetics and demonstrating pharmacological activity post-delivery. The next step is to build on these preclinical data and early stage clinical results and to develop effective iontophoretic patch systems for routine use by patients. Given the stability requirements of peptides and proteins and their susceptibility to degradation, aggregation and precipitation from solution, it may not be possible to use simple hydrogel systems as for small molecule therapeutics; dry patches where the biomolecule is hydrated immediately before use may need to be developed. In addition to the stability of the drug formulation, another major challenge will be the integrity of the other patch components, including the electronics; this will be especially critical in fully integrated patch designs. Physicochemical properties and drug pharmacokinetics/pharmacodynamics obviously put a limit on the number of peptide and protein candidates that can be delivered by transdermal iontophoresis from a realistically sized patch. For molecules with low potency, in theory there are several parameters that can be increased, including current density, duration of current application, drug loading, patch area and the use of pretreatments to impair skin barrier function, and there are many preclinical studies where these parameters have been investigated. However, for successful development of an iontophoretic product all of these 'options' need to be economically and clinically feasible and the product solutions must be

acceptable for patients – even more so for chronic therapy. For example, peptides and proteins are often expensive to produce – thus, increasing drug loading is undesirable because it might result in a product with an unacceptable final cost. The current density is normally limited to a maximum of 0.5 mA/cm^2; however, lower current densities are preferable for longer application periods and as the application area increases so as to minimize the risk of skin irritation. Moreover, lower currents are also preferred in terms of the power requirements of the device. Skin pretreatment may be feasible in preclinical studies but the increased risk of skin irritation means that it is seldom a viable option *in vivo*. In addition, to improve patient compliance the patch area should be as small as possible – preferably no more than 5 – 10 cm^{-2} if it is for prolonged use; a patch is undoubtedly better accepted if it is discrete. Other factors to be considered are ease of use and the ability of patients to manipulate the device. This is especially important for certain patients, for example, the geriatric population. Careful selection of drug candidates must be combined with well-thought-through product design and development programs that target unmet patient and therapeutic needs in order to realize the full potential of transdermal iontophoresis as a means finally to deliver biotechnology derived therapeutics non-invasively into the body.

Declaration of interest

The authors declare no conflict of interest. D Kalaria is supported by the Swiss State Secretariat for Education and Research in the framework of the Indo-Swiss Joint Research Program (ISJRP 123 143).

Bibliography

Papers of special note have been highlighted as either of interest (•) or of considerable interest (••) to readers.

1. Reichert J. Development trends for peptide therapeutics – A comprehensive quantitative analysis of peptide therapeutics in clinical development. Available from: www peptidetherapeutics org [Last accessed 30 September 2010]
2. Zompra AA, Galanis AS, Werbitzky O, Albericio F. Manufacturing peptides as active pharmaceutical ingredients. Fut Med Chem 2009;1:361-77
3. Vlieghe P, Lisowski V, Martinez J, Khrestchatisky M. Synthetic therapeutic peptides: science and market. Drug Discov Today 2010;15:40-56
4. Pichereau C, Allary C. Therapeutic peptides under the spotlight. Eur BioPharm Rev 2005:88-93
5. Ayoub M, Scheidegger D. Peptide drugs, overcoming the challenges, a growing business. Chim Oggi 2006;24:46-8
6. Haberkorn U, Eisenhut M. Molecular imaging and therapy – a programme based on the development of new biomolecules. Eur J Nucl Med Mol Imaging 2005;32:1354-9
7. Yuan L, Kurek I, English J, Keenan R. Laboratory-directed protein evolution. Microbiol Mol Biol Rev 2005;69:373-92
8. Ovadia O, Greenberg S, Laufer B, et al. Improvement of drug-like properties of peptides: the somatostatin paradigm. Expert Opin Drug Discov 2010;5:655-71
9. Werle M, Bernkop-Schnurch A. Strategies to improve plasma half life time of peptide and protein drugs. Amino Acids 2006;30:351-67
10. Chaturvedula A, Joshi DP, Anderson C, et al. In vivo iontophoretic delivery and pharmacokinetics of salmon calcitonin. Int J Pharm 2005;297:190-6
11. Zhang Q, Grice JE, Wang GJ, Roberts MS. Cutaneous metabolism in transdermal drug delivery. Curr Drug Metab 2009;10:227-35
12. Schuetz YB, Naik A, Guy RH, et al. Transdermal iontophoretic delivery of triptorelin in vitro. J Pharm Sci 2005;94:2175-82
13. Green PG. Iontophoretic delivery of peptide drugs. J Control Release 1996;41:33-48
•• **A good review article of iontophoretic delivery of peptides.**
14. Kalia YN, Naik A, Garrison J, Guy RH. Iontophoretic drug delivery. Adv Drug Deliv Rev 2004;56:619-58
•• **A comprehensive review covering all aspects of iontophoretic drug delivery.**
15. Burnette RR, Marrero D. Comparison between the iontophoretic and passive transport of thyrotropin releasing hormone across excised nude mouse skin. J Pharm Sci 1986;75:738-43
16. Marchand JE, Hagino N. Effect of iontophoresis of vasopressin on lateral septal neurons. Exp Neurol 1982;78:790-5
17. Siddiqui O, Sun Y, Liu JC, Chien YW. Facilitated transdermal transport of insulin. J Pharm Sci 1987;76:341-5
18. Stephen RL, Petelenz TJ, Jacobsen SC. Potential novel methods for insulin administration: I. Iontophoresis. Biomed Biochim Acta 1984;43:553-8
19. Subramony JA, Sharma A, Phipps JB. Microprocessor controlled transdermal drug delivery. Int J Pharm 2006;317:1-6
•• **A good review covering the principles involved in iontophoretic patch design.**
20. Phipps JB, Padmanabhan RV, Lattin GA. Iontophoretic delivery of model inorganic and drug ions. J Pharm Sci 1989;78:365-9
21. Abla N, Naik A, Guy RH, Kalia YN. Contributions of electromigration and electroosmosis to peptide iontophoresis across intact and impaired skin. J Control Release 2005;108:319-30
22. Delgado-Charro MB, Guy RH. Transdermal iontophoresis for controlled drug delivery and non-invasive monitoring. STP Pharm Sci 2001;11:403-14
23. Phipps JB, Gyory JR. Transdermal ion migration. Adv Drug Deliv Rev 1992;9:137-76
24. Sage BH, Riviere JE. Model systems in iontophoresis transport efficacy. Adv Drug Deliv Rev 1992;9:265-87
25. Mudry B, Guy RH, Begona Delgado-Charro M. Prediction of iontophoretic transport across the skin. J Control Release 2006;111:362-7
26. Mudry B, Guy RH, Delgado-Charro MB. Transport numbers in transdermal iontophoresis. Biophys J 2006;90:2822-30

27. Mudry B, Guy RH, Delgado-Charro MB. Electromigration of ions across the skin: determination and prediction of transport numbers. J Pharm Sci 2006;95:561-9

28. Kasting GB, Keister JC. Application of electrodiffusion theory for a homogeneous membrane to iontophoretic transport through skin. J Control Release 1989;8:195-210

29. Marro D, Guy RH, Delgado-Charro MB. Characterization of the iontophoretic permselectivity properties of human and pig skin. J Control Release 2001;70:213-17

30. Pikal MJ, Shah S. Transport mechanisms in iontophoresis. 3. An experimental-study of the contributions of electroosmotic flow and permeability change in transport of low and high-molecular-weight solutes. Pharm Res 1990;7:222-9

31. Pikal MJ. Transport mechanisms in iontophoresis. 1. A theoretical model for the effect of electroosmotic flow on flux enhancement in transdermal iontophoresis. Pharm Res 1990;7:118-26

• **This paper establishes a theoretical model to comprehend the effect of electroosmosis on flux, which was consistent with data in the literature.**

32. Pikal MJ, Shah S. Transport mechanisms in iontophoresis. 2. Electroosmotic flow and transference number measurements for hairless mouse skin. Pharm Res 1990;7:213-21

• **This paper validates the theoretical model developed for electroosmosis.**

33. Pikal MJ. The role of electroosmotic flow in transdermal iontophoresis. Adv Drug Deliv Rev 2001;46:281-305

34. Green PG, Hinz RS, Kim A, et al. Iontophoretic delivery of a series of tripeptides across the skin in vitro. Pharm Res 1991;8:1121-7

35. Cazares-Delgadillo J, Naik A, Ganem-Rondero A, et al. Transdermal delivery of cytochrome C-A 12.4 kDa protein-Across intact skin by constant-current iontophoresis. Pharm Res 2007;24:1360-8

• **This is the first report describing the transdermal iontophoretic delivery of a protein across intact skin.**

36. Schuetz YB, Naik A, Guy RH, et al. Transdermal iontophoretic delivery of vapreotide acetate across porcine skin in vitro. Pharm Res 2005;22:1305-12

37. Schuetz YB, Naik A, Guy RH, Kalia YN. Effect of amino acid sequence on transdermal iontophoretic peptide delivery. Eur J Pharm Sci 2005;26:429-37

38. Hirvonen J, Kalia YN, Guy RH. Transdermal delivery of peptides by iontophoresis. Nat Biotechnol 1996;14:1710-13

• **An important paper establishing a formal relationship between peptide sequence/structure and efficiency of delivery.**

39. Guy RH, Kalia YN, Delgado-Charro MB, et al. Iontophoresis: electrorepulsion and electroosmosis. J Control Release 2000;64:129-32

40. Dubey S, Kalia YN. Non-invasive iontophoretic delivery of enzymatically active ribonuclease A (13.6 kDa) across intact porcine and human skins. J Control Release 2010;145:203-9

• **This is the first report demonstrating the non-invasive iontophoretic delivery of a functional protein across the skin.**

41. Chang SL, Hofmann GA, Zhang L, et al. Stability of a transdermal salmon calcitonin formulation. Drug Deliv 2003;10:41-5

42. Patel SR, Zhong H, Sharma A, Kalia YN. In vitro and in vivo evaluation of the transdermal iontophoretic delivery of sumatriptan succinate. Eur J Pharm Biopharm 2007;66:296-301

43. Patel SR, Zhong H, Sharma A, Kalia YN. Controlled non-invasive transdermal iontophoretic delivery of zolmitriptan hydrochloride in vitro and in vivo. Eur J Pharm Biopharm 2009;72:304-9

44. Lau DT, Sharkey JW, Petryk L, et al. Effect of current magnitude and drug concentration on iontophoretic delivery of octreotide acetate (Sandostatin) in the rabbit. Pharm Res 1994;11:1742-6

45. Green P, Shroot B, Bernerd F, et al. In vitro and in vivo iontophoresis of a tripeptide across nude rat skin. J Control Release 1992;20:209-18

46. Craane-Vanhinsberg WHM, Bax L, Flinterman NHM, et al. Iontophoresis of a model peptide across human skin in-vitro – Effects of iontophoresis protocol, pH, and ionic strength on peptide flux and skin impedance. Pharm Res 1994;11:1296-300

47. Ledger PW. Skin biological issues in electrically enhanced transdermal delivery. Adv Drug Deliv Rev 1992;9:289-307

48. Huang YY, Wu SM, Wang CY. Response surface method: a novel strategy to optimize iontophoretic transdermal delivery of thyrotropin-releasing hormone. Pharm Res 1996;13:547-52

49. Knoblauch P, Moll F. In-vitro pulsatile and continuous transdermal delivery of buserelin by iontophoresis. J Control Release 1993;26:203-12

50. Kumar S, Hing C, Patel S, et al. Effect of Iontophoresis on in vitro skin permeation of an analog of growth-hormone releasing-factor in the hairless guinea-pig model. J Pharm Sci 1992;81:635-9

51. Abu Hashim II, Motoyama K, Abd-ElGawad AEH, et al. Potential use of iontophoresis for transdermal delivery of NF-kappa B decoy oligonucleotides. Int J Pharm 2010;393:127-34

52. Kanebako M, Inagi T, Takayama K. Evaluation of skin barrier function using direct current II: effects of duty cycle, waveform, frequency and mode. Biol Pharm Bull 2002;25:1623-8

53. Prausnitz MR. The effects of electric current applied to skin: a review for transdermal drug delivery. Adv Drug Deliv Rev 1996;18:395-425

54. Raiman J, Koljonen M, Huikko K, et al. Delivery and stability of LHRH and Nafarelin in human skin: the effect of constant/pulsed iontophoresis. Eur J Pharm Sci 2004;21:371-7

55. Rodriguez Bayon AM, Guy RH. Iontophoresis of nafarelin across human skin in vitro. Pharm Res 1996;13:798-800

56. Delgado-Charro MB, Guy RH. Characterization of convective solvent flow during iontophoresis. Pharm Res 1994;11:929-35

57. Delgado-Charro MB, Rodriguez-Bayon AM, Guy RH. Iontophoresis of Nafarelin – Effects of current density and concentration on electrotransport in vitro. J Control Release 1995;35:35-40

58. Delgado-Charro MB, Guy RH. Iontophoretic delivery of Nafarelin across the skin. Int J Pharm 1995;117:165-72

59. Hirvonen J, Guy RH. Iontophoretic delivery across the skin: electroosmosis and its modulation by drug substances. Pharm Res 1997;14:1258-63

60. Hoogstraate AJ, Srinivasan V, Sims SM, Higuchi WI. Iontophoretic enhancement of peptides – Behavior of Leuprolide versus model permeants. J Control Release 1994;31:41-7

61. Lu MF, Lee D, Carlson R, et al. The effects of formulation variables on iontophoretic transdermal delivery of Leuprolide to humans. Drug Dev Ind Pharm 1993;19:1557-71

- **Presents results from a pharmacokinetic/pharmacodynamic study into the delivery of a therapeutic peptide.**

62. Nair V, Panchagnula R. Physicochemical considerations in the iontophoretic delivery of a small peptide: in vitro studies using arginine vasopressin as a model peptide. Pharmacol Res 2003;48:175-82

63. Marro D, Kalia YN, Delgado-Charro MB, Guy RH. Contributions of electromigration and electroosmosis to iontophoretic drug delivery. Pharm Res 2001;18:1701-8

- **A good paper showing the contributions of electromigration and electroosmosis in the transport of various small molecules.**

64. Green PG, Hinz RS, Cullander C, et al. Iontophoretic delivery of amino acids and amino acid derivatives across the skin in vitro. Pharm Res 1991;8:1113-20

65. Panchagnula R, Bindra P, Kumar N, et al. Stability of insulin under iontophoretic conditions. Pharmazie 2006;61:1014-18

66. Tokumoto S, Higo N, Sugibayashi K. Effect of electroporation and pH on the iontophoretic transdermal delivery of human insulin. Int J Pharm 2006;326:13-19

67. Levin J, Maibach H. Human skin buffering capacity: an overview. Skin Res Technol 2008;14:121-6

68. Shukla C, Friden P, Juluru R, Stagni G. In vivo quantification of acyclovir exposure in the dermis following iontophoresis of semisolid formulations. J Pharm Sci 2009;98:917-25

69. Delgado-Charro MB. Recent advances on transdermal iontophoretic drug delivery and non-invasive sampling. J Drug Deliv Sci Technol 2009;19:75-88

70. Marro D, Kalia YN, Delgado-Charro MB, Guy RH. Optimizing iontophoretic drug delivery: identification and distribution of the charge-carrying species. Pharm Res 2001;18:1709-13

71. Alvarez-Figueroa MJ, Blanco-Mendez J. Transdermal delivery of methotrexate: iontophoretic delivery from hydrogels and passive delivery from microemulsions. Int J Pharm 2001;215:57-65

72. Haak RP, Gyory JR, Theeuwes F, et al. Iontophoretic delivery device and methods of hydrating same. US5320598; 1994

73. Fang JY, Hsu LR, Huang YB, Tsai YH. Evaluation of transdermal iontophoresis of enoxacin from polymer formulations: in vitro skin permeation and in vivo microdialysis using Wistar rat as an animal model. Int J Pharm 1999;180:137-49

74. Fang JY, Sung KC, Hu OYP, Chen HY. Transdermal delivery of nalbuphine and nalbuphine pivalate from hydrogels by passive diffusion and iontophoresis. Arzneimittelforschung 2001;51:408-13

75. Fang JY, Sung KC, Wang JJ, et al. The effects of iontophoresis and electroporation on transdermal delivery of buprenorphine from solutions and hydrogels. J Pharm Pharmacol 2002;54:1329-37

76. Jyoung JY, Shim BS, Cho DE, Hwang IS. Iontophoretic transdermal delivery of alendronate in hairless mouse skin. Polym Korea 2009;33:237-42

77. Taveira SF, Nomizo A, Lopez RFV. Effect of the iontophoresis of a chitosan gel on doxorubicin skin penetration and cytotoxicity. J Control Release 2009;134:35-40

78. Merclin N, Bramer T, Edsman K. Iontophoretic delivery of 5-aminolevulinic acid and its methyl ester using a carbopol gel as vehicle. J Control Release 2004;98:57-65

79. Banga AK, Chien YW. Hydrogel-based iontotherapeutic delivery devices for transdermal delivery of peptide/protein drugs. Pharm Res 1993;10:697-702

80. Tatavarti AS, Mehta KA, Augsburger LL, Hoag SW. Influence of methacrylic and acrylic acid polymers on the release performance of weakly basic drugs from sustained release hydrophilic matrices. J Pharm Sci 2004;93:2319-31

81. Essa EA, Bonner MC, Barry BW. Iontophoretic estradiol skin delivery and tritium exchange in ultradeformable liposomes. Int J Pharm 2002;240:55-66

82. Fang JY, Sung KC, Lin HH, Fang CL. Transdermal iontophoretic delivery of enoxacin from various liposome-encapsulated formulations. J Control Release 1999;60:1-10

83. Han I, Kim M, Kim J. Enhanced transfollicular delivery of adriamycin with a liposome and iontophoresis. Exp Dermatol 2004;13:86-92

84. Vutla NB, Betageri GV, Banga AK. Transdermal iontophoretic delivery of enkephalin formulated in liposomes. J Pharm Sci 1996;85:5-8

85. Manosroi A, Khositsuntiwong N, Gotz F, et al. Transdermal enhancement through rat skin of luciferase plasmid DNA loaded in elastic nanovesicles. J Liposome Res 2009;19:91-8

86. Kantaria S, Rees GD, Lawrence MJ. Gelatin-stabilised microemulsion-based organogels: rheology and application in iontophoretic transdermal drug delivery. J Control Release 1999;60:355-65

87. Sintov AC, Brandys-Sitton R. Facilitated skin penetration of lidocaine: combination of a short-term iontophoresis and microemulsion formulation. Int J Pharm 2006;316:58-67

88. Liu W, Hu M, Liu W, et al. Investigation of the carbopol gel of solid lipid nanoparticles for the transdermal iontophoretic delivery of triamcinolone acetonide acetate. Int J Pharm 2008;364:135-41

89. Joo HH, Lee HY, Kim JC, et al. Integrities and skin permeation-enhancing characteristics of behenic acid nanoparticles. J Dispers Sci Technol 2009;30:149-54

90. Li J, Zhai YL, Zhang B, et al. Methoxy poly(ethylene glycol)-block-poly(D, L-lactic acid) copolymer nanoparticles as carriers for transdermal drug delivery. Polym Int 2008;57:268-74

91. Miyazaki S, Takahashi A, Kubo W, et al. Poly n-butylcyanoacrylate (PNBCA) nanocapsules as a carrier for NSAIDs: in vitro release and in vivo skin penetration. J Pharm Pharm Sci 2003;6:238-45

92. Luengo J, Weiss B, Schneider M, et al. Influence of nanoencapsulation on human skin transport of flufenamic acid. Skin Pharmacol Physiol 2006;19:190-7

93. Stracke F, Weiss B, Lehr CM, et al. Multiphoton microscopy for the investigation of dermal penetration of nanoparticle-borne drugs. J Invest Dermatol 2006;126:2224-33

94. Boinpally RR, Zhou SL, Devraj G, et al. Iontophoresis of lecithin vesicles of cyclosporin A. Int J Pharm 2004;274:185-90

95. Abla N, Naik A, Guy RH, Kalia YN. Effect of charge and molecular weight on transdermal peptide delivery by iontophoresis. Pharm Res 2005;22:2069-78

96. Schuetz YB, Carrupt PA, Naik A, et al. Structure-permeation relationships for the non-invasive transdermal delivery of cationic peptides by iontophoresis. Eur J Pharm Sci 2006;29:53-9

97. Abla N, Geiser L, Mirgaldi M, et al. Capillary zone electrophoresis for the estimation of transdermal iontophoretic mobility. J Pharm Sci 2005;94:2667-75

98. Henchoz Y, Abla N, Veuthey JL, Carrupt PA. A fast screening strategy for characterizing peptide delivery by transdermal iontophoresis. J Control Release 2009;137:123-9

99. Banga AK, Chien YW. Characterization of in-vitro transdermal iontophoretic delivery of insulin. Drug Dev Ind Pharm 1993;19:2069-87

100. Langkjaer L, Brange J, Grodsky GM, Guy RH. Iontophoresis of monomeric insulin analogues in vitro: effects of insulin charge and skin pretreatment. J Control Release 1998;51:47-56

101. Pillai O, Panchagnula R. Transdermal iontophoresis of insulin – V. Effect of terpenes. J Control Release 2003;88:287-96

102. Pillai O, Borkute SD, Sivaprasad N, Panchagnula R. Transdermal iontophoresis of insulin – II. Physicochemical considerations. Int J Pharm 2003;254:271-80

103. Pillai O, Nair V, Panchagnula R. Transdermal iontophoresis of insulin: IV. Influence of chemical enhancers. Int J Pharm 2004;269:109-20

104. Li Y, Quan Y, Zang L, et al. Trypsin as a novel potential absorption enhancer for improving the transdermal delivery of macromolecules. J Pharm Pharmacol 2009;61:1005-12

105. Rastogi R, Anand S, Dinda AK, Koul V. Investigation on the synergistic effect of a combination of chemical enhancers and modulated iontophoresis for transdermal delivery of insulin. Drug Dev Ind Pharm 2010;36:993-1004

106. Rastogi SK, Singh J. Effect of chemical penetration enhancer and iontophoresis on the in vitro percutaneous absorption enhancement of insulin through porcine epidermis. Pharm Dev Technol 2005;10:97-104

107. Kanikkannan N, Singh J, Ramarao P. Transdermal iontophoretic delivery of bovine insulin and monomeric human insulin analogue. J Control Release 1999;59:99-105

108. Kari B. Control of blood-glucose levels in alloxan-diabetic rabbits by iontophoresis of insulin. Diabetes 1986;35:217-21

109. Tomohira Y, Machida Y, Onishi H, Nagai T. Iontophoretic transdermal absorption of insulin and calcitonin in rats with newly-devised switching technique and addition of urea. Int J Pharm 1997;155:231-9

110. Abla N, Naik A, Guy RH, Kalia YN. Iontohoresis: clinical applications and future challenges. In: Smith EW, Maibach HI, editors, Percutaneous penetration enhancers. 2nd edition; Taylor & Francis, Bristol PA, USA. 2005

111. Murthy SN, Zhao YL, Hui SW, Sen A. Synergistic effect of anionic lipid enhancer and electroosmosis for transcutaneous delivery of insulin. Int J Pharm 2006;326:1-6

112. Kogure K, Yamamoto M, Watanabe M, et al. Transdermal delivery of insulin-encapsulated liposomes via iontophoresis. Yakugaku Zasshi 2008;128:81-2

113. Chen HB, Zhu HD, Zheng JN, et al. Iontophoresis-driven penetration of nanovesicles through microneedle-induced skin microchannels for enhancing transdermal delivery of insulin. J Control Release 2009;139:63-72

- **This paper reported the transdermal delivery of insulin using a system containing various technologies such as iontophoresis, microneedles and nanotechnology.**

114. Torres-Lugo M, Peppas NA. Transmucosal delivery systems for calcitonin: a review. Biomaterials 2000;21:1191-6

115. Lee WA, Ennis RD, Longenecker JP, Bengtsson P. The bioavailability of intranasal salmon calcitonin in healthy volunteers with and without a permeation enhancer. Pharm Res 1994;11:747-50

116. Chang SL, Hofmann GA, Zhang L, et al. Transdermal iontophoretic delivery of salmon calcitonin. Int J Pharm 2000;200:107-13

117. Morimoto K, Iwakura Y, Nakatani E, et al. Effect of proteolytic-enzyme inhibitors as absorption enhancers on the transdermal iontophoretic delivery of calcitonin in rats. J Pharm Pharmacol 1992;44:216-18

118. Nakamura K, Katagai K, Mori K, et al. Transdermal administration of salmon calcitonin by pulse depolarization-iontophoresis in rats. Int J Pharm 2001;218:93-102

119. Santi P, Colombo P, Bettini R, et al. Drug reservoir composition and transport of salmon calcitonin in transdermal iontophoresis. Pharm Res 1997;14:63-6

120. Thysman S, Hanchard C, Preat V. Human calcitonin delivery in rats by iontophoresis. J Pharm Pharmacol 1994;46:725-30

121. Santi P, Volpato NM, Bettini R, et al. Transdermal iontophoresis of salmon calcitonin can reproduce the hypocalcemic effect of intravenous administration. Farmaco 1997;52:445-8

122. Suzuki Y, Iga K, Yanai S, et al. Iontophoretic pulsatile transdermal delivery of human parathyroid hormone (1-34). J Pharm Pharmacol 2001;53:1227-34

123. Suzuki Y, Nagase Y, Iga K, et al. Prevention of bone loss in ovariectomized rats by pulsatile transdermal iontophoretic administration

of human PTH(1-34). J Pharm Sci 2002;91:350-61

124. Bhatia KS, Singh J. Effect of dimethylacetamide and 2-pyrrolidone on the iontophoretic permeability of LHRH through porcine skin. Drug Dev Ind Pharm 1997;23:1215-18

125. Bhatia KS, Gao S, Singh J. Effect of penetration enhancers and iontophoresis on the FT-IR spectroscopy and LHRH permeability through porcine skin. J Control Release 1997;47:81-9

126. Bhatia KS, Singh J. Mechanism of transport enhancement of LHRH through porcine epidermis by terpenes and iontophoresis: permeability and lipid extraction studies. Pharm Res 1998;15:1857-62

127. Bhatia KS, Singh J. Synergistic effect of iontophoresis and a series of fatty acids on LHRH permeability through porcine skin. J Pharm Sci 1998;87:462-9

128. Bhatia KS, Singh J. Effect of linolenic acid ethanol or limonene ethanol and iontophoresis on the in vitro percutaneous absorption of LHRH and ultrastructure of human epidermis. Int J Pharm 1999;180:235-50

129. Chen LLH, Chien YW. Transdermal iontophoretic permeation of luteinizing hormone releasing hormone: characterization of electric parameters. J Control Release 1996;40:187-98

130. Heit MC, Monteiro-Riviere NA, Jayes FL, Riviere JE. Transdermal iontophoretic delivery of Luteinizing-Hormone-Releasing Hormone (LHRH) – Effect of repeated administration. Pharm Res 1994;11:1000-3

131. Heit MC, Williams PL, Jayes FL, et al. Transdermal iontophoretic peptide delivery: in vitro and in vivo studies with luteinizing hormone releasing hormone. J Pharm Sci 1993;82:240-3

132. Bayon AMR, Guy RH. Iontophoresis of nafarelin across human skin in vitro. Pharm Res 1996;13:798-800

133. Meyer BR, Kreis W, Eschbach J, et al. Successful transdermal administration of therapeutic doses of a polypeptide to normal human volunteers. Clin Pharmacol Ther 1988;44:607-12

134. Meyer BR, Kreis W, Eschbach J, et al. Transdermal versus subcutaneous leuprolide: a comparison of acute pharmacodynamic effect. Clin Pharmacol Ther 1990;48:340-5

135. Miller LL, Kolaskie CJ, Smith GA, Rivier J. Transdermal iontophoresis of gonadotropin releasing hormone (LHRH) and two analogues. J Pharm Sci 1990;79:490-3

136. Lelawongs P, Liu JC, Chien YW. Transdermal iontophoretic delivery of Arginine-Vasopressin. 2. Evaluation of electrical and operational factors. Int J Pharm 1990;61:179-88

137. Banga AK, Katakam M, Mitra R. Transdermal iontophoretic delivery and degradation of Vasopressin across human cadaver skin. Int J Pharm 1995;116:211-16

138. Nakakura M, Terajima M, Kato Y, et al. Effect of iontophoretic patterns on in-vivo antidiuretic response to Desmopressin Acetate administered transdermally. J Drug Target 1995;2:487-92

139. Nakakura M, Kato Y, Hayakawa E, et al. Effect of pulse on iontophoretic delivery of desmopressin acetate in rats. Biol Pharm Bull 1996;19:738-40

140. Nakakura M, Kato Y, Ito K. Prolongation of antidiuretic response to desmopressin acetate by iontophoretic transdermal delivery in rats. Biol Pharm Bull 1997;20:537-40

141. Kumar S, Char H, Patel S, et al. In vivo transdermal iontophoretic delivery of Growth-Hormone Releasing-Factor Grf (1-44) in hairless guinea-pigs. J Control Release 1992;18:213-20

142. Ellens H, Lai ZP, Marcello J, et al. Transdermal iontophoretic delivery of [H-3]GHRP in rats. Int J Pharm 1997;159:1-11

143. Bushara KO, Park DM, Jones JC, Schutta HS. Botulinum toxin–a possible new treatment for axillary hyperhidrosis. Clin Exp Dermatol 1996;21:276-8

144. Gregoriou S, Rigopoulos D, Makris M, et al. Effects of botulinum toxin-A therapy for palmar hyperhidrosis in plantar sweat production. Dermatol Surg 2010;36:496-8

145. Lowe NJ, Glaser DA, Eadie N, et al. Botulinum toxin type A in the treatment of primary axillary hyperhidrosis: a 52-week multicenter double-blind, randomized, placebo-controlled study of efficacy and safety. J Am Acad Dermatol 2007;56:604-11

146. Schnider P, Binder M, Kittler H, et al. A randomized, double-blind, placebo-controlled trial of botulinum A toxin for severe axillary hyperhidrosis. Br J Dermatol 1999;140:677-80

147. Kavanagh GM, Oh C, Shams K. BOTOX (R) delivery by iontophoresis. Br J Dermatol 2004;151:1093-5

• **This was the first report on the transdermal iontophoretic delivery of Botox in patients with severe palmar hyperhidrosis.**

148. Kavanagh GM, Shams K. Delivery of Botox (R) by iontophoresis: reply from authors. Br J Dermatol 2005;153:1076

149. Woolery-Lloyd H, Elsaie ML, Avashia N. Inguinal hyperhidrosis misdiagnosed as urinary incontinence: treatment with botulinum toxin A. J Drugs Dermatol 2008;7:293-5

150. Pacini S, Gulisano M, Punzi T, Ruggiero M. Transdermal delivery of Clostridium botulinum toxin type A by pulsed current iontophoresis. J Am Acad Dermatol 2007;57:1097-9

151. Chang SL, Hofmann GA, Zhang L, et al. The effect of electroporation on iontophoretic transdermal delivery of calcium regulating hormones. J Control Release 2000;66:127-33

152. Medi BM, Singh J. Electronically facilitated transdermal delivery of human parathyroid hormone (1-34). Int J Pharm 2003;263:25-33

153. Riviere JE, Monteiro-Riviere NA, Rogers RA, et al. Pulsatile transdermal delivery of LHRH using electroporation. J Control Release 1995;36:229-33

154. Badkar AV, Banga AK. Electrically enhanced transdermal delivery of a macromolecule. J Pharm Pharmacol 2002;54:907-12

155. Smyth HD, Becket G, Mehta S. Effect of permeation enhancer pretreatment on the iontophoresis of luteinizing hormone releasing hormone (LHRH) through human epidermal membrane (HEM). J Pharm Sci 2002;91:1296-307

156. Wu XM, Todo H, Sugibayashi K. Enhancement of skin permeation of high molecular compounds by a combination of microneedle pretreatment and iontophoresis. J Control Release 2007;118:189-95

157. Katikaneni S, Badkar A, Nema S, Banga AK. Molecular charge mediated transport of a 13 kD protein across

microporated skin. Int J Pharm 2009;378:93-100

158. Katikaneni S, Li G, Badkar A, Banga AK. Transdermal delivery of a approximately 13 kDa protein–an in vivo comparison of physical enhancement methods. J Drug Target 2010;18:141-7

159. Badkar AV, Smith AM, Eppstein JA, Banga AK. Transdermal delivery of interferon alpha-2B using microporation and iontophoresis in hairless rats. Pharm Res 2007;24:1389-95

- **This study demonstrates transdermal delivery of a therapeutic protein using a combination of two approaches.**

Affiliation

Taís Gratieri, Dhaval Kalaria & Yogeshvar N Kalia[†]
[†]Author for correspondence
University of Geneva,
School of Pharmaceutical Sciences,
30 Quai Ernest Ansermet,
1211 Geneva 4, Switzerland
Tel: +41 22 379 3355; Fax: +41 22 379 3360;
E-mail: Yogi.Kalia@unige.ch

Annexure 2

Supporting Information

Additional Supporting Information may be found in the online version of this article:

Figure S1. Calcitonin receptor–like receptor (CRLR) immunoreactivity was examined in 4-μm paraffin sections of healthy human scalp skin with a polyclonal rabbit antihuman CRLR antibody (Acris, SP4083P, 1:50).

Figure S2. Influence of CGRP on interferon (IFN)-γ-induced major histocompatibility complex (MHC) class I expression compared with controls – data from two other patients.

Figure S3. Influence of CGRP on connective tissue sheath (CTS) mast cells.

Please note: Wiley-Blackwell is not responsible for the content or functionality of any supporting materials supplied by the authors. Any queries (other than missing material) should be directed to the corresponding author for the article.

DOI:10.1111/j.1600-0625.2011.01429.x
www.blackwellpublishing.com/EXD

Letter to the Editor

Cutaneous iontophoretic delivery of CGP69669A, a sialyl Lewis^x mimetic, *in vitro*

Taís Gratieri[1], Beatrice Wagner[2], Dhaval Kalaria[1], Beat Ernst[2] and Yogeshvar N. Kalia[1]

[1]School of Pharmaceutical Sciences, University of Geneva & University of Lausanne, Geneva, Switzerland; [2]Institute of Molecular Pharmacy, University of Basel, Basel, Switzerland

Correspondence: Yogeshvar N. Kalia, School of Pharmaceutical Sciences, University of Geneva, 30 Quai Ernest Ansermet, 1211 Geneva 4, Switzerland, Tel.: 41-22-379-3355, Fax: 41-22-379-3360, e-mail: yogi.kalia@unige.ch

Abstract: The aim was to investigate the feasibility of using iontophoresis for the cutaneous delivery of the E-selectin antagonist CGP69669A, a sialyl Lewis^x-glycomimetic with potential activity against inflammatory skin diseases. The effects of current density and formulation on iontophoretic transport were evaluated in porcine and human skin *in vitro*. Cumulative permeation of CGP69669A increased with current density (69.73 ± 9.51, 113.97 ± 26.80 and 160.44 ± 13.79 $\mu g/cm^2$ at 0.1, 0.3 and 0.5 mA/cm^2, respectively) and drug concentration (37.42 ± 13.13, 78.96 ± 23.13 and 160.44 ± 13.79 $\mu g/cm^2$, at 1, 3 and 5 mg/ml, respectively). In contrast, passive delivery was negligible. Although permeation from a 2% hydroxyethyl cellulose gel was lower than that from aqueous solution, skin deposition – more relevant for the local treatment of dermatological conditions – was 3-fold higher. The results demonstrated that although CGP69669A cannot be delivered passively into the skin it is an excellent candidate for transdermal iontophoresis, a technique that is ideally suited to the delivery of glycomimetics.

Key words: glycomimetic – psoriasis – selectin antagonist – skin

Accepted for publication 30 November 2011

Background

Abnormal or excessive recruitment and influx of leukocytes is involved in the pathogenesis of several inflammatory diseases, such as psoriasis, atopic dermatitis or allergic contact dermatitis (1–4). Therefore, antagonism of the selectins, proteins involved in leukocyte trafficking between lymph nodes, blood and skin (5), might be an effective approach for the treatment of these diseases (6). However, many compounds have either not entered the clinic or failed in clinical trials (7,8). Challenges in targeting leukocyte migration into the skin with selectin antagonists include (i) functional overlaps (redundancies) of selectins – monospecific selectin antagonists are less effective (e.g. CDP-850) (7), (ii) low IC_{50} values (e.g. Cylexin) (9), which significantly increase dose and treatment costs and (iii) unfavorable pharmacokinetic properties – their high polarity decreases passive diffusion through the enterocyte layer in the small intestine, a prerequisite for oral availability, and they also suffer from fast renal excretion (10,11). The E-selectin antagonist CGP69669A is a sialyl Lewis^x (sLe^x)-glycomimetic (Fig. 1) (12,13,14). Although the potential of CGP69669A to block selectins has been established *in vitro* and in animal models (13), its efficacy in the treatment of skin inflammatory disorders has not been tested due to the challenges posed by its delivery. Topical administration offers a non-invasive targeted alternative to systemic administration. It targets skin lesions, reduces the amount of drug required for therapeutic effect and can be used to complement the administration of other therapeutic agents in multi-pronged approaches designed to overcome functional redundancy (10). However, due to its high polarity (CGP69669A is negatively charged in aqueous solution under physiological conditions, log D at pH 7.4: <−1.5), partitioning from a topical formulation into the lipid-rich intercellular space in the stratum corneum will be very low.

In contrast to passive delivery, which relies exclusively on the concentration gradient across the membrane, transdermal iontophoresis also employs an electrical potential gradient to enhance the delivery of hydrosoluble, ionized molecules that transit the skin through transport channels with more aqueous character (15). The potential gradient is a more effective driving force and can lead to order-of-magnitude increases in transport rates and significantly improve cutaneous delivery of therapeutic agents (16–19).

Questions addressed

Is it feasible to administer ''difficult-to-deliver'' glycomimetics, such as CGP69669A, into the skin using iontophoresis? How do

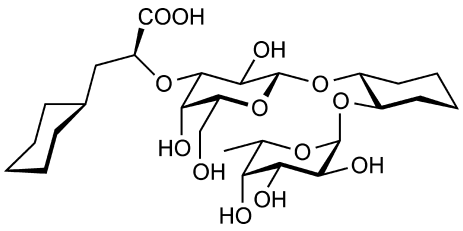

Figure 1. Structure of CGP69669A (MW 600.64 Da).

experimental variables (i.e., current density, drug concentration, and formulation) affect the iontophoretic transport rates?

Experimental design

CGP69669A was synthesized in-house (14). Transport experiments were performed across porcine and human skin *in vitro*. The effect of current density, drug concentration and formulation on iontophoretic transport rates was evaluated. Control experiments, in the absence of current, were performed to determine passive permeation of CGP69669A. Transport of CGP69669A was quantified by using HPAE-PAD (20). Full experimental details are provided in the Supporting Information.

Results

Control experiments confirmed that passive permeation of CGP69669A across intact dermatomed porcine skin and tape-stripped human skin was below the LOD (0.3 μg/ml). Furthermore, in both cases, no CGP69669A was detected after skin extraction, implying that <1.5 μg (considering the dilution of 5 ml for the extraction procedure) of CGP69669A was recovered from the skin. Since removal of the stratum corneum was unable to improve delivery, the results suggest that stratum corneum ablation techniques may not be able to enhance transport for molecules with such physicochemical properties and the presence of an additional driving force, e.g. the potential gradient employed in iontophoresis, is necessary for delivery.

Cumulative iontophoretic permeation and flux increased linearly with current density (0.1, 0.3 and 0.5 mA/cm^2) and was also linearly dependent on concentration (1, 3 and 5 mg/ml) (Table 1) (r^2 = 0.999 in both cases; ANOVA (α = 0.05) followed by Student Newman Keuls test). The extraction experiments showed that CGP69669A was retained within the membrane during iontophoresis. Similar amounts were recovered at 0.1 and 0.3 mA/cm^2; however, a further increase to 0.5 mA/cm^2 did result in a statistically significant increase in skin deposition (Table 1). A linear relationship between steady-state flux and either current density or donor concentration provides therapeutic flexibility, since drug input kinetics can be controlled by modifying either parameter. This may be of particular interest in the case of CGP69669A, which is a new molecule whose therapeutic dose is yet to be fully determined. Transport across porcine and human skin was statistically equivalent (160.44 ± 13.78 and 146.27 ± 37.33 μg/cm^2 after 6 h iontophoresis at 0.5 mA/cm^2). The iontophoretic transport efficiency of CGP69669A (as assessed by the iontophoretic permeability coefficient ($k_{p,ionto}$)) was similar to that of dexamethasone sodium phosphate, another anionic molecule with anti-inflammatory properties (cf. $k_{p,ionto}$ values of 5.1 and 4.7×10^{-3} cm/h, respectively) (21).

The preliminary iontophoretic transport studies were conducted with solution formulations; however, it is clear that in practice, a semi-solid hydrogel formulation would most likely be required in order to apply the drug in a patient-friendly form. Considering the total amount of drug delivered (sum of the amounts permeated and retained in the skin) there was no statistically significant difference between the solution and gel formulations (Table 1; Study 4 and Study 7, respectively). However, cumulative permeation from solution was two-fold higher than that from the gel while the amount of drug accumulated in the skin was approximately three-fold higher using the gel. Thus, even in a non-optimized form ~6.5% of the CGP69669A applied on the skin surface was retained – demonstrating the feasibility of using the gel for targeted local delivery. The selectivity for retention over permeation observed with the gel may have been due to the occlusive effect of the gel layer on the skin surface. This may increase the degree of skin hydration making the membrane a more thermodynamically favorable environment for hydrophilic substances, such as CGP69669A, resulting in an increase in skin deposition at the

Table 1. Effect of experimental parameters (formulation, drug concentration and current density) on cumulative permeation, steady state flux and skin deposition of CGP69669A after transdermal iontophoresis for 6 h

Study	Formulation	CGP69669A concentration (mg/ml)	Current density (mA/cm^2)	Cumulative permeation[1,2] (μg/cm^2)	Flux (μg/cm^2 h)	Skin retention[3] (μg/cm^2)	Total delivery[4] (μg/cm^2)
1[5]	Aq[6]	5	0.0	–[7]	–	–	–
2	Aq	5	0.1	69.73 ± 9.51[8]	11.09 ± 3.08	18.61 ± 3.82	88.34 ± 10.24
3	Aq	5	0.3	113.97 ± 26.8	18.55 ± 4.83	23.12 ± 6.06	137.09 ± 27.48
4	Aq	5	0.5	160.44 ± 13.79	25.41 ± 6.38	49.93 ± 12.43	210.37 ± 18.56
5	Aq	3	0.5	78.96 ± 23.13	14.35 ± 4.10	33.78 ± 7.57	112.74 ± 24.33
6	Aq	1	0.5	37.42 ± 13.13	7.08 ± 2.49	11.03 ± 3.14	48.45 ± 13.50
7	Gel[9]	5	0.5	68.92 ± 22.47	12.39 ± 3.72	163.29 ± 79.96	232.21 ± 83.06

[1]Statistically significant effect of increasing CGP69669A concentration in the formulation (ANOVA (α = 0.05) followed by Student Newman Keuls test).
[2]Statistically significant effect of increasing current density (ANOVA (α = 0.05) followed by Student Newman Keuls test).
[3]Statistically significant increase in skin retention observed in Study 4 (0.5 mA/cm^2 and 5 mg/ml of CGP69669A; ANOVA (α = 0.05) followed by Student Newman Keuls test). Use of the gel (Study 7) produced a further increase in the amount of CGP69669A retained in the skin.
[4]Total delivery is defined as the sum of the amounts permeated across and deposited within the skin.
[5]Study 1 measured passive permeation of CGP69669A, Study 2–4 determined the effect of current density, Study 4–6 investigated the effect of concentration and Study 7 quantified delivery from the gel formulation.
[6]Aqueous non-buffered solution (pH 7.5).
[7]Below limit of detection (0.3 μg/ml).
[8]Mean ± SD, $n \geq 4$.
[9]2% hydroxyethyl cellulose gel (pH 7.2).

expense of skin permeation. Given the amount of CGP69669A deposited in the skin and the dimensions of the skin sample, it was estimated that the CGP69669A concentration was 3.62 ± 1.77 mM, which is approximately 45-fold higher than the reported IC_{50} (0.08 mM) (9); however, further studies are obviously required to demonstrate efficacy *in vivo*.

Conclusions

This is the first report describing the successful iontophoretic delivery of a glycomimetic into the skin; molecules such as CGP69669A which cannot be delivered efficiently by passive diffusion are excellent candidates for iontophoresis. These results will be used to determine conditions for pharmacokinetic studies and investigations into the therapeutic efficacy of CGP69669A in the treatment of inflammatory skin disorders.

Acknowledgements

We would like to thank the Clinique Vert-Pré (Geneva, Switzerland), in particular, Dr. Gabor Varadi and Mrs. Amalia Vittoz-Rivero, for kindly providing us with excised human skin from aesthetic surgery procedures. Beatrice Wagner and Beat Ernst were responsible for the synthesis of CGP69669A and provided input with respect to experimental design and the manuscript. Taís Gratieri and Dhaval Kalaria performed the experiments, analysed data and wrote the manuscript. Yogeshvar N. Kalia was involved with experimental design, data analysis, manuscript writing and supervision of the project.

Conflict of interests

The authors have declared no conflicting interests.

References

1 Bock D, Philipp S, Wolff G. Expert Opin Investig Drugs 2006: **15**: 963–979.
2 Robert C, Kupper T S. N Engl J Med 1999: **341**: 1817–1828.
3 Armstrong A W, Voyles S V, Armstrong E J *et al.* Exp Dermatol 2011: **20**: 544–549.
4 Vocanson M, Hennino A, Rozieres A *et al.* Allergy 2009: **64**: 1699–1714.
5 Garbaraviciene J, Diehl S, Varwig D *et al.* Exp Dermatol 2010: **19**: 736–741.
6 Schön M P. Ther Clin Risk Manag 2005: **1**: 201–208.
7 Bhushan M, Bleiker T O, Ballsdon A E *et al.* Br J Dermatol 2002: **146**: 824–831.
8 Friedrich M, Philipp S, Hardtke M *et al.* J Invest Dermatol 2005: **124**: 232.
9 Schön M P, Ludwig R J. Expert Opin Ther Targets 2005: **9**: 225–243.
10 Boehncke W-H, Schön M P, Giromolomi G *et al.* Exp Dermatol 2005: **14**: 70–80.
11 Ernst B, Magnani J L. Nat Rev Drug Discov 2009: **8**: 661–677.
12 Titz A, Patton J, Smiesko M *et al.* Bioorg Med Chem 2010: **18**: 19–27.
13 Norman K E, Anderson G P, Kolb H C *et al.* Blood 1998: **91**: 475–483.
14 Kolb H C, Ernst B. Chem Eur J 1997: **3**: 1571–1578.
15 Kalia Y N, Naik A, Garrison J *et al.* Adv Drug Deliv Rev 2004: **56**: 619–658.
16 Gangarosa L P Sr, Ozawa A, Ohkido M *et al.* J Dermatol 1995: **22**: 865–875.
17 Zempsky W T, Sullivan J, Paulson D M *et al.* Clin Ther 2004: **26**: 1110–1119.
18 Welch M L, Grabski W J, McCollough M L *et al.* J Am Acad Dermatol 1997: **36**: 956–958.
19 Abla N, Naik A, Guy R H *et al.* Pharm Res 2006: **23**: 1842–1849.
20 Gratieri T, Wagner B, Kalaria D *et al.* Biomed Chromatogr 2011: doi: 10.1002/bmc.1695. (in press).
21 Cazares-Delgadillo J, Balaguer-Fernandez C, Calatayud-Pascual A *et al.* Eur J Pharm Biopharm 2010: **75**: 173–178.

Supporting Information

Additional Supporting Information may be found in the online version of this article:

Data S1. Materials and methods.

Please note: Wiley-Blackwell are not responsible for the content or functionality of any supporting materials supplied by the authors. Any queries (other than missing material) should be directed to the corresponding author for the article.

DOI:10.1111/j.1600-0625.2011.01437.x
www.blackwellpublishing.com/EXD

Letter to the Editor

8-Methoxypsoralen plus UVA treatment increases the proportion of CLA+ CD25+ CD4+ T cells in lymph nodes of K5.hTGFβ1 transgenic mice

Tej Pratap Singh[1], Michael P. Schön[2], Katrin Wallbrecht[2] and Peter Wolf[1]

[1]Department of Dermatology, Medical University of Graz, Graz, Austria; [2]Department of Dermatology, Venereology and Allergology, Georg August University, Göttingen, Germany

Correspondence: Peter Wolf, MD, Research Unit for Photodermatology, Medical University of Graz, Department of Dermatology, Auenbrugger Platz 8, A-8036 Graz, Austria, Tel.: +43 316 385-12371, Fax: +43 316 385-12466, e-mail: peter.wolf@medunigraz.at

Abstract: 8-Methoxypsoralen plus UVA (PUVA) photochemotherapy is an effective treatment for many skin diseases including psoriasis. However, its exact mechanism of therapeutic action is incompletely understood. Previously, in K5.hTGFβ1 transgenic psoriatic mice, we found that PUVA induces Foxp3+ CD25+ CD4+ regulatory T cells in both lymph node and spleen. Now, in the same model, we investigated whether cutaneous lymphocyte-associated antigen (CLA) mediates PUVA's effect on homing of CD25+ CD4+ T cells to the lymph nodes of K5.hTGFβ1 transgenic mice. We found that a low dose of topical PUVA maximally increased the proportion of CLA + CD25+ CD4 + T cells in the lymph nodes by up to 8-fold. We also observed an increased number of Foxp3+ CD25+ T cells in the skin of the mice after PUVA treatment. Together, these findings suggest that PUVA affects the homing of regulatory T cells.

Key words: cutaneous lymphocyte-associated antigen – psoralen – psoriasis – T-cell homing – UVA

Accepted for publication 14 December 2011

Annexure 3

Journal of Controlled Release 156 (2011) 53–59

Contents lists available at ScienceDirect

Journal of Controlled Release

journal homepage: www.elsevier.com/locate/jconrel

Erbium:YAG fractional laser ablation for the percutaneous delivery of intact functional therapeutic antibodies

Jing Yu [a,b], Dhaval R. Kalaria [a], Yogeshvar N. Kalia [a,*]

[a] School of Pharmaceutical Sciences, University of Geneva & University of Lausanne, 1211 Geneva, Switzerland
[b] School of Life Science and Biotechnology, Shanghai Jiaotong University, 200240 Shanghai, China

ARTICLE INFO

Article history:
Received 28 April 2011
Accepted 15 July 2011
Available online 22 July 2011

Keywords:
Antithymocyte globulin
Basiliximab
Composite tissue allotransplantation
Laser-assisted microporation
Topical delivery
Transdermal delivery

ABSTRACT

The physicochemical properties and stability requirements of therapeutic proteins necessitate their parenteral administration even for local therapy; however, unnecessary systemic exposure increases the risk of avoidable side-effects. The objective of this study was to use fractional laser ablation to enable the delivery of intact, functional therapeutic antibodies into the skin *in vitro* and *in vivo*. The laser-assisted delivery of Antithymocyte globulin (ATG) and Basiliximab – FDA-approved therapeutics for the induction of immunosuppression – was investigated. *In vitro* delivery experiments were performed using dermatomed porcine ear and human abdominal skins; an *in vitro/in vivo* correlation was shown using C57 BL/10 SCSnJ mice. Antibody transport was quantified by using ELISA methods developed in-house. Results showed that increasing the pore number from 300 to 450 and 900, increased total antibody delivery (sum of amounts permeated and deposited); e.g., for ATG, from 1.18 ± 0.10 to 3.98 ± 0.64 and 4.97 ± 0.83 μg/cm^2, respectively — corresponding to 19.7-, 66.3- and 82.8-fold increases over the control (untreated skin). Increasing laser fluence from 22.65 to 45.3 and 135.9 J/cm^2 increased total ATG delivery from 1.70 ± 0.65 to 4.97 ± 0.83 and 8.70 ± 1.55 μg/cm^2, respectively. The Basiliximab results confirmed the findings with ATG. Western blot demonstrated antibody identity and integrity post-delivery; human lymphocyte cytotoxicity assays showed that ATG retained biological activity post-delivery. Immunohistochemical staining was used to visualize ATG distribution in the epidermis. Total ATG delivery across porcine ear and human abdominal skin was statistically equivalent and an excellent *in vitro/in vivo* correlation was observed in the murine model. Based on published data, the ATG concentrations achieved in the laser-porated human skins were in the therapeutic range for providing local immunosuppression. These results challenge the perceived limitations of transdermal delivery with respect to biopharmaceuticals and suggest that controlled laser microporation provides a less invasive, more patient-friendly "needle-less" alternative to parenteral administration for the local delivery of therapeutic antibodies.

1. Introduction

Therapeutic antibodies and Fc-fusion proteins are a fast-growing segment of the global biopharmaceuticals market [1,2]. Their unique pharmacological properties put them at the forefront of new therapeutic approaches in oncology and in the treatment of autoimmune diseases [3–5]. Apart from notable exceptions such as the intravitreal administration of antiangiogenic agents to treat neovascular age-related macular degeneration [6], their physicochemical properties mean that systemic administration by intravenous (*i.v.*) or subcutaneous (*s.c.*) injection is the rule, even where targeted local pharmacological action is desired. For example, there are several reports describing *i.v.* or *s.c.* administration of monoclonal antibodies to treat dermatological conditions, including lichen planus, pyoderma gangrenosum, pemphigus and cutaneous B-cell lymphoma [7]. Similarly, in composite tissue allotransplantation, that is, the transplantation of a vascularized limb or a facial part because of surgical excision of tumors, accidents and congenital malformation [8], systemic immunosuppression is the norm [9]. This entails a significant pharmacological burden since the patient follows long-term immunosuppression with its attendant side effects for what is essentially not a life threatening condition; localized immunosuppression targeting the transplant site would be more efficient [10].

In common with parenteral administration, transdermal delivery avoids both proteolytic degradation in the gastrointestinal tract and the hepatic first pass effect and it is inherently more patient-friendly and enjoys high compliance [11]. However, transdermal delivery of large hydrophilic molecules across intact skin is a considerable challenge since their transport is restricted by the stratum corneum's excellent barrier function — which can be attributed to its unique structure and lipid-rich composition [12]. Hence, there has been considerable focus on the

* Corresponding author at: School of Pharmaceutical Sciences, University of Geneva, 30 Quai Ernest Ansermet, 1211 Geneva 4, Switzerland. Tel.: +41 22 3793355; fax: +41 22 3793360.
E-mail address: Yogi.Kalia@unige.ch (Y.N. Kalia).

0168-3659/$ – see front matter © 2011 Elsevier B.V. All rights reserved.
doi:10.1016/j.jconrel.2011.07.024

development of different strategies to reversibly impair this barrier and to enable drug transit [13], including the use of chemical and peptidic penetration enhancers [14,15], ultrasound [16], iontophoresis [17] and microneedles [18]. However, to date, there are no reports on the transdermal delivery of intact, biologically active therapeutic antibodies.

In this study, we have employed a novel laser microporation technique for the controlled fractional ablation of the stratum corneum and the upper layers of the epidermis. The P.L.E.A.S.E.® device (Precise Laser Epidermal System; Pantec Biosolutions, AG) uses a diode-pumped Er:YAG laser that emits energy at one of the principal absorption bands of water molecules present in the skin (2.94 μm) (Supplementary Fig. 1) [19,20]. Their excitation and evaporation leads to the fractional ablation of the skin and the creation of micropores, with a typical diameter of 100–150 μm that serve as transport conduits across the epidermis. The short duration of the energy pulses – less than the water thermal relaxation time – means that there is negligible heat transfer to neighboring skin tissue. The number of micropores to be created is programmed by the user and can be varied (Supplementary Fig. 2); the depth of each micropore is determined by the laser fluence (energy applied per unit area) used to create the pore and can be modulated to ensure either selective removal of the stratum corneum or to reach progressively further into the epidermis down to the dermal–epidermal junction (Supplementary Fig. 3). In practice, the device can create an array of several hundred micropores with a given depth in a few seconds and hence significantly increase molecular transport rates [20–22]. Although Er:YAG lasers have been used previously to facilitate skin transport [23–33], most of these studies did not use fractional ablation systems, employing instead devices where a single laser beam with a given spot diameter (e.g., 7 mm [24–30]) was used to ablate the skin. It is obvious that removal of this amount of skin surface to create a transport channel is impractical in the clinical setting due to the much longer healing time — thus, the move towards the development of fractional ablative systems where, as the name suggests, only a "fraction" of the skin surface area is removed. Recent reports describing the use of conventional fractional Er.YAG lasers to improve the delivery of 5-aminolevulinic acid and imiquimod employed a system that created a 13×13 micropore grid in the skin [31,32]; however, the operator was required to adjust the headpiece manually to predetermined positions to create additional micropores and had to ensure that there was no overlap of the irradiation areas of each pulse. The need for manual adjustment implicitly increases the risk of inhomogeneity. In addition, other systems perform fractional ablation by using a grid to split the applied laser beam into separate "microbeams" — thus fractionating the beam energy to create each individual pore [33]. The P.L.E.A.S.E.® device has several advantages over these existing systems. First, it is a diode-pumped system that combines the "cold ablation" features of conventional Er:YAG systems and the thermal impact of CO_2 lasers — the pulse duration can be varied from 10 to 300 μs (cf. 250–400 μs used in earlier studies [24–33]); thus, "cold ablation" can be done with high energy short duration pulses with limited or negligible heat transfer to surrounding tissue. Second, the number of pores (theoretically, it is possible to create several thousand pores) and the number of energy pulses used to create each pore are pre-programmed, reducing the risk of operator-induced inhomogeneity — the P.L.E.A.S.E.® system uses a scanner to generate the pore array meaning that the focus and energy used to create each micropore is identical (moreover, the pore diameter is 100–150 μm, cf. 7 mm for the "single beam" devices used previously [24–30]). Third, the high pulse repetition rate of up to 1 kHz – much higher than other fractional lasers – means that an array of several hundred sequentially-created identical pores can be generated in only a few seconds. Fourth, from a drug delivery perspective, the control over the number of pores created and their depth allows for the controlled, individualized delivery of therapeutic agents in response to patient needs.

The feasibility of using laser microporation with the P.L.E.A.S.E.® device to deliver biomacromolecules was investigated using two FDA-approved immunosuppressive antibodies, ATG (Thymoglobulin®; Genzyme Corp.) and Basiliximab (Simulect®; Novartis Pharmaceuticals Corp.), across different skins *in vitro* and *in vivo*. ATG is a rabbit-derived antithymocyte gamma globulin polyclonal antibody that recognizes a broad array of cell surface antigens on human T-lymphocytes; it has a nominal molecular weight of ~155 kDa. Basiliximab is a 144 kDa chimeric (murine/human) monoclonal antibody (IgG_{1K}) that binds to the interleukin-2 receptor α-chain (IL-2Rα, also known as CD25) on activated T-lymphocytes. The aims of this study were (i) to demonstrate the feasibility of using laser microporation to enable the delivery of functional antibodies into and across porcine and human skin *in vitro*, (ii) to investigate the effect of poration parameters on transport kinetics, (iii) to compare transport across murine skin *in vitro* and *in vivo* in order to establish whether there was a good *in vitro*/*in vivo* correlation and (iv) to evaluate whether topical antibody delivery was sufficient for local therapeutic applications.

2. Materials and methods

2.1. Skin source

Porcine ears were obtained from a local abattoir (CARRE; Rolle, Switzerland), the skin was excised (thickness 750 μm) with an air-dermatome (Zimmer; Etupes, France), wrapped in Parafilm™ and stored at −20 °C for a maximum period of 2 months. Human skin samples were collected immediately after surgery from the Department of Plastic, Aesthetic and Reconstructive Surgery, Geneva University Hospital (Geneva, Switzerland), fatty tissue was removed and the skin was wrapped in Parafilm™ before storage at −20 °C for a maximum period of 3 days. The study was approved by the Central Committee for Ethics in Research (CER: 08–150 (NAC08-051); Geneva University Hospital).

2.2. Laser microporation

Skin samples were equilibrated in 0.9% NaCl for 30 min prior to poration using the P.L.E.A.S.E.® device. After removing surface moisture, skin samples mounted in a custom designed assembly were placed at the focal length of the laser to create the micropores. Laser poration parameters, i.e., the pore number and the fluence (determined by the number of energy pulses applied to create each pore) were fixed using the device software.

2.3. In vitro delivery of therapeutic antibodies

In vitro transdermal delivery experiments were performed using 0.75 mm dermatomed porcine ear skin, human abdominal skin (~1.5 mm thickness) and intact C57 BL/10 SCSnJ murine skin at room temperature (RT). The experiments with human and porcine skins were conducted for 24 h; those with murine skin were of shorter duration – only 3 h – in order to enable direct comparison with the subsequent *in vivo* studies (see Section 2.4). Skin samples, either without laser treatment (control) or after laser microporation, were mounted in static Franz diffusion cells with a diffusional area of 2.9 cm^2 (PermeGear Inc., USA). ATG (Thymoglobulin®; Genzyme Corp., Switzerland) or Basiliximab (Simulect®, Novartis Pharmaceuticals Corp., Switzerland) in PBSS buffer (900 μl; PBS buffer containing 0.025% sodium azide, pH 7.4) was placed in the donor compartment; 9 ml PBSS buffer was used as the receptor solution, which was stirred at RT throughout the experiment. Aliquots (400 μl) were collected from the receiver compartment at 3, 6, 9, 21 and 24 h and analyzed by ELISA (see Section 2.5); each aliquot was replaced with fresh PBSS buffer. Experiments were performed to investigate the effects of pore number and laser fluence, as well as antibody concentration (1 or 5 mg/ml) on antibody cumulative permeation kinetics.

In addition to quantifying permeation, the amount of antibody retained within the porcine and human skin samples was also measured. After permeation, the area of the skin exposed to the antibody formulation was isolated, washed under running deionized water and gently blotted dry using a paper tissue. The isolated skin was then cut into small pieces and extracted in 10 ml PBSS buffer with stirring at RT for 4 h. The antibody recovery efficiency after skin extraction was ~75%. The extracted antibodies were analyzed by ELISA (see Section 2.5).

2.4. In vivo delivery of ATG

Twelve-week old C57 BL/10 SCSnJ mice (20–23 g) were anesthetized using a mixture of urethane (1.5 g/kg; Fluka, Switzerland) and diazepam (5 mg/kg; Sigma, Switzerland). The abdominal hair was trimmed using scissors. The donor compartment of a Franz diffusion cell was placed on the animal's abdomen and secured by silicon. ATG (900 µl; 1 mg/ml in PBSS) was then applied to the abdominal skin (either intact (control) or after P.L.E.A.S.E.® treatment) for 3 h. Blood was then collected directly from the animal's heart and centrifuged at 1000 *g* for 10 min to obtain the plasma. The concentration of ATG in the plasma was quantified by ELISA (see Section 2.5).

2.5. Quantitative analysis of ATG and Basiliximab by ELISA

2.5.1. ATG

A sandwich ELISA was developed to determine the concentration of ATG (the quantitative range was 5–300 ng/ml, the LOD and LOQ were 0.17 and 0.52 ng/ml, respectively and the CV was 2%). A Nunc-Immuno 96-well plate (Nunc, Denmark) was coated overnight at 4 °C with 100 µl of 10 µg/ml donkey anti-rabbit IgG (H + L) antibody (Jackson ImmunoResearch, USA). After washing three times with 200 µl PBST buffer (PBS buffer containing 0.05% Tween 20, pH 7.4), the plate was blocked with 200 µl of 3% (wt/vol) BSA (Sigma, Switzerland) in PBST for 1 h at RT. The plate was then washed and incubated with 100 µl of each sample (these were diluted in PBST buffer if required) for 2 h at RT. After washing, 100 µl of anti-rabbit IgG (whole molecule)–peroxidase antibody (Sigma, Switzerland) was added and incubated for a further 2 h at RT. Following additional washing, 100 µl substrate ABTS (Merck, Germany) was added and allowed to develop for 5–10 min. The reaction was terminated by addition of 100 µl 1% SDS and the absorbance measured at 405 nm (reference wavelength 490 nm) with a microtiter plate reader (Tecan Sunrise, Switzerland). Each sample was analyzed in triplicate.

2.5.2. Basiliximab

The concentration of Basiliximab was determined by using a similar ELISA method to that developed above (the quantitative range was 5–200 ng/ml, the LOD and LOQ were 0.61 and 1.86 ng/ml, respectively and the CV was 4%). Anti-mouse IgG (whole molecule) antibody (Sigma, Switzerland) was used to capture Basiliximab. Anti-human IgG (Fc fragment specific)–peroxidase antibody (Jackson ImmunoResearch, USA) was employed for detection. Each sample was analyzed in triplicate.

2.6. Western blot analysis

Antibodies and prestained markers (NEB, USA) were separated on 10% SDS-PAGE in Laemmli's Tris–glycine buffer system [34]. The separated proteins were then transferred onto a nitrocellulose membrane (Sigma, Switzerland) using a TransBlot semi-dry transfer cell (BIO-RAD, Switzerland) at 14 V for 1 h. Powdered fat-free milk (5% w/v) was used to block the membrane at 4 °C overnight. After three 5 min washings with PBST, the membrane was incubated at RT for 1.5 h with the corresponding detection antibody used in the ELISA method (ATG 1:5000 dilution; Basiliximab 1:60,000 dilution). The detected antibodies were visualized on the membrane by development with TMB (Sigma, Switzerland).

2.7. Immunohistochemistry

After ATG permeation, porcine skins were first washed with running deionized water to remove any excess antibody on the skin surface. Then, the skins were embedded in OCT medium, snap frozen in liquid nitrogen and vertically sectioned using a cryomicrotome. After fixation of the section with cold acetone, 10 µg/ml Alexa Fluor® 488 anti-rabbit antibody (Invitrogen, Switzerland) and Hoechst 33258 (Invitrogen, Switzerland) were used to stain the 10 µm sections. The images were documented using a Zeiss Axioplan fluorescence microscope equipped with a Zeiss Axiocam MRM digital camera system.

2.8. Functional analysis

A human lymphocyte cytotoxicity assay was performed in 96-well microplates (TPP, Switzerland) to evaluate the bioactivity of ATG post-delivery. Aliquots (75 µl) of transdermally delivered ATG or PBSF buffer (PBS buffer containing 2% fetal calf serum) were loaded into each well. Then, 25 µl of human lymphocytes (1×10^6 cells/ml in PBSF) and rabbit complement (Invitrogen, Switzerland) was added to each well. After incubation (37 °C, 5% CO_2) for 30 min, the supernatant was discarded. The cells were then resuspended in 200 µl propidium iodide (5 µg/ml in PBSF; Sigma, Switzerland) and Calcein-AM (Invitrogen, Switzerland) solution and incubated at RT for 10 min. The slide was prepared using 10 µl of suspension and imaged using the fluorescence microscope system described above.

2.9. Statistical analysis

Experimental data are shown as mean ± standard deviation (S.D.). Outliers determined using the *Grubbs test* were discarded. Statistical analyses were performed using the Data Analysis function in Microsoft Excel 2007. Results were evaluated statistically using either a two-tailed *Student t-test* or one way analysis of variance (*ANOVA*) followed by a *Student–Newman–Keuls* (*SNK*) post hoc test. The level of significance was fixed at $\alpha = 0.05$.

3. Results and discussion

3.1. Transdermal delivery of therapeutic antibodies in vitro

3.1.1. ATG

Transdermal delivery of ATG was first investigated into and across laser-porated dermatomed porcine ear skin (0.75 mm) *in vitro* and quantified by ELISA; control experiments were performed without laser treatment. Unsurprisingly, there was negligible delivery with untreated skin after 24 h; no ATG permeation was observed and deposition within the skin was only 0.06 ± 0.01 µg/cm^2 (most probably due to non-specific cross-reactions) (Fig. 1a, b). In contrast there was significant antibody transport after P.L.E.A.S.E.® treatment (Fig. 1a, b). Total ATG delivery (sum of the amounts permeated across and deposited within the skin) after 24 h, with 300, 450 and 900 pores at a fluence of 45.3 J/cm^2 per pore (enough to reach the deeper epidermis [19]), was 1.18 ± 0.10, 3.98 ± 0.64 and 4.97 ± 0.83 µg/cm^2, respectively (Fig. 1a). This corresponded to statistically significant 19.7-, 66.3- and 82.8-fold increases over the control ($P<0.05$; *ANOVA* followed by *Student–Newman–Keuls* (*SNK*) test). The effect of laser fluence was confirmed in a second series of experiments performed at a fixed pore number (900), where laser fluence was increased from 22.65 to 45.3 and 135.9 J/cm^2 per pore, ATG delivery increased significantly from 1.70 ± 0.65 to 4.97 ± 0.83 and 8.70 ± 1.55 µg/cm^2 ($P<0.05$; *ANOVA* and *SNK* test) (Fig. 1b). ATG transport kinetics (initial dose, 900 µl of 1 mg/ml

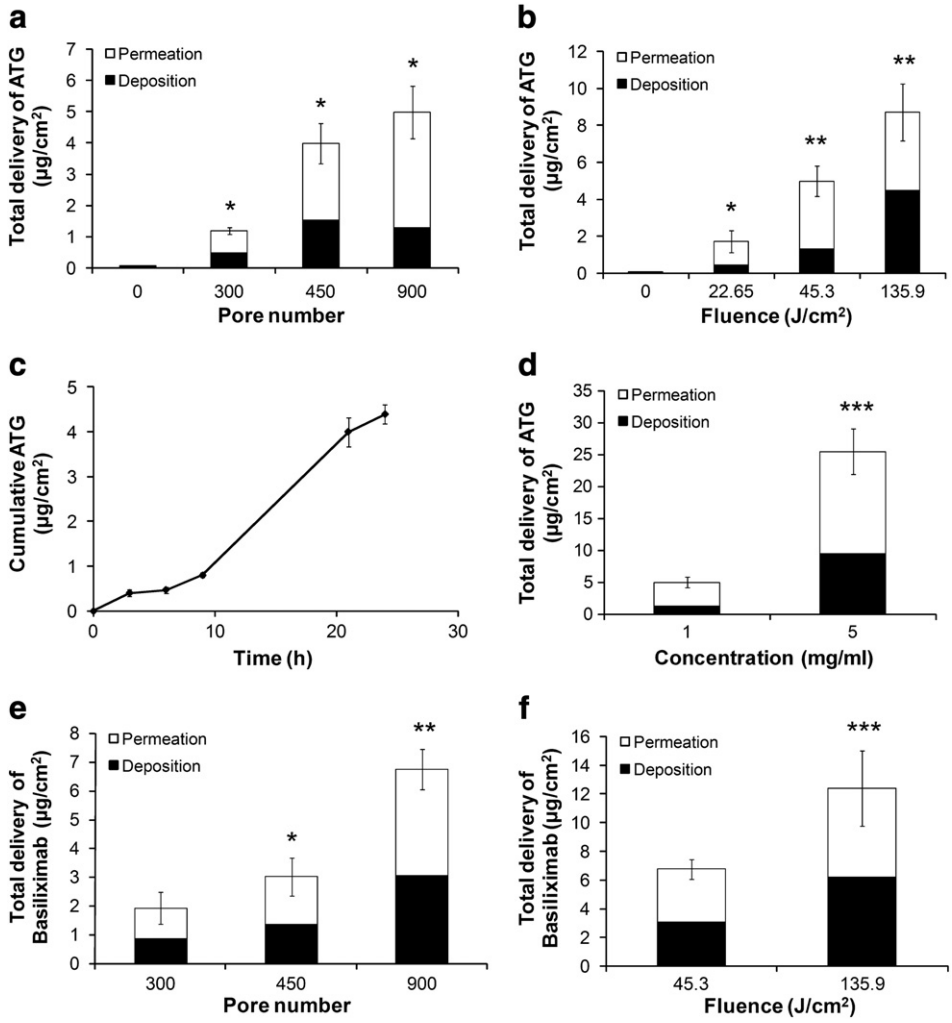

Fig. 1. Effect of laser poration parameters and formulation conditions on transdermal delivery of ATG and Basiliximab. Dermatomed porcine ear skins (0.75 mm) were mounted in Franz diffusion cells (2.9 cm^2) and 900 μl of either ATG or Basiliximab (1 mg/ml in PBSS buffer) was placed in the donor compartment for 24 h at RT. PBSS buffer was also placed in the receptor compartment. 400 μl aliquots were collected from the receptor at given time-points (3, 6, 9, 21, and 24 h) during permeation. The amount of antibody retained in the skin was extracted post-permeation in 10 ml PBSS for 4 h at RT. Antibody permeation and skin deposition were quantified by ELISA. (a) Effect of pore number (0, 300, 450 and 900 pores; fluence of 45.3 J/cm^2) on ATG delivery. (Mean ± S.D.; n ≥ 4). *P<0.05 (ANOVA (α = 0.05) and *Student–Newman–Keuls* (*SNK*) test). (b) Effect of fluence (0, 22.65, 45.3 and 135.9 J/cm^2; 900 pores) on ATG delivery. (Mean ± S.D.; n ≥ 4). *P<0.05, **P<0.01 (ANOVA (α = 0.05) and *SNK* test). (c) Cumulative permeation of ATG as a function of time over 24 h (900 pores and fluence of 135.9 J/cm^2). (Mean ± S.D.; n = 4). (d) Effect of concentration (1 or 5 mg/ml) on ATG delivery. (Mean ± S.D.; n ≥ 4). ***P<0.001 (*Student t-test* (α = 0.05)). (e) Effect of pore number (300, 450 and 900 pores; fluence 45.3 J/cm^2) on Basiliximab delivery. (Mean ± S.D.; n = 4). *P<0.05, **P<0.01 (ANOVA (α = 0.05) and *SNK* test). (f) Effect of fluence (45.3 and 135.9 J/cm^2; 900 pores) on Basiliximab transport. (Mean ± S.D.; n = 4) ***P<0.001 (*Student t-test*).

ATG) using 900 pores and 135.9 J/cm^2 were also investigated and the steady state flux was estimated to be 218 ng/cm^2 h (Fig. 1c). Increasing ATG concentration in the formulation from 1 to 5 mg/ml resulted in a 5-fold enhancement of ATG delivery across porated skin (900 pores and 45.3 J/cm^2) from 4.97 ± 0.83 to 25.46 ± 3.58 μg/cm^2 (P = 0.00003; *Student t-test*) (Fig. 1d). Thus, as for the delivery of small molecules across intact skin, increasing the antibody concentration gradient increased the thermodynamic driving force, resulting in an increase in flux.

3.1.2. Basiliximab

Transdermal delivery of Basiliximab across laser treated skins confirmed the trends observed with ATG. Comparable quantities of Basiliximab were delivered under the same experimental conditions. Basiliximab delivery increased linearly from 1.92 ± 0.48 to 3.02 ± 0.71 and 6.74 ± 0.66 μg/cm^2 when pore number was increased from 300 to 450 and 900, respectively, at a fluence of 45.3 J/cm^2 (Fig. 1e) (P<0.05; *ANOVA* and *SNK* test). A three-fold increase in laser fluence from 45.3 to 135.9 J/cm^2 resulted in a two-fold increase in Basiliximab delivery from 6.74 ± 0.66 to 12.36 ± 1.62 μg/cm^2 (P = 0.0007; *Student t-test*) using 900 pores (Fig. 1f). Hence, increasing either laser fluence or pore number could lead to substantive increases in antibody delivery.

3.2. Confirming structural integrity post-delivery

The identity and structural integrity of the antibodies post-delivery were confirmed by Western blot. Bands derived from ATG (Fig. 2a) and Basiliximab (Fig. 2b) post-delivery, and their respective standards, were detected under non-reducing conditions at a putative molecular weight of ~175 kDa on the membrane, indicating that the antibodies remained intact after transit.

3.3. Demonstrating biological activity post-delivery

In addition to confirming structural integrity, another objective was to confirm that antibody bioactivity was also retained post-delivery; this and subsequent *in vivo* studies (see below) were conducted using ATG alone. ATG functionality was tested by using a human lymphocyte cytotoxicity assay (Fig. 3). Active ATG can induce complement-dependent cytotoxicity in targeted human lymphocytes

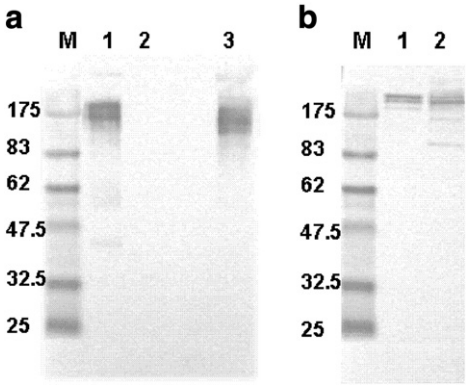

Fig. 2. Confirming antibody identity and integrity by Western blot analysis (non-reducing conditions). (a) ATG detected by anti-rabbit IgG (whole molecule)–peroxidase antibody. Lane M: Pre-stained protein marker; Lane 1: ATG standard; Lane 2: ATG delivered across untreated skins; Lane 3: ATG delivered following laser treatment. (b) Basiliximab detected by anti-human IgG (Fc fragment specific)–peroxidase antibody. Lane M: Pre-stained protein marker; Lane 1: Basiliximab standard; Lane 2: Basiliximab delivered following laser treatment.

[35]. In contrast to the negative control (in the absence of ATG) where the living cells were stained in green by Calcein-AM (Fig. 3a), an appreciable number of dead cells stained in red by propidium iodide, were observed upon the addition of post-permeation ATG samples (Fig. 3b). The extent of cell death was similar to that observed using an equal concentration of ATG standard (positive control; (Fig. 3c)). These results demonstrated that ATG biological activity, i.e., the cytotoxicity to human lymphocytes, was retained after delivery across laser porated skin.

3.4. Visualizing antibody distribution in the skin

Immunohistochemical staining was used to visualize ATG distribution within the skin and to demonstrate that antibody delivery was due to the presence of the micropores (Fig. 4). After ATG permeation for 24 h, skin samples were incubated with Alexa Fluor® 488 anti-rabbit antibodies. As expected no ATG was detected in the control (ATG applied to non-porated skins; (Fig. 4a)); however, intense green fluorescence derived from ATG was clearly visible in the laser-porated porcine ear skins following ATG permeation (Fig. 4b). The most intense green fluorescence was observed directly under the micropore; less intense fluorescence was observed in neighboring areas indicating radial diffusion of ATG in the viable epidermis along a concentration gradient emanating from the micropore.

3.5. Correlation between porcine and human skin

ATG delivery across dermatomed porcine skin was corroborated using human abdominal skin. Total ATG delivery across porcine and human skins in 24 h under the same experimental conditions (900 pores and 34 J/cm^2) was statistically equivalent (6.87 ± 0.23 and 8.03 ± 0.99 μg/cm^2, respectively) (Fig. 5). However, more ATG was deposited in human skin; this could have been due to its greater thickness (~1.5 mm vs. 0.75 mm). The similarity between antibody delivery across porcine and human tissue is consistent with earlier reports advocating the use of porcine ear skin as an *in vitro* model for percutaneous delivery across human skin [36,37].

3.6. Antibody delivery in vivo

In vivo proof-of-principle was demonstrated by delivering ATG in C57 BL/10 SCSnJ mice (12 weeks' old, 20–23 g). ATG (900 μl of 1 mg/ml ATG solution) was applied for 3 h to the animal's abdomen following laser-microporation (Fig. 6). The ATG concentration in the blood of mice treated with the laser was significantly higher than that in the control animals (without laser treatment) – 276.27 ± 50.61 and 6.71 ± 3.52 ng/ml, respectively ($P = 0.00004$; *Student t-test*) – the latter was probably due to cross reactions. Since mice are considered to have ~58.5 ml of total blood per kilogram of bodyweight [38], then given the animals' bodyweight of 20–23 g, ATG delivery *in vivo* at 3 h was estimated at 323 ± 59 ng. A direct *in vitro*/*in vivo* comparison was obtained by performing a similar experiment using isolated shaved abdominal skin from C57 BL/10 SCSnJ mice (12 weeks' old) *in vitro*. The results showed that 251 ± 67 ng of ATG was delivered after permeation for 3 h across laser-porated skin *in vitro*. There was statistical equivalence between laser-assisted delivery *in vitro* and *in vivo* (t (1.44) < t_{crit} (2.45); *Student t-test*) under identical experimental conditions (900 pores and 20.4 J/cm^2; Fig. 6). However, efficacy *in vivo* could not be validated in the murine model since ATG targets only human antigens.

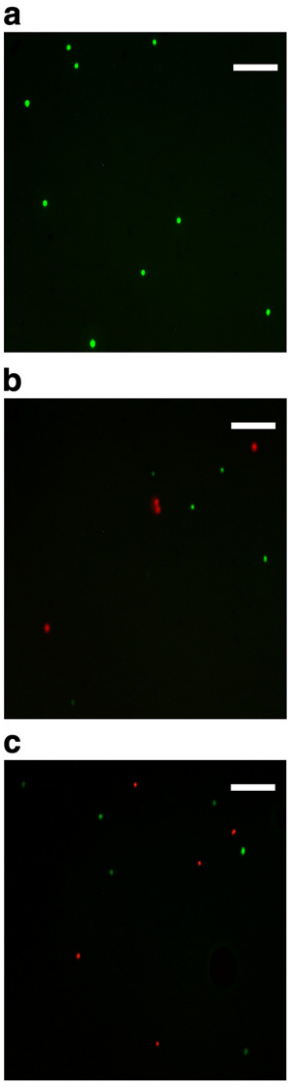

Fig. 3. Confirming functionality of ATG post-permeation. Micrographs of cytotoxicity assay results (a) without ATG (negative control), (b) following addition of ATG samples post-permeation (c) in the presence of an equivalent concentration of ATG standard (positive control). Buffer, post-permeation ATG sample or ATG standard (75 μl) was incubated with 25 μl of human lymphocytes (1×10^6 cells/ml in PBSF) and 25 μl of rabbit complement in a 96-well microplate well for 30 min at 37 °C. After removing the supernatant, the cells were stained with Calcein-AM (green) and propidium iodide (red); thus, living and dead human lymphocytes were specifically stained green or red, respectively. Bar = 300 μm.

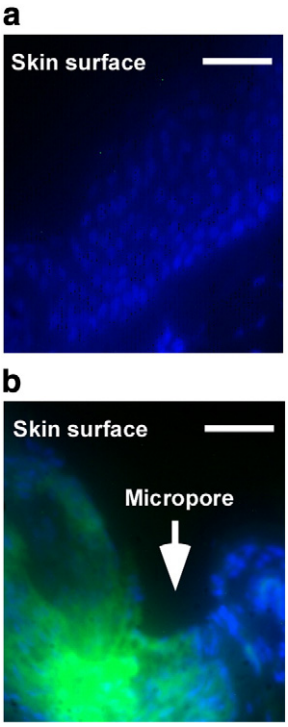

Fig. 4. Confirming ATG distribution in the epidermis. Immunohistochemistry micrograph showing ATG transport through (a) untreated and (b) laser-treated dermatomed porcine ear skin. 10 μm sections of skin samples following 24 h ATG application were prepared and stained with 10 μg/ml of Alexa Fluor® 488 anti-rabbit antibody (green) and Hoechst 33258 (blue). ATG distribution is indicated in green and cell nuclei in blue. The arrow denotes the micropore created by laser. Bar = 50 μm.

3.7. Delivering therapeutic amounts of antibody

These experiments demonstrate that laser microporation can deliver antibodies across the skin; moreover, the amounts delivered are therapeutically relevant. In the human skin study (see Section 3.5 and Fig. 5), ATG deposition after 24 h was 5.74 ± 0.72 μg/cm^2; taking into account the application area of 2.9 cm^2, this implies that 16.65 ± 2.09 μg ATG was retained in the skin sample. Since the samples had an average thickness of 1.5 mm, the ATG concentration in the skin samples can be estimated as 38.3 ± 4.8 μg/ml. It has been shown that ATG induces apoptosis in NK- and B-cells at 0.1 and 1 μg/ml [39,40]; it also down-regulates surface expression of CD16 on NK-cells at 0.1 μg/ml [40] and interferes with the expression of leukocyte function associated antigen-1 (CD11a/CD18, LFA-1), which is involved in intercellular adhesion, at 10 μg/ml [41]. Since rejection of composite tissue allografts appears to be

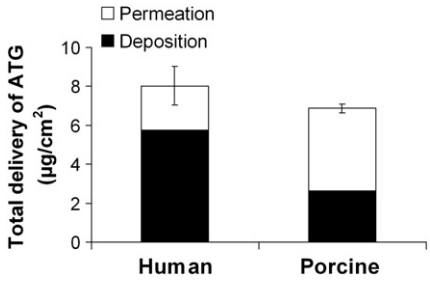

Fig. 5. Comparison of ATG delivery across human and porcine skin. *In vitro* transdermal delivery of ATG (900 μl, 1 mg/ml) using human and porcine skins in 24 h under the same laser poration conditions (900 pores/34 J/cm^2). The antibodies were collected and analyzed as in Fig. 1. (Mean ± S.D.; n ≥ 3).

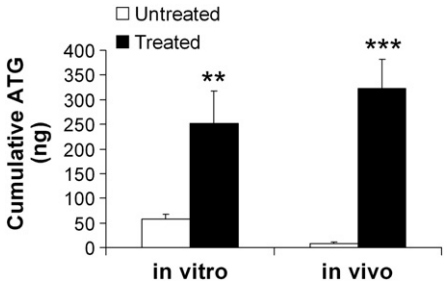

Fig. 6. The *in vitro/in vivo* correlation in C57 BL/10 SCSnJ mice. *In vitro/in vivo* comparison of ATG delivery through C57 BL/10 SCSnJ mice abdominal skin (12 weeks' old, 20–23 g) after 3 h using the same laser conditions (900 pores/20.4 J/cm^2). For the *in vivo* experiments, blood was collected directly from the heart after permeation for 3 h. The collected samples were diluted as required and analyzed by ELISA. (Mean ± S.D.; n ≥ 4) $^{**}P<0.01$, $^{***}P<0.001$ (*Student t-test*).

initiated in the skin (in the epidermis) [42], the key parameter in determining immunosuppressive efficacy could be the ATG concentration within the skin itself. Thus, given the reported pharmacological activities [39–42], the local concentrations observed in the skin in these studies appear to be in the therapeutic range.

4. Conclusions

Laser microporation using the P.L.E.A.S.E.® system was shown to be capable of delivering significant amounts of intact, biologically active antibody across porated murine, porcine and human skin *in vitro* and murine skin *in vivo*. Antibody transport was controlled by modulating pore number, laser fluence and antibody concentration in the formulation. The correlation between delivery across murine skin *in vitro* and *in vivo* suggests that laser microporation studies *in vitro* are good predictors for transport *in vivo*. Taken together with the delivery observed across porcine and human skin *in vitro*, these results point to the feasibility of delivering antibodies across human skin *in vivo*. The next step in the "ATG/Basiliximab" project will be to build upon these preliminary *in vitro* and *in vivo* data and to test the ability of laser-assisted antibody delivery to prevent graft rejection in a composite tissue allotransplantation animal model *in vivo*[42]. In conclusion, these findings provide the first report on the "needle-less" local delivery of functional antibodies across the skin at therapeutically relevant amounts and show that laser microporation may provide a new approach for the local administration of biopharmaceuticals.

Acknowledgements

We thank Olivier Dorchies, Yoshiko Nakae and Ophélie V. Pattey (School of Pharmaceutical Sciences, University of Geneva) for technical assistance with the immunohistochemical staining studies and the *in vivo* experiments. We would like to acknowledge Kouroche Amini (Department of Plastic, Aesthetic and Reconstructive Surgery, Geneva University Hospital) for providing human skin samples (the study was approved by the Central Committee for Ethics in Research (CER: 08–150 (NAC08-051); Geneva University Hospital)) and Christian Bloy (Genzyme Corp., France) and Deborah Wirth (Genzyme GmbH, Switzerland) for providing human lymphocytes. We would also like to thank Leonardo Scapozza and Remo Perozzo (School of Pharmaceutical Sciences, University of Geneva) and Aarti Naik (Triskel Integrated Services, Geneva) for reviewing the manuscript. Finally, we would like to acknowledge our colleague Yogeshwar Bachhav for help with the laser device and Arne Heinrich (Pantec Biosolutions AG, Ruggell, Liechtenstein) for laser technical support. This work was supported by the Swiss Innovation Promotion Agency (CTI: 9307.1 PFLS-LS), Genzyme GmbH and by Pantec Biosolutions AG.

Appendix A. Supplementary data

Supplementary data to this article can be found online at doi:10.1016/j.jconrel.2011.07.024.

References

[1] B. Leader, Q.J. Baca, D.E. Golan, Protein therapeutics: a summary and pharmacological classification, Nat. Rev. Drug Discovery 7 (1) (2008) 21–39.
[2] W.R. Strohl, D.M. Knight, Discovery and development of biopharmaceuticals: current issues, Curr. Opin. Biotechnol. 20 (6) (2009) 668–672.
[3] M.E. Chamuleau, A.A. van de Loosdrecht, P.C. Huijgens, Monoclonal Antibody therapy in haematological malignancies, Curr Clin. Pharmacol. 5 (3) (2010) 148–159.
[4] F. Perosa, M. Prete, V. Racanelli, F. Dammacco, CD20-depleting therapy in autoimmune diseases: from basic research to the clinic, J. Intern. Med. 267 (3) (2010) 260–277.
[5] D. Schrama, R.A. Reisfeld, J.C. Becker, Antibody targeted drugs as cancer therapeutics, Nat. Rev. Drug Discovery 5 (2) (2006) 147–159.
[6] S.B. Bressler, Introduction: understanding the role of angiogenesis and antiangiogenic agents in age-related macular degeneration, Ophthalmology 116 (10 Suppl) (2009) S1–S7.
[7] M.E. Sockolov, A. Alikhan, O. Zargari, Non-psoriatic dermatologic uses of monoclonal antibody therapy, J. Dermatol. Treat. 20 (6) (2009) 319–327.
[8] B. Gander, C.S. Brown, D. Vasilic, A. Furr, J.C. Banis Jr., M. Cunningham, O. Wiggins, C. Maldonado, I. Whitaker, G. Perez-Abadia, J.M. Frank, J.H. Barker, Composite tissue allotransplantation of the hand and face: a new frontier in transplant and reconstructive surgery, Transpl. Int. 19 (11) (2006) 868–880.
[9] V.S. Gorantla, J.H. Barker, J.W. Jones Jr., K. Prabhune, C. Maldonado, D.K. Granger, Immunosuppressive agents in transplantation: mechanisms of action and current anti-rejection strategies, Microsurgery 20 (8) (2000) 420–429.
[10] S.A. Gruber, M.V. Shirbacheh, J.W. Jones, J.H. Barker, W.C. Breidenbach, Local drug delivery to composite tissue allografts, Microsurgery 20 (8) (2000) 407–411.
[11] A. Naik, Y.N. Kalia, R.H. Guy, Transdermal drug delivery: overcoming the skin's barrier function, Pharm. Sci. Technol. Today 3 (9) (2000) 318–326.
[12] P.M. Elias, E.H. Choi, Interactions among stratum corneum defensive functions, Exp. Dermatol. 14 (10) (2005) 719–726.
[13] M.R. Prausnitz, S. Mitragotri, R. Langer, Current status and future potential of transdermal drug delivery, Nat. Rev. Drug Discovery 3 (2) (2004) 115–124.
[14] P. Karande, A. Jain, S. Mitragotri, Discovery of transdermal penetration enhancers by high-throughput screening, Nat. Biotechnol. 22 (2) (2004) 192–197.
[15] Y. Chen, Y. Shen, X. Guo, C. Zhang, W. Yang, M. Ma, S. Liu, M. Zhang, L.P. Wen, Transdermal protein delivery by a coadministered peptide identified via phage display, Nat. Biotechnol. 24 (4) (2006) 455–460.
[16] M. Ogura, S. Paliwal, S. Mitragotri, Low-frequency sonophoresis: current status and future prospects, Adv. Drug Deliv. Rev. 60 (10) (2008) 1218–1223.
[17] S. Dubey, Y.N. Kalia, Non-invasive iontophoretic delivery of enzymatically active ribonuclease A (13.6 kDa) across intact porcine and human skins, J. Control. Release 145 (2010) 203–209.
[18] G. Li, A. Badkar, S. Nema, C.S. Kolli, A.K. Banga, *In vitro* transdermal delivery of therapeutic antibodies using maltose microneedles, Int. J. Pharm. 368 (1–2) (2009) 109–115.
[19] Y.G. Bachhav, Y.N. Kalia, T. Bragagna, C. Böhler, Intraepidermal drug delivery: P.L.E.A.S.E.® — a new laser microporation technology, Drug Deliv. Technol. 8 (2008) 26–31.
[20] Y.G. Bachhav, S. Summer, A. Heinrich, T. Bragagna, C. Böhler, Y.N. Kalia, Effect of controlled laser microporation on drug transport kinetics into and across the skin, J. Control. Release 146 (1) (2010) 31–36.
[21] Y.G. Bachhav, A. Heinrich, Y.N. Kalia, Using laser microporation to improve transdermal delivery of diclofenac: increasing bioavailability and the range of therapeutic applications, Eur. J. Pharm. Biopharm. 78 (3) (2011) 408–414.
[22] N.H. Zech, M. Murtinger, P. Uher, Pregnancy after ovarian superovulation by transdermal delivery of follicle-stimulating hormone, Fertil. Steril. 95 (8) (2011) 2784–2785.
[23] P.L. Yun, R. Tachihara, R.R. Anderson, Efficacy of erbium:yttrium-aluminum-garnet laser-assisted delivery of topical anesthetic, J. Am. Acad. Dermatol. 47 (4) (2002) 542–547.
[24] K.H. Wang, J.Y. Fang, C.H. Hu, W.R. Lee, Erbium:YAG laser pretreatment accelerates the response of Bowen's disease treated by topical 5-fluorouracil, Dermatol. Surg. 30 (3) (2004) 441–445.
[25] J.Y. Fang, W.R. Lee, S.C. Shen, H.Y. Wang, C.L. Fang, C.H. Hu, Transdermal delivery of macromolecules by erbium:YAG laser, J. Control. Release 100 (1) (2004) 75–85.
[26] S.C. Shen, W.R. Lee, Y.P. Fang, C.H. Hu, J.Y. Fang, *In vitro* percutaneous absorption and *in vivo* protoporphyrin IX accumulation in skin and tumors after topical 5-aminolevulinic acid application with enhancement using an erbium:YAG laser, J. Pharm. Sci. 95 (4) (2006) 929–938.
[27] W.R. Lee, S.C. Shen, C.R. Liu, C.L. Fang, C.H. Hu, J.Y. Fang, Erbium:YAG laser-mediated oligonucleotide and DNA delivery via the skin: an animal study, J. Control. Release 115 (3) (2006) 344–353.
[28] W.R. Lee, T.L. Pan, P.W. Wang, R.Z. Zhuo, C.M. Huang, J.Y. Fang, Erbium:YAG laser enhances transdermal peptide delivery and skin vaccination, J. Control. Release 128 (3) (2008) 200–208.
[29] W.R. Lee, S.C. Shen, C.L. Fang, R.Z. Zhuo, J.Y. Fang, Topical delivery of methotrexate via skin pretreated with physical enhancement techniques: low-fluence erbium: YAG laser and electroporation, Lasers Surg. Med. 40 (7) (2008) 468–476.
[30] W.R. Lee, S.C. Shen, R.Z. Zhuo, K.C. Wang, J.Y. Fang, Enhancement of topical small interfering RNA delivery and expression by low-fluence erbium:YAG laser pretreatment of skin, Hum. Gene Ther. 20 (6) (2009) 580–588.
[31] W.R. Lee, S.C. Shen, M.H. Pai, H.H. Yang, C.Y. Yuan, J.Y. Fang, Fractional laser as a tool to enhance the skin permeation of 5-aminolevulinic acid with minimal skin disruption: a comparison with conventional erbium:YAG laser, J. Control. Release 145 (2) (2010) 124–133.
[32] W.R. Lee, S.C. Shen, S.A. Al-Suwayeh, H.H. Yang, C.Y. Yuan, J.Y. Fang, Laser-assisted topical drug delivery by using a low-fluence fractional laser: Imiquimod and macromolecules, J. Control. Release (2011) http://dx.doi.org/10.1016/j.jconrel.2011.03.015.
[33] B. Forster, A. Klein, R.M. Szeimies, T. Maisch, Penetration enhancement of two topical 5-aminolaevulinic acid formulations for photodynamic therapy by erbium:YAG laser ablation of the stratum corneum: continuous versus fractional ablation, Exp. Dermatol. 19 (9) (2010) 806–812.
[34] U.K. Laemmli, Cleavage of structural proteins during the assembly of the head of bacteriophage T4, Nature 227 (5259) (1970) 680–685.
[35] F. Ayuk, N. Maywald, S. Hannemann, U. Larsen, A. Zander, N. Kroger, Comparison of the cytotoxicity of 4 preparations of anti-T-cell globulins in various hematological malignancies, Anticancer. Res. 29 (4) (2009) 1355–1360.
[36] I.P. Dick, R.C. Scott, Pig ear skin as an *in-vitro* model for human skin permeability, J. Pharm. Pharmacol. 44 (8) (1992) 640–645.
[37] N. Sekkat, Y.N. Kalia, R.H. Guy, Biophysical study of porcine ear skin *in vitro* and its comparison to human skin *in vivo*, J. Pharm. Sci. 91 (11) (2002) 2376–2381.
[38] C.J. Brown, T.M. Donnelly, Rodent husbandry and care, Vet. Clin. North Am. Exot. Anim. Pract. 7 (2) (2004) 201–225 v.
[39] O. Penack, L. Fischer, C. Gentilini, A. Nogai, A. Muessig, K. Rieger, S. Ganepola, E. Thiel, L. Uharek, The type of ATG matters — natural killer cells are influenced differentially by Thymoglobulin, Lymphoglobulin and ATG-Fresenius, Transpl. Immunol. 18 (2) (2007) 85–87.
[40] D. Stauch, A. Dernier, E. Sarmiento Marchese, K. Kunert, H.D. Volk, J. Pratschke, K. Kotsch, Targeting of natural killer cells by rabbit antithymocyte globulin and campath-1H: similar effects independent of specificity, PLoS One 4 (3) (2009) e4709.
[41] M.C. Michallet, X. Preville, M. Flacher, S. Fournel, L. Genestier, J.P. Revillard, Functional antibodies to leukocyte adhesion molecules in antithymocyte globulins, Transplantation 75 (5) (2003) 657–662.
[42] T. Hautz, B. Zelger, J. Grahammer, C. Krapf, A. Amberger, G. Brandacher, L. Landin, H. Muller, M.P. Schon, P. Cavadas, A.W. Lee, J. Pratschke, R. Margreiter, S. Schneeberger, Molecular markers and targeted therapy of skin rejection in composite tissue allotransplantation, Am. J. Transplant. 10 (5) (2010) 1200–1209.

Annexure 4

Research article

Biomedical Chromatography

Received: 24 April 2011, Accepted: 5 July 2011 Published online in Wiley Online Library: 23 August 2011

(wileyonlinelibrary.com) DOI 10.1002/bmc.1695

Development and validation of a HPAE-PAD method for the quantification of CGP69669A, a sialyl Lewis^x mimetic, in skin permeation studies

Taís Gratieri,[a] Beatrice Wagner,[b] Dhaval Kalaria,[a] Beat Ernst[b] and Yogeshvar N. Kalia[a]*

ABSTRACT: A simple, rapid, precise and specific isocratic HPAE-PAD method for quantification of CGP69669A was developed and validated. CGP69669A is a glycomimetic of sialyl Lewis^x and an antagonist of E-selectin with potential application in the treatment of inflammatory skin disease. Quantification was performed using a Dionex CarboPac^{TM} PA-200 anion-exchange column (3 × 250 mm) with 100 mM NaOH solution as mobile phase, a flow rate of 0.50 mL/min and an injection volume of 10 μL. A quadruple potential waveform was used to detect the carbohydrate (+0.1 V from 0.00 to 0.40 s, −2.0 V from 0.41 to 0.42 s, +0.6 V at 0.43 s and −0.1 V from 0.44 to 0.50 s with current integrated between 0.20 and 0.40 s for detection) and rafinose was employed as an internal standard. The optimized conditions enabled rapid elution of CGP69669A (at 3.0 min) without interference from solvent peaks or substances present in the skin. The method showed good intra- and inter-day precision and accuracy and the response was linear from 1.0 to 25 μg/mL. This is the first validated direct method for the quantification of CGP69669A. It will now be employed in studies investigating the topical and transdermal delivery of CGP69669A *in vitro* and *in vivo* and it should also be of use for other applications of this molecule. Copyright © 2011 John Wiley & Sons, Ltd.

Keywords: CGP69669A; sialyl Lewis^x glycomimetic; E-selectin antagonist; HPAE-PAD; skin

Introduction

CGP69669A (Fig. 1) is a sialyl Lewis^x (sLex) glycomimetic antagonist of E-selectin (Kolb and Ernst, 1997, Norman *et al*., 1998; Titz *et al*., 2010). The tetrasaccharide sialyl Lewis^x (sLe^x) has been shown to be recognized by all three selectin adhesion molecules (E, P- and L-selectin) (Phillips *et al*., 1990; Berg *et al*., 1991). The interaction of selectins with their natural carbohydrate ligands has been shown to mediate the initial step of the recruitment of leukocytes in immune responses (Ley and Tedder, 1995; Ley, 1996; Rao *et al*., 2007). Since the abnormal or excessive recruitment and influx of leukocytes is involved in the pathogenesis of several inflammatory diseases, the antagonism of the selectins and the consequent inhibition of leukocyte trafficking between lymph nodes, blood and skin is considered to be a promising approach for the treatment of diseases such as psoriasis, eczematous disorders, atopic dermatitis or allergic contact dermatitis (Tanaka *et al*., 1996; Robert and Kupper, 1999; Vollmer *et al*., 2001; Schon, 2005; Bock *et al*., 2006; Vocanson *et al*., 2009).

The potential of CGP69669A to block selectins has been shown in animal models (Norman *et al*., 1998); however, to our knowledge, its efficacy in treating skin inflammatory disorders has never been tested. Possible reasons for the lack of studies may include: (i) the poor pharmacokinetic profile of CGP69669A owing to its high polarity and the presence of *O*-glycosidic bonds that are susceptible to hydrolysis; and (ii) the difficulty of quantification – the molecule possesses neither chromophore nor fluorophore groups, ruling out the use of direct UV–vis and fluorescence detection methods.

Given its physicochemical properties, CGP69669A is an interesting candidate for administration by iontophoresis, which involves the application of a mild electric current to enhance the transport of hydrosoluble, ionized molecules into and through the skin (Kalia *et al*., 2004). However, a reliable quantification method is required before the feasibility of using iontophoresis to deliver CGP69669A across the skin can be evaluated.

High-performance anion exchange chromatography coupled with pulsed amperometric detection (HPAE-PAD) is a relatively new technique that has been successfully applied for the analysis of complex carbohydrates (Hanko and Rohrer, 2000). Normally, an eluent of high pH is used and, owing to the weakly acidic nature of carbohydrates, separation can be carried out using a strong

* Correspondence to: Y. N. Kalia, School of Pharmaceutical Sciences, University of Geneva, 30 Quai Ernest Ansermet, 1211 Geneva 4, Switzerland. E-mail: yogi.kalia@unige.ch

[a] School of Pharmaceutical Sciences, University of Geneva and University of Lausanne, 30 Quai Ernest Ansermet, 1211 Geneva, Switzerland

[b] Institute of Molecular Pharmacy, University of Basel, Klingelbergstrasse 50, CH-4056 Basel, Switzerland

Abbreviations used: HPAE-PAD, high-performance anion exchange chromatography coupled with pulsed amperometric detection; PBS, phosphate-buffered saline; sLex, sialyl Lewis^x.

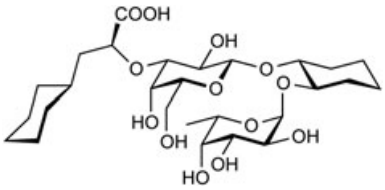

Figure 1. Molecular structure of CGP69669A (MW of 600.64 Da).

anion exchange stationary phase. Detection and quantification are possible by measuring the electrical current generated by the oxidation of the carbohydrate molecules after application of a positive potential at the surface of a gold electrode. In addition to its high sensitivity and specificity, the method enables rapid analysis of complex carbohydrate samples since no derivatization is required.

The aim of the present study was to develop and validate a simple, rapid, precise and specific isocratic HPAE-PAD method for quantification of CGP69669A that could be used in future skin permeation studies.

Experimental

Chemicals and reagents

CGP69669A was synthesized in-house (Kolb and Ernst, 1997). Rafinose and sodium hydroxide were purchased from Sigma-Aldrich (Buchs, Switzerland). Sucrose was purchased from AppliChem (Darmstadt, Germany). Sodium chloride, di-sodium hydrogen phosphate and potassium dihydrogenphosphate were purchased from Fluka (Buchs, Switzerland). Millex PVDF filters (0.45 μm) were purchased from Millipore (Bedford, MA, USA). All solutions were prepared using deionized reverse osmosis-filtered water (resistivity ≥ 18 MΩ cm). All other chemicals were at least of analytical grade.

Skin preparation

Porcine ears were obtained from a local abattoir shortly after slaughter (CARRE; Rolle, Switzerland). After cleaning under cold running water, the skin was excised (thickness 750 μm) with an air dermatome (Zimmer; Etupes, France), wrapped in aluminum foil and stored in polyethylene bags at −20 °C for a maximum period of 2 months.

Standard solution preparation

A stock solution of CGP69669A (50 μg/mL) was prepared by dissolving 5 mg of the carbohydrate in 100 mL phosphate-buffered saline (PBS; pH 7.4). Eleven standard solutions were prepared by suitable dilution of the stock solution in PBS (pH 7.4). The standard solutions were used to prepare the samples for the calibration curve.

Apparatus and chromatographic conditions

CGP69669A was quantified by HPAE-PAD. The system consisted of a GP50 gradient pump, an ED50A electrochemical detector with a gold working electrode, an AS50 autosampler, an AS50TC thermal compartment and a Chromeleon® chromatography workstation (Dionex Corporation, Sunnyvale, CA, USA). A Dionex CarboPac™ PA-200 anion-exchange column (3 × 250 mm) and a guard column (3 × 50 mm) were used for analysis. The mobile phase consisted of 100 mM NaOH solution. It was prepared in deionized water and purged with helium to minimize carbonate. The flow rate was 0.50 mL/min and the injection volume was 10 μL. Detection was performed using the quadruple potential waveform: +0.1 V from 0.00 to 0.4 s, −2.0 V from 0.41 to 0.42 s, +0.6 V at 0.43 s and −0.1 V from 0.44 to 0.50 s, using the combination Ag-AgCl pH reference electrode with the instrument set in pH mode and with current integration between 0.20 and 0.40 s for detection of the analyte (Rocklin *et al.*, 1998). Rafinose was used as an internal standard.

Method optimization

In order to obtain a sharp CGP69669A peak that was distinct and sufficiently separated from peaks due to substances released from the skin, mobile phases containing different amounts of sodium hydroxide and sodium acetate were tested at different flow rates. Two different anion-exchange columns were also evaluated: the Dionex CarboPac™ PA-10 and the Dionex CarboPac™ PA-200 with the respective pre-columns. Sucrose was also evaluated as an internal standard and compared with rafinose.

Method validation

The method was validated according to ICH guidelines Q2 (R1) (ICH, 2005) with respect to linearity, accuracy and precision, limit of detection and limit of quantification.

Linearity

CGP69669A concentrations of 1.0, 2.5, 5.0, 7.5, 10, 12.5, 15, 17.5, 20, 22.5 and 25 μg/mL in PBS buffer were used to prepare the calibration curves. A 50 μL aliquot of the internal standard solution (rafinose 55 μg/mL) was added to 1 mL of the CGP69669A sample. A standard curve of CGP69669A/rafinose peak area ratio against CGP69669A concentration was plotted and calibration curves were fitted using least squares linear regression.

Specificity

The specificity of the method was investigated by injecting samples of porcine skin extract in order to confirm that there was no interference from endogenous compounds present in the skin.

Accuracy and precision

Accuracy and precision were determined in terms of the recovery of known amounts of CGP69669A; both intra-day and inter-day variability were evaluated. Repeated analysis was performed for three concentrations of CGP69669A (1, 5 and 20 μg/mL) on the same day to determine intra-day variability and on two different days to establish inter-day variability.

Limit of detection and limit of quantification

The limit of detection was determined by first estimating the noise by injecting the mobile phase in triplicate. The peak area of the noise signal was determined at the CGP69669A retention time. The concentrations corresponding to 3 and 10 times the area of the noise peak were defined as the limits of detection and quantification, respectively.

Skin extraction method

The extraction method was validated by spiking the skin samples with two different known amounts of drug in ethanol solution (10 and 20 μg/mL). After solvent evaporation, skin samples were cut into small pieces and soaked in 5 mL of PBS buffer. Samples were left overnight under constant stirring at ambient temperature and then were filtered and analyzed using the HPAE-PAD method described above. The recovery of CGP69669A was determined by calculating the ratio of the amount extracted from the skin samples to the amount added, determined by direct injection of spiking solution in the absence of skin. The experiments were performed in triplicate.

Results and discussion

Optimization of chromatographic conditions

A sharp CGP69669A peak in PBS solution was obtained using the Dionex CarboPac™ PA-10 column; however, it was not possible to separate it from those of endogenous compounds released from the skin. Neither the use of mobile phases containing different amounts of sodium hydroxide (from 100 to 800 mM) nor the addition of sodium acetate (from 50 to 300 mM) at different flow rates (from 0.5 to 1.5 mL/min) enabled the resolution of the peaks. Separation of the CGP69669A peak was achieved by replacing the CarboPac™ PA-10 with a CarboPac™ PA-200 anion-exchange column, which provided much higher resolution. The optimal mobile phase was found to be 100 mM NaOH solution; this yielded a sharp CGP69669A peak with adequate retention time and without any interference. The flow rate of 0.5 mL/min was used according to the manufacturer's recommendations.

Another concern in using HPAE-PAD to quantify carbohydrate is the lowering of peak response with repeated analysis owing to fouling of the gold electrode caused by matrix components in the sample. Pulsed amperometric detection does not measure an intrinsic quantity of the analyte as, for example, in UV absorbance detection. Instead, the measured charge (in Coulombs) obtained by integration of the analyte oxidation current is proportional to the rate of the oxidation reaction. Therefore, a decreased response is obtained when the surface of the gold electrode is compromised or not clean (Rocklin *et al*., 1998). Since samples from transdermal transport studies will contain several endogenous compounds that might foul the electrode surface, and as these samples will be directly injected without prior treatment, two approaches were adopted in order to ensure reproducibility. First, a quadruple-potential waveform for detection was chosen (+0.1 V from 0.0 to 0.4 s, −2.0 V from 0.41 to 0.42 s, +0.6 V at 0.43 s and −0.1 V from 0.44 to 0.50 s, with current integrated between 0.20 and 0.40 s for detection). The short duration pulse at −2.0 V reduces adsorbed sugars and these are most likely displaced by adsorbed hydrogen owing to reduction of water (Rocklin *et al*., 1998). This waveform has been shown to minimize the dissolution and recession of the gold working electrode as a result of gold oxide formation/reduction cycles, improving long-term reproducibility. Second, another carbohydrate was also tested as an internal standard and calibration curves were constructed by plotting the CGP69669A/internal standard peak area ratio against CGP69669A concentration. In this way, in the event of lower peak response, the internal standard would also be affected and the CGP69669A/internal standard peak area ratio would remain the same.

Sucrose and rafinose were evaluated as internal standards for CGP69669A analysis. However, only rafinose eluted at a suitable retention time and could be completely separated from the CGP69669A peak. Figure 2 shows the overlaid chromatograms of CGP69669A in PBS buffer solution, with the internal standard (rafinose) and blank skin extract solution using the optimized conditions.

Method validation

Linearity. Good linearity was observed between response (CGP69669A/rafinose peak area ratio) and CGP69669A concentration (x) over a concentration range spanning 1.0–25 μg/mL (typical equation: $y = 0.0962\ x + 0.0436$). The results of least squares linear regression analysis showed that the correlation coefficients of all the standard curves were ≥0.997 (Fig. 3). The concentrations were back-calculated for each point by least squares linear regression and the RSD calculated. The resulting values were <10% for all of the points in the standard curves. Overlaid typical HPAE-PAD chromatograms of CGP69669A at different concentrations (1.0, 5.0, 10.0 and 20.0 μg/mL) in PBS buffer solution with rafinose are shown in Fig. 4.

Limit of detection and limit of quantification. The limits of detection and quantification were 0.3 and 1.0 μg/mL, respectively.

Specificity. The method was considered to be specific for CGP69669A ($t = 3.0$ min) as the peak was clearly separated from the solvent front and peaks from endogenous compounds released from the skin (Fig. 2).

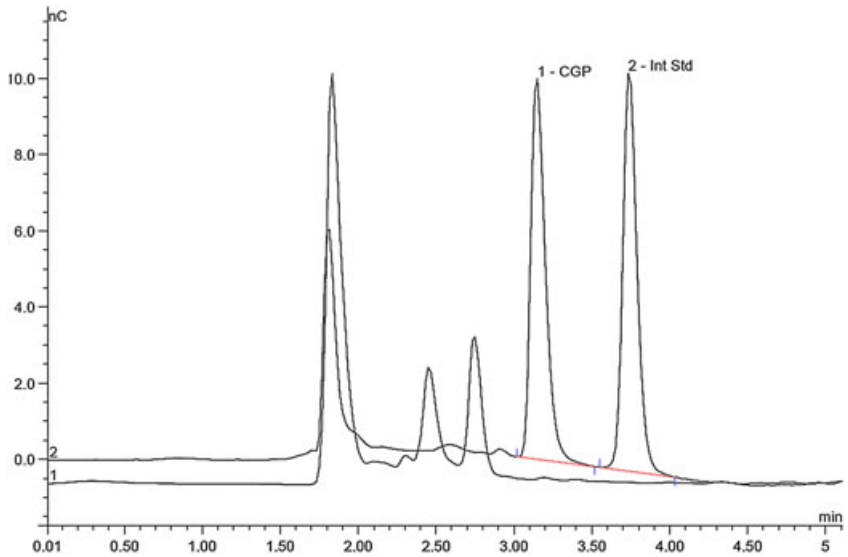

Figure 2. Overlaid HPAE-PAD chromatograms of (a) blank skin extract solution and (b) CGP69669A (20 μg/mL) in PBS buffer solution with internal standard (rafinose) obtained using the optimized conditions.

Precision and accuracy. The results of the intra- and inter-day precision and accuracy analyses of CGP69669A samples are shown in Table 1. For intra-day measurements, the mean recoveries ranged from 89.60 to 99.16% (RSD 2.16–4.74%). The mean recoveries for inter-day analysis on day 1 ranged from 92.09 to 101.02% (RSD 3.31–6.73%) and on day 2 they were between 94.58 and 104.00% (RSD 1.07–4.82%). All of these values are within the acceptance limits (ICH, 2005).

Application of the method: quantification of CGP69669A recovery from skin

The analytical method was used to determine the efficiency of the extraction process in recovering CGP69669A from the skin; the high yields obtained are shown in Table 2.

Conclusion

The present work describes the first validated direct isocratic HPAE-PAD method for the quantification of the E-selectin antagonist CGP69669A, a glycomimetic of the tetrasaccharide sialyl Lewis^x, with potential use for treating inflammatory skin diseases. The optimized conditions enabled rapid elution of CGP69669A (at 3.0 min) and internal standard (at 3.6 min) without interference from solvent peaks or substances present in the skin. The method was validated with respect to linearity over a concentration range of 1.0–25 μg/mL and the accuracy and precision, which were within acceptable limits for intra- and

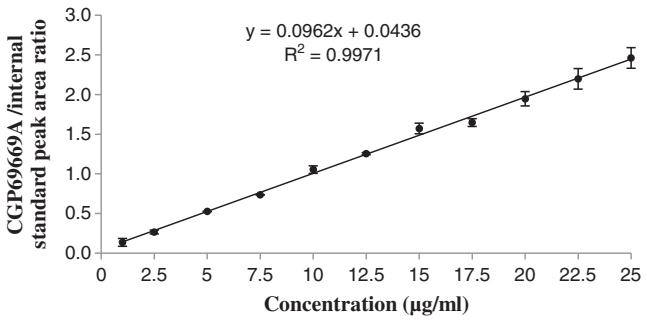

Figure 3. Calibration plot of CGP69669A internal standard peak area ratio against CGP69669A concentration ($n = 3$; mean ± SD).

Table 1. Precision and accuracy of the HPAE-PAD method to quantify CGP69669A

Theoretical concentration (μg/mL)	Experimental concentration (mean ± SD; μg/mL)	CV (%)[a]	Accuracy (%)[b]
Intra-day ($n = 5$)			
1.0	0.90 ± 0.06	4.74	89.60
5.0	4.96 ± 0.13	2.44	99.16
20.0	18.40 ± 0.41	2.16	91.98
Inter-day ($n = 5$)			
1.0	0.92 ± 0.07	4.90	92.09
5.0	5.05 ± 0.18	3.31	101.02
20.0	19.60 ± 1.35	6.73	97.99

[a]Precision = (SD/mean) × 100.
[b]Accuracy = (obtained concentration/theoretical concentration) × 100.

Table 2. Percentage recovery of CGP69669A from spiked skin samples following extraction with PBS buffer (pH 7.4)

Theoretical concentration (μg/mL)	Recovery (%)[a]
10.0	95.89 ± 11.42
20.0	103.46 ± 16.37

[a]Mean ± SD ($n = 3$).

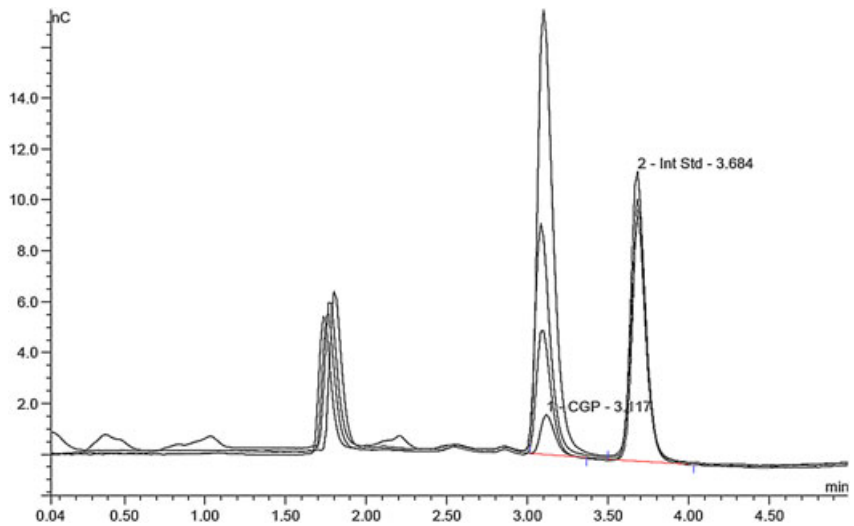

Figure 4. Overlaid HPAE-PAD chromatograms of CGP69669A at different concentrations (1.0, 5.0, 10.0 and 20.0 μg/mL) in PBS buffer solution with internal standard (rafinose).

inter-day analysis. It will now be used to quantify the iontophoretic transport of CGP69669A in skin permeation experiments. Furthermore, the HPAE-PAD method described here for CGP69669A may also prove to be a useful starting point for the development of similar analytical methods for the quantification of structurally related molecules.

References

Berg EL, Robinson MK, Mansson O, Butcher EC and Magnani JL. A carbohydrate domain common to both sialyl Le(a) and sialyl Le(X) is recognized by the endothelial cell leukocyte adhesion molecule ELAM-1. *Journal of Biological Chemistry* 1991; **266**: 14869–14872.

Bock D, Philipp S and Wolff G. Therapeutic potential of selectin antagonists in psoriasis. *Expert Opinion on Investigational Drugs* 2006; **15**: 963–979.

Hanko VP and Rohrer JS. Determination of carbohydrates, sugar alcohols, and glycols in cell cultures and fermentation broths using high-performance anion-exchange chromatography with pulsed amperometric detection. *Analytical Biochemistry* 2000; **283**: 192–199.

ICH. Q2(R1) *Validation of Analytical Procedures: Text and Methodology*. International Conference on Harmonization of Technical Requirements for Registration of Pharmaceuticals for Human Use: Geneva, 2005.

Kalia YN, Naik A, Garrison J and Guy RH. Iontophoretic drug delivery. *Advanced Drug Delivery Reviews* 2004; **56**: 619–658.

Kolb HC and Ernst B. Development of tools for the design of selectin antagonists. *Chemistry – a European Journal* 1997; **3**: 1571–1578.

Ley K. Molecular mechanisms of leukocyte recruitment in the inflammatory process. *Cardiovascular Research* 1996; **32**: 733–742.

Ley K and Tedder TF. Leukocyte interactions with vascular endothelium – new insights into selectin-mediated attachment and rolling. *Journal of Immunology* 1995; **155**: 525–528.

Norman KE, Anderson GP, Kolb HC, Ley K and Ernst B. Sialyl Lewis(x) (sLe(x)) and an sLe(x) mimetic, CGP69669A, disrupt E-selectin-dependent leukocyte rolling *in vivo*. *Blood* 1998; **91**: 475–483.

Phillips ML, Nudelman E, Gaeta FC, Perez M, Singhal AK, Hakomori S and Paulson JC. ELAM-1 mediates cell adhesion by recognition of a carbohydrate ligand, sialyl-Lex. *Science* 1990; **250**: 1130–1132.

Rao RM, Yang L, Garcia-Cardena G and Luscinskas FW. Endothelial-dependent mechanisms of leukocyte recruitment to the vascular wall. *Circulation Research* 2007; **101**: 234–247.

Robert C and Kupper TS. Inflammatory skin diseases, T cells, and immune surveillance. *New England Journal of Medicine* 1999; **341**: 1817–1828.

Rocklin RD, Clarke AP and Weitzhandler M. Improved long-term reproducibility for pulsed amperometric detection of carbohydrates via a new quadruple-potential waveform. *Analytical Chemistry* 1998; **70**: 1496–1501.

Schon MP. Inhibitors of selectin functions in the treatment of inflammatory skin disorders. *Journal of Therapeutics and Clinical Risk Management* 2005; **1**: 201–208.

Tanaka A, Takahama H, Kato T, Kubota Y, Kurokawa K, Nishioka K, Mizoguchi M and Yamamoto K. Clonotypic analysis of T cells infiltrating the skin of patients with atopic dermatitis: evidence for antigen-driven accumulation of T cells. *Human Immunology* 1996; **48**: 107–113.

Titz A, Patton J, Smiesko M, Radic Z, Schwardt O, Magnani JL and Ernst B. Probing the carbohydrate recognition domain of E-selectin: the importance of the acid orientation in sLex mimetics. *Bioorganic & Medicinal Chemistry* 2010; **18**: 19–27.

Vocanson M, Hennino A, Rozieres A, Poyet G and Nicolas JF. Effector and regulatory mechanisms in allergic contact dermatitis. *Allergy* 2009; **64**: 1699–1714.

Vollmer S, Menssen A and Prinz JC. Dominant lesional T cell receptor rearrangements persist in relapsing psoriasis but are absent from nonlesional skin: evidence for a stable antigen-specific pathogenic T cell response in psoriasis vulgaris. *Journal of Investigative Dermatology* 2001; **117**: 1296–1301.

LIST OF PUBLICATIONS

Publications

- Gratieri T, Kalaria D, Kalia YN. Non-invasive iontophoretic delivery of peptides and proteins across the skin. Expert Opin Drug Deliv, 2011; 8(5): 645-663.
- Yu J, Kalaria DR, Kalia YN. Erbium:YAG fractional laser ablation for the percutaneous delivery of intact functional therapeutic antibodies. J Control Release, 2011; 56(1): 53-59.
- Gratieri T, Wagner B, Kalaria D, Ernst B, Kalia YN. Cutaneous iontophoretic delivery of CGP69669A, a sialyl lewis^X Mimetic, *in vitro*. Exp Dermatol, 2012; 21(3): 226-228.
- Gratieri T, Wagner B, Kalaria D, Ernst B, Kalia YN. Development and validation of a HPAE-PAD method for the quantification of CGP69669A, a sialyl Lewis^x mimetic, in skin permeation studies. Biomed Chromatogr, 2012; 26 (4): 507-511.
- Kalaria DR, Patel P, Patravale V, Kalia YN. Comparison of the cutaneous iontophoretic delivery of rasagiline and selegiline across porcine and human skin *in vitro*. Int J Pharm, 2012; 438 (1-2) 202– 208.

Book chapters

- Kalaria DR, Dubey S, Kalia YN. Clinical applications of transdermal iontophoresis in: Topical and Transdermal Drug Delivery: Principles and Practice, Editors: Heather A.E. Benson, Adam C. Watkinson, 2011, John Wiley & Sons, United Kingdom.
- Dubey S, Kalaria D, Gratieri T, Kalia YN. Stratum corneum ablation techniques in: Physical methods to increase topical and transdermal drug delivery, Editors: Renata Fonseca Vianna Lopez, Tais Gratieri and Guilherme Martins Gelfuso, 2012 Research Signpost and Transworld Research Network, India.

Manuscripts in preparation

- Kalaria DR, Patravale V, Merino V, Kalia YN. Transdermal iontophoresis for the controlled delivery of pramipexole: Effect of iontophoretic and formulation parameters on electrotransport kinetics *in vitro* and *in vivo*.
- Kalaria DR, Patravale V, Merino V, Kalia YN. Controlled iontophoretic transport of huperzine A across skin *in vitro* and *in vivo*: Effect of delivery conditions and comparison of pharmacokinetic models.

- Kalaria DR, Merino V, Kalia YN. Anodal co-iontophoresis for the simultaneous transdermal delivery of pramipexole (dopamine agonist) and rasagiline (MAO-B inhibitor) for more effective treatment of Parkinson's Disease.

Conference communications/oral presentations

- Kalaria DR, Patel P, Patravale V, Kalia YN. Transdermal iontophoresis of huperzine A for the treatment of Alzheimer's Disease at 25th AAPS Annual Meeting and Exposition, Washington D.C., USA, 2011.
- Patel PA, Patil SC, Kalaria DR, Kalia YN, Patravale VB. Transdermal Delivery of huperzine A for the treatment of Alzheimer's disease at 25th AAPS Annual Meeting and Exposition, Washington D.C., USA, 2011.
- Patel PA, Kalaria DR, Patil SC, Kalia YN, Patravale VB. Influence of colloidal carriers on transdermal delivery of donepezil hydrochloride at 25th AAPS Annual Meeting and Exposition, Washington D.C., USA, 2011.
- Kalaria DR, Kalia YN. Co-iontophoresis of rasagiline and pramipexole for the treatment of Parkinsonism for Oral Podium Presentation at 38th Annual Meeting & Exposition of the Controlled Release Society, National Harbour, USA, August 2011.
- Kalaria DR, Gratieri T, Kalia YN. A topical microemulsion based formulation for tacrolimus at 38th Annual Meeting & Exposition of the Controlled Release Society, National Harbour, USA, August 2011.
- Gratieri T, Kalaria DR, Kalia YN. Drug delivery to the posterior eye segment: a new ex vivo model for ocular iontophoretic studies at 38th Annual Meeting & Exposition of the Controlled Release Society, National Harbour, USA, August 2011.
- Yu J, Kalaria D, Bachhav Y, Heinrich A, Böhler C, Kalia YN. Needle-less delivery of intact functional therapeutic antibodies: Turning fiction into reality at CTI Medtech Event, Bern, Switzerland 2010.
- Kalaria DR, Patravale VB, Kalia YN. Electromigration is the principal transport mechanism for the transdermal iontophoretic delivery of selegiline at 7th Pharmaceutics, Biopharmaceutics and Pharmaceutical Technology World Meeting, Malta, March 2010.

ACKNOWLEDGEMENTS

I would like to thank my supervisor Dr Yogeshvar N. Kalia for his guidance, untiring motivation and scientific inputs throughout my doctoral studies. I'm highly grateful to Prof. Leonardo Scapozza for giving me the opportunity to work under his direction for my thesis.

I'm thankful to Prof. Eric Allémann, Prof. Jouni Hirvonen, Prof. Patrizia Santi and Prof. Virginia Merino for accepting to evaluate this work.

I also thank Prof. Virginia Merino for giving me the opportunity to conduct in vivo studies at the Faculty of Pharmacy, University of Valencia. I'm grateful to our collaborator Prof. Vandana Patravale, Institute of Chemical Technology, Mumbai.

I would like to thank my friends and colleagues, past and present, FAPER and FABIP group members for their moral and technical support.

I acknowledge the financial support from Indo Swiss Joint Research Programme (ISJRP 123143).

Finally, I would like to thank my family for their constant moral support.